

Advances

in Clinical and Experimental Medicine

MONTHLY ISSN 1899-5276 (PRINT) ISSN 2451-2680 (ONLINE)

www.advances.umed.wroc.pl

2020, Vol. 29, No. 12 (December)

Impact Factor (IF) – 1.514
Ministry of Science and Higher Education – 40 pts.
Index Copernicus (ICV) – 155.19 pts.



WROCLAW
MEDICAL UNIVERSITY

Advances in Clinical and Experimental Medicine

ISSN 1899-5276 (PRINT)

ISSN 2451-2680 (ONLINE)

www.advances.umed.wroc.pl

MONTHLY 2020
Vol. 29, No. 12
(December)

Advances in Clinical and Experimental Medicine is a peer-reviewed open access journal published by Wrocław Medical University. Its abbreviated title is Adv Clin Exp Med. Journal publishes original papers and reviews encompassing all aspects of medicine, including molecular biology, biochemistry, genetics, biotechnology, and other areas. It is published monthly, one volume per year.

Editorial Office

ul. Marcinkowskiego 2–6
50-368 Wrocław, Poland
Tel.: +48 71 784 11 36
E-mail: redakcja@umed.wroc.pl

Publisher

Wrocław Medical University
Wybrzeże L. Pasteura 1
50-367 Wrocław, Poland

© Copyright by Wrocław Medical University,
Wrocław 2020

Online edition is the original version of the journal

Editor-in-Chief

Maciej Bagłaj

Vice-Editor-in-Chief

Dorota Frydecka

Editorial Board

Piotr Dziągpiel
Marian Klinger
Halina Milnerowicz
Jerzy Mozrzymas

Thematic Editors

Marzenna Bartoszewicz (microbiology)
Marzena Dominiak (dentistry)
Paweł Domoślawski (surgery)
Maria Ejma (neurology)
Jacek Gajek (cardiology)
Mariusz Kuształ
(nephrology and transplantology)
Rafał Matkowski (oncology)
Ewa Milnerowicz-Nabzdyk (gynecology)
Katarzyna Neubauer (gastroenterology)
Marcin Ruciński (basic sciences)
Robert Śmigiel (pediatrics)
Paweł Tabakow (experimental medicine)
Anna Wiela-Hojeńska
(pharmaceutical sciences)
Dariusz Wołowicz (internal medicine)

International Advisory Board

Reinhard Berner (Germany)
Vladimir Bobek (Czech Republic)
Marcin Czyz (UK)
Buddhadeb Dawn (USA)
Kishore Kumar Jella (USA)

Secretary

Katarzyna Neubauer

Piotr Ponikowski
Marek Sąsiadek
Leszek Szenborn
Jacek Szepietowski

Statistical Editors

Dorota Diakowska
Leszek Noga
Lesław Rusiecki

Technical Editorship

Paulina Kunicka
Marek Misiak

English Language Copy Editors

Eric Hilton
Sherill Howard Pociecha
Jason Schock
Marcin Tereszewski

Pavel Kopel (Czech Republic)
Tomasz B. Owczarek (USA)
Ivan Rychlík (Czech Republic)
Anton Sculean (Switzerland)
Andriy B. Zimenkovsky (Ukraine)

Editorial Policy

Advances in Clinical and Experimental Medicine (Adv Clin Exp Med) is an independent multidisciplinary forum for exchange of scientific and clinical information, publishing original research and news encompassing all aspects of medicine, including molecular biology, biochemistry, genetics, biotechnology and other areas. During the review process, the Editorial Board conforms to the "Uniform Requirements for Manuscripts Submitted to Biomedical Journals: Writing and Editing for Biomedical Publication" approved by the International Committee of Medical Journal Editors (www.ICMJE.org/). The journal publishes (in English only) original papers and reviews. Short works considered original, novel and significant are given priority. Experimental studies must include a statement that the experimental protocol and informed consent procedure were in compliance with the Helsinki Convention and were approved by an ethics committee.

For all subscription-related queries please contact our Editorial Office:
redakcja@umed.wroc.pl

For more information visit the journal's website:
www.advances.umed.wroc.pl

Pursuant to the ordinance No. 134/XV R/2017 of the Rector of Wrocław Medical University (as of December 28, 2017) from January 1, 2018 authors are required to pay a fee amounting to 700 euros for each manuscript accepted for publication in the journal Advances in Clinical and Experimental Medicine.

„Podniesienie poziomu naukowego i poziomu umiędzynarodowienia wydawanych czasopism naukowych oraz upowszechniania informacji o wynikach badań naukowych lub prac rozwojowych – zadanie finansowane w ramach umowy 784/p-DUN/2017 ze środków Ministra Nauki i Szkolnictwa Wyższego przeznaczonych na działalność upowszechniającą naukę”.



Indexed in: MEDLINE, Science Citation Index Expanded, Journal Citation Reports/Science Edition, Scopus, EMBASE/Excerpta Medica, Ulrich's™ International Periodicals Directory, Index Copernicus

Typographic design: Monika Kołęda, Piotr Gil
DTP: Wydawnictwo UMW
Cover: Monika Kołęda
Printing and binding: EXDRUK

Contents

Original papers

- 1379 Agnieszka Żok, Jadwiga Wiertelwska-Bielarz, Ewa Baum
Determinants of moral attitudes toward stem cells
- 1389 Beata Nowak, Agnieszka Matuszewska, Magdalena Tomanik, Jarosław Filipiak, Alicja Zofia Kucharska, Narcyz Piórecki, Diana Jędrzejuk, Krzysztof Zduniak, Małgorzata Trocha, Marek Bolanowski, Adam Szeląg, Tomasz Sozański
Cornelian cherry extract ameliorates osteoporosis associated with hypercholesterolemia in New Zealand rabbits
- 1399 Martyna Tomczyk-Socha, Dagmara Baczyńska, Joanna Przeździecka-Dołyk, Anna Turno-Kręcicka
MicroRNA-125b overexpression in pseudoexfoliation syndrome
- 1407 Jun Yu, Qiurong Ruan, Xiu Nie
Synthesis and characterization of atherosclerotic target anti-CD47 functionalized by nano- polyelectrolyte complexes between chitosan and hyaluronic acid and in vivo and in vitro targeting experiments
- 1417 Ayhan Korkmaz, Eser Oz Oyar, Zuhail Yildirim, Arzu Pampal, Nese Lortlar Unlu, Hakan Akbulut
Application of vascular endothelial growth factor at different phases of intestinal ischemia/reperfusion: What are its effects on oxidative stress, inflammation and telomerase activity?
- 1425 Ke Ma, Lvjun Yang, Mingde Liao, Yi Qin, Chao Luo, Lina Lin, Danyan Ye
Acute effect of a variable pulse width Nd:YAG laser combined with hematoporphyrin monomethyl ether-mediated photodynamic therapy on a cockscomb model of nevus flammeus
- 1433 Paweł Serek, Iwona Bednarz-Misa, Jadwiga Pietkiewicz, Bartłomiej Dudek, Magdalena Mierzchała-Pasierb, Katarzyna Jermakow, Marek Drab, Andrzej Gamian
Salmonella Typhimurium enolase-like membrane protein is recognized by antibodies against human enolase and interacts with plasminogen
- 1443 Jacek Marcin Zawadzki, Katarzyna Zimmer, Wojciech Przywara, Dorota Zyśko, Jadwiga Radziejewska, Agnieszka Sławuta, Jacek Gajek
The true nature of P wave dispersion
- 1449 Wojciech Grzebieluch, Urszula Kaczmarek, Tomasz Staniowski, Marcin Mikulewicz
Does image file transfer, exposure time and optimization algorithm affect digital intraoral radiographs?
- 1459 Paweł Duda, Brygida Knysz, Jacek Gąsiorowski, Bartosz Szetela, Ewa Piotrowska, Monika Bronkowska
Assessment of dietary habits and lifestyle among people with HIV
- 1469 Natalia Głódkowska, Katarzyna Emerich
The impact of environmental air pollution on the prevalence of molar incisor hypomineralization in schoolchildren: A cross-sectional study
- 1479 Xingyu Mei, Jie Huang, Yue Sun, Zhouwei Wu, Weimin Shi
Analysis of how obtaining melanocytes by magnetic cell separation contributes to autoepidermal transplantation technology in treating leucoderma

Multicenter study

- 1487 Ireneusz Honkisz, Janusz Sulisławski, Barbara Dobrowolska-Glazar, Caroline F. Kuijper, Rafał Chrzan
Foreskin healing after distal hypospadias repair: Does stenting affect the outcome?

Reviews

- 1491 Danuta Nowicka, Marta Bałaj-Oleszczuk, Joanna Maj
Infectious diseases of the skin in contact sports
- 1497 Jacek Arkowski, Marta Obremska, Kamil Kędzierski, Agnieszka Sławuta, Magdalena Wawrzyńska
Applications for graphene and its derivatives in medical devices: Current knowledge and future applications
- 1505 Paweł Kuźnicki, Radosław Kempański, Katarzyna Neubauer
The emerging role of mood disorders in inflammatory bowel diseases

Determinants of moral attitudes toward stem cells

Agnieszka Żok^{1,B–E}, Jadwiga Wiertlewska-Bielarz^{2,C–E}, Ewa Baum^{1,2,A–F}

¹ Division of Philosophy of Medicine and Bioethics, Poznan University of Medical Sciences, Poland

² Department of Social Sciences and Humanities, Poznan University of Medical Sciences, Poland

A – research concept and design; B – collection and/or assembly of data; C – data analysis and interpretation; D – writing the article; E – critical revision of the article; F – final approval of the article

Advances in Clinical and Experimental Medicine, ISSN 1899–5276 (print), ISSN 2451–2680 (online)

Adv Clin Exp Med. 2020;29(12):1379–1387

Address for correspondence

Agnieszka Żok
E-mail: agzok@ump.edu.pl

Funding sources

None declared

Conflict of interest

None declared

Received on June 10, 2020

Reviewed on July 2, 2020

Accepted on September 20, 2020

Abstract

Background. The paper presents an analysis of opinions concerning the use of stem cells (SCs), using tools developed in the field of moral psychology.

Objectives. To determine the factors that affect beliefs regarding the status of SCs and to evaluate the impact of these factors. The paper investigated whether factors of a moral nature prevail over the knowledge that makes it possible to use SCs in practice.

Material and methods. The analysis of psychological perception is based on a study carried out on a group of 172 Polish and 161 English-speaking first-year medical students. The study was conducted between 2005 and 2007, and in 2019 at the Poznan University of Medical Sciences (Poland).

Results. Knowledge is not the main factor that differentiates approaches towards the use of SCs. The importance of religion in the lives of the respondents has a significant impact on the perception of the use of SCs, and is associated with indications of ethically saturated terms. Focusing on the usefulness of cells is associated with lesser significance of religion and greater value placed on scientific knowledge.

Conclusions. Although the research results indicate a correlation between religiousness and the respondents' perception of the use of SCs, further research is needed into the relationship between the influence of scientific knowledge on views related to SCs.

Key words: stem cells, bioethics, moral psychology, medical ethics, education

Cite as

Żok A, Wiertlewska-Bielarz J, Baum E. Determinants of moral attitudes toward stem cells. *Adv Clin Exp Med.* 2020;29(12):1379–1387. doi:10.17219/acem/127678

DOI

10.17219/acem/127678

Copyright

© 2020 by Wrocław Medical University

This is an article distributed under the terms of the Creative Commons Attribution 3.0 Unported (CC BY 3.0) (<https://creativecommons.org/licenses/by/3.0/>)

Introduction

A significant problem that concerns contemporary researchers, doctors, medical students, ethicists, and philosophers is not whether we are technically capable of performing a complicated procedure, but whether we should perform it or whether we have a moral right to do so.¹ The disciplines that cause fundamental dilemmas and ethical controversies in modern biology and medicine are transplantology, regenerative medicine, genetic engineering and, in particular, the use of embryonic stem cells (ESCs) in modern therapy.² Ethical issues became a widely discussed topic in November 2018 when He Jankui of the Southern University of Science and Technology in Shenzhen, China, announced the birth of twin girls, Lulu and Nana, after he had edited the DNA in their embryos.³ Another example of ethically controversial research is to create animal embryos that contain human cells and transplant these into surrogate animals. This type of research was approved in 2019 in Japan.⁴ Still in need of improvement, genome editing therapy raises more ethical than technical controversies. An example is mitochondrial transfer (pronuclear transfer (PNT) and maternal spindle transfer (MST)), which despite its proven therapeutic effectiveness, is not approved in the EU (except for the UK) or the USA.

Stem cells (SCs) were defined in the 1940s and 1950s during studies on the effects of ionizing radiation on animals. They are characterized by their self-renewing potential and ability to reproduce and differentiate.⁵ Stem cells, based on their potential, are classified as totipotent, pluripotent, multipotent, and single-potent. The first ones are SCs that are present at the earliest stages of ontogenesis and can transform into all forms of embryo and placenta tissue. Stem cells can also be classified into 4 groups corresponding to their different origins: ESCs, fetal SCs, adult SCs, and induced pluripotent SCs.⁶ Research on the therapeutic use of SCs is constantly developing. Scientists are experimenting with ways to selectively target the blood-making cells within the body for destruction. Early studies suggest that the approach could make blood SCs transplants – powerful but dangerous procedures that are used mainly to treat blood cancers – safer and thereby broaden their use. The studies come as evidence piles up that such transplants can also treat some autoimmune disorders and genetic diseases.⁷ The possibilities of the therapeutic use of SCs are constantly increasing.

In 2019, according to a PubMed database search using the keywords “stem cells” and “human”, 7295 scientific articles were published concerning applications of SC therapy in human beings. An attempt has also been made to use pluripotent SCs with the clustered regularly interspaced short palindromic repeats (CRISPR) technique.⁸ Due to the ethical controversies that are still aroused by the use of SCs, despite their long-term therapeutic use, we have made an attempt to analyze students’ attitudes

towards this subject. In view of the ethical and social dilemmas involved, collecting, culturing and experimenting on embryonic and fetus SCs is legally restricted in many countries.⁶ Moreover, some experiments with ESCs have led to the formation of cancerous cells and teratomas. Work on the implementation of a safe ESC line is still in progress.⁹

The question of what really determines human moral judgment, and worldviews is becoming fundamental to the further development of biomedicine.¹⁰ Hence, a study was conducted at the University of Medical Sciences in Poznan (Poland) on a group of 172 Polish and 161 English-speaking first-year medical students in 2007 and again in 2019. The main objective of the study was to analyze the claim that the potential development and future success of SC therapy is determined not only by the progress of biological sciences but also by legal regulations and social approval of the issue in question. The problem lies in the fact that we cannot rely only on the technological capabilities of medicine, but also on our acceptance or rejection of controversial medical techniques. Ethical aspects must not be overlooked when making fundamental decisions, and at the same time, it can be assumed that attitudes towards the issues strongly correlate with the level of relevant knowledge.¹¹

Therefore, the specific objective of the study was to determine the attitudes of medical students towards transplantation techniques using SCs, taking into account the influence of factors such as the level of the respondents’ medical knowledge, their religious affiliation and the role it plays in their lives. Also included is an analysis of changes in the respondents’ knowledge and views over the course of 12 years. One particularly interesting factor is the influence of the students’ knowledge and their attitude towards religion on the terms they used to talk about SCs. This influence was analyzed from the perspective of moral psychology.

Material and methods

The study was based on questionnaire surveys conducted between 2005 and 2007, and again in 2019, involving 333 students of medical departments. The students were divided into 4 groups constituting statistical subgroups according to the year and language of their study curriculum (Table 1).

Table 1. The number of respondents

| Department of Medicine | Year of study | Survey year | Number of respondents |
|------------------------|---------------|-------------|-----------------------|
| Polish | 1 | 2007 | 100 |
| English | 1 | 2007 | 100 |
| Polish | 1 | 2019 | 72 |
| English | 1 | 2019 | 61 |

The questionnaire used to analyze the students' beliefs concerning the ethical dimensions of using SCs was based on the following questions:

1. Please indicate the sources of your knowledge concerning stem cells.
2. Do you know any sources of obtaining stem cells?
3. Which of the phrases listed below do you associate with embryonic stem cells?
4. Would you like to be involved in research on stem cells after graduating?

All the questions asked in the survey were open-ended, which made it possible to respond beyond the options provided. The students filled out the questionnaire independently and anonymously, and a section concerning their demographic and social affiliations was placed at the end of the form.

Subgroups were created on the basis of the answers to particular questions, and were compared as an important element of the research process. The results of the survey were analyzed using R v. 3.5.1 statistical software (R Foundation for Statistical Computing, Vienna, Austria; <http://www.R-project.org/>). The statistical significance of differences between the compared groups was determined using the Fisher–Freeman–Halton test. P-values under 0.05 were considered statistically significant. The results obtained were visualized as donut and alluvial diagrams generated using ggplot2 and RColorBrewer software (both from R Foundation for Statistical Computing).¹²

A constant common feature of all the respondents was studying at the Department of Medicine of the Poznan University of Medical Sciences. Religion, attitude toward religion, and toward specific issues in ethics and bioethics were treated as features; non-researchable variables included nationality, age, gender, and origin.¹³ A special focus was put on the changes in the features outlined above over a period of 12 years, which spanned a turbulent time in the development of the medical sciences, when many ethically questionable therapies were becoming standard. Stem cell therapy was chosen as an example.

Results

Our analysis of the findings included a comparison of the data from the questionnaires. The first step was to perform an analysis based on techniques characteristic of sociological research. The data obtained was also compared to trends observed in society. Following this, the analysis was carried out from the perspective of moral psychology.

As a source of knowledge about SCs, Polish and English-speaking students starting their medical education between 2005 and 2007 used university resources, for example lectures and seminars, university textbooks or other academic literature, as well as other sources of knowledge (the Internet, radio and television, press articles).

Both Polish and English-speaking students starting their education in 2019 were much more likely to gain knowledge about SCs from university textbooks and academic lectures. This may suggest that curricula and academic textbooks have been updated to include SC therapy. A difference was noted between the questionnaires from 2007 and 2019 in declarations concerning Internet-based knowledge. This is undoubtedly linked to the increase in web accessibility and the growing importance of popular science publications, where breakthroughs are often described even before they appear in peer-reviewed scientific journals, and which are easy to access via the Internet.

Over the course of the study, there was an increase in declared knowledge SC harvesting sources among both Polish and English-speaking students. However, it is interesting to note that the declared increase in knowledge among Polish students was much higher than among English-speaking students. The increase was just below the threshold of statistical significance. However, it should be stressed that as early as 2005 and 2007, English-speaking students declared much more knowledge than their Polish peers. This could be related to the fact that in the USA, for example, the use of ESCs in therapy began in 1998,¹⁴ whereas in Poland, the use of significantly less controversial cord blood cells in treatment did not start until 2000.¹⁵

Language is an important tool for reflecting and shaping moral judgments. In many instances, the language constructions used by the respondents reflected their worldviews and attitudes to the issues in question.

The students' responses to what they associated with the term ESCs indicate a significant difference between the responses obtained between 2005 and 2007 and in 2019. Today students are much more likely to consider SCs genetic material than those who started their studies 12 years ago. In 2019, definitely fewer students described SCs as human beings or potential human beings than in the 2005–2007 questionnaires. This may corroborate an increase in the students' scientific knowledge and a smaller share of philosophical values in moral decision-making.

The analysis of the responses provided by Polish and English-speaking students showed statistically significant differences in the students' attitudes in 2005–2007 and in 2019. In both time periods, English-speaking students were more willing to take up work related to SCs than their Polish peers. In both cases, however, the interest in conducting such research after graduating was higher (Fig. 1).

The answers provided by Polish and English-speaking medical students showed a clear tendency towards secularization: In the latest survey, students attached much less significance to religion in life than 12 years earlier. The secularization of students' views seems to correlate with the aforementioned increase in their interest in using SCs in therapy.



Fig. 1. Donation graphs showing the percentage distributions of the responses to the questions presented above the charts

A. Please indicate the sources of your knowledge concerning stem cells. B. Do you know any sources used to obtain stem cells? C. Which of the phrases listed below do you associate with embryonic stem cells? D. Would you like to be involved in research on stem cells after graduating? E–G. Religion and the significance of religion in life

Discussion

The results presented above form the basis of an interesting comparative study of changes that have taken place in the respondent groups. The findings can be elaborated on and analyzed from various points of view. One of the most intriguing aspects seems to be the shift in perception of the SCs status. Our analysis will argue that

the perception of SCs was of a moral nature. The main aim of the analysis is to show what plays an important role in forming beliefs concerning the status of SCs. Therefore, it seems appropriate to use tools developed in the field of moral psychology.

Moral psychology is a field that seeks to understand the specificity of morality as a property that modifies human behavioral-mental activity in relation to the presence

of another human. In particular, it seeks to explain why certain behaviors are absolutely acceptable or absolutely unacceptable, and why certain motives or objectives do not need to be justified while others are debatable. The doctrine of moral psychology must meet certain criteria.¹⁶ The aim of the psychology of morality is to analyze and explain in the most reliable manner possible the moral judgment that prevails in a given environment and the norms that prevail within it. Moral psychology tries to find the motives that push people toward behavior that is praised or punished in a given environment. The study of the theory in moral psychology has demonstrated that the current challenge for theory development and research in morality is to consider the complex and multifaceted nature of the psychological antecedents and implications of moral behavior connecting different mechanisms.¹⁷

Analysis of the findings concerning changes in how stem cells are perceived

To determine the status of SCs, a number of terms were used in the study, which differ mainly in the degree of moral/ethical saturation. Below they are presented from the most morally saturated to the most professional:

- a legal and sensitive member of society;
- a human being;
- a potential human being;
- an embryo with human dignity;
- genetic material;
- surplus genetic material;
- other.

Moral saturation means that these terms:

- 1) are frequently used in discussions of ethical concepts that reflect on morality;
- 2) have connotations associated with moral assessments;
- 3) are associated with perceptions of humans as having special properties, about which Ingarden wrote: “Man... is the only being who feels humiliated by his evil deeds and tries to atone for his guilt”.^{18,19}

The term ‘genetic material’ indicates that there are certain useful properties of SCs, while ‘surplus’ indicates a lack of such properties. The term ‘other’ is interpreted as indecision as to one’s attitude toward SCs, suggesting doubt as to what characteristics should be assigned to them. This is important, as shown by Wojciszke’s research²⁰ indicating that features belonging to the moral domain have a decisive influence on shaping the observer’s impression/perception. For example, it shows that:

- Moral judgment is more saturated with affect than competence;
- In the moral (M) domain, negative information is more decisive and diagnostic than positive information, whereas in the competence (C) domain, the opposite is true. The effect of this asymmetry is that the integration of incongruent information results in a negative bias in the M domain and a positive bias in the C domain.²⁰ It seems quite reasonable

to treat the terms used in the questionnaire as belonging to the M domain and the C domain. In the case of SCs, it is difficult to talk about personality, but by assigning a given status to SCs, the students clearly assigned to them specific features of a moral or competence-related nature.

Therefore, it can be concluded that over the course of 12 years, the status of SCs has changed in such a way that fewer and fewer people perceive them within a moral classification: Polish students from 67% in 2007 to 33% in 2019, and English-speaking students from 58% to 50%, respectively. With regard to designations indicating that SCs have a usable nature, the share of Polish students rose from 32% to 60%, and the share of English-speaking students slightly fell from 40% to 38%. In the case of the latter, there was a significant rise of 10% in responses indicating hesitancy or doubt (other) in comparison to +5% among Polish students. This means that the changes in the perception of SCs cannot be explained by a simple shift in beliefs. Whereas in Polish students it is possible to say that this is the case, in English-speaking students it is not. Consequently, it is necessary to look at correlations with other factors.

It is interesting that the shift in perceptions of SCs is accompanied by 3 other changes: in the respondents’ sources of information about SCs, in their ideas about the potency of SCs and in their declarations concerning the importance of religion in their lives. In the case of Polish students, the share of respondents for whom religion is not significant rose by 16%, and this is almost the same as the decline in respondents for whom religion is very significant, namely by 15%. With regard to English-speaking students, the increase was 15%, whereas the decrease was 13%. This comprises nearly complete symmetry. Moreover, these are extreme positions on the scale, referring to strong declarations. The “grey zone” concerning religious declarations is comparable in all the study situations, ranging between 63% and 60%. Thus, the secularization of both Polish and English-speaking students over the 12 years was comparable, so it would not account for significant differences in perceptions of SCs in those 2 groups.

Regarding the increase in knowledge, the most considerable shift of 38% is observed among Polish students, whereas among the English-speaking respondents, this is merely 6%. Thus, the increase in knowledge could explain why SCs are seen from a more useful perspective than before. This may undermine Wojciszke’s thesis that moral beliefs are of significant importance to perception.

Knowledge and emotion-related indicators

In the study, the students were not asked about their feelings towards or knowledge on SCs, albeit one can assume that the predictors of these are the students’ declarations concerning the significance of religion in their lives and their sources of knowledge on SCs. Religion was opposed to knowledge, and the fundamental difference between

them seemed to be in the irrational elements, including the presence of emotional elements.

As shown by research on the human brain, there are some coded universal evolutionary mechanisms that provide for generating moral judgments. According to Hauser, Baron-Cohen and Churchland,^{21–23} areas of the brain responsible for both rational thinking and experiencing feelings are activated in order to generate moral judgments. However, there is an ongoing debate on which is more important to the formation of moral judgments: the ability to think rationally or to experience emotions. The advocates of the first school of thought include Kant, the utilitarian philosophers, and Bloom,^{24,25} a contemporary moral psychologist. They do not eliminate emotions as a source of moral beliefs but are rather of the opinion that positively valenced behaviors require the involvement of rational thinking. Their opponents, whose precursor was Hume, include Haidt²⁶ and Damasio.²⁷ In particular, Haidt links emotions to religious beliefs. Another intriguing concept that seeks to explain humans' ability to generate opinions about the world is the so-called "left-brain interpreter" proposed by Gazzaniga, whereby humans have both the ability and the need to create a coherent (though not necessarily rational) explanation of the phenomena in the world.²⁸ Religion is a system of beliefs that explains these phenomena in a coherent but not a rational way.^{16,29} Moral psychology offers a strong argument for treating religious beliefs as a predictor of the existence of emotions. Christianity in particular perceives SCs within personal categories, namely, those to which we can attribute characteristics of competence (knowledge, free will) and emotions (for example, love, care and compassion).

An indicator that predicts knowledge of the competence-related features of SCs is the ability to identify the sources of this knowledge. This ability does not necessarily prove

the possession of such knowledge. Still, if one considers which sources the respondents identify, the assertion that students in 2019 had greater academic and scientific knowledge than in 2007 seems justified. There was a considerable increase in academic and scientific expertise among Polish students – 23% – whereas among English-speaking students the increase was 12%. The popularity of academic sources grew when the students did not use the Internet. However, at the starting point, the English-speaking students' knowledge was higher (+11%) than Polish students. Hence it is possible to see this as a specific balancing of these levels. The 2019 respondents did not look for information in popular sources, whose share in obtaining information fell by about 20%. In general, it is possible to assume that current students have greater knowledge, and that it is of better quality. Figures 2, 3 depict this situation in detail.

Considering the selected indicators as predictors of emotions and knowledge, one can say that when assigning a status to SCs, the respondents did so with a considerably less emotionally charged attitude than 12 years ago.³⁰ It should be noted that in the case of Polish students, this was related to a 'useful/objective' approach towards SCs. It would seem that this approach was brought about by an increase in high-quality knowledge, and by a decline in the proportion of respondents who declared involvement in religion. Despite this decline, the number of Polish students who declared religious involvement was still nearly twice as high as the number of English-speaking students. This indicates that emotions pertaining to faith/religion play a more significant role than knowledge in their attitude toward the use of SCs. The fact that the respondents were believers did not prevent them from simultaneously acknowledging the usefulness of SCs. What is more, 23% of Polish students declared that religion had no significance in their lives,

Please indicate the source that you obtain your knowledge concerning stem cells from, 2019 Program in Polish

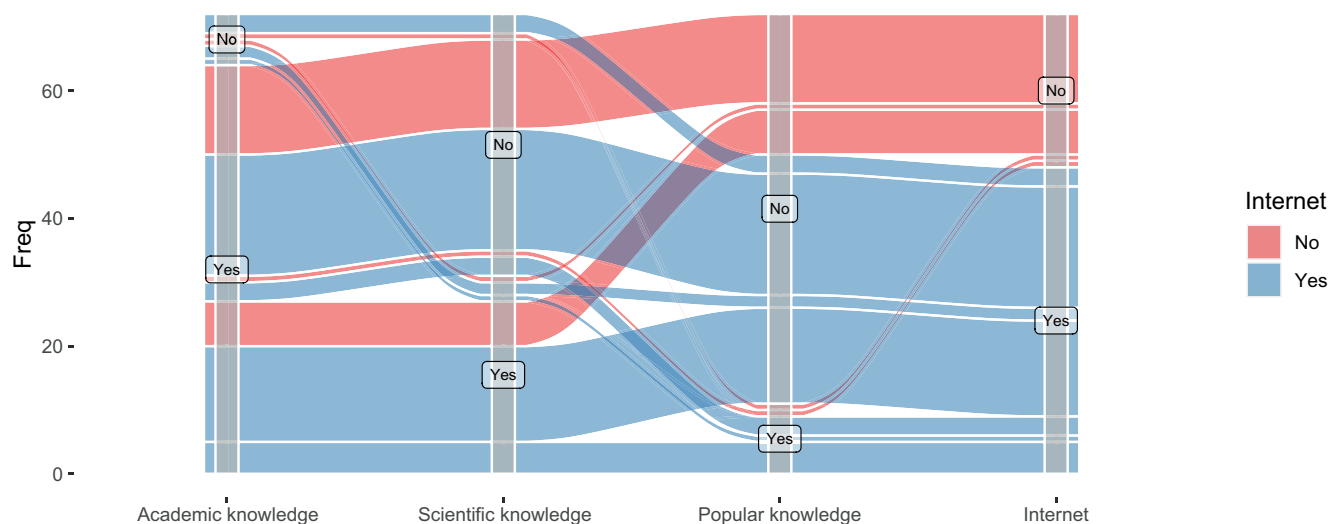


Fig. 2. Comparison of knowledge declared by Polish students with information obtained from the Internet

Please indicate the source that you obtain your knowledge concerning stem cells from, 2019 Program in English

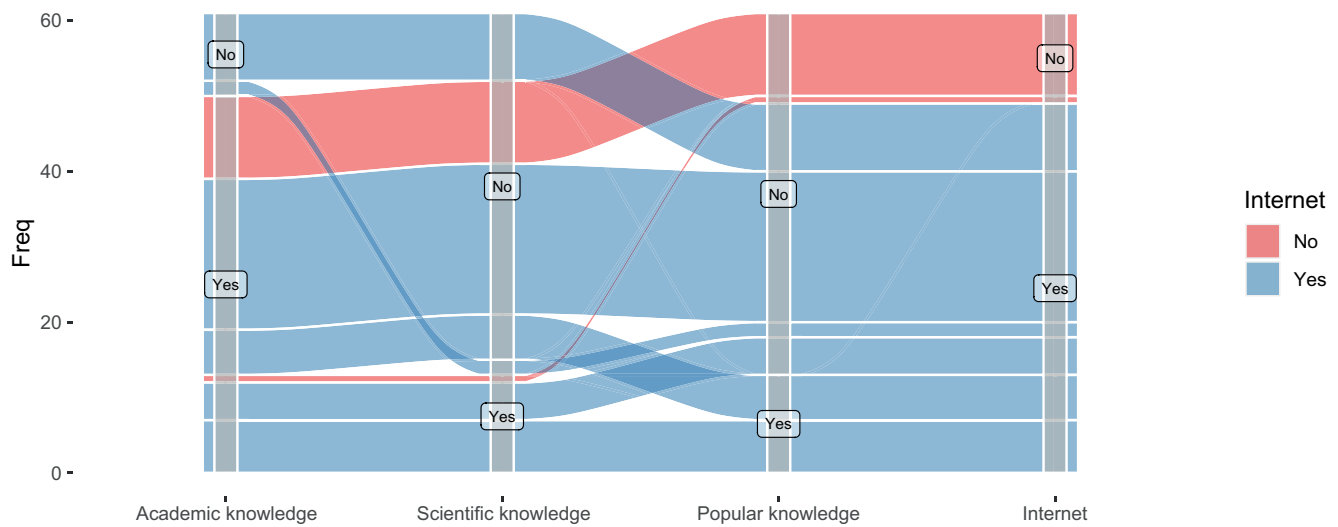


Fig. 3. Comparison of knowledge declared by English-speaking students with information obtained from the Internet

2019 Program in Polish

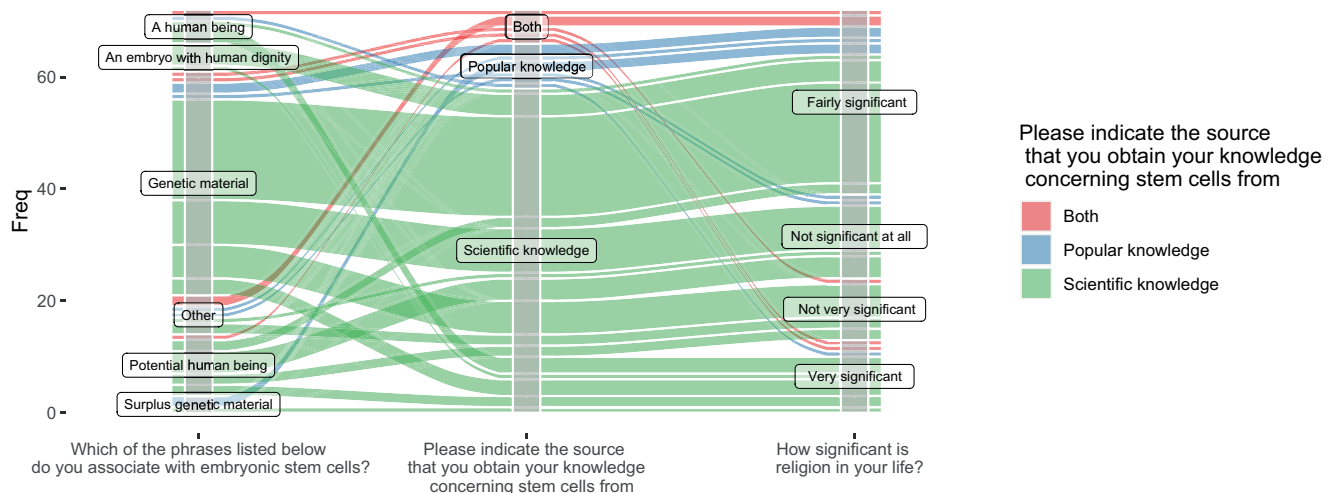


Fig. 4. Comparison of knowledge declared by Polish students with the significance of religion in their lives

which according to our theory would mean they determined the status of SCs based on knowledge only. This means that they should have viewed this issue strictly from the perspective of useful or non-useful features, but many of these students see SCs as potential human beings. This would mean that knowledge is a modifier rather than a major factor that impacts on their perception of SCs, which would correspond to the findings of Wojciszke.

As far as the English-speaking students were concerned, the share of respondents who declared that religion was of no significance in their lives was 26%, i.e., slightly above the percentage of Polish students stating that. Despite this, it is possible to observe an even wider variety of attitudes towards the status of SCs than among Polish students. The current English-speaking students were less eager to attach moral features to SCs than 12 years ago, but

at the same time, they did not see them from a utilitarian point of view; they expressed doubts about their status.

Finally, it is worth noting that the increase in knowledge declared by the students in 2019 was not paralleled by an increase in their interest in using SCs in therapy in the future.

Figures 4, 5 show the relationships between the respondents' knowledge, religion and perceptions of the SCs status.

Conclusions

As demonstrated above, knowledge is not the main factor that differentiates approaches towards SCs. Polish students with scientific knowledge defined SCs in various

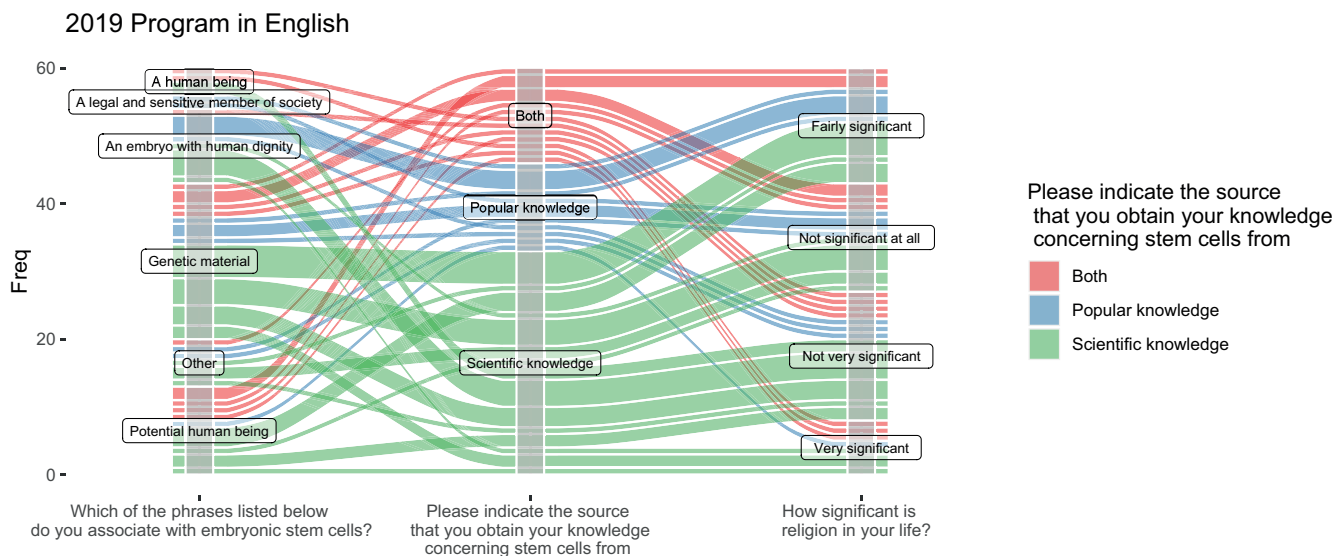


Fig. 5. Comparison of knowledge declared by English-speaking students with the significance of religion in their lives

ways. What differentiates their definitions is the significance of religion in their lives. In the case of students who declared that religion was (very) important to them, terms that were ethically saturated definitely outweighed the other terms, with the exception being 'legal and sensitive member of society', which is an extreme term that nobody chose. When religion was unimportant in student's life, less ethically saturated terms like 'genetic material', 'other' and to a lesser extent 'potential human being' were used. Knowledge may modify attitudes in the case of respondents who indicated the term 'surplus genetic material'. These respondents declared that their knowledge was derived from popular sources, and, at the same time, that religion was fairly important to them. In this situation, it is religion that determines the non-usefulness of SCs. In the case of respondents who did not have a definite attitude towards religion, terms indicating the usefulness of SCs prevailed over other terms.

In the case of the English-speaking students, one can observe a greater polarization of terms concerning the status of SCs: 50% of the terms were morally saturated, 38% were utilitarian and 12% were unspecified. In general, the proportions were similar to those among the Polish students. Nonetheless, contrary to their Polish peers, the English-speaking students did not select terms expressing a non-useful nature (e.g., 'surplus'), but, interestingly, 3% of them selected an extremely ethically saturated term (i.e., 'a legal and sensible member of society'). This 3% consisted of respondents who used non-scientific knowledge and, intriguingly, those for whom religion either did not matter at all or was quite meaningful. It may be possible to hypothesize that the significance of religion connects with the selection of ethically saturated terms, while usefulness saturation is connected with attaching less meaning to faith.

Although the results of this research indicate something about the respondents' religiousness, their sources of information and their perceptions of SCs, this study is only preliminary. The influence of scientific knowledge on students' views needs to be further analyzed, since it should be the basis of decisions made by scientists and workers in healthcare systems.

ORCID iDs

Agnieszka Żok <https://orcid.org/0000-0002-5560-5432>
 Jadwiga Wiertelwska-Bielarz <https://orcid.org/0000-0003-3655-2790>
 Ewa Baum <https://orcid.org/0000-0002-0503-0562>

References

- Centre for Public Opinion Research. Survey No. 3383: Values and norms in the lives of Poles [Wartości i normy w życiu Polaków]. Warszawa, Poland: CBOS; 2005.
- Centre for Public Opinion Research. Survey No. BS/100/2007: Opinions on organ transplantation [Opinie o przeszczepianiu narządów]. Warszawa, Poland: CBOS; 2007.
- Sample I. Gene mutation meant to protect from HIV 'raises risk of early death', *The Guardian*. June 3, 2019. <https://www.theguardian.com/science/2019/jun/03/gene-mutation-protect-hiv-raises-risk-early-death>. Accessed June 15, 2019.
- Cyranoski D. Japan approves first human-animal embryo experiments. <https://www.theguardian.com/science/2019/jun/03/gene-mutation-protect-hiv-raises-risk-early-death>. Accessed June 15, 2019.
- Olszewska-Stonina DM, Styczyński J, Drewa TA, Czajkowski R. Komórki niezróżnicowane – źródła i plastyczność. *Adv Clin Exp Med*. 2006; 15(3):497–503.
- Koźlik M, Wójcicki P. The use of stem cells in plastic and reconstructive surgery. *Adv Clin Exp Med*. 2014;23(6):1011–1017.
- Ledford H. Targeted stem cell attack could make transplanted safer. *Nature*. 2019;576(7785):18–19.
- Hazelbaker DZ, Beccard A, Angelini G, et al. A multiplexed gRNA piggyBac transposon system facilitates efficient induction of CRISPRi and CRISPRa in human pluripotent stem cells. *Sci Rep*. 2020;10(1):635. doi:10.1038/s41598-020-57500
- Ye J, Bates N, Soteriou D, et al. High quality clinical grade human embryonic stem cell lines derived from fresh discarded embryos. *Stem Cell Res Ther*. 2017;8(1):128. doi:10.1186/s13287-017-0561-y

10. Singer P, ed. *A Companion to Ethics*. Oxford, UK: Blackwell Publishing; 2016.
11. Meith D. Going to the roots of the stem cell debate. The ethical problems of using embryos for research. *EMBO Rep*. 2000;1(1):4–6.
12. Wickham H. *ggplot2: Elegant Graphics for Data Analysis*. New York, USA: Springer; 2016.
13. Babbie E. *The Practise of Social Research*. Boston, MA: Wadsworth Publishing; 2012.
14. Thomson JA, Itskovitz EJ, Shapiro SS, et al. Embryonic stem cell lines derived from human blastocysts. *Science*. 1998;282(5391):1145–1147.
15. Styczyński J. Przeszczepianie krwi pępowinowej. *Forum Pediatr Prakt*. 2018;13(2):49–55.
16. Haidt J, Kesebir S. Morality. In: Fiske S, Gilbert D, Lindzey G, eds. *Handbook of Social Psychology*. Hoboken, NJ: Wiley Blackwell; 2010:797–832.
17. Ellemers N, Toorn van der J, Paunov Y, Leeuwen van T. The psychology of morality: A review and analysis of empirical studies published from 1940 through 2017. *Pers Soc Psychol Rev*. 2019;23(4):332–366. doi:10.1177/1088868318811759
18. Ingarden R. *Książeczka o człowieku*. Kraków, Poland: Wydawnictwo Literackie; 2003.
19. Andersen Nawrot AM. *The Utopian Human Right to Science and Culture*. London, UK: Routledge; 2016.
20. Wojciszke B, Bazińska R, Jaworski M. On dominance of moral categories in impression formation. *Pers and Soc Psychol Bull*. 1998;24(12):1251–1263.
21. Hauser M. The liver and the moral organ. *Soc Cogn Affect Neurosci*. 2006;1(3):214–220. doi:10.1093/scan/nsl026
22. Churchland PS. A neurophilosophical slant on consciousness research. *Prog Brain Res*. 2005;149:285–293.
23. Churchland PS. The significance of neuroscience for philosophy. *Funct Neurol*. 2008;23(4):175–178.
24. Bloom P. *Against Empathy: The Case for Rational Compassion*. New York, USA: Ecco; 2016.
25. Bloom P. *Just Babies: The Origins of Good and Evil*. New York, USA: The Crown Publishing Group; 2013.
26. Haidt J. The emotional dog and its rational tail: A social intuitionist approach to moral judgment. *Psychol Rev*. 2001;108(4):814–834.
27. Damasio A. *The Strange Order of Things: Life, Feeling, and the Making of Cultures*. New York, USA: Pantheon; 2018.
28. Gazzaniga M. *Who's in Charge? Free Will and the Science of the Brain*. New York, USA: Ecco/HarperCollins; 2012.
29. Damasio H, Grabowski T, Frank R, Galaburda AM, Damasio AR. The return of Phineas Gage: Clues about the brain from the skull of a famous patient. *Science*. 1994;264(5162):1102–1105. doi:10.1126/science.8178168
30. Baum E, Musielak M. Approach of Polish medical students to ethical problems related to transplantation. *Arch Perinat Med*. 2008;14(3):51–53.

Cornelian cherry extract ameliorates osteoporosis associated with hypercholesterolemia in New Zealand rabbits

Beata Nowak^{1,A–F}, Agnieszka Matuszewska^{1,A–F}, Magdalena Tomanik^{2,B,C,E,F}, Jarosław Filipiak^{3,B,C,E,F}, Alicja Zofia Kucharska^{4,B,F}, Narcyz Piórecki^{5,B,F}, Diana Jędrzejuk^{6,C,F}, Krzysztof Zduniak^{7,B,C,E,F}, Małgorzata Trocha^{1,C,F}, Marek Bolanowski^{6,E,F}, Adam Szela^{1,E,F}, Tomasz Sozański^{1,A,B,E,F}

¹ Department of Pharmacology, Wrocław Medical University, Poland

² Student's Scientific Club, Faculty of Mechanical Engineering, Wrocław University of Science and Technology, Poland

³ Faculty of Mechanical Engineering, Wrocław University of Science and Technology, Poland

⁴ Department of Fruit, Vegetable and Plant Nutraceutical Technology, Wrocław University of Environmental and Life Sciences, Poland

⁵ Arboretum Bolestraszyce and Institute of Physiography, University of Rzeszów, Poland

⁶ Department of Endocrinology, Diabetes and Isotope Therapy, Wrocław Medical University, Poland

⁷ Department of Pathology, Wrocław Medical University, Poland

A – research concept and design; B – collection and/or assembly of data; C – data analysis and interpretation; D – writing the article; E – critical revision of the article; F – final approval of the article

Advances in Clinical and Experimental Medicine, ISSN 1899–5276 (print), ISSN 2451–2680 (online)

Adv Clin Exp Med. 2020;29(12):1389–1397

Address for correspondence

Beata Nowak
E-mail: beata.nowak@umed.wroc.pl

Funding sources

This work was supported by Wrocław Medical University, Poland (grant No. ST A080.17.035) and by National Science Centre, Poland, (grant No. 2016/21/B/NZ7/02759).

Conflict of interest

None declared

Received on March 27, 2020

Review on June 15, 2020

Accepted on September 20, 2020

Cite as

Nowak B, Matuszewska A, Tomanik M, et al. Cornelian cherry extract ameliorates osteoporosis associated with hypercholesterolemia in New Zealand rabbits. *Adv Clin Exp Med.* 2020;29(12):1389–1397. doi:10.17219/acem/127683

DOI

10.17219/acem/127683

Copyright

© 2020 by Wrocław Medical University

This is an article distributed under the terms of the Creative Commons Attribution 3.0 Unported (CC BY 3.0) (<https://creativecommons.org/licenses/by/3.0/>)

Abstract

Background. Results of animal studies show that a high-cholesterol diet increases bone resorption and decreases bone formation, thus leading to osteoporosis. Previously, we reported on the beneficial influence of Cornelian cherry (*Cornus mas* L.) fruit on lipid profile in an animal model of diet-induced hypercholesterolemia.

Objectives. To investigate the influence of *Cornus mas* L. extract and loganic acid (LA) on cholesterol-induced bone changes.

Material and methods. The study was conducted on 50 New Zealand rabbits. The animals were given either standard chow (group P) or the same standard chow enriched with 1% cholesterol (other groups). Additionally, the group CHOL+EX received *Cornus mas* L. extract, group CHOL+LA – loganic acid, and group CHOL+SIM – simvastatin. Serum concentration of bone turnover markers, bone mineral density (BMD) and bone micro-computed tomography (microCT) were assessed.

Results. In the CHOL group, a decrease in osteocalcin (OC) and an increase in C-terminated telopeptide of type I collagen (CTX) levels were detected (CHOL vs P 0.674 ± 0.159 ng/mL vs 1.003 ± 0.297 ng/mL and 10.049 ± 1.276 ng/mL vs 7.721 ± 1.187 ng/mL, respectively). The EX and LA ameliorated cholesterol-induced changes in serum OC (0.857 ± 0.160 ng/mL and 1.103 ± 0.356 ng/mL, respectively) and CTX (7.735 ± 1.045 ng/mL and 8.128 ± 1.106 ng/mL, respectively). There was a significant decrease in femoral BMD in CHOL group (0.429 ± 0.11 g/cm² vs 0.449 ± 0.020 g/cm²). The EX and LA ameliorated those changes (0.458 ± 0.016 g/cm² and 0.449 ± 0.021 g/cm², respectively). The microCT revealed increased bone volume ratio (BV/TV) and trabecular thickness (Tb.Th.) in the CHOL+EX group.

Conclusions. *Cornus mas* L. inhibited bone resorption and stimulated bone formation, thereby preventing the development of cholesterol-induced osteoporosis.

Key words: osteoporosis, cholesterol, bone mineral density, bone micro-computed tomography, *Cornus mas* L.

Introduction

Osteoporosis is a prevalent systemic bone disease characterized by loss of bone mass and deterioration of its microstructure. Reduced bone mass and disturbances in bone architecture associated with osteoporosis lead to increased risk of fragility fractures representing the main clinical consequence of osteoporosis. Fragility fractures are associated with significant pain and suffering of patients; they lead to disability and even increase the risk of premature death. Hip fragility fracture is the most common reason for elderly people to undergo emergency surgery, and up to 1/3 of those patients die within a year after the osteoporotic fracture.¹ Osteoporosis is associated with significant physical, psychosocial and financial consequences, and it is becoming a growing public health problem. In 2010 in the EU, 27.5 million people were estimated to have osteoporosis and 3.5 million new fragility fractures were diagnosed.²

As bone loss occurs with advancing age, the prevalence of the osteoporosis increases with age. Apart from aging and postmenopausal estrogen deficiency in female, there are many other factors that may accelerate or even induce osteoporosis development. Various drugs (e.g., corticosteroids, systemic antiviral, antacids, antiepileptics, and antithrombotic drugs)^{3–5} and chronic diseases (e.g., diabetes mellitus, hyperthyroidism, hypercortisolemia, hypogonadism, chronic inflammatory diseases, malabsorption etc.)⁶ may influence bone metabolism and lead to excessive loss of bone mass. In recent years, the link between lipid levels and osteoporosis has been described. Many observational studies investigated the association between dyslipidemia, cardiovascular disease and bone mineral density (BMD).^{7–9} Cardiovascular disease and osteoporosis seriously affect quality of life and mortality of middle-aged and elderly people and there is growing evidence that they may share common pathological mechanisms other than age.¹⁰ Zhang et al. found the significant correlation between BMD and arterial stiffness.¹¹ The inverse relationship between BMD and serum total cholesterol and low-density lipoprotein (LDL) level in postmenopausal women was described.¹² The association between serum triglyceride level and the risk of osteoporotic fractures has also been reported.¹³ The analysis by Lian et al. suggests that serum LDL and total cholesterol levels are major risk factors for senile osteoporosis.¹⁰ Some evidence suggests that hypercholesterolemia increases the risk of high-turnover osteoporosis.¹⁴ Results of animal studies show that a high cholesterol diet increases bone resorption and decreases bone formation, thus leading to decreased in BMD in rats.¹⁵ However, results of studies regarding the effect of lipid-lowering therapies on bone metabolism are ambiguous.¹⁶

The 2016 American College of Physicians (ACP) guidelines recommend bisphosphonates (alendronate, risedronate, zoledronate) or denosumab in the treatment of osteoporosis in men and women.¹⁷ Therapy with bisphosphonates and denosumab, although effective, may be associated with various side effects, such as gastrointestinal disturbances,

acute phase reaction, nephrotoxicity, atypical fractures, or osteonecrosis of jaw.¹⁸ Drug toxicity that may necessitate discontinuation of treatment may affect patient compliance. As plants are a rich sources of potentially bioactive substances and many of them have been a part of traditional folk medicine for ages, many researchers focus on herbal drugs that may be useful in osteoporosis therapy.^{19,20}

Cornus mas L. (*C. mas* L.) is a flowering plant cultivated for decorative purposes and as a source of fruits. Cornelian cherry fruit has been studied for various biological properties. There are reports about the beneficial influence of *C. mas* L. fruit on diabetes, different microbial infections, inflammation, and oxidative stress.²¹ Previously, we reported on beneficial influence of *C. mas* L. fruit on lipid profile in an animal model of diet-induced hypercholesterolemia²² and diet-induced atherosclerosis.^{23–26} The beneficial influence of *C. mas* L. fruit on lipid profile, glycemic indexes and leptin levels was also described by Gholamrezayi et al.²⁷ Taking into account the possible common pathogenesis of atherosclerosis and osteoporosis, and our previous results, we decided to investigate the influence of *C. mas* L. extract (EX) and loganic acid (LA), present in *C. mas* L. extract, on cholesterol-induced bone changes.

This study was specifically approved by the First Local Ethic Committee for Animal Experiments in Wrocław, Poland (2013 and 2014), and animal experiments were, therefore, performed in accordance with ethical standards laid down in the 1964 Declaration of Helsinki and its later amendments.

Material and methods

Chemicals and materials

Acetonitrile for liquid chromatography-mass spectrometry (LC-MS) was purchased from POCH (Gliwice, Poland). Acetonitrile (anhydrous, 99.8%), formic acid (reagent grade, ≥95%), acetic acid (≥99.7%), and methanol (≥99.9%) were purchased from Sigma-Aldrich (Steinheim, Germany). Loganic acid (≥99%), *p*-coumaric acid (≥90%), caffeic acid (≥99%), ellagic acid (≥95%), quercetin 3-*O*-glucoside (≥98.5%), kaempferol 3-*O*-glucoside (≥99%), and cyanidin 3-*O*-glucoside (≥90%) were purchased from Extrasynthese (Lyon, France). Morbital® (1 mL containing 133.3 mg of sodium pentobarbital and 26.7 mg of pentobarbital) was purchased from Biowet Puławy Sp. z o.o. (Poland).

Plant materials and samples preparation of extract and loganic acid

Cornelian cherry fruits were collected in the Arboretum Bolestraszyce and Institute of Physiography, Bolestraszyce, Poland. The plant material was verified by Jakub Dolatowski and the voucher specimen (BDPA 3967) has been deposited at the Arboretum Herbarium and Institute of Physiography in Bolestraszyce. The investigated extract

Table 1. Identification and the content (mg/100 g dw) of main compounds of extracts from Cornelian cherry fruits using UPLC-ESI-qTOF-MS/MS and HPLC-PDA

| Peak No. | t_R [min] | Compound | UV λ_{max} [nm] | $[M - H]^-/[M + H]^+$ [m/z] | Other ions [m/z] | Content [mg/100 g dw] |
|----------------|-------------|----------------------------------|-------------------------|-----------------------------|------------------|-----------------------|
| Iridoids | | | | | | |
| 1 | 4.9 | loganic acid | 246 | 375 (377+) | 213 (215+) | 10870.20 ±15.86 |
| 2 | 16.1 | cornuside | 245/273 | 541 (543+) | 169 (171+) | 1549.28 ±3.43 |
| total | | | | | | 12419.48 |
| Anthocyanins | | | | | | |
| 3 | 6.3 | delphinidin 3-O-galactoside | 524 | 463+ | 303+ | 44.06 ±1.77 |
| 4 | 7.6 | cyanidin 3-O-galactoside; | 515 | 449+ | 287+ | 809.70 ±0.55 |
| 5 | 8.3 | cyanidin 3-O-robinobioside | 516 | 595+ | 287+ | 369.94 ±1.41 |
| 6 | 8.8 | pelargonidin 3-O-galactoside | 501 | 433+ | 271+ | 1542.22 ±0.84 |
| 7 | 9.5 | pelargonidin 3-O-robinobioside | 501 | 579+ | 271+ | 297.18 ±0.44 |
| 8 | 12.6 | cyanidin | 523 | 287+ | – | 222.98 ±31.61 |
| 9 | 15.1 | pelargonidin | 509 | 271+ | – | 396.55 ±67.49 |
| total | | | | | | 3682.63 |
| Phenolic acids | | | | | | |
| 10 | 4.1 | caffeoyl hexoside | 326 | 341 | 179 | 120.28 ±3.00 |
| 11 | 4.6 | <i>p</i> -coumaroilquinic acid 1 | 316 | 337 | 163 | 33.91 ±1.40 |
| 12 | 5.8 | caffeoylquinic acid | 324 | 353 | 191 | 471.45 ±1.42 |
| 13 | 7.9 | <i>p</i> -coumaric acid | 309 | 163 | – | 12.40 ±0.21 |
| 14 | 8.3 | <i>p</i> -coumaroilquinic acid 2 | 313 | 337 | 191/163 | 279.91 ±3.50 |
| 15 | 10.0 | <i>p</i> -coumaroilquinic acid 3 | 312 | 337 | 191/163 | 20.91 ±1.88 |
| 16 | 12.3 | ellagic acid | 254/362 | 301 | – | 124.21 ±1.64 |
| total | | | | | | 1063.07 |
| Flavonols | | | | | | |
| 17 | 13.2 | quercetin 3-O-glucuronide | 354 | 477 | 301 | 306.28 ±22.62 |
| 18 | 13.7 | quercetin 3-O-glucoside | 353 | 463 | 301 | 31.64 ±1.58 |
| 19 | 14.8 | kaempferol 3-O-galactoside | 348 | 447 | 285 | 215.45 ±2.61 |
| 20 | 15.6 | kaempferol 3-O-glucuronide | 351 | 461 | 285 | 35.94 ±1.38 |
| total | | | | | | 589.30 |

(EX) was prepared from *C. mas* L. fruits by the Department of Fruit, Vegetable and Plant Nutraceutical Technology at Wrocław University of Environmental and Life Sciences according to the method described by Kucharska et al.²⁸ and Sozański et al.²⁹ The extract of iridoids and phenolic compounds (EX) was obtained after purification on XAD-16 Amberlite resin (Rohm and Haas, Chauny, France) in a column, concentration using a Rotavapor (Unipan, Warszawa, Poland), and lyophilization (Alpha 1–4 LSC; Martin Christ Gefriertrocknungsanlagen GmbH, Osterode am Harz, Germany).²⁸ The extract was qualitatively and quantitatively characterized using LC-MS and high-performance liquid chromatography (HPLC) (Table 1).

Identification of compounds by UPLC-ESI-qTOF-MS/MS

Compounds were identified with the method described by Kucharska et al.,³⁰ using the Acquity ultra-performance liquid chromatography (UPLC) system coupled with

a quadrupole time of flight (q-TOF) MS instrument (Waters Corp., Milford, USA), with an electrospray ionization (ESI) source. Separation was achieved with an Acquity BEH C18 column (100 mm × 2.1 mm i.d., 1.7 µm; Waters). The mobile phase was a mixture of 2.0% aq. formic acid v/v (solvent A) and acetonitrile with formic acid (solvent B). The instrument was operated both in the positive (iridoids and anthocyanins) and the negative (iridoids, phenolic acids, flavonols, and anthocyanins) ion mode, scanning m/z from 100 to 1500.

Quantification of compounds by HPLC-PDA

Iridoids and anthocyanins were assayed using the method described by Kucharska et al.³⁰ with a Dionex HPLC Ultimate 3000 system (Germering, Germany) equipped with the diode array detector. The Cadenza Imtakt (Portland, USA) column C5-C18 (75 × 4.6 mm, 5 µm) was used. The mobile phase was composed of solvents: A (4.5% aq. formic acid, v/v) and B (acetonitrile with formic acid),

as described by Kucharska et al.³⁰ Runs were monitored at wavelengths of 245 nm (iridoids), 254 nm (ellagic acid), 320 nm (phenolic acids), 360 nm (flavonols), and 520 nm (anthocyanins). Peaks corresponding to standards were quantified, and iridoid was quantified as LA, anthocyanins as cyanidin 3-*O*-glucoside, phenolic acid as *p*-coumaric acid, caffeic acid and ellagic acid, and flavonols as quercetin 3-*O*-glucoside and kaempferol 3-*O*-glucoside.

Animal model and protocol

The study was conducted on 50 male sexually mature New Zealand rabbits, aged 8–12 months and weighing 4.5–5.5 kg. The animals were housed in individual chambers with temperature maintained at 21–23°C on a regular 12 h light/dark cycle. During the experiment the animals had water ad libitum and received the same daily portion of chow (40 g/kg). The animals were acclimated for 3 weeks prior to being used in the sixty-day study. After acclimatization, the animals were randomly divided into 5 groups (NT, CHOL, CHOL+EX, CHOL+LA, and CHOL+SIM) of 10 animals each. For 60 consecutive days of the experiment, the animals were given either standard chow (group NT) or the same standard chow enriched with 1% cholesterol (groups CHOL, CHOL+EX, CHOL+LA, and CHOL+SIM). Once daily, in the morning, the following test substances were administered orally to the rabbits: group NT and CHOL – normal saline solution, group CHOL+EX – *C. mas* L. extract, group CHOL+LA – loganic acid, and group CHOL+SIM – simvastatin (Table 2).

On day 60, blood samples were collected from each animal from the margin vein of the ear or the saphenous vein. Serum was separated using centrifugation (at 1500 × g) and then stored at 70°C until required for bone metabolic marker assays.

On day 60, the animals were euthanized with terminal anesthesia, using Morbital® (Biovet, Puławy, Poland; 1 mL containing 133.3 mg of sodium pentobarbital and 26.7 mg of pentobarbital) at a dose of 2 mL/kg given intraperitoneally (i.p.). The femur and tibia were cleaned off all soft tissues and carefully separated. Left femurs were fixed in buffered formaldehyde for further histological examination. Right femurs and tibias were frozen and stored at the temperature of –70°C for further examination (dual-energy X-ray absorptiometry (DXA) and micro-computed tomography (microCT)).

Table 2. Experimental groups

| Group | Chow | Tested substance | Dose of tested substance |
|----------|--------------------------------|--------------------------|--------------------------|
| P | standard chow | none | none |
| CHOL | standard chow + 1% cholesterol | none | none |
| CHOL+EX | standard chow + 1% cholesterol | Cornelian cherry extract | 50 mg/kg |
| CHOL+LA | standard chow + 1% cholesterol | loganic acid | 20 mg/kg |
| CHOL+SIM | standard chow + 1% cholesterol | simvastatin | 5 mg/kg |

P – placebo; CHOL – cholesterol; EX – *C. mas* L. extract; LA – loganic acid; SIM – simvastatin.

Measurement of relevant serum parameters

Serum total calcium and inorganic phosphorus were measured with Architect plus ci4100 (Abbott, Chicago, USA) using commercial tests (Calcium Architect/Aeroset REF 3L79-21 and 3L79-31 304328/R1, Abbott; Phosphorus Architect REF 7D71 305532/R02, Abbott).

Serum osteocalcin (OC) and C-terminated telopeptide of type I collagen (CTX) levels (sensitive biochemical markers of bone formation and bone resorption, respectively) were determined using commercial OC (Rabbit Osteocalcin (OC) ELISA Kit, Wuhan USCN Cloud-Clone Corp, Wuhan, China) and CTX (Rabbit CTXI (Cross Linked C-telopeptide of Type I Collagen) ELISA Kit, Fine Test, Wuhan Fine Biotech Corp, Wuhan, China) enzyme-linked immunosorbent assay (ELISA) kits. All ELISA tests were performed according to their manufacturers' instructions.

Determination of bone mineral density

Bone mineral density of the right femoral bones was measured by trained examiners using DXA with Hologic DXA equipment (Hologic Discovery W 81507; Hologic, Mississauga, Canada) using software for small animals. The results were obtained as grams of mineral content per square centimeter of bone area (g/cm²). The scanner was calibrated daily using a phantom provided by the manufacturer.

MicroCT evaluation of the bone structure

In order to evaluate the bone structure from each group, 5 randomly selected tibias (n = 25) were scanned with high-resolution microCT (SkyScan 1172; Bruker®, Billerica, USA). For acquiring the images with 9.0-μm pixel size, the X-ray tube was set at 95 kV and 104 μA, along with a copper-aluminium (CuAl) filter. For the quantitative evaluation, only the distal part of the tibia was taken under consideration. After the reconstruction process, a set of 2D cross-sections representing the bone structure of the specimens was obtained.

Prior to the 3D morphometric analyses, the images were aligned with the bone major axis and the set of trabecular and cortical volumes of interests (VOIs) were selected,

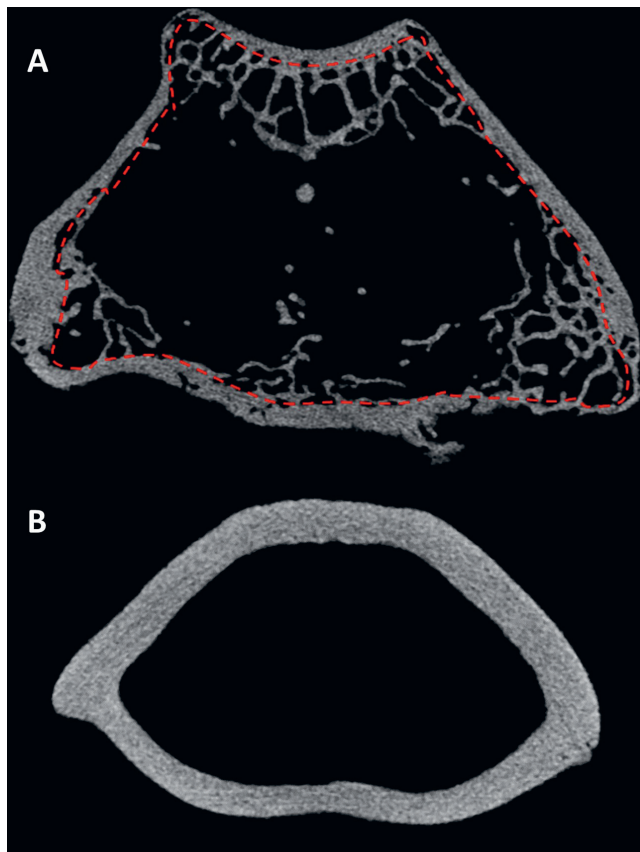


Fig. 1. The representative microCT cross sections of (A) the trabecular region (within the red line) and (B) cortical region

with reference to the growth plate. The selection of both regions of interest (trabecular and cortical) was based on the commonly accepted procedure used for small animals.^{31,32} Within each VOI, the automatic selection of a specific bone (Fig. 1) was applied; then, the images were segmented, using an adaptive global threshold algorithm. Quantitate analysis (CTAnn; Bruker®) of the cancellous bone structure took into account bone volume ratio (BV/TV), bone surface ratio (BS/BV) trabecular thickness (Tb.Th), number (Tb.N) and pattern (Tb.Pf), as well as structural model index (SMI). Apart from the basic parameters (BV/TV and BV/BS), the cortical thickness (Cr.Th) was calculated for the cortical bone. Furthermore, to complete

the densitometric analysis for the cortical bone datasets, X-ray absorption, defined as the attenuation coefficient (AC [mm⁻¹]) determining both by mass density and elemental composition of the material, was calculated.

Thickness of femoral cortical bone

Left femoral bones were fixed in 10% neutral-buffered formaldehyde and were then decalcified in 5% formic acid and 5.6% hydrochloric acid solution for 14 days. Next, the bones were embedded in paraffin and fixed, and 4-μm histological sections, stained with hematoxylin and eosin (H&E), were subsequently prepared. Histological slides were scanned with the NanoZoomer v. 2.0 (Hamamatsu Photonics K.K., Hamamatsu, Japan). The thickness of the cortical bone was measured 40 mm from the distal metaphysis of the femur.

Statistical analysis

Parametric data was expressed as means ± standard deviation (SD). The statistical analysis was carried out using STATISTICA v. 13 (StatSoft, Inc., Tulsa, USA). The normality of all continuous variables was verified with the Shapiro–Wilk test. One-way analysis of variance (ANOVA) with least significant difference (LSD) Fisher’s post hoc test was performed for a comparison involving 3 or more groups. The limit of significance was set at $p < 0.05$.

Results

Serum concentration of bone turnover markers

Serum total calcium and inorganic phosphorus levels, and serum concentration of OC and CTX are presented in Table 3. A decrease in serum calcium was detected in animals fed with a cholesterol-rich diet and receiving *C. mas* L. deviates or simvastatin. Inorganic phosphorus levels were increased only in animals fed with a cholesterol-rich diet and receiving *C. mas* L. extract and LA ameliorated cholesterol-induced

Table 3. Selected serum parameters measured on day 60

| Parameter [unit] | Experimental groups | | | | |
|-------------------------------|---------------------|-------------------|----------------------|------------------|-------------------|
| | P (n = 10) | CHOL (n = 10) | CHOL+EX (n = 10) | CHOL+LA (n = 10) | CHOL+SIM (n = 10) |
| Total calcium [mmol/L] | 3.547 ± 0.193 | 3.394 ± 0.148 | 3.283 ± 0.224** | 3.380 ± 0.126* | 3.348 ± 0.152* |
| Inorganic phosphorus [mmol/L] | 1.489 ± 0.183 | 1.935 ± 0.569 | 4.428 ± 1.259***,### | 2.731 ± 1.210## | 1.452 ± 0.201 |
| OC [ng/mL] | 1.003 ± 0.297** | 0.674 ± 0.159## | 0.857 ± 0.160 | 1.103 ± 0.356* | 0.722 ± 0.190# |
| CTX [ng/mL] | 7.721 ± 1.187*** | 10.049 ± 1.276### | 7.735 ± 1.045*** | 8.128 ± 1.106*** | 7.252 ± 1.064*** |

P – placebo; OC – osteocalcin; CTX – C-termined telopeptide of type I collagen; * $p < 0.05$; ** $p < 0.01$; *** $p < 0.001$ compared to CHOL; # $p < 0.05$; ## $p < 0.01$; ### $p < 0.001$ compared to P.

decrease in OC concentration, whereas in the simvastatin group OC level remained lower than in the placebo group. We observed normalization of cholesterol-induced increase in CTX level in animals receiving *C. mas* L. extract, LA and simvastatin.

Bone mineral density

Femoral BMD is presented in Fig. 2. There is a significant decrease in femoral BMD in the CHOL group in comparison to the not-treated (NT) one ($0.429 \pm 0.11 \text{ g/cm}^2$ vs $0.449 \pm 0.020 \text{ g/cm}^2$, $p = 0.033$). The *C. mas* L. extract and LA ameliorate cholesterol-induced changes in BMD ($0.458 \pm 0.016 \text{ g/cm}^2$, $p = 0.004$ and $0.449 \pm 0.021 \text{ g/cm}^2$, $p = 0.039$, respectively). There was no difference between CHOL and CHOL+SIM group ($0.422 \pm 0.021 \text{ g/cm}^2$).

Histopathological examination

A histopathological examination revealed no significant difference in the thickness of the femoral cortical bone between groups (NT: $0.910 \pm 0.056 \text{ mm}$, CHOL: $0.872 \pm 0.092 \text{ mm}$, CHOL+EX: $0.895 \pm 0.055 \text{ mm}$, CHOL+LA: $0.887 \pm 0.076 \text{ mm}$ and CHOL+SIM: $0.878 \pm 0.086 \text{ mm}$).

MicroCT morphometry

Microstructural cancellous and cortical bone parameters are presented in Table 4, and examples of cross-sections in 3 orthogonal planes are shown in Fig. 3. In the CHOL-EX group, the bone volume ratio was 29% higher than in the CHOL group. Such an increase was not detected in the CHOL+SIM group. Apart from this, bone

trabeculae were 14% thicker in the CHOL+EX group than in animals receiving simvastatin. We detected no influence of investigated substances on cortical bone.

Discussion

Osteoporosis is characterized by the imbalance between osteoblast and osteoclast activity, leading to bone loss and disturbances in its microarchitecture. Hypercholesterolemia seems to be a possible triggering factor that may affect homeostasis between bone formation and bone resorption, thus leading to osteoporosis. You et al. reported increased serum CTX level with decreased serum OC level in rats fed with cholesterol-rich diet.¹⁵ In cholesterol-fed rats, they observed inhibition of proliferation and differentiation of osteoblasts and decreased BMP2 (bone morphogenic protein 2) expression, leading to decreased bone formation. In the conducted study, we also noticed an increase in serum CTX level and a decrease in serum OC level in animals fed with cholesterol-rich diet, which is a sign of increased bone resorption and decreased bone formation. In our study, changes in concentrations of bone turnover markers were associated with decreased femoral BMD, as reported by You et al.¹⁵ These changes are similar to those observed in postmenopausal osteoporosis and in ovariectomy-induced osteoporosis in animal models.^{33,34} The *C. mas* L. extract (50 mg/kg), LA (20 mg/kg) and simvastatin (5 mg/kg) given simultaneously with cholesterol-rich diet prevented the increase in CTX level, which is evidence of their anti-resorptive activity. In the CHOL+EX and CHOL+LA group, we detected no decrease in OC levels, which suggest that they may stimulate bone formation. The beneficial effect

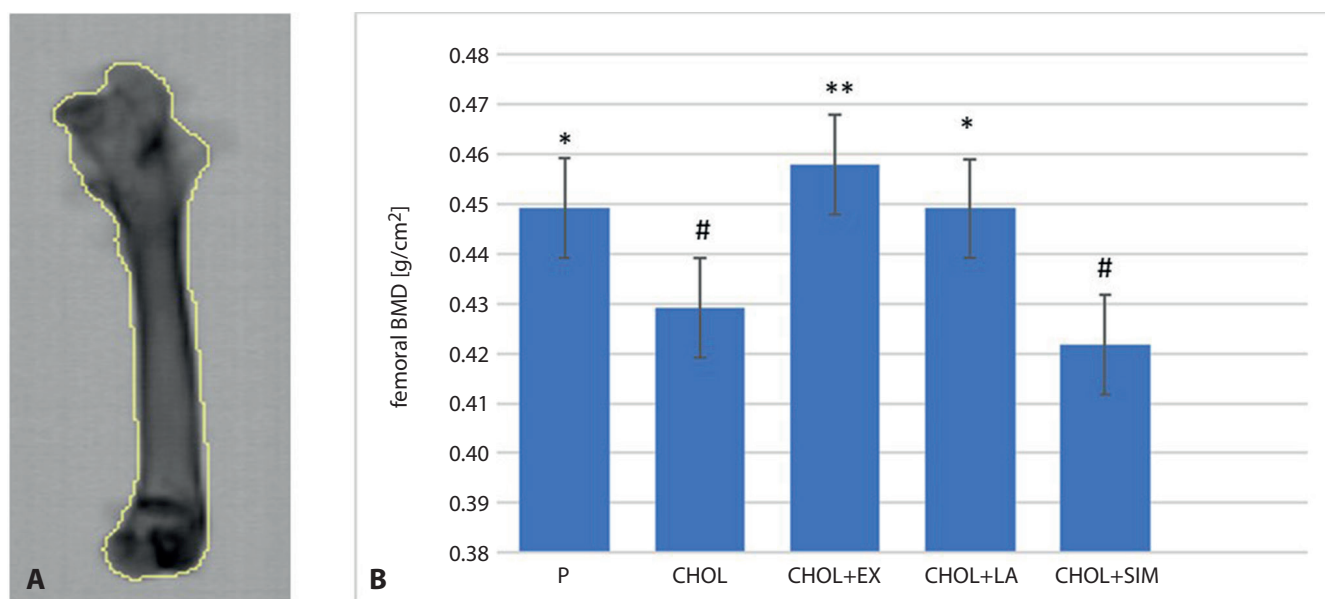


Fig. 2. Femoral BMD examination

A – DXA scan of right femur; B – femoral BMD in experimental groups (P – placebo; CHOL – 1% cholesterol; CHOL+EX – 1% cholesterol + Cornelian cherry extract 50 mg/kg; CHOL+LA – 1% cholesterol + LA 20 mg/kg; CHOL+SIM – 1% cholesterol + simvastatin 5 mg/kg); * $p < 0.05$; ** $p < 0.01$ vs CHOL; # $p < 0.05$ vs P.

Table 4. Microstructural parameters obtained for cancellous and cortical bone of distal tibia metaphysis, microCT evaluation. Results presented as: mean ±SD. Experimental groups: P – placebo, CHOL – 1% cholesterol, CHOL+EX – 1% cholesterol + Cornelian cherry extract 50 mg/kg, CHOL+LA – 1% cholesterol + loganic acid 20 mg/kg, CHOL+SIM – 1% cholesterol + simvastatin 5 mg/kg

| Parameter [units] | Experimental groups | | | | |
|-------------------|--------------------------|----------------------------|-----------------------------|----------------------------|-----------------------------|
| | P (n = 5) | CHOL (n = 5) | CHOL+EX (n = 5) | CHOL+LA (n = 5) | CHOL+SIM (n = 5) |
| Cancellous bone | | | | | |
| BV/TV (%) | 9.53 ±0.72 | 9.37 ±1.94 | 12.11 ±3.30 ^{#**°} | 10.11 ±2.18 | 9.09 ±3.81 |
| BS/BV [1/U] | 25.11 ±2.55 [°] | 24.51 ±1.99 ^{°°} | 23.55 ±1.26 ^{°°°} | 23.59 ±1.45 ^{°°°} | 27.28 ±2.31 ^{#,**} |
| Tb.Th. [mm] | 0.162 ±0.021 | 0.157 ±0.014 | 0.173 ±0.014 [°] | 0.166 ±0.013 | 0.152 ±0.007 |
| Tb.N. [1/mm] | 0.594 ±0.073 | 0.600 ±0.137 | 0.708 ±0.222 | 0.609 ±0.118 | 0.597 ±0.219 |
| Tb.Pf. [ratio] | 7.611 ±1.277 | 6.858 ±1.255 ^{°°} | 7.525 ±0.852 | 6.775 ±0.599 ^{°°} | 8.634 ±1.777 ^{**} |
| SMI [1] | 1.812 ±0.190 | 1.680 ±0.273 | 1.922 ±0.244 | 1.726 ±0.160 | 1.900 ±0.274 |
| Cortical bone | | | | | |
| BV/TV (%) | 34.77 ±1.97 | 34.10 ±5.49 | 37.58 ±2.57 | 36.01 ±2.38 | 33.92 ±4.39 |
| BS/BV [1/U] | 3.88 ±0.22 | 4.17 ±0.98 | 4.15 ±1.04 | 3.89 ±0.39 | 4.44 ±0.84 |
| Cr.Th. [mm] | 0.837 ±0.048 | 0.825 ±0.137 | 0.831 ±0.144 | 0.855 ±0.058 | 0.763 ±0.087 |
| AC [1/mm] | 0.0253 ±0.0012 | 0.0256 ±0.0011 | 0.0267 ±0.0011 | 0.0266 ±0.0007 | 0.0268 ±0.0013 [#] |

microCT – micro-computed tomography; P – placebo; BV/TV – bone volume ratio; BS/BV – bone surface ratio; Tb.Th. – trabecular thickness; Tb.N. – trabecular number; Tb.Pf. – trabecular pattern; SMI – structural model index; Cr.Th. – cortical thickness; AC – attenuation coefficient; * p < 0.05; ** p < 0.01 compared to CHOL; # p < 0.05 compared to P; ° p < 0.05; °° p < 0.01; °°° p < 0.001 compared to CHOL + SIM.

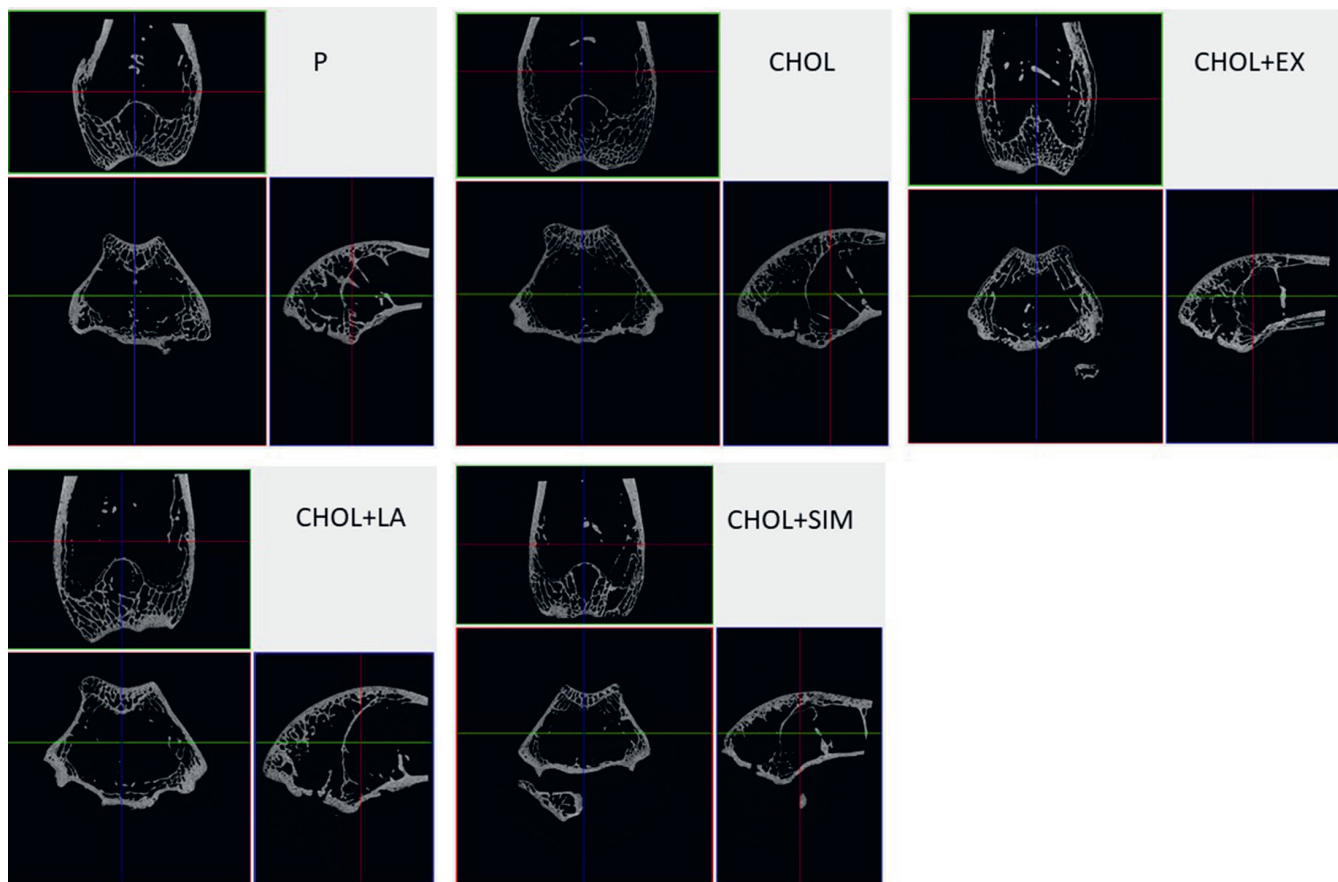


Fig. 3. MicroCT scans of tibias in experimental groups

P – placebo; CHOL – 1% cholesterol; CHOL+EX – 1% cholesterol + Cornelian cherry extract 50 mg/kg; CHOL+LA – 1% cholesterol + LA 20 mg/kg; CHOL+SIM – 1% cholesterol + simvastatin 5 mg/kg

of simvastatin on bone metabolism was described by some authors. Simvastatin local delivery and high systemic doses had a beneficial effect on fractures healing.³⁵ Simvastatin was reported to alleviate bone resorption and bone loss.^{36,37} Some authors also described its beneficial effect on bone formation,³⁸ but we did not observe such an effect in our study.

The difference in the calcium level between the CHOL group and the animals receiving additionally Cornelian cherry derivatives or simvastatin may be attributed to the anti-resorptive properties of Cornelian cherry extract, LA and simvastatin. The inhibition of bone resorption decreases the mobilization of calcium from bone tissue, and as a consequence lower serum calcium level is observed. The increased level of inorganic phosphorus in the CHOL+EX and CHOL+LA groups needs further explanation.











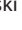

In CHOL+EX and CHOL+LA groups, we did not observe cholesterol-induced bone loss. Simvastatin did not exert a protective effect on femoral BMD. Shahrezaee et al. reported an increase in BMD in ovariectomized rats treated with simvastatin.³⁹ However, the discrepancy with our study may be a consequence of the fact that Shahrezaee et al. investigated higher doses of simvastatin (25 mg/kg) and used a different animal model. Shahrezaee et al. investigated the influence of simvastatin on estrogen-deficiency-induced osteoporosis and they used a classical animal model for such a condition. However, ovariectomy does not induce lipid changes in rats, so it does not allow us to predict the influence of simvastatin on cholesterol-induced bone changes. As we planned to concentrate on atherosclerosis-associated bone changes, we used cholesterol-fed rabbit model, which is a standard model used in animal studies on atherosclerosis.⁴⁰ In the CHOL+EX group, femoral BMD was even higher than in the placebo group, which supports the hypothesis that Cornelian cherry extract may induce new bone formation. *Cornus mas* L. extract seems to have a beneficial influence on cancellous bone, as in the CHOL+EX group we found an increase in bone volume ratio (BV/TV). Apart from that, the trabeculae were thicker in animals receiving Cornelian cherry extract than in rabbits receiving simvastatin.

As Cornelian cherry extract exerted effects that were not observed in simvastatin-treated animals, we suspect that these effects may not be limited to its lipid lowering properties.

Conclusions

To our knowledge, this is the first in vivo study investigating the influence of *C. mas* L. on the disturbances of bone metabolism and structure. Our study revealed the beneficial influence of *C. mas* L. and LA on cholesterol-induced osteopenia in rabbits. However, further research is needed to establish the mechanism of the observed effects, and to investigate the influence of Cornelian cherry on other forms of osteoporosis.

ORCID iDs

Beata Nowak  <https://orcid.org/0000-0003-0014-6344>
 Agnieszka Matuszewska  <https://orcid.org/0000-0003-1082-0793>
 Magdalena Tomanik  <https://orcid.org/0000-0002-7249-6266>
 Jarosław Filipiak  <https://orcid.org/0000-0002-9380-0642>
 Alicja Zofia Kucharska  <https://orcid.org/0000-0002-2172-0408>
 Narcyz Piórecki  <https://orcid.org/0000-0002-0256-5510>
 Diana Jędrzejuk  <https://orcid.org/0000-0001-7053-142X>
 Krzysztof Zduniak  <https://orcid.org/0000-0003-4652-4478>
 Małgorzata Trocha  <https://orcid.org/0000-0002-3951-205X>
 Marek Bolański  <https://orcid.org/0000-0002-2360-6596>
 Adam Szeląg  <https://orcid.org/0000-0001-8104-5267>
 Tomasz Sozański  <https://orcid.org/0000-0003-1722-3190>

References

- Johansen A, Tsang C, Boulton C, Wakeman R, Moppett I. Understanding mortality rates after hip fracture repair using ASA physical status in the National Hip Fracture Database. *Anaesthesia*. 2017;72(8):961–966. doi:10.1111/anae.13908
- Hernlund E, Svedbom A, Ivergård M, et al. Osteoporosis in the European Union: Medical management, epidemiology and economic burden. *Arch Osteoporos*. 2013;8(1–2):136. doi:10.1007/s11657-013-0136-1
- Panday K, Gona A, Humphrey MB. Medication-induced osteoporosis: Screening and treatment strategies. *Ther Adv Musculoskelet Dis*. 2014;6(5):185–202. doi:10.1177/1759720X14546350
- Matuszewska A, Nowak B, Rzeszutko M, et al. Effects of long-term administration of pantoprazole on bone mineral density in young male rats. *Pharmacol Reports*. 2016 68(5):1060–1064. doi:10.1016/j.pharep.2016.06.012
- Nowak B, Matuszewska A, Filipiak J, et al. The influence of bexarotene, a selective agonist of the retinoid receptor X (RXR), and tazarotene, a selective agonist of the retinoid acid receptor (RAR), on bone metabolism in rats. *Adv Med Sci*. 2016;61(1):85–89. doi:10.1016/j.advms.2015.09.001
- Sheu A, Diamond T. Secondary osteoporosis. *Aust Prescr*. 2016;39(3):85–87. doi:10.18773/austprescr.2016.038
- Bagger YZ, Rasmussen HB, Alexandersen P, et al. Links between cardiovascular disease and osteoporosis in postmenopausal women: Serum lipids or atherosclerosis per se? *Osteoporos Int*. 2007;18(4):505–512. doi:10.1007/s00198-006-0255-2
- Ackert-Bicknell CL. HDL cholesterol and bone mineral density: Is there a genetic link? *Bone*. 2012;50(2):525–533. doi:10.1016/j.bone.2011.07.002
- Hu X, Ma S, Yang C, Wang W, Chen L. Relationship between senile osteoporosis and cardiovascular and cerebrovascular diseases. *Exp Ther Med*. 2019;17(6):4417–4420. doi:10.3892/etm.2019.7518
- Lian XL, Zhang YP, Li X, Jing LD, Cairang ZM, Gou JQ. Exploration on the relationship between the elderly osteoporosis and cardiovascular disease risk factors. *Eur Rev Med Pharmacol Sci*. 2017;21(19):4386–4390.
- Zhang M, Bai L, Kang J, Ge J, Peng W. Links between arterial stiffness and bone mineral density in middle-aged and elderly Chinese individuals: A cross-sectional study. *BMJ Open*. 2019;9(8):e029946. doi:10.1136/bmjopen-2019-029946
- Makovey J, Chen JS, Hayward C, Williams FMK, Sambrook PN. Association between serum cholesterol and bone mineral density. *Bone*. 2009;44(2):208–213. doi:10.1016/j.bone.2008.09.020
- Wang Y, Dai J, Zhong W, Hu C, Lu S, Chai Y. Association between serum cholesterol level and osteoporotic fractures. *Front Endocrinol (Lausanne)*. 2018;9:30. doi:10.3389/fendo.2018.00030
- Zhou Y, Deng T, Zhang H, et al. Hypercholesterolaemia increases the risk of high-turnover osteoporosis in men. *Mol Med Rep*. 2019; 19(6):4603–4612. doi:10.3892/mmr.2019.10131
- You L, Sheng Z, Tang C, Chen L, Pan L, Chen J. High cholesterol diet increases osteoporosis risk via inhibiting bone formation in rats. *Acta Pharmacol Sin*. 2011;32(12):1498–1504. doi:10.1038/aps.2011.135
- An T, Hao J, Sun S, et al. Efficacy of statins for osteoporosis: A systematic review and meta-analysis. *Osteoporos Int*. 2017;28(1):47–57. doi:10.1007/s00198-016-3844-8
- Qaseem A, Forciea MA, McLean RM, Denberg TD; Clinical Guidelines Committee of the American College of Physicians. Treatment of low bone density or osteoporosis to prevent fractures in men and women: A clinical practice guideline update from the American College of Physicians. *Ann Intern Med*. 2017;166(11):818. doi:10.7326/M15-1361

18. Yang YL, Xiang ZJ, Yang JH, Wang WJ, Xiang RL. The incidence and relative risk of adverse events in patients treated with bisphosphonate therapy for breast cancer: A systematic review and meta-analysis. *Ther Adv Med Oncol*. 2019;11:1758835919855235. doi:10.1177/1758835919855235
19. Gupta T, Das N, Imran S. The prevention and therapy of osteoporosis: A review on emerging trends from hormonal therapy to synthetic drugs to plant-based bioactives. *J Diet Suppl*. 2019;16(6):699–713. doi:10.1080/19390211.2018.1472715
20. He J, Li X, Wang Z, et al. Therapeutic anabolic and anticatabolic benefits of natural Chinese medicines for the treatment of osteoporosis. *Front Pharmacol*. 2019;10:1344. doi:10.3389/fphar.2019.01344
21. Tiptiri-Kourpeti A, Fitsiou E, Spyridopoulou K, et al. Evaluation of antioxidant and antiproliferative properties of *Cornus mas* L. fruit juice. *Antioxidants (Basel)*. 2019;8(9):377. doi:10.3390/antiox8090377
22. Sozański T, Kucharska AZ, Szumny A, et al. The protective effect of the *Cornus mas* fruits (cornelian cherry) on hypertriglyceridemia and atherosclerosis through PPAR α activation in hypercholesterolemic rabbits. *Phytomedicine*. 2014;21(13):1774–1784. doi:10.1016/j.phymed.2014.09.005
23. Sozański T, Kucharska AZ, Rapak A, et al. Iridoid–loganic acid versus anthocyanins from the *Cornus mas* fruits (cornelian cherry): Common and different effects on diet-induced atherosclerosis, PPARs expression and inflammation. *Atherosclerosis*. 2016;254:151–160. doi:10.1016/j.atherosclerosis.2016.10.001
24. Sozański T, Kucharska AZ, Szumny D, et al. Cornelian cherry consumption increases the L-arginine/ADMA ratio, lowers ADMA and SDMA levels in the plasma, and enhances the aorta glutathione level in rabbits fed a high-cholesterol diet. *J Funct Foods*. 2017;34:189–196. doi:10.1016/j.jff.2017.04.028
25. Sozański T, Kucharska AZ, Wiśniewski J, et al. The iridoid loganic acid and anthocyanins from the cornelian cherry (*Cornus mas* L.) fruit increase the plasma L-arginine/ADMA ratio and decrease levels of ADMA in rabbits fed a high-cholesterol diet. *Phytomedicine*. 2019;52:1–11. doi:10.1016/j.phymed.2018.09.175
26. Sozański T, Kucharska AZ, Szumny A, et al. The protective effect of the *Cornus mas* fruits (cornelian cherry) on hypertriglyceridemia and atherosclerosis through PPAR α activation in hypercholesterolemic rabbits. *Phytomedicine*. 2014;21(13):1774–1784.
27. Gholamrezayi A, Aryaeian N, Rimaz S, et al. The effect of *Cornus mas* fruit extract consumption on lipid profile, glycemic indices, and leptin in postmenopausal women: A randomized clinical trial. *Phyther Res*. 2019;33(11):2979–2988. doi:10.1002/ptr.6476
28. Kucharska AZ, Szumny A, Sokół-Letowska A, Piórecki N, Klymenko SV. Iridoids and anthocyanins in cornelian cherry (*Cornus mas* L.) cultivars. *J Food Compos Anal*. 2015;40:95–102. doi:10.1016/j.jfca.2014.12.016
29. Sozański T, Kucharska AZ, Wiśniewski J, et al. The iridoid loganic acid and anthocyanins from the cornelian cherry (*Cornus mas* L.) fruit increase the plasma L-arginine/ADMA ratio and decrease levels of ADMA in rabbits fed a high-cholesterol diet. *Phytomedicine*. 2019;52:1–11. doi:10.1016/j.phymed.2018.09.175
30. Kucharska A, Sokół-Letowska A, Oszmiański J, Piórecki N, Fecka I. Iridoids, phenolic compounds and antioxidant activity of edible honeysuckle berries (*Lonicera caerulea* var. *kamtschatica* Sevest). *Molecules*. 2017;22(3):405. doi:10.3390/molecules22030405
31. Campbell GM, Sophocleous A. Quantitative analysis of bone and soft tissue by micro-computed tomography: Applications to ex vivo and in vivo studies. *Bonekey Rep*. 2014;3:564. doi:10.1038/bonekey.2014.59
32. Verdels K, Lukashova L, Atti E, et al. MicroCT morphometry analysis of mouse cancellous bone: Intra- and inter-system reproducibility. *Bone*. 2011;49(3):580–589. doi:10.1038/jid.2014.371
33. Nowak B, Matuszewska A, Szandrak M, et al. Effect of long-term administration of mangiferin from *Belamcanda chinensis* on bone metabolism in ovariectomized rats. *J Funct Foods*. 2018;46:12–18. doi:10.1016/j.jff.2018.04.048
34. Komori T. Animal models for osteoporosis. *Eur J Pharmacol*. 2015;759:287–294. doi:10.1016/j.ejphar.2015.03.028
35. Moshiri A, Sharifi AM, Oryan A. Role of simvastatin on fracture healing and osteoporosis: A systematic review on in vivo investigations. *Clin Exp Pharmacol Physiol*. 2016;43(7):659–684. doi:10.1111/1440-1681.12577
36. Kim AR, Kim J-H, Kim A, et al. Simvastatin attenuates tibial bone loss in rats with type 1 diabetes and periodontitis. *J Transl Med*. 2018;16. doi:10.1186/S12967-018-1681-6
37. Yang CN, Kok SH, Wang HW, et al. Simvastatin alleviates bone resorption in apical periodontitis possibly by inhibition of mitophagy-related osteoblast apoptosis. *Int Endod J*. 2019;52(5):676–688. doi:10.1111/iej.13055
38. Oryan A, Kamali A, Moshiri A. Potential mechanisms and applications of statins on osteogenesis: Current modalities, conflicts and future directions. *J Control Release*. 2015;215:12–24. doi:10.1016/j.jconrel.2015.07.022
39. Shahrezaee M, Oryan A, Bastami F, Hosseinpour S, Shahrezaee MH, Kamali A. Comparative impact of systemic delivery of atorvastatin, simvastatin, and lovastatin on bone mineral density of the ovariectomized rats. *Endocrine*. 2018;60(1):138–150. doi:10.1007/s12020-018-1531-6
40. Fan J, Kitajima S, Watanabe T, et al. Rabbit models for the study of human atherosclerosis: From pathophysiological mechanisms to translational medicine. *Pharmacol Ther*. 2015;146:104–119. doi:10.1016/j.pharmthera.2014.09.009

MicroRNA-125b overexpression in pseudoexfoliation syndrome

Martyna Tomczyk-Socha^{1,A–D}, Dagmara Baczyńska^{2,A–C,E,F}, Joanna Przeździecka-Dołyk^{1,C,E}, Anna Turno-Kręcicka^{1,A–C,E,F}

¹ Department of Ophthalmology, Wrocław Medical University, Poland

² Department of Molecular and Cellular Biology, Faculty of Pharmacy with Division of Laboratory Diagnostics, Wrocław Medical University, Poland

A – research concept and design; B – collection and/or assembly of data; C – data analysis and interpretation;

D – writing the article; E – critical revision of the article; F – final approval of the article

Advances in Clinical and Experimental Medicine, ISSN 1899–5276 (print), ISSN 2451–2680 (online)

Adv Clin Exp Med. 2020;29(12):1399–1405

Address for correspondence

Martyna Tomczyk-Socha

E-mail: martyna_tomczyk@wp.pl

Funding sources

This study constitutes statutory activity of the Department of Ophthalmology, supported with the Wrocław Medical University grant No. ST C240.17.014.

Conflict of interest

None declared

Received on September 11, 2019

Reviewed on February 18, 2020

Accepted on June 7, 2020

Abstract

Background. MicroRNAs (miRs) are small non-coding RNAs. MiR-125b has been described as being down-regulated in cataract tissue when compared to a transparent lens.

Objectives. The aims of the study were: 1) to establish the expression of miR-125b in cataracts complicated by pseudoexfoliation syndrome (PEX), glaucoma or PEX glaucoma; and 2) to determine whether any environmental factors influence miR-125b expression.

Material and methods. Anterior lens capsules were obtained from 150 patients. The patients were subdivided into 1 of 4 groups: those with PEX (PEXg), those with primary open-angle glaucoma (Gg) and those with PEX glaucoma (PEXgG), plus gender-matched controls with cataracts alone (control group – Cg). Quantitative polymerase chain reaction (qPCR) expression of microRNA-125b was examined in every group.

Results. The mean age of the 150 patients was 75.18 years (standard deviation (SD) ± 9.12 years). Our investigation indicated, for the first time, that miR-125b expression was increased 3.33 times in the PEXg ($p = 0.015$). The quantitative analysis of miR-125b expression conducted between combined groups of all the patients that have PEX syndrome (with or without glaucoma) and the Cg revealed a statistically significant difference ($p = 0.04$). Lower miR-125b expression was found in the patients who smoked compared to those who did not ($p = 0.01$).

Conclusions. Our data revealed the possible role of miR-125b in PEX syndrome development. There are 2 possible interpretations of these results: either the co-existence of PEX acts as a moderator of miR-125b expression in the anterior lens capsule, or increased expression of miR-125b can play a role in the pathogenesis of PEX.

Key words: microRNA, pseudoexfoliation syndrome, pseudoexfoliation glaucoma, miR-125b, lens capsule

Cite as

Tomczyk-Socha M, Baczyńska D, Przeździecka-Dołyk J, Turno-Kręcicka A. MicroRNA-125b overexpression in pseudoexfoliation syndrome. *Adv Clin Exp Med.* 2020;29(12):1399–1405. doi:10.17219/acem/123623

DOI

10.17219/acem/123623

Copyright

© 2020 by Wrocław Medical University

This is an article distributed under the terms of the Creative Commons Attribution 3.0 Unported (CC BY 3.0) (<https://creativecommons.org/licenses/by/3.0/>)

Introduction

MicroRNAs (miRs) are a group of small endogenous non-coding RNAs, generally consisting of 21–23 nucleotides. They regulate posttranscriptional gene expression through complementary or partial complementary binding with the 3' untranslated region of target mRNA.¹ The miRs represent a prominent class of gene regulators.^{2–4} A single miR can modulate the expression of several mRNAs, and conversely, a single mRNA strand can interfere with multiple miRs.⁵ Mature miRs have long half-lives, are not rapidly degraded and can influence different biological pathways by binding to different mRNAs.⁵ While miRs usually act as negative modulators of gene expression, they can also stimulate translation.⁶ Previous studies have demonstrated that expression of miRs, such as miR-760, miR-186, miR-20a, miR-24, miR-34a, miR-106a, and miR-449a, can be involved in senescence or age-related diseases including neurological disorders, diabetes, degenerative arthritis, and cataracts.^{2,7}

Distinct expression profiles of miRs in the central epithelium of transparent human lenses and age-related cataract-affected human lenses have been reported previously.⁸ In transparent lenses, a high expression of miR-184, miR-1826, miR-125b, miR-1308, miR-26a, miR-638, miR-923, and let-7b has been observed. In age-related cataract-affected lenses, other miRs have been identified, including miR-184, miR-1826, let-7b/c, miR-24, miR-23b, miR-23a, and miR-923.⁸ It is possible that all the identified miRs are involved in a multifactorial pathogenesis of cataract formation, in which processes of senescence, as well as multiple genetic and environmental factors, have been implicated. Specifically, miR-34a may play an important role in lens senescence, given that its expression in the lens epithelium is positively correlated with age and the severity of the cataract.⁹ There are probably also different exclusively age-specific gene expression changes in human lenses.¹⁰

The pathogenesis of a cataract is still poorly understood, but Li et al. described lens epithelial cell apoptosis as a common cellular process in cataract development.¹¹ Specifically, the TP53 gene is closely associated with lens epithelial cell apoptosis.¹² Qin et al. described that microRNA-125b (miR-125b) directly targets P53: miR-125b was downregulated in age-related cataract tissue when compared with healthy transparent lens tissue, and inversely related to the level of P53.¹³

With its monolayer structure and direct exposure to ultraviolet radiation, the lens capsule epithelium seems to be an important subject for investigating complex factors playing roles in cellular aging, including genetics and environmental influences.¹⁰ Senescence has been implicated in cataract, pseudoexfoliation syndrome (PEX) and primary open-angle glaucoma, but disease-specific mechanisms remain elusive.

Pseudoexfoliation syndrome is a common multifactorial age-related and genetically determined elastosis.

Pathologic pseudoexfoliation material (PEXM) accumulates as a result of excessive production and abnormal netting of elastic fibers, resulting in the accumulation of elastic fiber aggregates in tissues of the eye and other organs.¹⁴

Our study aimed to: 1) establish the expression of miR-125b in cataract complicated by other eye diseases; and 2) to determine whether any environmental factors have any influence on miR-125b expression. For the first time we quantified the expression of miR-125b in lens capsules of patients with cataract, PEX, primary open-angle glaucoma, and PEX glaucoma.

Material and methods

This prospective, controlled study was approved by the Regional Ethics Review Board and was conducted in accordance with the principles set forth in the Guidelines for Good Clinical Practice and the Declaration of Helsinki (and its amendments) (approval No. KB 272/2017 from 26/04/2017).

Fresh specimens of anterior lens capsules were obtained from 150 patients between 46 and 92 years of age (mean: 75.18 years, standard deviation (SD) \pm 9.12 years) during cataract phacoemulsification surgery. All lens samples were obtained with intact continuous curvilinear capsulorhexis 5–6 mm in diameter.

Each patient underwent a complete ophthalmological examination comprising an interview, anterior segment slit lamp biomicroscopy before and after dilation of the pupil, intraocular pressure (IOP) and funduscopy examination. Patients who had previously undergone eye surgery or who had other ophthalmic diseases (e.g., diabetic retinopathy, uveitis, trauma) were excluded.

The patients were consecutively selected and assigned to 1 of 4 groups:

1. group of patients with cataract and PEX (PEXg) – 38 patients;
2. group of patients with cataract and primary open-angle glaucoma (Gg) – 37 patients;
3. group of patients with cataract, PEX and glaucoma (PEX glaucoma group – PEXGg) – 30 patients;
4. group of patients with cataract – the control group (Cg) – 45 patients.

The severity of the cataracts was similar in each study group. Information regarding current ophthalmic medication usage (timolol, brymonidine, prostaglandin analog, dorzolamide) and lifestyle data, such as smoking habits, were elicited through a patient interview prior to surgery.

RNA isolation and relative real-time RT-PCR

Fragments of lens capsules from patients with cataract were homogenized using MagNA Lyser Green Beads (Roche Diagnostics GmbH, Mannheim, Germany) in a lysis

buffer. Total RNA was isolated using a NucleoSpin RNA II kit (Macherey-Nagel & Co., Düren, Germany) following the manufacturer’s protocol. Reverse transcription reaction (RT) was performed using 3 µL of extracted total RNA, TaqMan MicroRNA Reverse Transcription Kit (Thermo Fisher Scientific, Foster City, USA) and specific RT primers for RNU6B (Thermo Fisher Scientific) and miR-125b (Thermo Fisher Scientific) in a final volume of 15 µL according to the manufacturer’s instructions. Kapa PROBE Master Mix (Kapa Biosystems Inc., Boston, USA) and specific TaqMan MicroRNA Assays (Thermo Fisher Scientific) were used to assess microRNA expression according to the manufacturers’ instructions. We added 1.33 µL of twice-diluted RT product to single real-time polymerase chain reaction (RT-PCR). All the reactions were performed in triplicate in 96-well plates under the following thermal cycling conditions: 20 s at 95°C followed by 40 cycles of 1 s at 95°C and 20 s at 60°C. The reactions were run in the 7900HT Fast Real-Time PCR System (Thermo Fisher Scientific) and the threshold cycle data (Ct) were collected using SDS v. 2.2 software (Thermo Fisher Scientific). The relative expression of miR-125b in each sample was calculated using the comparative Ct method ($2^{-\Delta\Delta Ct}$). The patients’ samples were normalized to RNU6B, calibrated to the Cg and presented as a relative quantity (RQ).

Statistical analysis

A qualitative analysis (χ^2 test) used to form a categorized table and a quantitative analysis (Student’s t-test) were performed. Analysis of variance (ANOVA) with a post hoc least significant difference (LSD) evaluation was used to define the differences between the groups. A partial analysis was performed at intervals of RQ (and logRQ) defined with the χ^2 method. In addition, the correlation between miR-125b and the age of the patients was assessed. Logistic regression was used to assess the probability of influence of the RQ in each specified group. The results were considered statistically significant at a p-value less than 0.05. All the calculations were carried out using STATISTICA v. 12 software. (StatSoft Inc., Tulsa, USA) and MedCalc (MedCalc Software Ltd., Ostend, Belgium).

Results

MiR-125b expression

In order to determine the expression level of miR-125b in every group, relative RT-PCR was performed. The level of miR-125b expression was increased in each of the study groups (PEXg, Gg and PEXGg) compared to the Cg (Fig. 1). The qualitative analysis (χ^2 test) revealed statistically significant increases in the miR-125b levels in the PEXg cohort compared to the Cg cohort (3.33 times higher; $p = 0.015$, Table 1). There were no statistically significant differences in miR-125b levels between the samples from the Gg and Cg cohorts.

Table 1 shows the mean and standard deviations of RQ values; however, the RQ distributions are right-skewed. Therefore, the ANOVA test was used after the RQ logarithm transformation. An LSD test was used as a post hoc test after the ANOVA. No differences in sex distribution between groups was found ($p = 0.4822$). In the PEXg compared to the other 2 groups (Gg and PEXGg), the number of patients with an RQ value >0.6 was increased by 10%, while 10% fewer patients had an RQ value <-0.3 . This further supports the statistical difference between the groups described (Fig. 2).

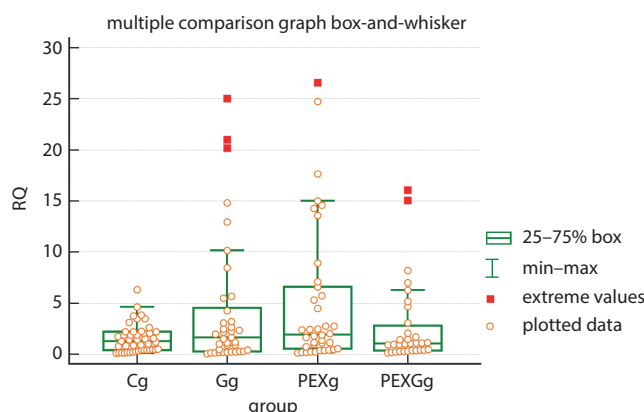


Fig. 1. Comparison of miR-125b expression levels in PEXg, Gg, PEXGg, and Cg. The observed values were higher in the study groups with an ophthalmic disease compared to the Cg, but the only statistically significant difference was in PEXg compared to Cg $p = 0.046$ (median – horizontal line inside of the 25–75% box).

Table 1. Mean expression of miR-125b in every group (LSD test as post hoc test)

| Group | Number of patients | Mean age [†] | Sex proportion in each group (female:male) [†] | Mean RQ | SD | p-value (tested group vs Cg) |
|------------|--------------------|-----------------------|---|---------|------|------------------------------|
| PEXg | 38 | 77 | 15:4 | 5.11 | 6.92 | 0.015 |
| Gg | 37 | 72 | 25:12 | 4.30 | 6.44 | 0.14 |
| PEXGg | 30 | 76 | 22:8 | 2.78 | 4.10 | 0.45 |
| Cg | 45 | 73 | 29:16 | 1.53 | 1.38 | x |
| All groups | 150 | 75 | 53:22 | 3.37 | 5.27 | x |

[†] no statistically significant differences between groups ($p > 0.05$); LSD – least significant difference; SD – standard deviation; RQ – relative quantity; PEX – pseudoexfoliation; PEXg – patients cataract and PEX; PEXGg – patients with cataract, glaucoma and PEX; Gg – patients with cataract and primary open-angle glaucoma; Cg – control group.

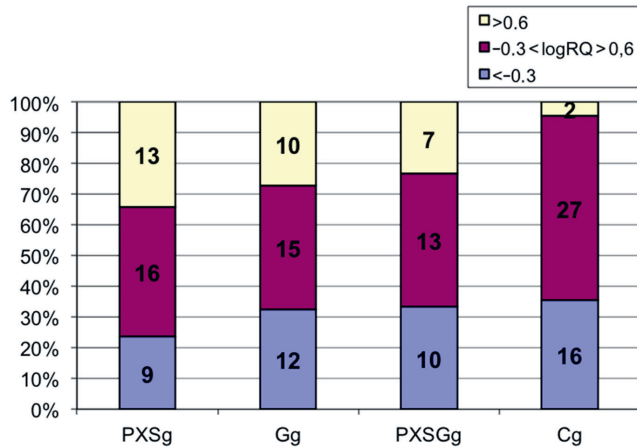


Fig. 2. MiR-125b expression analysis in PEXg, Gg, PEXGg, and Cg with subdivisions into the different value ranges of logRQ (the number of patients in each group is on the bar)

The quantitative analysis of miR-125b expression (Student's t-test) conducted between PEXg+PEXGg (the combined group of all the patients that have the PEX syndrome,

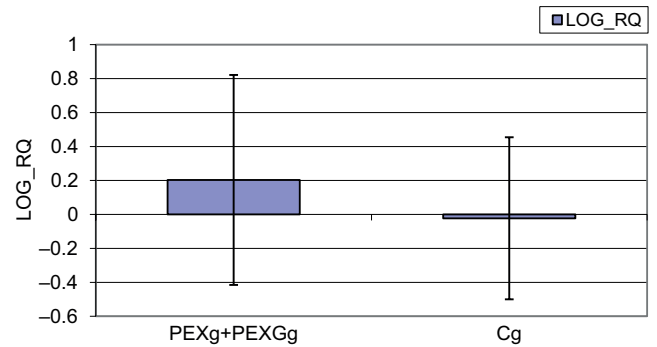


Fig. 3. MiR-125b expression (logRQ values) in all the patients with PEX syndrome compared to the Cg (mean logRQ PEXg+PEXGg = 0.203; Cg = -0.0228; p = 0.04)

with or without glaucoma) and Cg revealed a statistically significant difference (p = 0.04, Fig. 3).

Additionally, the logistic regression model (Fig. 4) revealed a statistically significant correlation (probability >50%) between the level of RQ and the diagnoses outlined in the study: A) existing PEX with or without glaucoma;

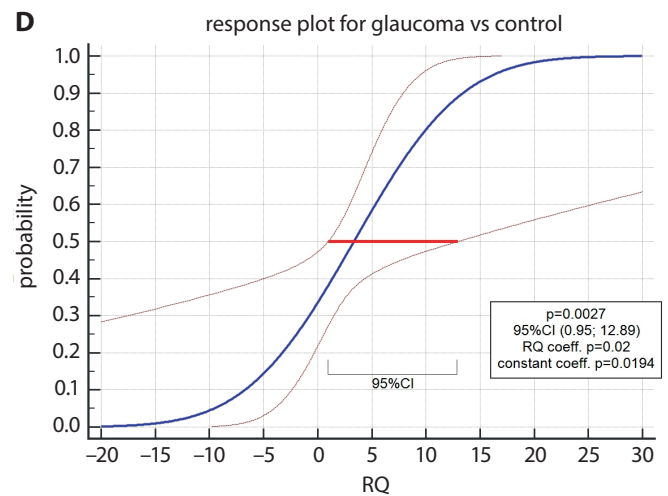
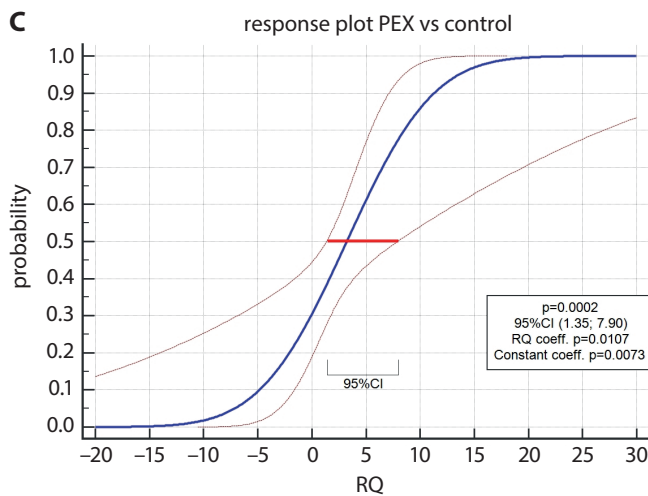
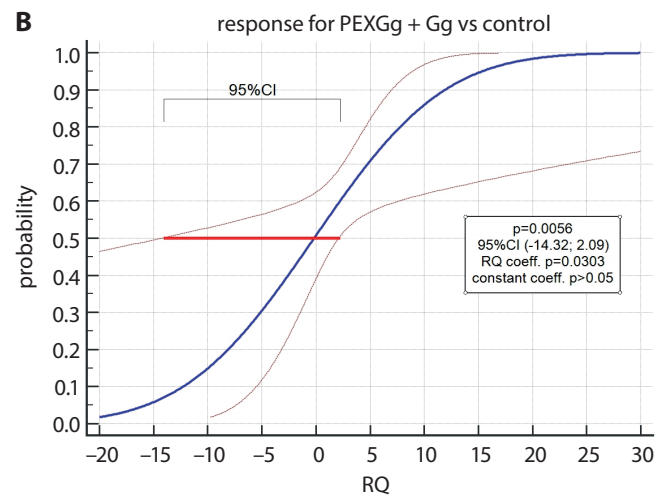
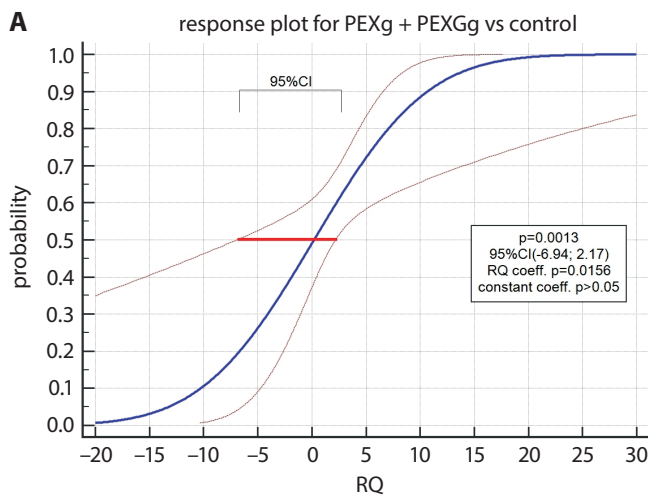


Fig. 4. Logistic regression analysis for different categorical outcomes (A) existing PEX with or without glaucoma, (B) existing glaucoma with or without PEX, (C) only PEX, and (D) only glaucoma compared to the Cg. The PEXGg is the factor that reverses the 95% CI RQ values from predominantly positive in the PEXg and Gg into the predominantly negative in the combined groups such as PEXg+PEXGg and PEXGg+Gg

B) existing glaucoma with or without PEX, C) only PEX; and D) only glaucoma compared to the Cg. The PEXG is a factor that reverses the 95% confidence interval (95%) CI RQ values from predominantly positive in the PEXg and Gg into the predominantly negative in the combined groups, such as PEXg+PEXGg and PEXGg+Gg. The p-values and 95% CI ranges are: 0.0013, -6.94–2.17; 0.0056, -14.32–2.09; 0.0002, 1.35–7.90; and 0.0027, 0.95–12.89, respectively, for PEXg+PEXGg, PEXGg+Gg, PEXg, and Gg.

Factors that may affect miR-125b expression

There were no statistically significant correlations between the levels of miR-125b and the age of the patients. During the assessment of relationships between levels of miR-125b and important factors obtained from patients' history records (current cigarettes smoking, drops for glaucoma), only 1 statistically significant difference was found: a lower level of miR-125b expression was found in patients who smoked compared to those who did not ($p = 0.01$, Table 2). Cigarette smoking was noted in the histories of 5.26% of the patients with PEXg (2 of 38 patients), 16.67% of the patients with PEXGg (5 of 30 patients), 8.1% of the patients with Gg (3 of 37 patients), and 8.89% of the patients in the Cg (4 of 45 patients).

Discussion

Our study is the first to present the correlation between the level of miR-125b and PEX syndrome in patients with cataracts and PEX compared to patients with cataracts alone.

MiR-125b has been demonstrated to be inversely related to the level of P53 in age-related cataract tissue and is involved in aging induced by the DNA damage response, which is mainly governed by the P53 pathway.¹³ Some confirmed risk factors for cataract formation, like chronic

ultraviolet light exposure and oxidative stress, cause DNA damage as a result of the cumulative effects of reactive oxygen species (ROS).⁹

In our study, we observed no differences in the levels of expression of miR-125b in the lens capsules of patients with cataracts alone and those with both cataract and primary open-angle glaucoma. The main finding of our study is that miR-125b is significantly increased in lens capsules of patients with PEXg. The results obtained in this and in prior studies allow to us assume that in the examined population, the co-existence of PEX and cataracts was the main moderator of miR-125b expression in the lens capsules and that the increased expression of miR-125b may be a cause of PEX. It should be emphasized that our research, which reflects miR-125b expression levels close to those seen in vivo, was carried out on a large number of sampled capsules from a patient population that was relatively homogenous in terms of age and disease severity.

Numerous mechanisms, such as disruptions in the proteolytic balance of the extracellular matrix, chronic inflammatory processes of low intensity, chronic or recurrent ischemia/hypoxia, regulation disturbances at the cellular level, and oxidative stress, have all been implicated in the formation of PEXM complexes.^{4,15,16} These factors interplay in creating conditions specific for PEX and the upregulation of miR-125b in capsular lens tissue can be either a cause or an effect of these processes.

Altered expression of miR-125b has been demonstrated in a number of chronic diseases and malignancies, including prostate, breast and pancreatic cancer and primary hepatocellular carcinoma.^{17–20} MiR-125b expression is associated with classic phenotypic and genotypic sequelae of reduced P53 expression, including altered sensitivity to genotoxic agents and reduced expression of P53-related transcriptional targets such as miR-34a/b/c.²¹

Excessive oxidative stress has been shown to augment expression of miR-125b.²¹ Upregulation of miR-125b expression has been identified in acute cerebral ischemia.^{22,23} Also, miR-125b has been shown to increase in settings

Table 2. Summary of additional factors in the analysis of miR-125b expression

| Medical history information | | Mean | | Number of valid cases | | SD | | p-value |
|-----------------------------|-----------------|------|------|-----------------------|-----|------|------|---------|
| | | no | yes | no | yes | no | yes | |
| Medications | timololi maleas | 1.91 | 1.84 | 131 | 19 | 0.72 | 0.76 | 0.57 |
| | brimonidine | 1.90 | 2.00 | 131 | 19 | 0.70 | 0.88 | 0.96 |
| | prostaglandins | 1.89 | 2.00 | 137 | 13 | 0.72 | 0.71 | 0.77 |
| Habits | smoking | 1.95 | 1.43 | 136 | 14 | 0.72 | 0.51 | 0.01 |
| Comorbidities | DM | 1.88 | 1.97 | 119 | 31 | 0.72 | 0.75 | 0.52 |
| | heart failure | 1.87 | 1.95 | 91 | 59 | 0.70 | 0.75 | 0.95 |
| | HT | 1.88 | 1.91 | 52 | 98 | 0.70 | 0.73 | 0.90 |
| | dementia | 1.90 | 1.80 | 145 | 5 | 0.73 | 0.45 | 0.69 |
| | vertigo | 1.91 | 1.75 | 138 | 12 | 0.72 | 0.75 | 0.60 |

DM – diabetes mellitus; HT – hypertension; SD – standard deviation.

of hypoxia.²⁴ Thus, oxidative stress and hypoxia appear to play a major role in the modification of gene expression.

The impact of smoking on the incidence of PEX has not been clearly assessed, but Spečkauškas et al. reported that the age-adjusted odds ratio (OR) for PEX increased 3.1% with each year of smoking, but that the number of cigarettes smoked per day had no effect on PEX.²⁵ However, other researchers, like You et al., found no relationship between smoking and the occurrence of PEX in a large cohort study.²⁶

The present study showed significantly reduced miR-125b expression in cigarette smokers. Analyzing the distribution of smokers among the study groups, the percentage of smoking patients in the PEXGg was close to double that in the other groups (16.67% compared to 5.26% in PEXg, 8.1% in Gg and 8.89% in Cg).

In the present study, there was no significant elevation in the expression of miR-125b in PEXGg. Increased expression was statistically significant for PEXg and for the combined group of all patients with PEX (PEXg+PEXGg). If smoking reduces the expression level of miR-125b, and more patients who smoke cigarettes are found in PEXGg than in the other groups, it can be assumed that the reason for the absence of a statistically significant increase in miR-125b expression in the PEXGg may be the increased percentage of smokers. In the group of all patients with PEX, the percentage of smoking patients was equalized (10.29% in the PEXg+PEXGg group compared to 8.89% in the Cg) and significantly increased miR-125b expression was noted in all the PEX patients.

The central fragment of the anterior lens capsule was the material examined to assess the miR-125b level. The lens capsule is an ideal source of information about PEX, as it is constantly exposed to damaging factors that participate in the disease pathogenesis, such as UV rays. It is a region in which the molecules comprising PEXM are deposited and bound in insoluble structures. The lens capsule is avascular and is washed by aqueous fluid. The components of the aqueous fluid can impact the lens capsule. According to the protein sink model, the anterior chamber of PEX eyes reflects a breakdown of the blood–eye barrier.¹⁴ Chronic inflammatory changes of the aqueous humor may lead to dysregulation of miR expression and influence P53 activity, leading to the transcription of numerous genes responsible for senescence or apoptosis by activation of the target mRNA.²⁷


Conclusions

An interesting and innovative aspect of our preliminary study was the correlation of PEX and miR-125b expression in the eye tissue examined. Further studies are needed to determine the role of miR in eye pathologies. Dysregulation of miR expression and activity can contribute to stress-related chronic diseases such as PEX. Even with

the advances in the field in the last decade, effective novel therapeutic approaches are still lacking for PEX. An improved understanding of the impact of epigenetic factors, such as DNA hypermethylation and histone modifications in the regulation of miR expression, is needed. The results of this study suggest that miR shows a potential to be a future avenue for effective diagnosis and therapeutic strategies for PEX.

ORCID iDs

Martyna Tomczyk-Socha  <https://orcid.org/0000-0002-1472-4996>

Dagmara Baczyńska  <https://orcid.org/0000-0001-6781-6758>

Joanna Przeździecka-Dołyk  <https://orcid.org/0000-0002-1099-4876>

Anna Turno-Kręcicka  <https://orcid.org/0000-0001-6732-1851>

References

- Dogini DB, Pascoal VD, Avansini SH, Vieira AS, Pereira TC, Lopes-Cendes I. The new world of RNAs. *Genet Mol Biol.* 2014;37(1 Suppl): 285–293.
- Lee YH, Kim SY, Bae YS. Upregulation of miR-760 and miR-186 is associated with replicative senescence in human lung fibroblast cells. *Mol Cells.* 2014;37(8):620–627.
- Chen K, Rajewsky N. The evolution of gene regulation by transcription factors and microRNAs. *Nat Rev Genet.* 2007;8(2):93–103.
- Peng CH, Liu JH, Woung LC, et al. MicroRNAs and cataracts: Correlation among let-7 expression, age and severity of lens opacity. *Br J Ophthalmol.* 2012;96(5):747–751.
- Kowlru RA, Kowlru A, Mishra M, Kumar B. Oxidative stress and epigenetic modifications in the pathogenesis of diabetic retinopathy. *Prog Retin Eye Res.* 2015;48:40–61.
- Vasudevan S, Tong Y, Steitz JA. Switching from repression to activation: MicroRNAs can up-regulate translation. *Science.* 2007;318(5858): 1931–1934.
- Khee SG, Yusof YA, Makpol S. Expression of senescence-associated microRNAs and target genes in cellular aging and modulation by tocotrienol-rich fraction. *Oxid Med Cell Longev.* 2014;725929. doi:10.1155/2014/725929
- Wu C, Lin H, Wang Q, et al. Discrepant expression of microRNAs in transparent and cataractous human lenses. *Invest Ophthalmol Vis Sci.* 2012;53(7):3906–3912.
- Chien KH, Chen SJ, Liu JH, Chang HM, Woung LC, Liang CM. Correlation between microRNA-34a levels and lens opacity severity in age-related cataracts. *Eye (Lond).* 2013;27(7):883–888.
- Hawse JR, Hejtmancik JF, Horwitz J, Kantorow M. Identification and functional clustering of global gene expression differences between age-related cataract and clear human lenses and aged human lenses. *Exp Eye Res.* 2004;79(6):935–940.
- Li WC, Kuszak JR, Dunn K, et al. Lens epithelial cell apoptosis appears to be a common cellular basis for non-congenital cataract development in humans and animals. *J Cell Biol.* 1995;130(1):169–181.
- Geatrell JC, Gan PM, Mansergh FC, et al. Apoptosis gene profiling reveals spatio-temporal regulated expression of the p53/Mdm2 pathway during lens development. *Exp Eye Res.* 2009;88(6):1137–1151.
- Qin Y, Zhao J, Min X, et al. MicroRNA-125b inhibits lens epithelial cell apoptosis by targeting p53 in age-related cataract. *Biochim Biophys Acta.* 2014;1842(12 Pt A):2439–2447.
- Lee RK. The molecular pathophysiology of pseudoexfoliation glaucoma. *Curr Opin Ophthalmol.* 2008;19(2):95–101.
- Wu C, Liu Z, Ma L, et al. MiRNAs regulate oxidative stress related genes via binding to the 3' UTR and TATA-box regions: A new hypothesis for cataract pathogenesis. *BMC Ophthalmol.* 2017;17(1):142.
- Zenkel M, Kruse FE, Naumann GO, Schlötzer-Schrehard U. Impaired cytoprotective mechanisms in eyes with pseudoexfoliation syndrome/glaucoma. *Invest Ophthalmol Vis Sci.* 2007;48(12):5558–5566.
- Wojciechowska A, Braniewska A, Kozar-Kamińska K. MicroRNA in cardiovascular biology and disease. *Adv Clin Exp Med.* 2017;26(5):865–874.
- Shi XB, Xue L, Yang J, et al. An androgen-regulated miRNA suppresses Bak1 expression and induces androgen-independent growth of prostate cancer cells. *Proc Natl Acad Sci U S A.* 2007;104(50):19983–19988.

19. Thomson JM, Newman M, Parker JS, Morin-Kensicki EM, Wright T, Hammond SM. Extensive post-transcriptional regulation of microRNAs and its implications for cancer. *Genes Dev.* 2006;20(16):2202–2207.
20. Xu J, Li J, Zheng TH, Bai L, Liu ZJ. MicroRNAs in the occurrence and development of primary hepatocellular carcinoma. *Adv Clin Exp Med.* 2016;25(5):971–975.
21. Selbach M, Schwanhäusser B, Thierfelder N, Fang Z, Khanin R, Rajewsky N. Widespread changes in protein synthesis induced by microRNAs. *Nature.* 2008;455(7209):58–63.
22. Lukiw WJ, Pogue AI. Induction of specific microRNA (miRNA) species by ROS-generating metal sulfates in primary human brain cells. *J Inorg Biochem.* 2007;101(9):1265–1269.
23. Sepramaniam S, Tan JR, Tan KS, et al. Circulating microRNAs as biomarkers of acute stroke. *Int J Mol Sci.* 2014;15(1):1418–1432.
24. Kulshreshtha R, Ferracin M, Wojcik SE, et al. A microRNA signature of hypoxia. *Mol Cell Biol.* 2006;27(5):1859–1867.
25. Spečkauskas M, Tamošiūnas A, Jašinskas V. Association of ocular pseudoexfoliation syndrome with ischaemic heart disease, arterial hypertension and diabetes mellitus. *Acta Ophthalmol.* 2012;90(6):e470–e475.
26. You QS, Xu L, Wang YX, et al. Pseudoexfoliation: Normative data and associations – the Beijing eye study 2011. *Ophthalmology.* 2013;120(8):1551–1558.
27. Liu B, Chen Y, Clair DK. ROS and p53: A versatile partnership. *Free Radic Biol Med.* 2008;44(8):1529–1535.

Synthesis and characterization of atherosclerotic target anti-CD47 functionalized by nano- polyelectrolyte complexes between chitosan and hyaluronic acid and in vivo and in vitro targeting experiments

Jun Yu^{1,A}, Qiurong Ruan^{2,E}, Xiu Nie^{1,E}

¹ Department of Pathology, Union Hospital, Tongji Medical College, Huazhong University of Science and Technology, Wuhan, China

² Institute of Pathology, Tongji Hospital, Tongji Medical College, Huazhong University of Science and Technology, Wuhan, China

A – research concept and design; B – collection and/or assembly of data; C – data analysis and interpretation;

D – writing the article; E – critical revision of the article; F – final approval of the article

Advances in Clinical and Experimental Medicine, ISSN 1899–5276 (print), ISSN 2451–2680 (online)

Adv Clin Exp Med. 2020;29(12):1407–1415

Address for correspondence

Jun Yu

E-mail: 89679676@qq.com

Funding sources

This work was financially supported by the National Natural Science Foundation of China (81200104), and the Youth Foundation of Huazhong University of Science and Technology (02.03.2017-314).

Conflict of interest

None declared

Received on October 14, 2019

Reviewed on June 29, 2020

Accepted on September 20, 2020

Cite as

Yu J, Ruan Q, Nie X. Synthesis and characterization of atherosclerotic target anti-CD47 functionalized by nano- polyelectrolyte complexes between chitosan and hyaluronic acid and in vivo and in vitro targeting experiments. *Adv Clin Exp Med.* 2020;29(12):1407–1415. doi:10.17219/acem/127685

DOI

10.17219/acem/127685

Copyright

© 2020 by Wrocław Medical University

This is an article distributed under the terms of the Creative Commons Attribution 3.0 Unported (CC BY 3.0) (<https://creativecommons.org/licenses/by/3.0/>)

Abstract

Background. In several different atherosclerotic model mice, blocking CD47 with anti-CD47 antibody significantly reduced accumulation of arterial plaque.

Objectives. We described the development of multifunctional positively charged polyelectrolyte complex (PEC) nanoparticles, designed to be stable at physiological salt concentrations and pH for effective targeted delivery in atherosclerosis.

Material and methods. These nanoparticles were obtained by charge neutralization using chitosan (CS) as the polycation and hyaluronic acid (HA) as the polyanion. An atherosclerotic-model antibody, the anti-CD47 antibody, was sorbed onto the particle surfaces in water and phosphate-buffered saline (PBS) for 4 h. The synthetic nanocarriers were exposed to vascular endothelial cells (VECs) in vitro to study their targeted adsorption to the cells, and the targeted distribution of nanocarriers was evaluated in vivo.

Results. We showed that the complexation process and the physicochemical properties of the resulting colloids were impacted by external parameters such as the charge mixing ratio and the polymer concentrations. Nonstoichiometric colloidal PECs were obtained in water or PBS (pH 7.4) and remained stable for 1 month. The morphology was studied with scanning electron microscopy (SEM). The average size of the CS-HA/CD47 nanoparticles was 375–620 nm, with a positive zeta potential. The CD47-targeted nanocarriers could be efficiently adsorbed to the surface of VECs in vitro, and their targeted distribution was evaluated in vivo.

Conclusions. Targeted nanocarriers can be effectively adsorbed to the surface of a VEC line and atheromatous plaque in vitro and in vivo. These results demonstrated that CS-HA/CD47 can be an effective carrier for targeted drug delivery in atherosclerosis.

Key words: atherosclerosis, chitosan, hyaluronic acid, polyelectrolyte complexes, anti-CD47

Introduction

In a recent study, researchers from the Stanford University School of Medicine (USA) found that cells with surface antigen CD47 are extremely abundant in atherosclerotic plaque, and that CD47-blocking antibodies reverse defects in efferocytosis, normalize the clearance of diseased vascular tissue and ameliorate atherosclerosis in multiple mouse models. In several different atherosclerotic mouse models, blocking CD47 with anti-CD47 antibody significantly reduced arterial plaque accumulation.¹ However, how to use CD47 antibody to achieve effective drug delivery remains a key issue to be solved in future research.

In the past few years, the preparation of polyelectrolyte complexes (PECs) through the electrostatic interaction of oppositely charged polyions, especially as a drug carrier or gene delivery system, has been widely studied by researchers.^{2,3} The preparation of PEC nanoparticles is relatively simple, and the synthesis requires minimal technical expertise and equipment. Without the need for toxic organic solvents and chemical cross-linking agents, PEC nanoparticles can be prepared under mild conditions and easily controlled.

There are many factors that influence the formation and physical properties of PEC nanoparticles, such as pH, temperature, ionization, ionic strength, and interaction time. The stability of PECs depends on the relative molecular weight and charge mixing ratio.⁴ Chitosan (CS) is a polysaccharide obtained by partially deacetylated chitin. Chitosan has some properties that are particularly suitable for medical applications, such as biocompatibility,⁵ biodegradability and non-toxicity,⁶ in addition to being relatively inexpensive.⁷ The glucosamine residue of the primary amino group ($-NH_2$) can be protonated in a weakly acidic environment. Therefore, CS can be combined with various anionic forms of PECs such as dextran sulfate,⁸ chondroitin sulfate,⁹ sodium alginate-carboxymethylcellulose,^{10–12} carrageenan, polygalacturonic acid,^{13,14} and DNA. Hyaluronic acid (HA) is a low-density, multi-component weak acid that is part of the extracellular matrix of all higher animals. It has high lubricity, water absorption and water retention, all of which affect the migration, adhesion and proliferation of various cells.¹⁵ Biomedical applications of HA include ophthalmic surgery, arthritis treatment, wound healing stents, tissue engineering, and implant materials.^{16–18} Hyaluronic acid can be used in biomedical applications with other polymers such as polylysine^{19,20} and silk fibroin to form PECs. Recent studies have shown that chitosan-hyaluronic acid PEC (CS-HA PEC) nanoparticles can be used as a vector for gene delivery,^{21–23} with vector efficiency of up to 60%.²⁴

Based on the above, the aim of this study was to combine the advantages of CS and HA to develop a polyelectrochemical composite PEC nanoparticle for CD47 antibody adsorption, and to study whether colloidal PEC nanoparticles are stable to the CD47 antibody. In vivo and in vitro cytology experiments with the synthetic anti-CD47-targeted nanocarriers were performed to evaluate the targeted

adsorption of vascular endothelial cells (VECs) and atherosclerotic plaque.

This study was approved by the Ethics Committee of Tongji Medical College of Huazhong University of Science and Technology (Wuhan, China).

Material and methods

Chitosan with varying degrees of acetylation (DA) was provided by Jinan Haidebei Marine Biological Engineering Co., Ltd. (Jinan, China). The DA for the CS used were 5% and 48% and the molar molecular weight (Mw) ranged from 100×10^3 g/mol to 600×10^3 g/mol. The samples were dissolved in aqueous acetic acid, filtered through a Millipore membrane with reduced porosity (Millipore Sigma, Burlington, USA), precipitated with ammonia, rinsed to neutral with deionized water, and lyophilized. The purified high molar mass CS was acetylated with acetic anhydride in a homogeneous medium. The CS was dissolved at 0.5% (w/v) in 0.2 M acetic acid with 0.1 M sodium acetate buffer. We added 0.15 M sodium nitrite solution to the CS solution to obtain nitrite/glucosamine at a molar ratio of 0.5. The reaction was carried out for various durations (15–60 min) under moderate magnetic stirring according to the target Mw. The CS was recovered through ammonia precipitation, washed several times with deionized water until neutral and finally freeze-dried.

Hyaluronic acid with varying Mw, ranging from 1500×10^3 g/mol to 50×10^3 g/mol, was provided by Zhenjiang Dongyuan Biotechnology Co., Ltd. (Jiangsu, China). Anti-CD47 (CD47) antibody was provided by Santa Cruz Biotechnology (Santa Cruz, USA) and the concentrations were confirmed using a Pierce bicinchoninic acid (BCA) assay according to the manufacturer's instructions (Thermo Fisher Scientific, Hudson, USA).

Preparation of polyelectrolyte solution

The CS was dispersed in water or phosphate-buffered saline (PBS) at a concentration of 0.1% by mass. The solution was adjusted to pH = 4.0 with 0.1 M sodium hydroxide or hydrochloric acid. All the CS solutions were filtered through a 0.22- μ m pore size Millipore membrane prior to use. A 0.1% strength HA solution was prepared directly in water or PBS medium with magnetic stirring.

Formation of polyelectrolyte complexes

Under non-stoichiometric conditions ($R = n+/n- \geq 1$, where R is the mixed molar charge ratio), excess polymer was added to the magnetic stirrer in 1 portion. A colloidal PEC (750 rpm) was formed with magnetic stirring at room temperature. The final particle dispersion volume was 30 mL and the solid content was 0.1%. The substrate was precipitated from the solution by centrifugation

at 7000 rpm and 20°C for 10 min. The supernatant was removed and the pellet was resuspended in deionized water or PBS. In all the experiments performed in this study, the initial solution of CS was adjusted to pH = 4.0 to ensure full protonation. Chitosan with an Mw of 100×10^3 g/mol and DA of 5% as well as with an Mw of 200×10^3 g/mol and DA of 48% was used. The average molar mass of the HA used ranged from 50×10^3 g/mol to 1500×10^3 g/mol. Hyaluronic acid was complexed to CS and the charge ratio of the complex was controlled to be $(N+/N-) = 1.5$.

Determination of particle solid content

The solid content is defined as the ratio between the weight of the particles after drying at 60°C for 24 h and the initial weight of the solution.

Physical and chemical characterization of complex dispersions

Dynamic light scattering measurements of the PEC dispersion were performed using a Malvern Nanosizer SZ (Malvern Instruments, Malvern, UK) at the Huazhong University of Science and Technology Analytical Testing Center (Wuhan, China) with a parameter of $\lambda = 633$ nm (at a 173° scattering angle), operated using a 10 mW He/Ne laser beam. All the dynamic light scattering measurements were performed at least 3 times at 25°C. The polydispersity index (PI) is derived from an algorithm provided by the software and is defined as $\mu_2/(\Gamma)^2$, where μ_2 is the second cumulative amount of the correlation function and (Γ) is the average decay rate. Each polydispersity index measurement is the average of 6 measurements in 3 experiments. The zeta potential was measured using the electrophoretic mobility (μE) from the Smoluchowski equation. The μE of the particles was measured at 25°C using the Malvern Nanosizer SZ, and the measurements were carried out by suspending the washed dispersion in a 10^{-3} M sodium chloride solution. The average of 10 measurements was used with a relative error of 5%. A scanning electron microscope (SEM) image was obtained at 5 kV on a Hitachi S-4800 microscope (Hitachi Ltd., Tokyo, Japan). A 0.01% (v/v) nanoparticle dispersion droplet was deposited on a sample holder, air dried at room temperature for 12 h and coated under an argon atmosphere with a palladium cathode evaporator (Structure Probe; Inc./SPI Supplies, West Chester, USA). Scanning electron microscope examinations were performed at the Center for Analysis and Testing Technology of Huazhong University of Science and Technology.

CD47 antibody adsorbed onto CS-HA polyelectrolyte nanocolloid

Chitosan-hyaluronic acid polyelectrolytic nanocolloid (CS Mw 200×10^3 g/mol and DA = 48%, HA Mw = 50×10^3 g/mol) was mixed with different

concentrations of the CD47 antibody solution with moderate agitation, so that the final mixed molar charge ratio of the mixture was $R = 1.5$. After the mixture was centrifuged at 14,000 g for 10 min, the supernatant was removed and the pellet was resuspended in the same volume of buffer. The anti-CD47 adsorption yield was calculated as follows: anti-CD47 adsorption rate = $((\text{anti-CD47 input} - \text{anti-CD47 residue})/\text{anti-CD47 input}) \times 100\%$, where anti-CD47 input is the concentration of anti-CD47 titrated in the original control sample solution for each independent experiment, and anti-CD47 residue refers to the concentration of anti-CD47 measured with titration in the supernatant.

In vitro targeting of VECs by anti-CD47-CS-HA polyelectrochemical complex

The anti-CD47 nanocarrier was labeled with fluorescein isothiocyanate (FITC) fluorescent secondary antibody in vitro. The VEC strain was routinely cultured. When the cells were grown to 80% confluency, the medium was changed to a serum-free medium and cultured for 3 days in the absence of serum medium. The cells were added to 50 $\mu\text{g}/\text{mL}$ ox-LDL for 72 h, and then inoculated into a 24-well cell culture plate, co-cultured with anti-CD47 nano adjuvant for 24 h and washed with PBS. The medium was exchanged and the suspension of the adsorbed nanocarriers was simultaneously counterstained with DAPI. The number and proportion of green fluorescent cells were observed under a fluorescence microscope.

Targeted experiment with synthetic anti-CD47-CS-HA polyelectrochemical complex for atherosclerotic plaque

Atherosclerosis-prone apolipoprotein E-deficient (ApoE $-/-$) mice display poor lipoprotein clearance with subsequent accumulation of cholesterol ester-enriched particles in the blood, which promote the development of atherosclerotic plaque. Therefore, the ApoE $-/-$ mouse model is well established for the study of atherosclerosis. A total of 24 ApoE mice were purchased from the Experimental Animal Center of Nanjing University (China). The mice were fed a high-fat and high-cholesterol diet, and were fostered in the Specific Pathogen-Free (SPF) animal room at the Experimental Animal Center of Tongji Medical College at Huazhong University of Science and Technology (Wuhan, China). After 20 weeks of feeding, the model of atherosclerosis was ready. For the last 8 weeks of the 20-week period, the animals were divided into 3 groups: the P group ($n = 8$), which was administered Cy5.5-anti-CD47-CS-HA-PECs; the M group ($n = 8$), given cy5.5 dye solution; and the G group ($n = 8$), which got CS-HA-PECs. Each mouse was injected with 0.2 mL of its assigned component in the tail vein once a week for 8 weeks. After

the injections were completed in the 20th week, the health status and blood cell count of each mouse were checked. Normal mice were used for follow-up experiments.

In vivo targeting of atherosclerotic plaque in ApoE mice by Cy5.5-CD47 antibody-CS-HA-PECs

Each group of mice began fasting 6 h before imaging to reduce potential background interference caused by gastrointestinal foods. Group G was injected with 0.2 mL PBS through the tail to dissolve 10 mg/mL CS-HA-PECs, whereas group P was injected with 0.2 mL PBS to dissolve Cy5.5-labeled (25 μ g) anti-CD47-CS-HA-PECs (10 mg/mL). The control group (M) was injected with 0.1 mL of a free Cy5.5 dye solution (1 mg/mL) through the tail vein. Twenty four hours after the injection, the mice were anesthetized with an intraperitoneal injection of 10% chloral hydrate solution (0.35 mL per 100 mg of body weight). After anesthesia, the mice were depilated to reduce the background fluorescence interference generated by the hair and fixed onto the treatment bed with tape in a supine position. The small animal in vivo imaging system IVIS 200 (Perkin Elmer, Waltham, USA) was used to image the entire body; the thorax was imaged with the fluorescence scanning in vivo imaging system of the same device. The images of the animals emitting fluorescence in vivo were recorded and the distribution of the fluorescent complex Cy5.5-CD47 antibody-CS-HA-PECs was analyzed. The fluorescence distribution of the negative and positive control groups was compared. After the imaging, the aortas were harvested and tissue sections were prepared. The limbs of the mice were fixed in an anatomical tray, and the chest and abdomen were smeared with 75% alcohol until the skin was moist. The abdominal skin was lifted with a sterilized shaver and surgically cut with scissors. A gap was carefully cut to open the chest and abdominal cavity and expose the heart. Physiological saline was used to perfuse the heart followed by an infusion of 10% formaldehyde for about 40 min. The blood vessel and surrounding connective tissue were removed from the root of the aorta, and the abdominal aorta was harvested. Several 1–1.5-cm specimens were cut and fixed with 10% formaldehyde. After 48 h, the tissues were embedded in paraffin and 0.2-cm samples with a thickness of 5 μ m were evenly sliced from the aortic root. Five sections per blood vessel were observed with fluorescence microscopy.

Statistical analysis

All data was expressed as means \pm standard deviation (SD), and the statistical analyses were performed using IBM SPSS Statistics for Windows v. 20.0 (IBM Corp., Armonk, USA). Comparisons among groups were analyzed using a one-way analysis of variance (ANOVA), followed by the Student–Newman–Keuls test. A $p < 0.05$ was considered statistically significant.

Results and discussion

Formation of polyelectrolyte complexes

Chitosan interacts with the ionized carboxyl group (COO⁻) between ionized aminoglycan (NH₃⁺) and HA to form PECs (Fig. 1). The various colloidal dispersions obtained in the study were measured to determine their average size and the particle size distribution after complexation. An increase in the molar mass of HA resulted in a significant increase in the particle size (Fig. 2; the data represented the mean \pm SD of 3 independent tests; * $p < 0.05$). The 1500 $\times 10^3$ g/mol HA sample did not form particles in the experiment; only a precipitate was obtained. This indicates that such a high Mw polymer cannot be unraveled to form a single particle, and only aggregated precipitates can be formed. Therefore, further experiments were not performed with HA at this molar mass. According to the trend shown in Fig. 2, as the molar mass of HA increases, the particle diameter of the resulting polyelectrolyte increases and the dynamic light scattering PI of the dispersion also increases. Therefore, the optimum molar mass for sodium hyaluronate – i.e., the smallest particle size and PI of the particles – was 50 $\times 10^3$ g/mol.

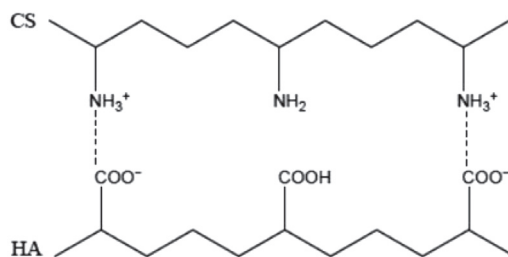


Fig. 1. Schematic diagram of a polyelectrolyte complexation reaction between CS and HA²⁴

As shown in Fig. 3, increasing the molar mass of CS increased the average particle size of the polyelectrochemical composite PECs regardless of the acetylation rate, and the PI followed the same trend. These results suggest that an increase in the molar mass of CS will increase the size of CS-HA polyelectrolyte nanoparticles (data taken from the mean of 3 independent tests \pm SD, $p < 0.05$). The results show that there is a critical molar mass for CS. Above this point, the diameter of the polyelectro-composite nanoparticles will increase sharply. The critical molar mass is 200 $\times 10^3$ g/mol when the acetylation rate is 5% and 48%. When the molar mass of CS is lower than this value, the granular structure formed is dense and uniform.

Therefore, to obtain small and fairly uniformly dispersed particles, low to medium molar masses of CS (about 200 $\times 10^3$ g/mol or less) and 50 $\times 10^3$ g/mol HA are required. The results also show that the CS acetylation rate has a limited effect on the formation of polyelectro-composite nanoparticles.

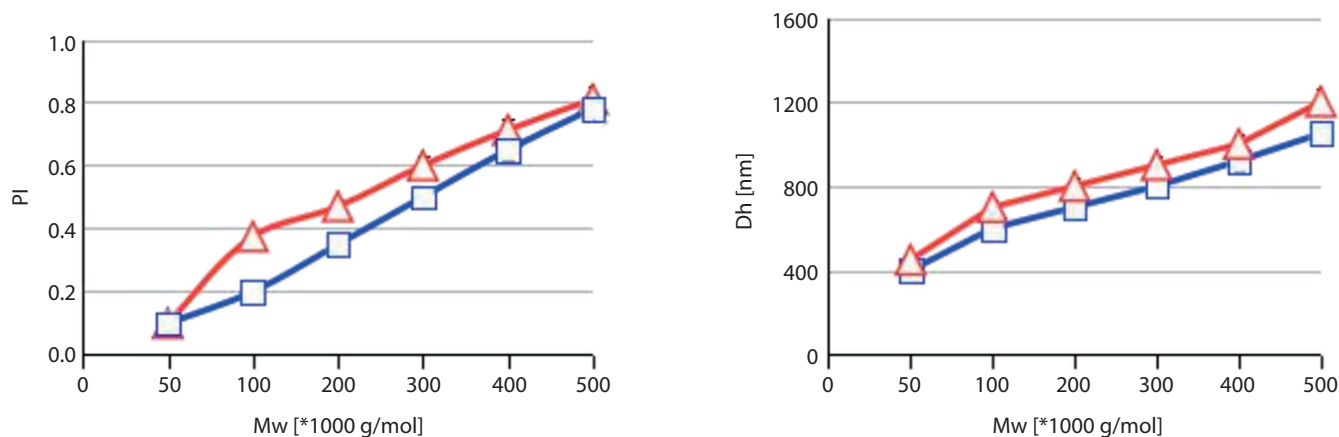


Fig. 2. The effect of HA with different Mw on the size and dispersion index (PI) of PECs was studied. The complex reacted with CS with a Mw of 10×10^3 g/mol and a degree of acetylation (DA) of 5% (\blacktriangle), as well as with CS with a Mw of 200×10^3 g/mol and a DA rate of 48% (\blacksquare), with a charge ratio R of 1.5 in water. The data represents the average value and SD of 3 independent experiments ($p < 0.05$)

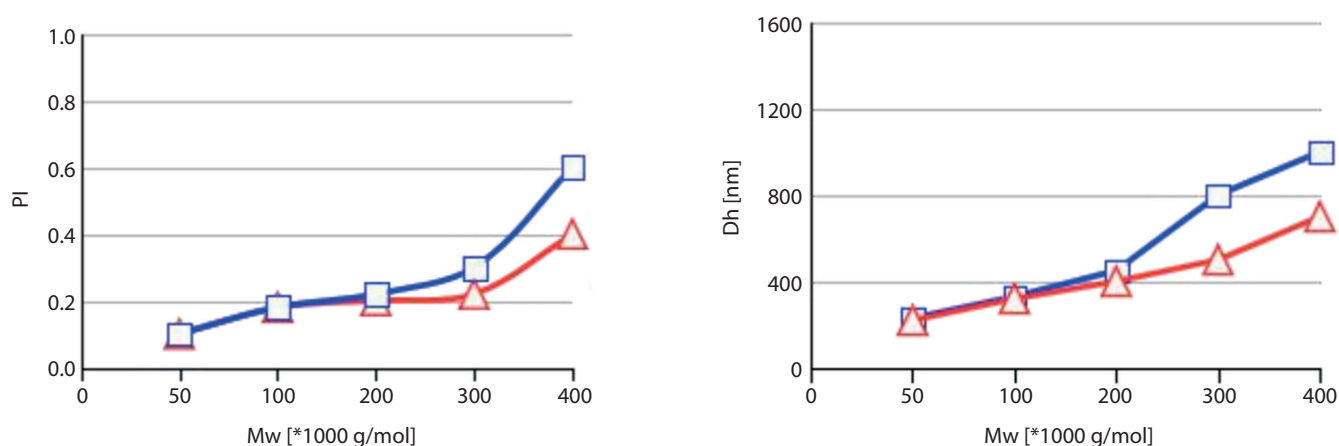


Fig. 3. Particle size and Mw distribution (PI) of polyelectrolyte complexes (PECs) affected by the Mw of CS. Chitosan DA was 5% (\blacktriangle) and 48% (\blacksquare). Chitosan with Mw ranging from 20×10^3 g/mol to 500×10^3 g/mol and HA with a molar mass of 50×10^3 g/mol reacted in water at a charge-to-charge ratio of R = 1.5. The data represents the average value and SD of 3 independent experiments ($p < 0.05$)

The effect of charge change on the physical and chemical properties of the formed polyelectrochemical complex

As described above, the anionic and cationic polyelectrolyte in the mixed solution form a sub-electrolyte complex, and in both extreme cases, a completely water-soluble complex or precipitate is obtained. In order to obtain PEC nanocolloids that do not accumulate over time, the experiments in this study were focused on the effect of charge changes on the stability of the formed polyelectrochemical complex. The DA of CS was 48%, the molar mass was 200×10^3 g/mol, and the low molar mass of HA was 50×10^3 g/mol in water or PBS with a charge ratio $R(N^+/N^-)$: 0.5, 1.5, 2.5, and 3.5. Polyelectrolyte nanoparticles were obtained in water and PBS. Table 1 lists the size, PI, zeta potential and appearance of these nanoparticles (Table 1).

When $R(N^+/N^-) = 0.5$, flocculation was observed with naked eye, as well as after reconstitution 24 h later. This

may be due to the rearrangement of the initially formed complex and thus the observed re-dissolution. More HA participates in the reaction during polymerization, resulting in the redistribution of neutralized fragments, thereby forming a soluble complex. When the charge ratio is close to 1, the size of the particles is significantly increased due to the complete neutralization of the charge. Due to the neutral, non-charged environment, there is no electrostatic charge to counteract the van der Waals interactions, leading to precipitation of the particles. When the charge ratio is increased from 1, the particle size is reduced, and the colloidal stability is enhanced due to an increase in the amount of net charge on the particles. When $R(N^+/N^-)$ is from 1.5 to 3.5, the polyelectrolyte nanoparticles have a diameter distribution between 230 nm and 320 nm in water and a diameter of 330–590 nm in PBS. The zeta potential of the polyelectrochemical complex is positive. As the CS incorporated into the colloid increases, the charge ratio R increases and so did the zeta potential,

Table 1. Physicochemical characteristics of colloidal PECs after synthesis at different charge ratios: CS (DA 48%, Mw 200×10^3 g/mol) and HA (Mw 50×10^3 g/mol)

| CS-HA | Charge ratio (n+/n-) | Solid content (%) | Size [nm] | PI | Zeta potential [mV] | Appearance |
|-------|----------------------|-------------------|-----------|-----|---------------------|------------------|
| Water | 0.5 | – | 1050 | 1 | – | precipitation |
| | 1.5 | 5 | 320 | 0.1 | 25 ± 1.63 | medium turbidity |
| | 2.5 | 2 | 260 | 0.1 | 31 ± 0.23 | medium turbidity |
| | 3.5 | 1 | 230 | 0.1 | 43 ± 0.17 | low turbidity |
| PBS | 0.5 | – | 1180 | 1 | – | precipitation |
| | 1.5 | 4 | 590 | 0.1 | 32 ± 0.13 | medium turbidity |
| | 2.5 | 3 | 392 | 0.1 | 42 ± 0.27 | medium turbidity |
| | 3.5 | 1 | 330 | 0.1 | 45 ± 0.31 | low turbidity |

PEC – polyelectrolyte complex; HA – hyaluronic acid; CS – chitosan; PBS – phosphate-buffered saline; PI – polydispersity index; DA – degree of acetylation; Mw – molecular weight.

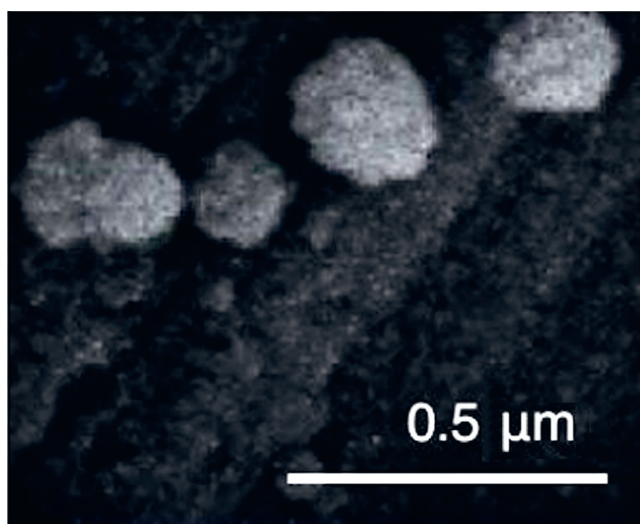


Fig. 4. Scanning electron microscopy images showing the ultrastructure of the CS-HA polyelectrolyte complex (CS: DA 48%, molar mass 200×10^3 g/mol; HA: 500×10^3 g/mol, charge ratio R = 1.5:1)

as expected. Scanning electron microscopy was used to detect the spherical morphology of CS-HA nanoparticles. Figure 4 shows the ultrastructure of the CS-HA PEC composite that had R = 1.5, and the particles clearly show a rough surface.

Colloidal stability

The average size of the particles was measured with elastic light scattering. Most samples in aqueous solution are stable for at least 1 month. When R = 1.5, the dispersion index PI value increased significantly on the 30th day of observation (Tables 2, 3).

The colloidal particles of the polyelectrochemical composite PECs have a smaller particle size in water than in PBS, reflecting the electrostatic stability mode of the PEC composite. Due to the hydrophobic action, the chain inside the CS extends to the hydrophilic peripheral region, thereby preventing aggregation of the polymer. Due to the electrostatic action of salt ions in the PBS solution, the stabilization process for the PEC polymer is not as effective as in water, and thus the particles have a larger average diameter. As shown in Table 3, we observed 2 significant characteristics of the change in particle diameter: First, as the charge ratio R increased, the diameter of the particles became smaller. Second, regardless of the type of solution and the ratio of charge, the diameter of the particle decreased with time. This may be due to the reorganization of the particle structure during the process. Nonetheless, after storage for 1 month at room temperature, the particle size distribution PI index of the solution increased, indicating that the dispersion range of the particles had expanded.

Table 3. CS-HA nanoparticle colloidal stability with time as a function of charge ratio in PBS (CS: DA 48%, molar mass 200×10^3 g/mol; HA: 50×10^3 g/mol)

| Time [days] | CS-HA in PBS | | | | | |
|-------------|----------------------------|-----|----------------------------|-----|----------------------------|-----|
| | Charge ratio (n+/n-) = 1.5 | | Charge ratio (n+/n-) = 2.5 | | Charge ratio (n+/n-) = 3.5 | |
| | size [nm] | PI | size [nm] | PI | size [nm] | PI |
| 0 | 603 | 0.1 | 404 | 0.2 | 398 | 0.1 |
| 7 | 591 | 0.1 | 381 | 0.2 | 365 | 0.1 |
| 14 | 553 | 0.1 | 372 | 0.2 | 320 | 0.1 |
| 30 | 306 | 0.3 | 225 | 0.2 | 216 | 0.2 |

HA – hyaluronic acid; CS – chitosan; PBS – phosphate-buffered saline; PI – polydispersity index; DA – degree of acetylation; Mw – molecular weight.

Table 2. CS-HA nanoparticle colloidal stability with time as a function of charge ratio in water (CS: DA 48%, molar mass 200×10^3 g/mol; HA: 50×10^3 g/mol)

| Time [days] | CS-HA in water | | | | | |
|-------------|----------------------------|-----|----------------------------|-----|----------------------------|-----|
| | Charge ratio (n+/n-) = 1.5 | | Charge ratio (n+/n-) = 2.5 | | Charge ratio (n+/n-) = 3.5 | |
| | size [nm] | PI | size [nm] | PI | size [nm] | PI |
| 0 | 320 | 0.1 | 280 | 0.1 | 260 | 0.1 |
| 7 | 300 | 0.1 | 242 | 0.1 | 253 | 0.1 |
| 14 | 250 | 0.2 | 223 | 0.1 | 203 | 0.1 |
| 30 | 152 | 0.3 | 201 | 0.2 | 121 | 0.2 |

HA – hyaluronic acid; CS – chitosan; PI – polydispersity index; DA – degree of acetylation; Mw – molecular weight.

In vitro targeted adsorption of VECs by synthetic anti-CD47-CS-HA nanopolymerization complex

The DAPI staining highlighted the nuclei of all VECs, which appeared green under the fluorescence microscope, showing anti-CD47-targeting nanoparticles adsorbed onto the VECs. The results demonstrated that anti-CD47-targeting nanocarriers can effectively adsorb to VECs. On the surface, the effective adsorption rate

was about 90%, and the formula for the effective adsorption rate = the number of green fluorescent positive cells/ the number of DAPI blue fluorescent positive cells (Fig. 5).

Synthesis of anti-CD47-CS-HA nanopolymer complex for targeted adsorption of atherosclerotic plaque

The results showed that compared with the control group, the fluorescently labeled CD47 antibody-CS-HA-PECs

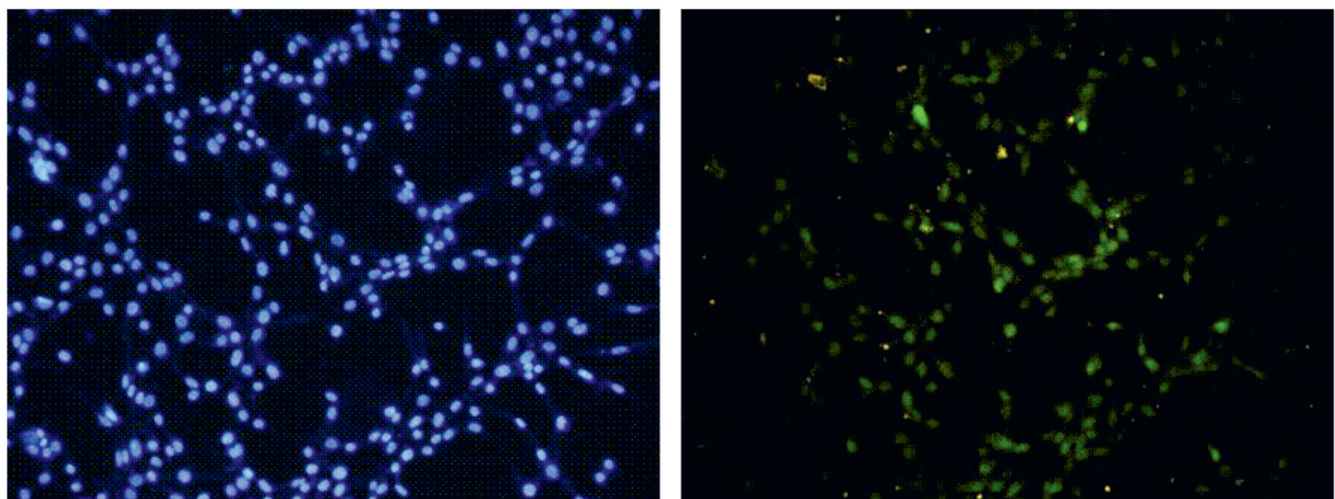


Fig. 5. The interaction of FITC-labeled anti-CD47-targeting CS-HA nanoelectro complex with cultured VEC lines in vitro

A – DAPI staining showed the nuclei of all VECs; B – FITC fluorescence microscopy showed that anti-CD47-targeting nanoparticles were absorbed on VECs. The experimental results showed that anti-CD47-targeting nanocarriers could be effectively absorbed to the surface of vascular endothelium.

Table 4. CD47 sorption yield from protein solutions in water or PBS at different concentrations. CS-HA particles at a ratio R = 1.5 (CS: Mw 200×10^3 g/mol and DA = 48%; HA: Mw = 50×10^3 g/mol)

| Time [h] | Adsorption rate (%) | | | | | |
|----------|----------------------------|-----|-----|------------------------------|-----|-----|
| | input of CD47 in PBS [g/L] | | | input of CD47 in water [g/L] | | |
| | 0.1 | 0.3 | 0.5 | 0.2 | 0.4 | 0.6 |
| 2 | 95 | 91 | 90 | 93 | 91 | 85 |
| 4 | 97 | 98 | 95 | 95 | 93 | 90 |
| 6 | 100 | 99 | 97 | 99 | 99 | 95 |
| 16 | 100 | 100 | 100 | 100 | 100 | 100 |
| 24 | 100 | 100 | 100 | 100 | 100 | 100 |

PEC – polyelectrolyte complex; HA – hyaluronic acid; CS – chitosan; PBS – phosphate-buffered saline; PI – polydispersity index; DA – degree of acetylation; Mw – molecular weight.

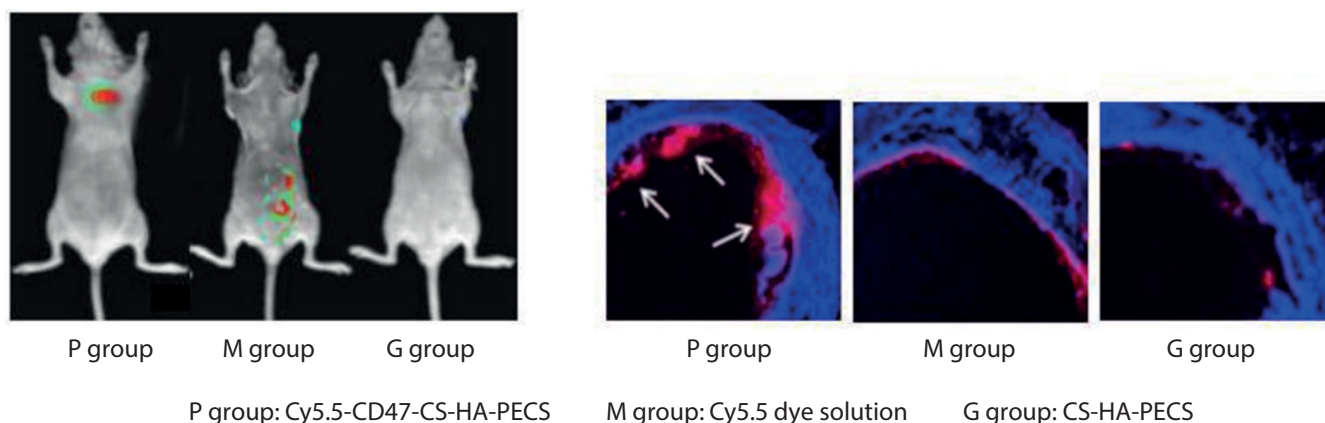


Fig. 6. Targeted adsorption of anti-CD47-CS-HA nanocomposite on atherosclerotic plaque. Using the IVIS 200 in vivo imaging system for small animals, images of fluorescence emission from animals were recorded and the Cy5.5-CD47 antibody-CS-HA-PECS were distributed around atherosclerotic plaques in vivo and compared with the control group. No fluorescence was detected in group G mice, which lacked antibody targeting labeling. The fluorescence distribution in group M labeled with fluorescent Cy5.5 dye solution alone is shown (left). After imaging, the aorta was harvested and sliced into sections. Five sections were taken from each vessel and the nuclei were stained with DAPI. Fluorescence microscopy confirmed the targeting of CD47 antibody-CS-HA-PECS to atherosclerotic plaque in vivo (right)

were distributed around the atherosclerotic plaque in vivo. Group G, without the antibody-targeted marker, showed no fluorescence in the body. The fluorescence distribution of the control group (M) labeled with the Cy5.5 dye solution was not localized to the plaque (Fig. 6). The fluorescence of the CD47 antibody-CS-HA-PECS was confirmed in vivo to target atherosclerotic plaque (Fig. 6).

Conclusions

In this work, experiments were conducted to obtain positively charged PEC nanoparticles from HA and CS which maintained their colloidal stability in physiological media for 30 days at room temperature. Antibodies can be quantitatively adsorbed at the particle interface without changing colloidal stability.

With reference to the relevant literature and our preliminary results, the following parameters were selected: low and medium molar mass CS (about 200×10^3 g/mol and lower), HA with a molar mass of about 50×10^3 g/mol and a charge ratio R ($n+/n-$) maintained in the range from 1.5 to 3.5. The experiments were carried out in deionized water or PBS and the pellet solid content was increased to 5% after centrifugation and re-dispersion. The diameter of the resulting nanoparticles decreased as R increased, but the conversion of the polymer to a colloid decreased. The results showed that the acetylation ratio of CS has little effect on the particle formation process.

The association of anti-CD47 with CS-HA nanoparticles resulted in rapid kinetics and high load capacity in both water and PBS. After anti-CD47 loading, the particle sizes observed in water and PBS were 375 nm and 620 nm, respectively, and the zeta potential remained positive. The CS-HA/anti-CD47 polyelectron nanoparticles remained stable for 3 weeks in both buffers. These results indicate that CS-HA polyelectron nanoparticles

have a high loading capacity for CD47 antibody and maintain good colloidal stability in PBS. More importantly, anti-CD47 nanocarriers were labeled with FITC fluorescent secondary antibody in vitro. The VEC strain was inoculated into a 24-well cell culture plate and co-cultured with CD47 nano-adjuvant for 24 h. The results showed that the anti-CD47-targeted nanocarrier can effectively adsorb to VECs. On the surface, the effective adsorption rate was about 90% and the nanoparticles targeted atherosclerotic plaques in in vivo experiments. Therefore, both CS and HA are non-toxic polysaccharides derived from biomass, laying the foundation for further research on the use of CD47 antibodies to target functional biopharmaceutical delivery nanosystems against atherosclerosis.

ORCID iDs

Jun Yu <https://orcid.org/0000-0002-3390-5901>
 Qiorong Ruan <https://orcid.org/0000-0002-7015-7666>
 Xiu Nie <https://orcid.org/0000-0002-1001-7709>

References

- Kojima Y, Volkmer JP, McKenna K, et al. CD47-blocking antibodies restore phagocytosis and prevent atherosclerosis. *Nature*. 2016; 536(7614):86–90. doi:10.1038/nature18935
- Lankalapalli S, Kolapalli VRM. Polyelectrolyte complexes: A review of their applicability in drug delivery technology. *Indian J Pharm Sci*. 2009;71(5):481. doi:10.4103/0250-474x.58165
- Sun W, Mao S, Mei D, Kissel T. Self-assembled polyelectrolyte nanocomplexes between chitosan derivatives and enoxaparin. *Eur J Pharm Biopharm*. 2008;69(2):417–425. doi:10.1016/j.ejpb.2008.01.016
- Vaidyanathan K, Gopalakrishnan S. Nanomedicine in the diagnosis and treatment of atherosclerosis: A systematic review. *Cardiovasc Hematol Disord Drug Targets*. 2017;17(2):119–131. doi:10.2174/1871529x17666170918142653
- Vila A, Sánchez A, Tobío M, Calvo P, Alonso M. Design of biodegradable particles for protein delivery. *J Control Release*. 2002;78(1):15–24. doi:10.1016/s0168-3659(01)00486-2
- Rodrigues FC, Singh K, Thakur G. Pharmaceutical application of chitosan derivatives. In: Nayak AK, Hasnain S, Pal D, eds. *Natural Polymers for Pharmaceutical Applications*. Vol. 2. New York, NY: Apple Academic Press; 2019:141–163. doi:10.1201/9780429328299-6

7. Kean T, Thanou M. Biodegradation, biodistribution and toxicity of chitosan. *Adv Drug Deliv Rev.* 2010;62(1):3–11. doi:10.1016/j.addr.2009.09.004
8. Kim SJ, Yoon SG, Lee KB, Park YD, Kim SI. Electrical sensitive behavior of a polyelectrolyte complex composed of chitosan/hyaluronic acid. *Solid State Ionics.* 2003;164(3):199–204. doi:10.1016/j.ssi.2003.08.005
9. Chen WB, Wang LF, Chen JS, Fan SY. Characterization of polyelectrolyte complexes between chondroitin sulfate and chitosan in the solid state. *J Biomed Mater Res A.* 2005;75(1):128–137. doi:10.1002/jbm.a.30393
10. Komoto D, Furuike T, Tamura H. Preparation of polyelectrolyte complex gel of sodium alginate with chitosan using basic solution of chitosan. *Int J Biol Macromol.* 2019;126:54–59. doi:10.1016/j.ijbiomac.2018.12.195
11. Karzar Jeddi M, Mahkam M. Magnetic nano carboxymethyl cellulose-alginate/chitosan hydrogel beads as biodegradable devices for controlled drug delivery. *Int J Biol Macromol.* 2019;135:829–838. doi:10.1016/j.ijbiomac.2019.05.210
12. Volod'ko AV, Davydova VN, Nedashkovskaya OI, et al. Morphology, electrokinetic characteristics and the effect on biofilm formation of carrageenan: Chitosan polyelectrolyte complexes. *Int J Biol Macromol.* 2018;117:1118–1124. doi:10.1016/j.ijbiomac.2018.05.215
13. Khanna R, Katti KS, Katti DR. Bone nodules on chitosan-polygalacturonic acid-hydroxyapatite nanocomposite films mimic hierarchy of natural bone. *Acta Biomater.* 2011;7(3):1173–1183. doi:10.1016/j.actbio.2010.10.028
14. Liu W, Sun S, Cao Z, et al. An investigation on the physicochemical properties of chitosan/DNA polyelectrolyte complexes. *Biomaterials.* 2005;26(15):2705–2711. doi:10.1016/j.biomaterials.2004.07.038
15. Prestwich GD. Hyaluronic acid-based clinical biomaterials derived for cell and molecule delivery in regenerative medicine. *J Control Release.* 2011;155(2):193–199. doi:10.1016/j.jconrel.2011.04.007
16. Yun YH, Goetz DJ, Yellen P, Chen W. Hyaluronan microspheres for sustained gene delivery and site-specific targeting. *Biomaterials.* 2004;25(1):147–157. doi:10.1016/s0142-9612(03)00467-8
17. Oh EJ, Park K, Kim KS, et al. Target specific and long-acting delivery of protein, peptide, and nucleotide therapeutics using hyaluronic acid derivatives. *J Control Release.* 2010;141(1):2–12. doi:10.1016/j.jconrel.2009.09.010
18. Yamane S, Iwasaki N, Majima T, et al. Feasibility of chitosan-based hyaluronic acid hybrid biomaterial for a novel scaffold in cartilage tissue engineering. *Biomaterials.* 2005;26(6):611–619. doi:10.1016/j.biomaterials.2004.03.013
19. Hahn SK, Hoffman AS. Preparation and characterization of biocompatible polyelectrolyte complex multilayer of hyaluronic acid and poly-L-lysine. *Int J Biol Macromol.* 2005;37(5):227–231. doi:10.1016/j.ijbiomac.2005.11.010
20. Malay O, Batigün A, Bayraktar O. pH- and electro-responsive characteristics of silk fibroin-hyaluronic acid polyelectrolyte complex membranes. *Int J Pharm.* 2009;380(1–2):120–126. doi:10.1016/j.ijpharm.2009.07.011
21. Lu HD, Zhao HQ, Wang K, Lv LL. Novel hyaluronic acid-chitosan nanoparticles as non-viral gene delivery vectors targeting osteoarthritis. *Int J Pharm.* 2011;420(2):358–365. doi:10.1016/j.ijpharm.2011.08.046
22. Duceppe N, Tabrizian M. Factors influencing the transfection efficiency of ultra-low molecular weight chitosan/hyaluronic acid nanoparticles. *Biomaterials.* 2009;30(13):2625–2631. doi:10.1016/j.biomaterials.2009.01.017
23. Verheul RJ, Slütter B, Bal SM, Bouwstra JA, Jiskoot W, Hennink WE. Covalently stabilized trimethyl chitosan-hyaluronic acid nanoparticles for nasal and intradermal vaccination. *J Control Release.* 2011;156(1):46–52. doi:10.1016/j.jconrel.2011.07.014
24. Chua PH, Neoh KG, Kang ET, Wang W. Surface functionalization of titanium with hyaluronic acid/chitosan polyelectrolyte multilayers and RGD for promoting osteoblast functions and inhibiting bacterial adhesion. *Biomaterials.* 2008;29(10):1412–1421. doi:10.1016/j.biomaterials.2007.12.019

Application of vascular endothelial growth factor at different phases of intestinal ischemia/reperfusion: What are its effects on oxidative stress, inflammation and telomerase activity?

Ayhan Korkmaz^{1,A,B,F}, Eser Oz Oyar^{2,A,F}, Zuhul Yildirim^{3,A–F}, Arzu Pampal^{4,A,C,D,F}, Nese Lortlar Unlu^{5,C,F}, Hakan Akbulut^{6,C,F}

¹ Department of Physiology, Faculty of Medicine, Gazi University, Ankara, Turkey

² Department of Physiology, Faculty of Medicine, Katip Celebi University, Izmir, Turkey

³ Etimesgut Public Health Laboratory, Ankara, Turkey

⁴ Department of Pediatric Surgery, Faculty of Medicine, Ufuk University, Ankara, Turkey

⁵ Department of Histology and Embrology, Faculty of Medicine, Bahcesehir University, Istanbul, Turkey

⁶ Department of Medical Oncology, Faculty of Medicine, Ankara University, Turkey

A – research concept and design; B – collection and/or assembly of data; C – data analysis and interpretation;

D – writing the article; E – critical revision of the article; F – final approval of the article

Advances in Clinical and Experimental Medicine, ISSN 1899–5276 (print), ISSN 2451–2680 (online)

Adv Clin Exp Med. 2020;29(12):1417–1424

Address for correspondence

Zuhul Yildirim

E-mail: zyildirim2004@yahoo.com

Funding sources

None declared

Conflict of interest

None declared

Received on March 29, 2020

Reviewed on April 20, 2020

Accepted on August 11, 2020

Cite as

Korkmaz A, Oyar EO, Yildirim Z, Pampal A, Unlu NL, Akbulut H. Application of vascular endothelial growth factor at different phases of intestinal ischemia-reperfusion: What are its effects on oxidative stress, inflammation and telomerase activity? *Adv Clin Exp Med.* 2020;29(12):1417–1424. doi:10.17219/acem/126297

DOI

10.17219/acem/126297

Copyright

© 2020 by Wrocław Medical University

This is an article distributed under the terms of the Creative Commons Attribution 3.0 Unported (CC BY 3.0) (<https://creativecommons.org/licenses/by/3.0/>)

Abstract

Background. Intestinal ischemic reperfusion injury (IRI) represents a great challenge in clinical practice, with high morbidity and mortality. Vascular endothelial growth factor (VEGF), as a signal protein, contributes to vasculogenesis and angiogenesis.

Objectives. To evaluate the local effectiveness of VEGF following intestinal IRI and its relation with application time.

Material and methods. Thirty Wistar albino rats were allocated to 5 groups and underwent laparotomy. The superior mesenteric arteries (SMA) were dissected in 4 groups, while the control group (Gr C) underwent a resection of small and large intestines. The VEGF group (Gr V) received VEGF following SMA dissection, with no further intervention, and the remaining 3 groups were subjected to ischemia for 90 min through occlusion of SMA and reperfusion for 4 h. Ischemic reperfusion group (Gr I/R) received no additional medication, while the remaining 2 groups received VEGF just before ischemia (Gr V+I/R) and during reperfusion (Gr I/R+V).

Results. Both applications of VEGF caused decreases in plasma levels of interleukin 6 (IL-6), tumor necrosis factor α (TNF- α), intestinal malondialdehyde (MDA), oxidized glutathione, protein carbonyl levels, and increases in intestinal total glutathione and superoxide dismutase (SOD) levels. Telomerase activity, which disappeared for Gr I/R, was found to be elevated following both treatment groups. Similarly, the histopathological scores were found better for both treatment groups, but Gr V-I/R represented best outcomes.

Conclusions. The findings of our study revealed that VEGF, applied either before ischemia or during reperfusion, is effective on local damage following intestinal IRI. By interpreting the biochemical analysis and histopathological findings, we conclude either treatment option to be considered according to the reason of intestinal IRI.

Key words: inflammation, VEGF, telomerase activity, intestinal ischemic reperfusion injury, oxidative stress

Introduction

Intestinal ischemic reperfusion injury (IRI), due to the occlusion at the level of superior mesentery artery (SMA), is connected to parenchymal damage at the intestine as a result of hypoxia, resultant adenosine triphosphate (ATP) depletion and intracellular acidosis at the early phase. The intestinal mucosa and submucosa show deterioration resulting from ischemic damage and ischemia, which also causes stagnation in the bowel and damage to the intestinal barriers. If the condition is untreated, the initial damage is exacerbated and ischemia of the muscle layers becomes inevitable, possibly leading to intestinal perforation, sepsis and even death.¹ As the clinical problem is resolved in IRI, the main problem at the tissue level is the additional inflammatory process taking place due to reperfusion.^{2,3} Evidence supports local and systemic effects of IRI, as many injurious substances and factors are activated during IRI and are released to systemic circulation through venous and/or lymphatic routes.²⁻⁵ Moreover, IRI has been shown to induce apoptosis of not only intestinal cells but also remote organs as a result of reactive oxygen species (ROS) and pro-inflammatory cytokine production.⁴

Vascular endothelial growth factor (VEGF) is a participant of vital signaling proteins. As a mitogen agent for endothelium, VEGF induces vascular growth and increases microvascular permeability. It acts via nitric oxide (NO) dependent pathways and stimulates vasodilation.⁵ Vessel growth is induced by means of pre-existing vasculature and this expansion is important, especially in case of inadequate blood supply. Hypoxia contributes to angiogenesis, as it is the major stimulant producing VEGF and its receptors.⁶

The VEGF was demonstrated as a recuperative agent of IRI of various organs like myocardium, liver and spinal cord.⁷⁻¹¹ Thus, we wanted to establish whether it is as effective on intestinal IRI as other organs – and if so, does the timing of its application matter. We designed a study in order to evaluate the effectiveness of VEGF on intestinal IRI used either before ischemia or during reperfusion.

Material and methods

The permission for the experimental study was granted by Animal Ethics Committee of Gazi University (Ankara, Turkey) and the study was completed due to the dictates of the Research Committee at the Experimental Research Center of Gazi University School of Medicine.

Thirty male adult Wistar albino rats weighing 220–270 g (mean weight 240 ± 10 g) were included in the study. All animals were housed under standard temperature and humidity with light and dark cycles of 10 h and 14 h, respectively. No water, food and light restrictions were applied to animals. During the experiments, humane care was given to all animals according to Principles of Laboratory Animal Care and the Guide for the Care and Use

of Laboratory Animals of National Health Institutes (NHS; Bethesda, USA). The animals were anaesthetized using xylazine hydrochloride (5 mg/kg) (Alfazyne; Ege Vet, Izmir, Turkey) and ketamine hydrochloride (40 mg/kg) (Ketalar; Eczacibasi, Istanbul, Turkey), and every surgical procedure was performed under sterile conditions by the surgeon of the team (AP).

All the rats were randomly allocated to 5 groups and underwent a median laparotomy:

- Control group (Gr C, n = 6) underwent excision of small and large intestines with no further intervention.

- VEGF group (Gr V, n = 6) underwent only dissection of SMA and received VEGF (0.8 µg/kg) through the caudal caval vein.

- IRI group (Gr I/R, n = 6) underwent dissection and occlusion of SMA. After the dissection of SMA, the vessel was occluded for 90 min using a microclamp at the point where it branches from abdominal aorta. Pulseless mesenteric artery accompanying pale jejunoileal segments confirmed the ischemia.

- VEGF-IRI group (Gr V-I/R, n = 6) received VEGF (0.8 µg/kg) through caudal caval vein before the surgical procedure. The animals in this group underwent dissection, and occlusion of SMA for 90 min following drug administration.

- IRI-VEGF group (Gr I/R-V, n = 6) underwent dissection, and occlusion of SMA for 90 min. The animals in this group received VEGF (0.8 µg/kg) through the caudal caval vein at the beginning of reperfusion.

The infusion dose for VEGF was chosen as the minimum effective dose as defined according to the previous study by Oz Oyar et al.⁷ Animals in all groups but Gr C underwent a relaparotomy at the 4th hour of reperfusion, and small bowel and proximal large bowel segments of the animals were removed. The rats were sacrificed with aspiration of cardiac blood and the blood samples were placed in EDTA tubes. Plasma samples were separated by centrifugation (3000 × g for 10 min at 4°C) and frozen at –80°C. The excised bowel segment was washed in cold 0.9% NaCl, wiped, and weighed. To perform biochemical analysis and histopathological evaluation, the bowel was cut into 3 equal pieces. The 1st (representing the most proximal portion) and 3rd (representing the most distal portion) pieces were fixed in liquid nitrogen and kept frozen at –80°C, whereas the 2nd (representing the middle portion) piece was laid in 10% neutral buffered formalin.

Biochemical analysis

Western blot analysis

Intestinal tissues were weighed, diluted with lysis buffer and homogenized at a ratio of 1/10 (w/v). Homogenates were centrifuged at 2500 rpm for 10 min at +4°C. To quantify the protein levels, BCA Assay Kit (Pierce, Waltham, USA) was used. The heat shock protein (HSP70) (Rabbit,

SPA810; Stressgen, San Diego, USA) and catalase (CAT) (Rabbit, ab1877; Abcam, Cambridge, UK) primary antibodies, used for western blotting analysis and β -actin, were used as housekeeping proteins in order to quantify the other primary antibodies.

Determination of intestinal malondialdehyde levels

Lipid peroxidation was measured using the test published by Gérard-Monnier et al.¹² The malondialdehyde (MDA) levels were also recalculated from our MDA standards produced by the acid hydrolysis of 1,1,3,3-tetramethoxypropane.

Determination of intestinal superoxide dismutase activity

Superoxide dismutase (SOD) activity was measured using nitroblue tetrazolium (NBT) reduction in order to inhibit SOD activity. A superoxide generator (xanthine and xanthine oxidase) was used to trigger inhibition and the amount of SOD required to produce 50% inhibition was accepted to define 1 IU.¹³

Determination of intestinal protein carbonyl group levels

Protein carbonyl group (PC) levels were measured and described by Buss et al.¹⁴ Carbonyl residues were determined using 2,4-dinitrophenylhydrazine (DNPH) and carbonyl contents were calculated by obtaining the enzyme-linked immunosorbent assay (ELISA) of the DNPH-treated samples at 480 nm.

Determination of intestinal total and oxidized glutathione levels

Total glutathione (TGSH) and oxidized glutathione (GSSG) levels were determined with glutathione reductase (GR) as described by Tietze.¹⁵

Determination of intestinal telomerase activity

Telo TAGGG Telomerase PCR ELISA Plus kit (Roche, Mannheim, Germany) was used to determine the telomerase activity. Reactive telomerase activity was quantified with photometric enzyme immunoassay using TRAP and presented as percentage.

Determination of intestinal hypoxia inducible factor 1 α levels

Hypoxia-inducible factor 1 α (HIF-1 α) levels were defined with a solid phase sandwich ELISA (Rat HIF-1 α ELISA Kit; USCN Life Science Inc Wuhan, China; Cat No. E90798Ra, Lot No. 111011285).

Plasma tumor necrosis factor α and interleukin 6 measurements

Plasma tumor necrosis factor α (TNF- α) and interleukin 6 (IL-6) levels were also determined by a solid phase sandwich ELISA (Rat TNF- α ELISA Kit; Cat No. ER3TNFA, Lot No. LF144120, Rat IL-6 ELISA Kit; Cat No. EH2IL-6, Lot No. KL138035; Thermo Fisher Scientific, Waltham, USA).

Histopathological evaluation

The intestinal pieces laid in 10% buffered formalin were fixed for 72 h and set in paraffin blocks. Afterwards, five-micrometer-thick sections were cut axially using a microtome (RM 2245; Leica, Wetzlar, Germany). Hematoxylin and eosin (H&E) staining was performed for the sections and the slides were evaluated under a light microscope (DMI 4000 B; Leica, Wetzlar, Germany) by the histologist of the team (NLU) who was blind to the study groups. In order to quantify the ischemic changes at the mucosal level, a scoring system described by Chiu et al. was used.¹⁶

Immunohistochemical evaluation

After fixing in formalin, embedding in paraffin and cutting sections 5 μ m in thickness, tissue sections were placed in an incubator at 37°C for a night and at 60°C for 1 h. Xylol was applied twice for 15 min. The slides were then placed in 96% absolute alcohol, 80% ethanol for 10 min and distilled water twice for 5 min. For caspase-3 immunoperoxidase, the slides were placed in a high temperature microwave oven in 10% citrate buffer. After the tissue was left for 20 min at room temperature, it was marked with a hydrophobic pen (Super PAP PEN IM3580; Immunotech, Beckman Coulter Co., Brea, USA). In order to block endogenous peroxidase activity, the tissue was washed with distilled water and 0.02 M PBS (pH 7.2) (Lab Vision Corp., Fremont, USA) and 0.3% hydrogen peroxide (Thermo Fisher Scientific) was applied thereafter for 10 min. After washing with PBS, ultra V block (TA-125-UB; Thermo Fisher Scientific) was utilized. Primary antibody including caspase-3 (rabbit polyclonal antibody; Lab Vision/Neo Markers Corp.) was applied for 1 h, the samples were washed with phosphate-buffered saline (PBS), and a post-PBS level was applied (biotinylated goat anti-polyvalent and streptavidin peroxidase, respectively). After having been rewashed with PBS, the specimens were placed for 10 min in AEC (3-amino, 9-ethylcarbazole) (TA_125-HA; Thermo Fisher Scientific) chromogen. Finally, the counterstain with Mayer hematoxylin was performed for 2 min. All the slides were evaluated using a light microscope (DMI 4000 b; Leica) by the same histologist (NLU). The relative intensity of immunoreactivity staining was quantified as described by McCarty et al., focusing on the intensity and the distribution of a specific stain.¹⁷ A histological score (H-score) was formulated as the sum of the percentages

of positively stained cells multiplied by the weighted intensity of staining. The H-score was calculated with the formulation of $\sum Pi(I + 1)$, as I represented intensity of staining (0 – none; 1 – mild; 2 – moderate; and 3 – intense) and Pi represented the fraction of stained cells for each intensity.

Statistical analysis

Statistical package SPSS for Windows v. 18.0 (SPSS Inc., Chicago, USA) was used for analyses with the descriptive statistics presented as mean \pm standard deviation (SD). Kruskal–Wallis test and Mann–Whitney U test were used for statistical analyses and Spearman's correlation test was used to evaluate the correlation between variables. A p-value less than 0.05 was considered to be statistically significant.

Results

All the animals survived the experiment. The results obtained from each group are presented in Tables 1, 2.

Intestinal MDA levels

The MDA levels for proximal and distal intestinal segments of Gr I/R were elevated when compared to Gr C ($p < 0.05$). All treatment groups, not being superior to one another, represented a significant decrease of MDA level at the proximal segment whereas only Gr V-I/R represented a significant decrease at the distal segment (Table 1).

Table 1. Biochemical analysis of intestinal segments and plasma

| Parameter | Group | | | | |
|-----------------------------------|--------------------|--------------------|---------------------|---------------------------------|------------------------------------|
| | Control | VEGF | I/R | V-I/R | I/R-V |
| MDA-proximal [μ M] | 4.08 \pm 0.40 | 4 \pm 0.18 | 8.16 \pm 1.56* | 4.87 \pm 0.58 [#] | 4.99 \pm 0.68 [#] |
| MDA-distal [μ M] | 3.29 \pm 0.46 | 3.3 \pm 0.71 | 8.44 \pm 2.97* | 4.84 \pm 1.19 [#] | 6.84 \pm 1.51 |
| TGSH-proximal [μ M] | 326 \pm 32.78 | 317.2 \pm 13.6 | 183.16 \pm 31.5* | 299.66 \pm 86.48 [#] | 250.33 \pm 48.74 |
| TGSH-distal [μ M] | 488.45 \pm 48.76 | 467.26 \pm 60.55 | 160.63 \pm 35.77* | 341 \pm 42.78 [#] | 290.32 \pm 60.9 [#] |
| GSSG-proximal [μ M] | 3.93 \pm 1.39 | 3.91 \pm 0.76 | 8.29 \pm 1.46* | 3.62 \pm 1.19 [#] | 4.66 \pm 0.83 [#] |
| GSSG-distal [μ M] | 5.28 \pm 1.36 | 5.5 \pm 1.37 | 14.03 \pm 2.19* | 6.07 \pm 0.97 [#] | 6.58 \pm 1.01 [#] |
| SOD-proximal [AU] | 6.15 \pm 1.32 | 6.9 \pm 0.31 | 3.32 \pm 0.75* | 5.92 \pm 0.89 | 5.33 \pm 1.71 |
| SOD-distal [AU] | 8.54 \pm 2.07 | 8.65 \pm 1.52 | 3.54 \pm 0.94* | 7.02 \pm 2.28 [#] | 5.35 \pm 1.31 [#] |
| PC-proximal [AU] | 0.103 \pm 0.013 | 0.101 \pm 0.005 | 0.114 \pm 0.011 | 0.097 \pm 0.010 | 0.105 \pm 0.006 |
| PC-distal [AU] | 0.191 \pm 0.004 | 0.194 \pm 0.002 | 0.199 \pm 0.003* | 0.172 \pm 0.027 [#] | 0.184 \pm 0.008 [#] |
| CAT-proximal [AU] | 0.83 \pm 0.06 | 0.84 \pm 0.16 | 0.47 \pm 0.09* | 0.55 \pm 0.1 [#] | 0.67 \pm 0.15 |
| CAT-distal [AU] | 1.13 \pm 0.14 | 1.18 \pm 0.13 | 0.69 \pm 0.12 | 0.79 \pm 0.04 | 0.85 \pm 0.12 |
| HSP70-proximal [AU] | 0.51 \pm 0.24 | 0.49 \pm 0.2 | 0.82 \pm 0.18* | 0.67 \pm 0.2 | 0.64 \pm 0.39 |
| HSP70-distal [AU] | 0.74 \pm 0.13 | 0.75 \pm 0.16 | 1.06 \pm 0.55 | 0.81 \pm 0.21 | 0.79 \pm 0.17 |
| Telomerase activity (%) | 100 | 83.33 | 0* | 50 [#] | 66.67 [#] |
| Intestinal HIF-1 α [ng/mL] | 9.62 \pm 4.02 | 13.89 \pm 2.45 | 15.01 \pm 0.51* | 13.84 \pm 2.02 | 13.56 \pm 3.51 |
| Plasma TNF- α [pg/mL] | 124.22 \pm 20.70 | 110.39 \pm 19.90 | 326.27 \pm 84.93* | 139.06 \pm 5.05 [#] | 114.76 \pm 14.93 [#] |
| Plasma IL-6 [pg/mL] | 16.30 \pm 1.81 | 29.78 \pm 5.41 | 280.24 \pm 89.96* | 131.69 \pm 24.87 [#] | 73.65 \pm 6.67 ^{#&} |

Biochemical analysis of intestinal segments and plasma, results presented as mean \pm standard deviation (SD); * $p < 0.05$ compared to control group; [#] $p < 0.05$ compared to I/R; [&] $p < 0.05$ when compared to V-I/R group; VEGF – vascular endothelial growth factor; MDA – malondialdehyde; TGSH – total glutathione; GSSG – oxidized glutathione; SOD – superoxide dismutase; PC – protein carbonyl group; CAT – catalase; HSP – housekeeping protein; HIF-1 α – hypoxia-inducible factor 1 α ; TNF- α – tumor necrosis factor α ; IL-6 – interleukin 6.

Table 2. Mean histopathological scoring, intestinal caspase-3 immunoreactivity and MMP-9 levels for all groups

| Parameter | Control | VEGF | I/R | V-I/R | I/R-V |
|-------------------------------------|-----------------|-----------------|------------------|------------------------------|------------------------------|
| Mean histopathologic scores (grade) | 0.16 | 0.33 | 2.66* | 0.5 ^{#&} | 1.16 [#] |
| Caspase-3 | 0.85 \pm 0.37 | 1.07 \pm 0.41 | 2.95 \pm 0.45* | 1.02 \pm 0.45 [#] | 1.2 \pm 0.44 [#] |
| MMP-9 | 1.78 \pm 0.35 | 1.83 \pm 0.42 | 3.07 \pm 0.20* | 2.15 \pm 0.46 [#] | 2.32 \pm 0.28 [#] |

Intestinal caspase-3 immunoreactivity and MMP-9 levels, results presented as mean \pm standard deviation (SD); * $p < 0.05$ compared to control group; [#] $p < 0.05$ when compared to I/R group; [&] $p < 0.05$ compared to I/R-V group; VEGF – vascular endothelial growth factor; MMP-9 – matrix metalloproteinase 9.

Intestinal SOD activity

The SOD activity of both proximal and distal intestinal segments of Gr I/R were found decreased when compared to Gr C ($p < 0.05$). Either treatment represented a significant elevation only for the distal segment (Table 1).

Intestinal PC levels

The PC levels of distal intestinal segments of Gr I/R were found increased when compared to Gr C ($p < 0.05$) and either treatment represented significant fall for the same segment (Table 1).

Intestinal CAT activity

Catalase activity was found to decrease significantly at the proximal segment in Gr I/R when compared to Gr C ($p < 0.05$) and the rise of CAT was statistically significant only at the proximal segment for Gr V-I/R (Table 1).

Intestinal TGS and GSSG levels

A statistically significant increase in TGS level and a statistically significant decrease in GSSG level were seen at both proximal and distal intestinal segments of Gr I/R when compared to Gr C. Gr V-I/R represented a significant increase in TGS for both segments, whereas Gr I/R-V represented a significant rise at the distal segment. Both treatment groups represented a significant decrease in GSSG for both segments, but neither treatment was found superior (Table 1).

Intestinal telomerase activity

Telomerase activity was found to decrease to 0 in Gr I/R when compared to Gr C ($p < 0.05$) and all treatment groups recuperated the telomerase activity significantly (Table 1).

Intestinal HIF-1 α levels

The HIF-1 α levels were found increased in Gr I/R when compared to Gr C ($p < 0.05$), but the decrease in treatment groups were insignificant (Table 1).

Plasma TNF- α , and IL-6 levels

Both of the parameters were found significantly increased in Gr I/R when compared to Gr C. Either treatment group represented a significant decrease for TNF- α , and IL-6 when compared to Gr I/R. Despite no changes in TNF- α levels, Gr I/R-V had a more significant decrease to Gr V-I/R in terms of decrease in IL-6 levels ($p < 0.05$) (Table 1).

Histopathological evaluation

Gr I/R represented significant ischemic changes, such as generalized desquamation and moderate to severe mucosal congestion, when compared to Gr C. Both treatment groups represented enhanced histopathological findings, such as focal desquamation and mild mucosal congestion (Fig. 1). The comparison of histopathological scoring of treatment groups revealed a better outcome for Gr V-I/R when compared to Gr I/R-V with a statistically significant difference (Table 2). In terms of caspase activity and matrix metalloproteinase 9 (MMP-9) scores, Gr I/R represented the highest score and both treatment groups represented better scores when compared to Gr I/R ($p < 0.05$) (Table 2).

Discussion

The VEGF is a key signal protein that stimulates expansion of new vasculature from surviving vessels in case of hypoxia.⁷ This angiogenic activity is also supported by the vasodilator effect of protein through nitric oxide (NO) production. The VEGF is also shown to have antioxidant effects and to modulate endothelial dysfunction during IRI. In this study, we aimed to evaluate the effectiveness of VEGF on intestinal IRI during the different phases of the injury. For this purpose, experimental intestinal IRI model was established as described by Dwivedi et al. and an intravenous VEGF dose of 0.8 $\mu\text{g}/\text{kg}$ was used for treatment, as this dose was proven to be the minimal effective concentration in an earlier study.^{11,18} The VEGF was applied either before ischemia or during the reperfusion of the experimental intestinal IRI model and it was found that the drug was effective in both situations. This is also the first study that evaluated the changes of the bowel at separate levels (proximal and distal bowel segments) after ischemia and reperfusion. Both of the treatment groups represented enhancement in terms of tissue MDA, TGS/GSSG, SOD, PC, and CAT levels for both intestinal segments. However, some of the parameters showed different distributions – for example, better results with distal intestinal segments and better results with VEGF treatment before intestinal I/R. The differences between proximal and distal intestinal segments can be attributed to the anatomic settlement. Marginal artery (of Drummond) is the major anastomosis between superior and inferior mesenteric arteries. The marginal artery forms a continuous arterial circle along the inner border of the colon and it is probable that during SMA occlusion and reperfusion period the distal segments of the intestine was supported by inferior mesenteric artery (IMA) and presented better results. We observed that some parameters were recuperated only for Gr V-I/R (like MDA for distal segments, TGS and MDA for proximal segments). Application time of VEGF resulted in a difference that is of interest and difficult to justify.

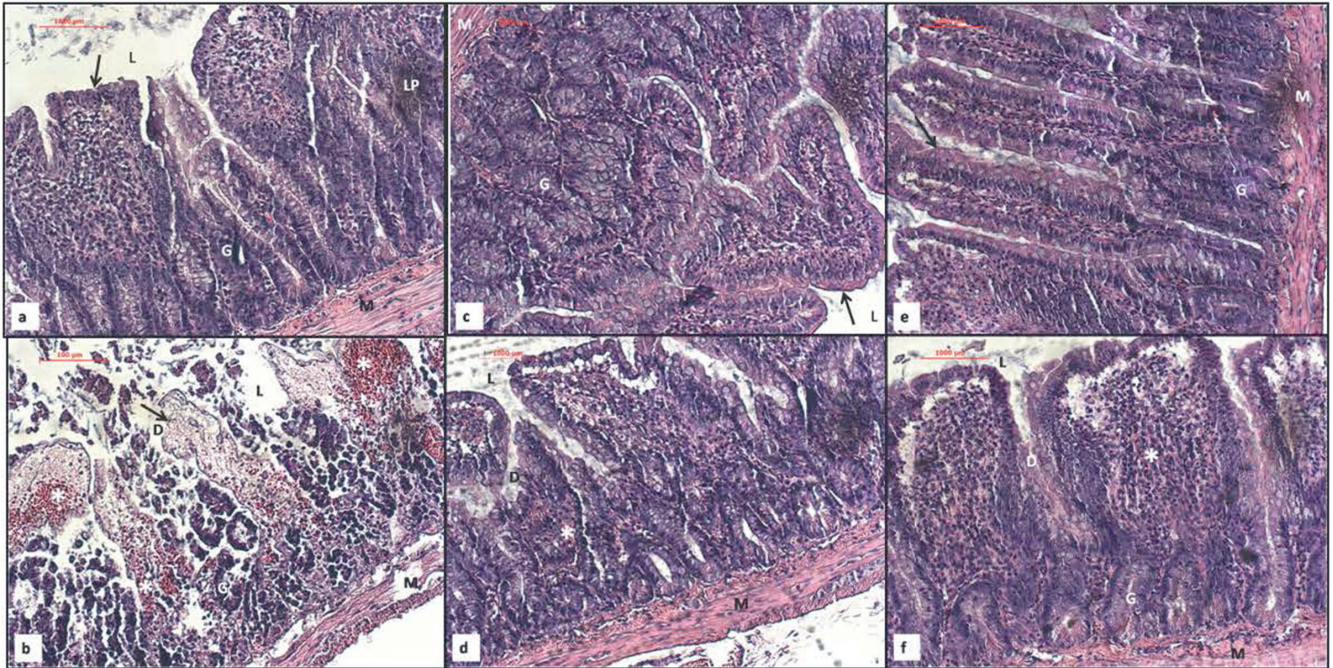


Fig. 1. Histopathological view of intestinal segments stained with H&E in all groups. Panel (a) represents intestinal structures of Gr C within normal limits; (b) represents generalized desquamation (D) within intestinal epithelium and mucosal congestion (*) in Gr I/R; (c) represents intestinal structures of Gr V within normal limits; (d) represents localized desquamation (D) and mucosal congestion (*) with intact muscular layer in Gr I/R-V; (e) represents intestinal structures within normal limits of Gr V-I/R; and (f) represents localized desquamation (D) and mucosal congestion (*) of Gr V-I/R. Arrow – intestinal epithelium; L – intestinal lumen; G – intestinal secretory glands; LP – lamina propria; M – muscular layer; Bar = 1000 μ

Tissue hypoxia is inevitable as a result of capillary perfusion failure. Activation of hypoxia-inducible factor (HIF-1), which is the main regulator of pathophysiological response to hypoxia, has been shown to play an important role in inducing intestinal damage. This is why HIF-1 α , the subunit of heterodimeric transcription factor HIF-1, is accepted as the main transcriptional regulator for cellular hypoxia. However, HIF-1 α , constantly produced and kept low under normoxic conditions, increases rapidly during hypoxia and dimerizes with constitutively present HIF-1 β to stimulate VEGF production.^{19,20} Studies evaluating the effects of IRI on HIF-1 α at separate organs revealed that the ischemic injury is related to elevation of HIF-1 α .^{21,22} Also, Poynter et al. represented the relation between HIF-1 α and VEGF in an experimental ischemic myocardial injury.²¹ The findings of our study supported HIF-1 α elevation in Gr I/R, but apart from the other studies, even the treatment groups represented a decrease in HIF-1 α levels; such decrease was statistically insignificant. As mentioned previously, HIF-1 α is increased rapidly during hypoxia and dimerized with HIF-1 β in order to stimulate VEGF production and induce angiogenesis. Although a decrease in HIF-1 α levels is expected in the case of exogenous administration of VEGF, no such relationship was found in the findings of our study. It is probable that either HIF-1 α production is not affected by VEGF levels or the appearance of free radicals resulted in HIF-1 α being suspended in intestinal tissues despite its short half-life period.

Telomere is a DNA-protein complex consisting of 6 base repetitive sequences and telomere binding proteins at the end of the chromosomes of eukaryotic organisms. Telomeres protect against events such as disruption of the terminal regions of chromosomes. However, telomere segments are shortened by the cell cycle and cell division, which triggers cellular apoptosis.²³ Telomerase is a ribonucleoprotein reverse transcriptase that adds telomeric DNA repeat sequences to the 3'-end of chromosomes. Despite its essential role for telomere homeostasis, its activation leads to unlimited cell proliferation, probably resulting in neoplastic transformation. However, this reverse transcriptase also reactivates during tissue repair.²⁴ Eckers et al. reported that oxidative stress and elevated ROS are closely related to endothelial cell apoptosis and endothelial dysfunction, loss of telomerase activity and telomere shortening.²⁵ Werner et al. presented the protective effect of upregulated telomerase activity against endothelial apoptosis in case of oxidative stress.²⁶ Zaccagnini et al. showed that there was a positive regulation of VEGF and telomerase activity in a hind limb ischemia study in rats.²⁷ The IRI related oxidative stress was also obtained in our study and we found that telomerase activity disappeared in the I/R group, and both treatment groups exhibited elevated telomerase activity, supporting reactivation of telomerase against injury.

The heat shock proteins are a class of molecular chaperons that exist in cell cytoplasm in order to prevent

the formation of nonfunctional structures. It is thought to act as a cytosolic chaperone that plays a role in facilitating protein folding, degradation, complex assembly, and translocation. The best known members are the heat-inducible form, also known as HSP72 or HSP70i, and are also present in the structural form, also called HSC70, HSP73 or HSC73.²⁸ HSP70 interacts with hydrophobic peptide parts of proteins that are not ATP-bound. These cytoprotective proteins are induced by many factors, such as infection, oxidative stress, osmotic stress, hyperthermia, ultraviolet exposure, and heavy metals. In the presence of these inducers, chaperone properties have been reported to reduce protein aggregates and intracellular inclusions. The catalytic unit of telomerase (TERT) is known to interact with chaperone proteins. The 70 kDa heat shock proteins (HSP70), as a chaperone protein was shown not to be vital for telomerase activity but also to be important for telomerase stability.²⁴ The literature review revealed a number of IRI studies on various organs representing elevation of HSP70.²⁹ We also evaluated the HSP70 levels in our study and found the significant elevation of HSP70 at only the proximal intestinal segment, where IMA does not supply in Gr I/R, supporting the vascular compromise in that region. HSP70 was shown to be a cell-protector for apoptosis, but its overexpression was generally proven to be related to poor prognosis.³⁰ Despite insignificant changes in HSP70 in our treatment groups, caspase activity was found to be elevated with IRI and the treatment with VEGF normalized this activity. Even though the last step of either intrinsic or extrinsic pathways of apoptosis is caspase-3 activation, DNA damage and heat shock proteins are mainly involved in intrinsic pathway. However, the increase of HSP70 and caspase-3 in Gr I/R is rational, but the presence of caspase activation in the treatment groups despite low HSP70 is beyond our predictions. These findings supported the claim that the extrinsic pathway stimulated abundantly during I/R is somehow less affected.

Intestinal IRI is a clinical entity related to life-threatening conditions, such as mesenteric artery occlusion, intestinal transplantation, intussusceptions, acute blood loss, and trauma. Each of these conditions, however, causes the same physiological consequence and requires separate approaches in the clinical settings. In this study, we applied VEGF either before ischemia or during the reperfusion of the experimental intestinal IRI model and aimed to evaluate whether any changes occur. We found that the drug was effective in terms of enhancing intestinal IRI in both situations; apart from that, the treatment before ischemic process was found slightly superior to the other therapy. In the light of these findings, we can probably speculate on the benefits of VEGF usage of different timetables for different causes of intestinal IRI. It is obvious that further studies are needed to support this inference.

Conclusions

Intestinal IRI is a clinical entity related to life-threatening conditions like mesenteric artery occlusion, intestinal transplantation, intussusception, acute blood loss, and trauma. Each of these conditions, however, causes the same physiological consequence and has separate approaches in the clinical settings. That is why, the use of VEGF at different timetables of the ischemic reperfusion process could serve different outcomes for different reasons of IRI.

ORCID iDs

Ayhan Korkmaz  <https://orcid.org/0000-0001-5702-8184>
 Eser Oz Oyar  <https://orcid.org/0000-0003-1805-4149>
 Zuhal Yildirim  <https://orcid.org/0000-0002-2808-7860>
 Arzu Pampal  <https://orcid.org/0000-0002-7771-0380>
 Nese Lortlar Unlu  <https://orcid.org/0000-0002-1716-9350>
 Hakan Akbulut  <https://orcid.org/0000-0003-1631-5739>

References

- Schellekens D, Reisinger KW, Lenaerts K. SM22: A plasma biomarker for human transmural intestinal ischemia. *Ann Surg.* 2018;268(1):120–126.
- Kesik V, Guven A, Vurucu S, et al. Melatonin and 1400 W ameliorate both intestinal and remote organ injury following mesenteric ischemia/reperfusion. *J Surg Res.* 2009;157(1):97–105.
- Sagiroglu T, Sezer A, Altaner S, Umit H, Yalta T, Yagci MA. The effects of sirolimus on target organs during mesenteric ischemia and reperfusion damage in an experimental rat model. *Curr Ther Res Clin Exp.* 2011;72(2):79–93.
- Al-Salam S, Hashmi S. Myocardial ischemia reperfusion injury apoptotic, inflammatory and oxidative stress role of galectin-3. *Cell Physiol Biochem.* 2018;50(3):1123–1139.
- Oz Oyar E, Korkmaz A, Kardeş O, Ömeroğlu S. Aortic cross-clamping-induced spinal cord oxidative stress in rabbits: The role of a novel antioxidant adrenomedullin. *J Surg Res.* 2008;147(1):143–147.
- Ferrara N. Role of vascular endothelial growth factor in regulation of physiological angiogenesis. *Am J Physiol Cell Physiol.* 2001;280(6):1358–1366.
- Oz Oyar E, Kardeş O, Korkmaz A, Ömeroğlu S. Effects of vascular endothelial growth factor on ischemic spinal cord injury caused by aortic cross-clamping in rabbits. *J Surg Res.* 2009;151(1):94–99.
- Kirisci M, Oktar GL, Ozogul C, et al. Effects of adrenomedullin and vascular endothelial growth factor on ischemia/reperfusion injury in skeletal muscle in rats. *J Surg Res.* 2013;185(1):56–63.
- Yang Y, Shi C, Hou X, et al. Modified VEGF targets the ischemic myocardium and promotes functional recovery after myocardial infarction. *J Control Release.* 2015;213:27–35.
- Li GH, Luo B, Lv YX, et al. Dual effects of VEGF-B on activating cardiomyocytes and cardiac stem cells to protect the heart against short- and long-term ischemia-reperfusion injury. *J Transl Med.* 2016;14(1):116–130.
- Cao D, Wang M, Gong J, Wei S, Gong J, Li J. Exogenous vascular endothelial growth factor delivery prior to endothelial precursor cell transplantation in orthotopic liver transplant-induced hepatic ischemia reperfusion injury. *Liver Transplant.* 2017;23(6):804–812.
- Gérard-Monnier D, Erdelmeier I, Régnard K, Moze-Henry N, Yadan JC, Chaudière J. Reactions of 1-methyl-2-phenylindole with malondialdehyde and 4-hydroxyalkenals: Analytical applications to a colorimetric assay of lipid peroxidation. *Chem Res Toxicol.* 1998;11(10):1176–1183.
- Beauchamp C, Fridovich I. Superoxide dismutase: Improved assays and an assay applicable to acrylamide gels. *Anal Biochem.* 1971;44(1):276–287.
- Buss H, Chan TP, Shis KB, Domigan NM, Winterboum CC. Protein carbonyl measurement by a sensitive ELISA method. *Free Radic Biol Med.* 1997;23(3):361–366.
- Tietze F. Enzymic method for quantitative determination of nanogram amounts of total and oxidized glutathione: Applications to mammalian blood and other tissues. *Anal Biochem.* 1969;27(3):502–522.

16. Chiu CJ, McArdle AH, Brown R, Scott HJ, Gurd FN. Intestinal mucosal lesion in low-flow states. I. A morphological, hemodynamic, and metabolic reappraisal. *Arch Surg*. 1970;101:478–483.
17. McCarty KS Jr, Miller LS, Cox EB, Konrath J, McCarty KS Sr. Estrogen receptor analyses: Correlation of biochemical and immunohistochemical methods using monoclonal antireceptor antibodies. *Arch Pathol Lab Med* 1985;109(8):716–721.
18. Dwivedi AJ, Wu R, Nguyen E, et al. Adrenomedullin and adrenomedullin-binding protein-1 prevent acute lung injury after gut ischemia-reperfusion. *J Am Coll Surg*. 2007;205(2):284–293.
19. Hoeben A, Landuyt B, Highley MS, Wilders H, Van Oosterom AT, De Bruijn EA. Vascular endothelial growth factor and angiogenesis. *Pharmacol Rev*. 2004;56(4):549–580.
20. Mahfoudh-Boussaid A, Zaouali MA, Hadj-Ayed K, et al. Ischemic preconditioning reduces endoplasmic reticulum stress and upregulates hypoxia inducible factor-1 α in ischemic kidney: The role of nitric oxide. *J Biomed Sci*. 2012;19(1):7–15.
21. Poynter JA, Manukyan MC, Wang Y, et al. Systemic pretreatment with dimethylallylglycine increases myocardial HIF-1 α and VEGF production and improves functional recovery after acute ischemia/reperfusion. *Surgery*. 2011;150(2):278–283.
22. Grenz A, Clambey E, Eltzschig HK. Hypoxia signaling during intestinal ischemia and inflammation. *Curr Opin Crit Care*. 2012;18(2):178–185.
23. Wyatt HD, West SC, Beattie TL. InTERTpreting telomerase structure and function. *Nucleic Acids Res*. 2010;38(17):5609–5622.
24. Pandita TK. Role of HSPs and telomerase in radiotherapy. *Int J Hyperthermia*. 2005;21(8):689–694.
25. Eckers A, Altschmied J, Haendeler J. Oxidative stress in endothelial cells and in diabetes type 2 [in German]. *Z Gerontol Geriatr*. 2012;45(2):90–94.
26. Werner C, Gensch C, Pöss J, Haendeler J, Böhm M, Laufs U. Pioglitazone activates aortic telomerase and prevents stress-induced endothelial apoptosis. *Atherosclerosis*. 2011;216(1):23–34.
27. Zaccagnini G, Gaetano C, Pietra LD, et al. Telomerase mediates vascular endothelial growth factor-dependent responsiveness in a rat model of hind limb ischemia. *J Biol Chem*. 2005;280(15):14790–14798.
28. Quyang YB, Giffard RG. MicroRNAs regulate the chaperone network in cerebral ischemia. *Transl Stroke Res*. 2013;4(6):693–703.
29. Xiao B, Ma LL, Xiao CL, et al. Protective effect of heat shock protein 70 and magnesium sulfate supplementation on renal ischemia reperfusion injury [in Chinese]. *Beijing Da Xue Xue Bao*. 2011;43(4):525–530.
30. Kim BK, Kim BR, Lee HJ, et al. Tumor-suppressive effect of a telomerase-derived peptide by inhibiting hypoxia-induced HIF-1 α -VEGF signaling axis. *Biomaterials*. 2014;35(9):2924–2933.

Acute effect of a variable pulse width Nd:YAG laser combined with hematoporphyrin monomethyl ether-mediated photodynamic therapy on a cockscomb model of nevus flammeus

Ke Ma^{1,A,F}, Lvjun Yang^{2,B,E}, Mingde Liao^{1,B}, Yi Qin^{3,C}, Chao Luo^{4,D}, Lina Lin^{5,E}, Danyan Ye^{2,D}

¹ Department of Plastic & Cosmetic Surgery, The First Affiliated Hospital of Guangxi Medical University, Nanning, China

² Research Center for Translational Medicine, Shantou University Medical College, Shantou, China

³ Department of Anesthesiology, The First Affiliated Hospital of Guangxi Medical University, Nanning, China

⁴ School of Life Science, Central South University, Changsha, China

⁵ Department of Gynecology, The First Affiliated Hospital of Guangxi Medical University, Nanning, China

A – research concept and design; B – collection and/or assembly of data; C – data analysis and interpretation; D – writing the article; E – critical revision of the article; F – final approval of the article

Advances in Clinical and Experimental Medicine, ISSN 1899–5276 (print), ISSN 2451–2680 (online)

Adv Clin Exp Med. 2020;29(12):1425–1431

Address for correspondence

Ke Ma

E-mail: 1037579997@qq.com

Funding sources

This work was supported by the National Natural Science Foundation of China (grant No. 81472054) and the Guangxi Science and Technology Major Project (grant No. AA17204085).

Conflict of interest

None declared

Received on March 25, 2020

Reviewed on March 30, 2020

Accepted on August 11, 2020

Cite as

Ma K, Zhao J, Yang L, et al. Acute effect of a variable pulse width Nd:YAG laser combined with hematoporphyrin monomethyl ether-mediated photodynamic therapy on a cockscomb model of nevus flammeus. *Adv Clin Exp Med.* 2020;29(12):1425–1431. doi:10.17219/acem/126300

DOI

10.17219/acem/126300

Copyright

© 2020 by Wrocław Medical University

This is an article distributed under the terms of the Creative Commons Attribution 3.0 Unported (CC BY 3.0) (<https://creativecommons.org/licenses/by/3.0/>)

Abstract

Background. Nevus flammeus (NF) is a congenital vascular malformation.

Objectives. To investigate the acute effect of a variable pulse width Nd:YAG laser combined with hematoporphyrin monomethyl ether (HMME)-mediated photodynamic therapy (PDT) on a cockscomb model of NF.

Material and methods. Forty-two leghorn roosters were randomly divided into the following 7 groups: group A1 (treated with HMME-mediated PDT; energy density of 75 J/cm²), group A2 (treated with HMME-mediated PDT; 125 J/cm²), group A3 (treated with HMME-mediated PDT; 150 J/cm²), group A4 (treated with HMME-mediated PDT; 175 J/cm²), group B (treated with a variable pulse width Nd:YAG laser), group C (treated with a variable pulse width Nd:YAG laser and HMME-mediated PDT), and group D (the control group). Changes in the cockscomb tissues were observed visually and microscopically on days 1, 3, 7, and 14 after treatment. The capillary reduction and the ratio of collagen type I to type III were examined.

Results. The response rate was higher in groups A3 and A4 than in group B. In group A, a higher energy density resulted in a higher response rate and a greater capillary reduction ($p < 0.05$ for all). However, we concluded that PDT at an energy density of 175 J/cm² is not suitable for treating NF, as severe tissue damage, markedly lower capillary numbers, and markedly higher collagen type I:III ratios were observed in the cockscombs treated at this energy density; instead, 150 J/cm² may be a more appropriate energy density. Moreover, HMME-mediated PDT at 150 J/cm² combined with a variable pulse width Nd:YAG laser achieved better treatment outcomes than PDT or a variable pulse width Nd:YAG laser alone ($p < 0.05$ for both).

Conclusions. Compared to PDT or a variable pulse width Nd:YAG laser alone, the combination of the 2 therapies achieved a better acute effect in treating a cockscomb model of NF, and 150 J/cm² may be a suitable energy density for PDT.

Key words: photodynamic therapy, laser, nevus flammeus, hematoporphyrin monomethyl ether

Introduction

Nevus flammeus (NF), also known as port-wine stain, is a congenital vascular malformation characterized by ectasia of capillaries and venules; it often occurs in dermal papillary and reticular layers.^{1,2} The disease does not resolve without treatment, and the incidence rate is about 0.4% in children.^{3,4} Treatment options for NF include laser therapy, cryotherapy and surgery.^{5–7} A pulsed dye laser, which is the most widely used therapy for NF, can achieve good results but may cause irreversible vessel injury, thereby increasing the risk of purpura. Moreover, there may be a recurrence after pulsed dye laser therapy, and it is ineffective in some NF cases.^{7,8} Therefore, it is essential to find a more effective method for the treatment of NF.

In recent years, photodynamic therapy (PDT) has been considered a good method for treating NF.⁹ In this therapy, photosensitizers can accumulate selectively in the vascular endothelial cells, and the recurrence rate is low. The greatest advantage of PDT is that it has high selectivity in the target tissue. Some studies have demonstrated that hematoporphyrin monomethyl ether (HMME) displays characteristic absorption peaks in multiple wavelengths, and a 532-nm laser is often used in PDT for treating NF.^{10,11} Therefore, a 532-nm continuous laser was chosen for our experiment. During PDT, the capillary malformation is targeted by substances generated from the reaction between the laser and photosensitizers. This therapy can be applied in large-area skin damage and offers a low recurrence rate.¹² However, most of the studies to date investigated only the effect of PDT on patients in clinical practice and no effective animal experiments were carried out; moreover, the energy densities applied in those studies were empirical doses. The effectiveness of PDT in the treatment of NF has been demonstrated in many studies.^{5,9,11,13} Different energy densities (75 J/cm², 100 J/cm² and 150 J/cm²) were investigated in some of these studies, but the effects of different energy densities on the treatment outcomes were not thoroughly compared. Therefore, in order to find a suitable energy density for treating NF, we compared 4 energy densities in our experiments. It has been revealed that a variable pulse width Nd:YAG laser can achieve good efficacy in treating some skin diseases.¹⁴ In this therapy, a 532-nm wavelength is often used to treat NF, as a laser at this wavelength can deeply penetrate the skin, cause a large area of thermal damage and achieve good coagulation; the effect of a variable pulse width Nd:YAG laser at a wavelength of 532 nm is especially noteworthy in the management of deep vascular malformation.^{15,16} However, no other study has been performed on the effect of combined variable pulse width Nd:YAG laser and PDT. Therefore, in this study, we investigated the effect of the combined use of the 2 methods and compared the efficacy of such use to the efficacy of a variable pulse width Nd:YAG laser or PDT alone.

Material and methods

Study subjects

Forty-two leghorn roosters (age: 8–9 months; weight: approx. 3 kg) were chosen as subjects. The cockscombs (thickness: 7–9 mm) were ruddy and without damage, necrosis or ulcers. The subjects were divided into the following 7 groups: group A1 (treated with HMME-mediated PDT; an energy density of 75 J/cm²), group A2 (treated with HMME-mediated PDT; 125 J/cm²), group A3 (treated with HMME-mediated PDT; 150 J/cm²), group A4 (treated with HMME-mediated PDT; 175 J/cm²), group B (treated with variable pulse width Nd:YAG laser), group C (treated with variable pulse width Nd:YAG laser and HMME-mediated PDT), and group D (the control group). The study was approved by the Animal Ethics Committee of our hospital.

The cockscombs of the leghorn roosters met the criteria for the disease model of NF.¹⁷

Treatment methods

Photodynamic therapy

The HMME is the most commonly used photosensitizer in PDT. For the treatment in our study, HMME (Fudan-Zhangjiang Bio-Pharmaceutical, Shanghai, China) was diluted with normal saline solution (10 mg/mL/kg). The subjects received chloral hydrate (2 mL/kg) orally for anesthesia, and the experimental area on the left side of the comb was marked in a circle with a diameter of 1.5 cm. The HMME was then injected intravenously into the root of the chicken wings in group A, and laser radiation with a power density of 150 mW/cm² was applied to the experimental areas. During the radiation, both the experimental and non-experimental areas were covered. The energy densities in groups A1, A2, A3, and A4 were 75 J/cm², 125 J/cm², 150 J/cm², and 175 J/cm², respectively.

Variable pulse width Nd:YAG laser

Before applying the variable-pulse frequency-doubled Nd:YAG (532 nm) laser, the subjects received chloral hydrate (2 mL/kg) orally for anesthesia, and the experimental areas on the combs were marked in the same way as that in the PDT groups. The energy density was 20 J/cm², the pulse-width was 10–50 ms and the spot diameter was 8 cm.

Combination therapy

After comparing the effects in the 4 PDT groups, we chose 150 J/cm² as the most suitable energy density and applied it with the variable pulse width Nd:YAG laser for the combination therapy. The PDT was first conducted, followed by variable pulse width Nd:YAG laser treatment 10 min later. The 2 procedures were carried out in the same way as described above.

Outcome measures

Main outcome measures

On days 1, 3, 7, and 14 after treatment, samples from the experimental areas of the combs were collected in each group for visual and microscopic inspection, and the non-experimental area was used as a control. The blood capillaries in the combs were observed under a microscope, and the percentage decrease of the capillary number was calculated with the following formula: percentage decrease of the capillary number = (the number of capillaries before treatment – the number of capillaries after treatment)/the number of capillaries before treatment × 100%.

Secondary outcome measures

On day 14 after treatment, 5 fields in the experiment area of each comb were randomly picked and drilled for immunohistochemistry staining to examine the levels of collagen types I and III. The samples were fixed with 10% formaldehyde, sectioned after paraffin embedment, and then dewaxed and hydrated. After antigen retrieval, the samples were blocked with serum and incubated with primary antibodies to collagen types I and III. Next, the samples were incubated with the secondary antibodies after rewarming. Then, they were stained with DAB followed by counterstaining with hematoxylin. The sections were then sealed for observation, and the ratio of collagen type I to type III were calculated.

The response rate in each group was observed and classified into 5 levels as listed in Table 1.¹⁸ The total response rate = the total number of samples with response rate in levels 1, 2 and 3/the total number of samples × 100%.

Adverse reactions in each group such as pigmentation, blistering and scar formation were recorded 14 days after treatment.

Statistical analysis

SPSS v. 19.0 software (IBM Corp., Armonk, USA) was used for the statistical analysis. The measurement data is expressed as means ± standard deviation (SD). Comparison between 2 groups was conducted using a t-test for independent samples. Measurement data at different time points between the 2 groups were compared with repeated-measures analysis of variance (ANOVA) and a Bonferroni post hoc test. A p-value <0.05 was considered to indicate a statistically significant difference.

Results

Results of visual inspection

After treatment, the color and morphology remained the same in the combs of group D and on the right side of the combs (opposite to the experimental side) in other groups. In contrast, changes were observed in the experimental areas of combs in groups A, B and C. In groups A1–4, the higher energy density resulted in a better clearance of NF. However, the energy density in group A4 was not optimal, as scars were formed on the combs in this group 14 days after treatment. Therefore, we chose the energy density from group A3 for PDT in the combination therapy. The results showed that the outcome in group C was much better than that of the other groups. In group C, 14 days after treatment, marked blanching was observed in some areas and no noticeable scars had formed (Table 2).

Results of microscopic observation

On days 1, 3, 7, and 14 after treatment, the combs in each group were observed under a microscope. Prior to the treatment, the structure of the stratum corneum and the dermis was intact in each group; however, changes were observed after treatment in the blood vessels in the experimental areas of groups A, B and C, whereas the combs in group D and the right side of the combs in other groups remained unchanged. As with the results of the visual inspection, good clearance of NF was achieved in group A4, but proliferative collagen fibers, which could lead to scars, were observed in this group. Thus, the energy density from group A3 was chosen for the combination therapy. Fourteen days after treatment in group C, the capillaries had almost disappeared, the epidermis had thickened, no blisters had formed, and the results of the treatment were much better than that of other groups (Table 3).

Capillary reduction in each group

Compared to group D at each time point, the other groups had a higher percentage of decrease in capillary number ($p < 0.05$ for all), suggesting that the treatment in these groups may have damaged the blood vessels. In groups A1–4, we found that a higher energy density resulted in a greater percentage of decrease in capillary number. Moreover, compared to groups B and A3, group C had a greater percentage decrease in capillary number ($p < 0.05$ for both; Table 4).

Table 1. Response rate level

| Variable | Level 1: Excellent response | Level 2: Good response | Level 3: Fair response | Level 4: Poor response | Level 5: No response |
|----------------------------|--------------------------------|---------------------------|---------------------------|---------------------------|-------------------------|
| Percentage of NF clearance | 80–100% | 60–79% | 40–59% | 20–39% | 0–19% |

NF – nevus flammeus.

Table 2. Results of visual inspection in each group

| Group | Before treatment | 1 day after treatment | 3 days after treatment | 7 days after treatment | 14 days after treatment |
|----------|-------------------------------|---|--|---|--|
| Group A1 | The comb was ruddy and intact | No noticeable edema was observed. The skin color in the experimental area was darker compared with the surrounding area | The skin was slightly yellowish-white. No skin damage was observed. | The blanching became more noticeable. | The blanching decreased, and the color in part of the experimental area was restored to normal. |
| Group A2 | | Mild edema was observed. Part of the skin was slightly purplish-red. | Edema was gone. Evident blanching was observed in part of the experimental area. | The purplish-red color faded in some areas. The blanching became more evident. | The blanching decreased, and the skin color became darker compared with the surrounding area and was not restored to normal. |
| Group A3 | | Moderate edema occurred. Evident purplish-red was observed in part of the experimental area. | The edema reduced partially, and the purplish-red color faded slightly. | The edema decreased significantly. The blanching was noticeable in the experimental area. | The edema was gone. The blanching decreased slightly. Thin crust was formed on the skin. No blister or scar was formed. |
| Group A4 | | Severe edema occurred. Part of the skin was purplish-black. Blister was formed | The edema was noticeable. Part of the skin was deep to moderate purplish-red. | The edema reduced. The blanching was evident in some areas. The skin was mild purplish-red. Crust was formed on the skin. | The edema was gone. The blanching was evident in some areas. The purplish-red color faded. The scar was formed. |
| Group B | | Mild edema occurred. Blanching was observed in part of the experimental area. | Edema was gone. The blanching became more evident. | The blanched area turned darker. | The blanching reduced significantly but the skin color still looked a little different from the normal skin color. |
| Group C | | Moderate to severe edema occurred. The skin was deep purplish-red. No blister was formed. | Both the edema and the purplish-red color were in a moderate level. | The edema and the purplish-red color became mild. Blanching was evident in some areas. | The edema and the purplish-red color was gone. Blanching was evident in some areas. No scar was formed. |
| Group D | | | No noticeable changes were observed. | | |

Collagen type I:III ratio in each group

The collagen type I:III ratios in groups A1, A2, A3, B, and C were similar to that in group D, while group A4 had a higher ratio than group D ($p < 0.05$). This result indicates that the energy density in group A4 was too high and that it may cause a risk of fibrosis in the combs (Fig. 1).

Response rate and adverse reactions in each group

The results from groups A1–4 demonstrated that the response rate increased with the increase of energy density. In fact, the energy density of 175 J/cm^2 used in group A4 could easily cause blisters and scarring. Considering that NF usually occurs on the facial and neck area, any therapy that may lead to blisters and scarring in these areas is not suitable for clinical treatment. Thus, we chose an energy density of 150 J/cm^2 for further experiments. The results showed that group C achieved a better response rate than groups A3 and B ($p < 0.05$ for both), and had a similar incidence rate of adverse reactions in comparison to groups A3 and B (29.2% vs 29.2%, 29.2% vs 25.0%; $p > 0.05$ for both; Tables 5, 6).

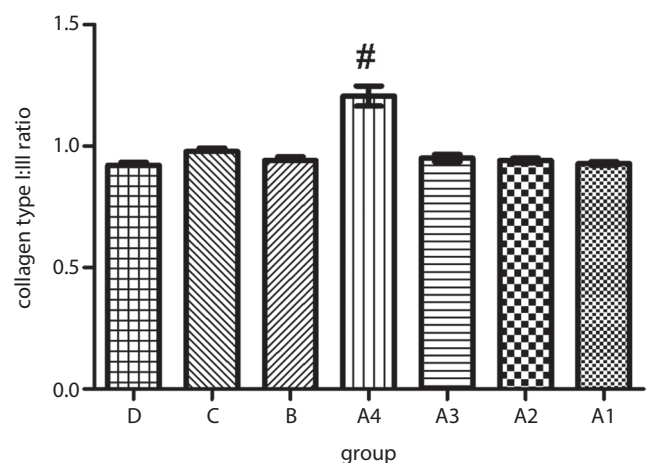


Fig. 1. Collagen fiber type I:III ratios in the experimental area of each group (# $p < 0.05$ vs group D)

Discussion

Methods for treating NF include surgical incision, cryotherapy with liquid nitrogen and skin grafting if the wound is large.^{19,20} However, these methods cannot achieve excellent results and are likely to cause scarring or pigmentation.

Table 3. Results of microscopic observation in each group

| Group | Before treatment | 1 day after treatment | 3 days after treatment | 7 days after treatment | 14 days after treatment |
|----------|--|--|--|---|--|
| Group A1 | The epidermal layer was intact. Many dilated capillaries were observed in the dermis. Plenty of red blood cells were present in the vessels. | Mild edema occurred in the epidermal layer. Mild exudation was observed in the dermis. The number of capillaries slightly decreased. | The edema in the epidermal layer slightly reduced. Exudation in the dermis still existed. The capillary number and vessel diameter decreased. | Edema disappeared in the epidermal layer. Exudation in the dermis reduced. | There was no noticeable edema or exudation. The capillary number and the vessel diameter reduced slightly. |
| Group A2 | | Mild to moderate edema and exudation occurred. A small number of inflammatory cells were observed. The number of superficial capillaries in dermis reduced. The vessel diameter decreased. | Edema and exudation in dermis were aggravated a bit. The number of inflammatory cells increased a little. | Edema and exudation reduced in the epidermal and dermal layers. The number of inflammatory cells reduced. | No evident exudation or edema was observed. The number of inflammatory cells reduced. The capillary number decreased significantly. The vessel diameter reduced. |
| Group A3 | | Moderate to severe edema and exudation occurred. Many inflammatory cells were observed. The capillary number and the vessel diameter reduced markedly. | Edema and exudation were aggravated. The number of inflammatory cells increased. The capillary number and the vessel diameter reduced further. | Edema and exudation decreased. The number of inflammatory cells began to decline. The capillary number and the vessel diameter reduced further. | Edema and exudation reduced markedly. The number of inflammatory cells reduced markedly. The epidermal layer was thickened. No blister was formed. The capillary number and the vessel diameter reduced significantly. |
| Group A4 | | Severe edema and exudation occurred. Blisters were present in dermis. Infiltration of many inflammatory cells was observed. The capillary number and the vessel diameter reduced markedly. | Edema and exudation were aggravated. The capillary number and the vessel diameter reduced further. | Moderate to severe edema and exudation occurred. The number of inflammatory cells did not decrease significantly. The capillaries were almost gone. | Edema and exudation began to decrease. Inflammatory cells reduced. More capillaries disappeared. Proliferative collagen fibers were formed. |
| Group B | | Mild to moderate edema and exudation occurred. Few inflammatory cells were present. The number of superficial capillaries in dermis reduced. The vessel diameter decreased. | Edema and exudation in dermis were aggravated a little. The number of inflammatory cells increased. | Edema and exudation in epidermal and dermal layer reduced markedly. The number of inflammatory cells reduced markedly. | No evident exudation or edema was observed. The inflammatory cells almost disappeared. The capillary number and the vessel diameter reduced. |
| Group C | | Moderate to severe exudation occurred. Many inflammatory cells were observed. The capillary number and the vessel diameter reduced markedly. | Exudation and edema were aggravated. The number of inflammatory cells increased. Capillary number and the vessel diameter reduced further. | Edema and exudation decreased. The number of inflammatory cells decreased. Capillary number and the vessel diameter reduced further. | Edema and exudation reduced markedly. The number of inflammatory cells reduced markedly. The epidermal layer was thickened. No blister was formed. Capillaries almost disappeared. |
| Group D | | No noticeable changes were observed. | | | |

Table 4. Decrease in the number of capillaries (% , ±SD)

| Group | 1 day after treatment | 3 days after treatment | 7 days after treatment | 14 days after treatment |
|----------|----------------------------|-----------------------------|-----------------------------|-----------------------------|
| Group A1 | 15.43 ±5.21 [#] | 18.54 ±4.22 [#] | 24.21 ±5.92 ^{##} | 27.64 ±4.11 ^{###} |
| Group A2 | 25.67 ±6.31 ^{##} | 31.88 ±4.23 ^{###} | 37.23 ±5.43 ^{###} | 40.21 ±4.37 ^{###} |
| Group A3 | 43.65 ±5.26 ^{###} | 59.35 ±4.77 ^{####} | 74.68 ±5.43 ^{###} | 86.55 ±5.29 ^{####} |
| Group A4 | 55.42 ±6.91 ^{###} | 70.67 ±4.16 ^{###} | 87.37 ±6.15 ^{###} | 93.23 ±5.54 ^{###} |
| Group B | 26.44 ±4.25 ^{###} | 32.17 ±4.16 ^{####} | 40.51 ±5.24 ^{####} | 45.33 ±4.65 ^{####} |
| Group C | 52.87 ±4.69 ^{###} | 68.53 ±5.21 ^{###} | 86.33 ±6.89 ^{###} | 94.25 ±4.11 ^{###} |
| Group D | 1.22 ±3.54 | 1.34 ±3.61 | 2.11 ±2.24 | 1.18 ±3.85 |

Compared with Group D: [#]p < 0.05, ^{##}p < 0.01, ^{###}p < 0.001; compared with Group C: *p < 0.05, **p < 0.01, ***p < 0.001.

Table 5. Efficacy in each group

| Group | Excellent response | Good response | Fair response | Poor response | No response | Total response rate (%) |
|----------|--------------------|---------------|---------------|---------------|-------------|-------------------------|
| Group A1 | 0 | 0 | 2 | 3 | 1 | 33.3 |
| Group A2 | 0 | 2 | 1 | 2 | 1 | 50.0 |
| Group A3 | 3 | 2 | 0 | 1 | 0 | 83.3** |
| Group A4 | 5 | 1 | 0 | 0 | 0 | 100.0** |
| Group B | 0 | 2 | 2 | 1 | 1 | 66.7## |
| Group C | 6 | 0 | 0 | 0 | 0 | 100 |

Compared with Group C: #p < 0.05, ##p < 0.01; compared with Group B: *p < 0.05, **p < 0.01.

Table 6. Adverse reactions in each group

| Variable | Blister | Scar | Pigmentation | Discoloration |
|----------|---------|--------|--------------|---------------|
| Group A1 | 0 | 0 | 0 | 1 |
| Group A2 | 0 | 0 | 1 | 2 |
| Group A3 | 0 | 0 | 3 | 4 |
| Group A4 | 5 | 6 | 6 | 6 |
| Group B | 0 | 0 | 4 | 2 |
| Group C | 1 | 0 | 3 | 3 |
| p-value | <0.001 | <0.001 | <0.001 | <0.001 |
| χ^2 | 23.546 | 25.264 | 28.153 | 21.823 |

χ^2 – chi square test.

Therefore, it is essential to find a safer and more effective method for treating NF. In recent years, PDT and variable pulse width Nd:YAG lasers have often been employed in clinical practice. The PDT can achieve good results for treating superficial vascular lesions, but not for deep vascular malformations, due to its weak laser penetration. In contrast, variable pulse width Nd:YAG lasers, with stronger laser penetration, can treat the capillary malformations in deep tissues.^{15,21} Therefore, in order to effectively treat both superficial and deep vascular malformations in NF, we investigated the effect of a combination therapy of PDT and a variable pulse width Nd:YAG laser.

We found that in the PDT groups, the clearance improved with increased energy density, and that PDT at an energy density of 175 J/cm² achieved the highest clearance rate. However, the group with this energy density had the most adverse reactions, including severe blistering and scarring, and had markedly higher collagen type I:III ratios, suggesting the potential risk, or even the presence, of fibrosis in the combs.²² Therefore, an energy density of 175 J/cm² cannot be employed clinically; instead, 150 J/cm² may be considered a suitable energy density. The PDT at 150 J/cm² in group A3 was found to achieve a good clearance rate and a similar incidence rate of adverse reactions as found in groups B and C; likewise, PDT at this energy density did not cause a noticeable elevation in the collagen type I:III ratio, indicating a low risk of fibrosis.

In this study, we found that the combination of PDT and a variable pulse width Nd:YAG laser was able to achieve

a better outcome than PDT or variable pulse width Nd:YAG laser alone. The combination therapy achieved a similar response rate with a lower incidence of adverse reactions in comparison with the PDT therapy at 175 J/cm². The combined use of PDT and a variable pulse width Nd:YAG laser can treat both deep and superficial capillary malformations. So far, many scholars have explored the combination of 2 or more therapies for treating NF, including cryotherapy combined with laser therapy, surgery combined with laser therapy, microneedle therapy combined with PDT, and pulsed dye laser therapy combined with long-pulse 1064-nm Nd:YAG laser therapy. However, many of these methods can easily cause adverse reactions, including scarring and pigmentation. The combination of microneedle therapy and PDT, even though it can achieve good outcomes, requires a more complicated operation than the combination of PDT and a variable pulse width Nd:YAG laser. Therefore, the combined use of PDT and variable pulse width Nd:YAG laser therapy can be recommended for further clinical trials.

Due to time constraints, there were some limitations in our study. Firstly, there are still some differences between cockscomb skin and human skin, even though the cockscomb can be used as a disease model of NF. Secondly, since human facial skin is more delicate, whether PDT at 150 J/cm² can be used to treat faces needs to be investigated further. In this study, we found that the combination of 2 therapies, even though it did not increase the incidence of adverse reactions, could still lead to blisters and scars on the subjects.

Therefore, we do not recommend its clinical application on facial areas to avoid scarring or other adverse reactions. Lastly, the study only demonstrated the short-term effect within 14 days of treatment, and more studies need to be carried out in the future to investigate the adverse reactions and recurrence rate after a longer course of treatment.

Conclusions

In conclusion, 150 J/cm² can serve as a suitable energy density in PDT for the treatment of NF, and the combination of HMME-mediated PDT and variable pulse width Nd:YAG laser therapy can achieve a better outcome than PDT or such a laser alone, so it can be recommended for clinical application.

ORCID iDs

Ke Ma  <https://orcid.org/0000-0002-7982-5536>
 Jinmin Zhao  <https://orcid.org/0000-0002-4341-9317>
 Lvjun Yang  <https://orcid.org/0000-0002-9300-0549>
 Mingde Liao  <https://orcid.org/0000-0001-5499-3106>
 Yi Qin  <https://orcid.org/0000-0002-7039-4549>
 Chao Luo  <https://orcid.org/0000-0003-1943-6659>
 Lina Lin  <https://orcid.org/0000-0001-8106-568X>
 Danyan Ye  <https://orcid.org/0000-0003-0482-4085>

References

- Sharma M, Hu X, Geddes GC, Acharya K. Microcephalic newborn with forehead nevus flammeus, bulging eyes, and clenched fists. *Neoreviews*. 2019;20(3):e170–e173. doi:10.1542/neo.20-3-e170
- Takkar B, Saxena H, Sharma B, Rathi A. Generalised nevus flammeus, episcleral capillary malformation and glaucoma. *BMJ Case Rep*. 2018;2018:bcr2018227248. doi:10.1136/bcr-2018-227248
- Shruti S, Siraj F, Ramesh V, Ramesh V. Recurrent pyogenic granuloma over nevus flammeus. *Indian J Dermatol Venereol Leprol*. 2019;85(2):236–236. doi:10.4103/ijdv.IJDVL_80_17
- Combalia A, Rojano-Fritz L, Podlipnik S, Ferrando J. Nuchal nevus flammeus and alopecia areata: When size matters. *Int J Trichology*. 2018;10(6):275–277. doi:10.4103/ijtr.ijt_82_18
- Burns JM, Jia W, Nelson JS, Majaron B, Anvari B. Photothermal treatment of port-wine stains using erythrocyte-derived particles doped with indocyanine green: A theoretical study. *J Biomed Opt*. 2018;22(12):121616. doi:10.1117/1.JBO.23.12.121616
- Yu W, Zhu J, Wang L, et al. Double pass 595 nm pulsed dye laser does not enhance the efficacy of port wine stains compared with single pass: A randomized comparison with histological examination. *Photomed Laser Surg*. 2018;36(6):305–312. doi:10.1089/pho.2017.4392
- Lipner SR. Topical adjuncts to pulsed dye laser for treatment of port wine stains: Review of the literature. *Dermatol Surg*. 2018;44(6):796–802. doi:10.1097/DSS.0000000000001507
- Lin L, Guo P, Wang X, et al. Effective treatment for hypertrophic scar with dual-wave-length PDL and Nd:YAG in Chinese patients. *J Cosmet Laser Ther*. 2019;21(4):228–233. doi:10.1080/14764172.2018.1516889
- Zhang Y, Yang Y, Zhang Z, et al. Clinical study on hemoporfin PDT for infant facial port-wine stains. *Photodiagnosis Photodyn Ther*. 2019;25:106–110. doi:10.1016/j.pdpdt.2018.09.012
- Wen L, Zhang Y, Zhang L, et al. Application of different noninvasive diagnostic techniques used in HMME-PDT in the treatment of port wine stains. *Photodiagnosis Photodyn Ther*. 2019;25:369–375. doi:10.1016/j.pdpdt.2019.01.008
- Wang Y, Liao X-H, Gu Y, Chen R, Zeng J. The change of reflection spectra and fluorescence spectra of port wine stains during PDT [in Chinese]. *Guang Pu Xue Yu Guang Pu Fen Xi*. 2011;31(1):2969–2972.
- Huang NY. What is the optimal PDT protocol for treating port wine stains (PWS)? *Photodiagnosis Photodyn Ther*. 2007;4:145–146. doi:10.1016/j.pdpdt.2007.07.005
- Gu Y, Huang NY, Liang J, Pan YM, Liu FG. Clinical study of 1949 cases of port wine stains treated with vascular photodynamic therapy (Gu's PDT) [in French]. *Anna Dermatol de Venereol*. 2007;134(3 Pt 1):241–244. doi:10.1016/s0151-9638(07)91816-5
- Abdul Latif AA, Abdel-Hameed AKS, Salama OAAM. Immediate post-irradiation dermoscopic vascular changes versus purpura as a therapeutic endpoint in pulsed-dye laser treatment of port wine stains. *Dermatol Ther*. 2019;32(6):e13094–e13094. doi:10.1111/dth.13094
- Xing L, Chen B, Li D, Wu W, Wang G. Nd:YAG laser combined with gold nanorods for potential application in port-wine stains: An in vivo study. *J Biomed Opt*. 2017;22(11):1–10. doi:10.1117/1.JBO.22.11.115005
- Chang HS, Kim Y-G, Lee JH. Treatment using a long pulsed nd: yag laser with a pulsed dye laser for four cases of blebbed port wine stains. *Ann Dermatol*. 2011;23(Suppl 1):S75–S78. doi:10.5021/ad.2011.23.S1.S75
- Cong T, Liu L, Zhang H, Wang L, Jiang X. Port-wine stains associated with large vestibular aqueduct syndrome caused by mutations in GNAQ and SLC26A4 genes: A case report. *J Dermatol*. 2020;47:78–81. doi:10.1111/1346-8138.15130
- Stephens MR, Putterman E, Yan AC, Castelo-Soccio L, Perman MJ. Acquired port-wine stains in six pediatric patients. *Pediatr Dermatol*. 2020;37(1):93–97. doi:10.1111/pde.14019
- Mathes EF, Frieden IJ. Early use of laser for port-wine stains: Timing, efficacy, and shared decision-making. *JAMA Dermatol*. 2019;155(4):421–423. doi:10.1001/jamadermatol.2018.5189
- Jeon H, Bernstein LJ, Belkin DA, Ghalili S, Geronemus RG. Pulsed dye laser treatment of port-wine stains in infancy without the need for general anesthesia. *JAMA Dermatol*. 2019;155(4):435–441. doi:10.1001/jamadermatol.2018.5249
- Pençe B, Aybey B, Ergenekon G. Outcomes of 532 nm frequency-doubled Nd:YAG laser use in the treatment of port-wine stains. *Dermatol Surg*. 2005;31(5):509–517. doi:10.1111/j.1524-4725.2005.31152
- Lorenz S, Scherer K, Wimmershoff MB, Landthaler M, Hohenleutner U. Variable pulse frequency-doubled Nd:YAG laser versus flashlamp-pumped pulsed dye laser in the treatment of port wine stains. *Acta Derm Venereol*. 2003;83(3):210–213. doi:10.1080/00015550310007238

Salmonella Typhimurium enolase-like membrane protein is recognized by antibodies against human enolase and interacts with plasminogen

Paweł Serek^{1,A–F}, Iwona Bednarz-Misa^{1,A,C–F}, Jadwiga Pietkiewicz^{1,C,E}, Bartłomiej Dudek^{2,C,E},
Magdalena Mierzchała-Pasierb^{1,D,E}, Katarzyna Jermakow^{3,B}, Marek Drab^{4,B}, Andrzej Gamian^{1,5,E,F}

¹ Department of Medical Biochemistry, Wrocław Medical University, Poland

² Department of Microbiology, Faculty of Biological Sciences, University of Wrocław, Poland

³ Department of Microbiology, Wrocław Medical University, Poland

⁴ Unit of Nano-Structural Bio-Interactions, Hirsfeld Institute of Immunology and Experimental Therapy, Polish Academy of Sciences, Wrocław, Poland

⁵ Medical Microbiology Laboratory, Hirsfeld Institute of Immunology and Experimental Therapy, Polish Academy of Sciences, Wrocław, Poland

A – research concept and design; B – collection and/or assembly of data; C – data analysis and interpretation;
D – writing the article; E – critical revision of the article; F – final approval of the article

Advances in Clinical and Experimental Medicine, ISSN 1899–5276 (print), ISSN 2451–2680 (online)

Adv Clin Exp Med. 2020;29(12):1433–1441

Address for correspondence

Paweł Serek

E-mail: pawel.serek@umed.wroc.pl

Funding sources

The project was financed by the National Science Centre (Poland) grant No. DEC-2015/17/N/NZ6/02148.

Conflict of interest

None declared

Received on July 1, 2020

Reviewed on July 12, 2020

Accepted on October 8, 2020

Published online on November 27, 2020

Cite as

Serek P, Bednarz-Misa I, Pietkiewicz J, et al. *Salmonella* Typhimurium enolase-like membrane protein is recognized by antibodies against human enolase and interacts with plasminogen. *Adv Clin Exp Med*. 2020;29(12):1433–1441. doi:10.17219/acem/128233

DOI

10.17219/acem/128233

Copyright

© 2020 by Wrocław Medical University

This is an article distributed under the terms of the Creative Commons Attribution 3.0 Unported (CC BY 3.0) (<https://creativecommons.org/licenses/by/3.0/>)

Abstract

Background. Enolase is generally known as the glycolytic pathway enzyme present in the cytoplasm of eukaryotic cells and in some microorganisms. In human cells, it is also a component of cell surface membranes, where it functions as a human plasminogen receptor.

Objectives. The study aimed to purify *Salmonella enterica* serovar Typhimurium cytosolic enolase and obtain the antibodies against this protein; to identify enolase on the surface of bacteria; and to find cross-reactivity and plasminogen binding properties.

Material and methods. Cytosolic enolase from *S. Typhimurium* was purified using a five-step preparation method. Anti-cytosolic enolase antibodies combined with scanning electron microscopy (SEM) allowed us to detect enolase on the surface of intact *S. Typhimurium* cells. The binding of plasminogen to surface enolase and the cross-reactivity of this protein with antibodies against human enolases were tested with western blot.

Results. Antibodies against human α - and β -enolases cross-reacted with *S. Typhimurium* membrane protein, the identity of which was further confirmed using a mass spectrometry analysis of enolase tryptic peptides. The enolase from bacterial membrane also bound plasminogen.

Conclusions. The cross-reactivity of membrane enolase with antibodies against human enolases suggests that this bacterium shares epitopes with human proteins. Surface exposition of enolase and the demonstrated affinity for human plasminogen indicates that *Salmonella* membrane enolase could play a role in the interaction of *S. Typhimurium* with host cells.

Key words: membrane proteins, *Salmonella*, Typhimurium, enolase

Introduction

The World Health Organization (WHO) reported that every year about 600 million people fall ill after eating contaminated food and 420 000 die, making it the leading cause of mortality worldwide. In addition, children under 5 years of age carry 40% of the foodborne disease burden, with 125 000 deaths every year. Streptococci, staphylococci and *Enterobacteriaceae* are major contributors to bacterial disease.^{1,2}

Salmonella spp. are Gram-negative, rod-shaped bacteria that belong to the *Enterobacteriaceae* family. There are 2 species within the genus *Salmonella*: *S. enterica* and *S. bongori*. *Salmonella enterica* is a pathogenic bacteria and is further divided into more than 2500 serotypes.³ *Salmonella enteritidis* and *S. Typhimurium* are 2 of the most common clinical serotypes of salmonellosis agents isolated worldwide.⁴

There are 2 main clinical types of *Salmonella* infection. The first one is caused by non-typhoidal *Salmonella* strains. The symptoms of this type are limited to the gastrointestinal tract and typically include acute gastritis and enteritis, high fever, spasmodic abdominal pain, and bloody mucus diarrhea. The 2nd clinical type is typhoid fever, caused by *Salmonella typhi* infection, and resulting in a systemic inflammatory response, usually requiring antibiotic treatment. For both, the first phase in the infection process is bacterial adhesion to the intestinal epithelium, which impedes the host's ability to naturally remove the bacterium from the digestive tract. This allows the bacteria to survive, multiply and colonize the host environment.⁵

Outer membrane proteins (OMPs) play a crucial role in the infection and colonization processes. They participate in bacterial contact with host tissues, in initiating the process of degradation of the host tissue and in stimulating the development of infections. They are also important factors in bacterial adaptation to the host environment.^{6,7}

Enolase (Enzyme Commission (EC) 4.2.1.11) is a glycolytic enzyme found in the cytoplasm of eukaryotes and prokaryotes.⁸ It is also an external component of cell membranes in the epithelium and endothelium, in monocytes, leukocytes and neutrophils.^{9,10} Enolase acts as a receptor for plasminogen, which plays a unique role in the defense system of the human body.⁸ For example, active plasmin degrades fibrin in the process of fibrinolysis, which is critical for maintaining hemostasis. Plasminogen also permits cell migration to areas of inflammation. Interestingly, bacteria also have exposed surface plasminogen binding receptors on their cell surfaces. Plasminogen, once cleaved to become the active form called plasmin, allows bacteria to migrate through host tissues. Another example of such a receptor is the surface enolase-like protein, whose properties were described for *Streptococcus pneumoniae*.¹¹

During inflammation caused by Gram-positive or Gram-negative bacteria, the host develops enolase-targeted

antibodies.^{6,12} Since there is greater than 50% homology among enolases of different species,⁸ the structural similarity between human and bacterial enolase can lead to the phenomenon of molecular mimicry. Molecular mimicry is the mechanism whereby antibodies produced by a host against foreign antigens cause cross-reactivity with epitopes of the host's own protein; this can result in autoimmune diseases.¹³ The presence of anti- α -enolase antibodies has been observed in disorders like Behçet's disease, Hashimoto's encephalopathy and Sjögren's syndrome.^{14–16}

Since the enolase from *Salmonella* spp. has not been previously characterized, the purpose of this study was to isolate, purify and perform an immunochemical characterization of the enolase from *S. Typhimurium* bacteria. Deeper insights into the properties of this protein will help to further elucidate its pathogenesis in the development of autoimmune diseases. This paper describes how we identified enolase as a component of *S. Typhimurium* surface proteins and demonstrates the binding of surface enolase to human plasminogen.

Material and methods

Bacterial strain, media and growth conditions

Salmonella enterica serovar Typhimurium (Polish Collection of Microorganisms (PCM) 2713) was obtained from the PCM at the Institute of Immunology and Experimental Therapy, Polish Academy of Sciences, Wrocław, Poland. The bacteria were cultured on tryptic soya agar (Graso Biotech, Owidz, Poland) solid media at 37°C for 18 h.

Extraction and purification of *S. Typhimurium* cytoplasmic proteins

Protein extraction was performed according to the method described by Bednarz-Misa et al.,¹⁷ with minor modifications. The bacterial mass was suspended in 10 mM Tris-HCl, pH 8.4 (Sigma-Aldrich, St Louis, USA) with 1 mM MgSO₄ (Chempur, Piekary Śląskie, Poland), 1% glycerol (v/v) (Chempur), 0.5 mM β -mercaptoethanol (Sigma-Aldrich), and a protease inhibitor cocktail (Merck Millipore, Burlington, USA). The bacterial cells were lysed using the Vibra-Cell YC-130PB ultrasonic processor (Labo-Plus, Warszawa, Poland) at 4°C for 30 min, during 40-second cycles on ice. To remove unbroken cells, the suspension was centrifuged (4000 \times g, 4°C, 1 h). The collected supernatant was re-centrifuged (100,000 \times g, 4°C, 1 h) to obtain the cytosolic fraction (supernatant) and the cell membrane fraction (saved for later purification). For the initial removal of unwanted proteins, 3 stages of protein precipitation with increasing ammonium sulfate (Chempur) saturation (0–30%, 30–80% and 80–100%) were completed. The 1st purification step was carried out through ion exchange

chromatography with a strong anionite Sepharose Q Fast Flow column (GE Healthcare, Chicago, USA). The proteins were precipitated with 30–80% ammonium sulfate and dialyzed into elution buffer (20 mM Tris-HCl, pH 8.4, 1 mM MgSO₄ and 1 mM β-mercaptoethanol). The procedure was carried out on the AKTA Explorer 100 GE chromatograph (GE Healthcare). The column was equilibrated with elution buffer and 50 mg of cytosolic protein extract was applied and separated at a flow of 2 mL/min in an ionic strength gradient of 1 M NaCl (Chempur) as follows: 6 column volumes (CVs) elution buffer, 3 CVs 8% isocratic gradient, 6 CVs gradient 8–70%, and 5 CVs gradient 100% to release the remaining proteins from the column. Protein concentration was determined spectrophotometrically at 280 nm. To quantify the enolase, an absorption coefficient of $A_{0.1\%} = 0.89$ was used, determined for rabbit muscle enolase at a concentration of 1 mg/mL.¹⁸ The enzymatic activity for cytosolic enolase was assessed spectrophotometrically (EnviSense UV-1800; EnviSense, Lublin, Poland) at room temperature (RT) at 240 nm as an increase in phosphoenolpyruvate (PEP) concentration in the reaction buffer (50 mM imidazole-HCl, pH 8.4 (Sigma-Aldrich), 1 mM MgSO₄, 400 mM KCl (Chempur) and 1 mM 2-phosphoglyceric acid (2-PGA)). One unit of enolase activity is defined as the amount of protein that under these conditions catalyzes the synthesis of 1 μmol of PEP from 2-PGA in 1 min.¹⁹ The active fractions were eluted from the 20–35% gradient, and then collected, concentrated and dialyzed into a sodium chloride-free buffer using Centri-con 30K filters (Merck Millipore).

The protein fractions collected in the 1st chromatography step (20 mg) were then applied to a Sephadex G-100 column (GE Healthcare). The column was equilibrated with 20 mM Tris-HCl buffer, pH 8.4 with 300 mM NaCl (Chempur), 1 mM MgSO₄ and 1 mM β-mercaptoethanol. Chromatographic separation was carried out at a flow of 0.1 mL/min on an AKTA Explorer 100 HPLC system (GE Healthcare). The final purification step used preparative electrophoresis on the PrepCell 491 device (Bio-Rad, Hercules, USA). Discontinuous separation was carried out at 280 V under native conditions in 4% stacking gel and 10% separating gel in 25 mM Tris and 192 mM glycine (BioShop Canada Inc., Burlington, Canada), pH 8.3.

Extraction and purification of *S. Typhimurium* OMPs

The pellet fraction obtained after centrifugation at 100,000 × g was used for purification of the OMP. The pellet was washed twice with 20 mM Tris-HCl buffer, pH 7.2, using a tissue grinder. The suspension was then centrifuged (100,000 × g, 4°C, 1 h). The pellet collected at this step was resuspended in 20 mM Tris-HCl, pH 7.4, and 80 mM CHAPS detergent (BioShop Canada Inc.). Membrane protein extraction was carried out for 30 min at 4°C. The suspension was again centrifuged (100,000 × g,

4°C, 1 h) and the supernatant containing the extracted membrane protein was collected. The protein concentration was measured using a bicinchoninic acid (BCA) assay (Thermo Fisher Scientific, Waltham, USA).

For the final purification step the extracted membrane proteins were diluted 1:1 with ×2 Laemmli sample buffer (Bio-Rad) and incubated for 5 min at 100°C. The proteins were separated at 200 V and 1 mL/min with the PrepCell 491 device (Bio-Rad) using 10% and 12% separating gel in an electrode buffer: 25 mM Tris and 192 mM glycine, 0.5% SDS, pH 8.3 (Bio-Rad).

All procedures involving animals were in accordance with the ethical standards of Wroclaw Medical University and approved by the Local Ethics Committee for Animal Experiments (approval No. 55/2017).

Preparation of rabbit polyclonal antibodies specific to *S. Typhimurium* cytosolic enolase

A male New Zealand rabbit weighing 2 kg was immunized with a total of 1.5 mg of *S. Typhimurium* enolase. The 1st multipoint intradermal injection was performed with 0.5 mg of enolase diluted in 0.5 mL of phosphate buffered saline (PBS) (BioShop Canada Inc.) mixed with an equal volume of incomplete Freund's adjuvant (Sigma-Aldrich). After 3 weeks, a 2nd immunization was performed in the same way. The 3rd injection of protein was performed after another 3 weeks. Two weeks later, the animal was bled. The collected antisera were filtered and incubated at 56°C for 30 min to inactivate the complement. IgG antibodies were isolated on a Protein A Protein G GraviTrap column (GE Healthcare) according to the manufacturer's instructions.

Electrophoresis and immunoblotting

The bacterial enolase-like protein was detected with western blot analysis using rabbit anti-cytosolic enolase *S. Typhimurium* antibodies. The *S. Typhimurium* OMP fraction (10 μg) obtained during preparative electrophoresis and purified *S. Typhimurium* cytosolic enolase (10 μg) were diluted 1:1 with ×2 Laemmli sample buffer containing 5% 2-mercaptoethanol, followed by denaturation for 5 min at 95°C. The samples were resolved with SDS-PAGE electrophoresis²⁰ using a 4.5% stacking gel and a 12% resolving gel. The proteins were then visualized with Coomassie brilliant blue G-250 (BioShop Canada Inc.) staining or transferred to an Immobilon P membrane (Merck Millipore) for 90 min at 200 mA.¹² The membrane was blocked with 1% casein blocking buffer (Sigma-Aldrich) at 37°C for 1 h. After washing, the membrane was incubated with IgG antibodies obtained from a rabbit immunized with *Salmonella* cytosolic enolase in TBS-T buffer (20 mM Tris-HCl, pH 7.0, 50 mM NaCl, 0.05% Tween-20 (Sigma-Aldrich), pH 7.0). Unbound antibodies were removed through washing with TBS-T

buffer. Next, the membrane was incubated with goat anti-rabbit IgG antibodies (Abcam, Cambridge, UK) conjugated with horseradish peroxidase (HRP) at 37°C for 1 h. The western blot was visualized using a colorimetric reaction with substrate 3-amino-9-ethylcarbazole (Sigma-Aldrich).

Immunoblotting with human plasminogen was performed with the *S. Typhimurium* OMP fraction (10 µg) obtained during preparative electrophoresis and with purified *S. Typhimurium* cytosolic enolase (10 µg). The SDS-PAGE, protein transfer and membrane blocking were performed as outlined above. After washing, the membranes were incubated with 20 µg of human plasminogen (R&D Systems, Minneapolis, USA) in TBS buffer (20 mM Tris-HCl, 50 mM NaCl, pH 7.0) at 37°C for 1 h, then overnight at 4°C. Unbound plasminogen was removed through washing with TBS-T buffer. The membranes were then incubated with rabbit anti-human plasminogen antibodies (Abcam) and, after further washing, with HRP goat anti-rabbit IgG antibodies (Abcam). The western blot was visualized using a colorimetric reaction with substrate 3-amino-9-ethylcarbazole (Sigma-Aldrich).

The reactive fraction of OMPs from *S. Typhimurium* was separated by two-dimensional electrophoresis (2-DE), as described earlier.²¹ The OMPs for transfer (40 µg) or for silver staining (20 µg) were separated with pH 4–7 immobilized pH gradient strips (7 cm, from (Bio-Rad)). The 2-DE analysis was carried out with the Mini-PROTEAN® Tetra Cell System (Bio-Rad). Prior to resolving the first dimension, precast IPG strips were rehydrated with 120 µL of rehydration buffer (Bio-Rad) for 16 h at room temperature. Isoelectric focusing (IEF) was conducted through stepwise voltage increases: 250 V for 20 min, 4000 V for 120 min (linear) and 4000 V (rapid) until the total volt-hours reached 14 kWh. After IEF separation, the strips were equilibrated in 6 M urea (BioShop Canada Inc.), 375 mM Tris, pH 8.8, 2% SDS, reduced with 2% (w/v) dithiothreitol (DTT) (BioShop Canada Inc.) and alkylated with 135 mM iodoacetamide (Sigma-Aldrich). The IPG strips were then loaded onto a 9–12.5% gradient polyacrylamide gel (10 × 8 cm, 1.0 mm thick) using 0.5% agarose (Bio-Rad) in the running buffer. Molecular mass standards (Precision Plus Protein™ Standards; Bio-Rad) were applied at the basic end of the IPG strips. Electrophoresis was performed at 4°C with constant power (1 W). Following separation in the second dimension, the gels were silver stained.²² Spot patterns were visualized under white light and photographed using a GelDoc XR camera system (Bio-Rad).

Then 2-DE OMPs were transferred from gel to the Immobilon P membrane as described above. The membranes were blocked with 1% casein blocking buffer (Sigma-Aldrich) at 37°C for 1 h. After washing, the membranes were incubated with either mouse anti-human α -enolase and/or with anti-human β -enolase antibodies (both from Santa-Cruz Biotechnology, Dallas, USA) at 37°C for 1 h. Secondary antibody incubation was performed using HRP goat anti-mouse IgG (Novus Biologicals, Centennial, USA) and

the proteins were visualized using a colorimetric reaction with substrate 3-amino-9-ethylcarbazole (Sigma-Aldrich).

In-gel protein digestion and mass spectrometry protein identification

The appropriate protein spot was excised from the gel and analyzed using liquid chromatography coupled with mass spectrometry in the Laboratory of Mass Spectrometry, Institute of Biochemistry and Biophysics, Polish Academy of Sciences (Warszawa, Poland). Samples were subjected to standard trypsin digestion, during which the proteins were reduced with 10 mM DTT for 30 min at 56°C, alkylated with iodoacetamide in the dark for 45 min at room temperature and digested with 10 ng/µL trypsin overnight. The resulting peptide mixtures were concentrated and desalted on a RP-C18 pre-column (Waters, Milford, USA) and further peptide separation was achieved on a nano-Ultra Performance Liquid Chromatography (UPLC) RP-C18 column (Waters, BEH130 C18 column, 75 µm i.d., 250 mm long; Waters) using a 45-minute linear acetonitrile gradient in the presence of 0.1% formic acid. The column outlet was directly coupled to the Orbitrap Velos MS ion source (Thermo Electron Corp., San Jose, USA). Mass spectra were obtained with a full scan on an Orbitrap mass analyzer in data dependent acquisition (DDA) mode, followed by MS/MS scans in the ion trap. A blank run to ensure the absence of cross-contamination from previous samples preceded each analysis.

The acquired MS/MS data was pre-processed with Mascot Distiller software v. 2.6 (Matrix Science Ltd., London, UK) and the search was performed using the Mascot Search Engine (Matrix Science Ltd.) against the National Center for Biotechnology Information (NCBI; US National Library of Medicine, Bethesda, USA) NCBI nr database (176 222 799 sequences; 64 284 901 062 residues), with a *S. Typhimurium* filter (101 607 sequences). To reduce mass errors, the peptide and fragment mass tolerance settings were established after a measured mass recalibration,²³ resulting in a value of 6.5 ppm for parent and 0.01 Da for fragment ions. The rest of the search parameters were as follows: enzyme, trypsin; missed cleavages, 1; fixed modifications, carbamidomethyl (C); variable modifications, oxidation (M); instrument, HCD. The Decoy Mascot functionality was used to keep the false discovery rate (FDR) for peptide identifications below 1%.

Scanning electron microscopy

To demonstrate the immunostaining pattern of pathogens detected with the polyclonal *S. Typhimurium* cytosolic enolase antibody, cells were further treated with secondary anti-rabbit antibody labelled with 30 nm colloidal gold. Bacteria treated only with secondary antibodies were used as a control. Scanning electron microscopy (SEM) was processed with low accelerating voltage of the primary beam (low-voltage field-emission SEM – LV-FESEM) without

any coating of the sample.²⁴ The bacterial colonies were stamped with polished silicon chips by pressing the chip against the bacterial colony for 5 min at room temperature. The samples were fixed with 2.5% formaldehyde in 100 mM cacodylate buffer at 4°C for 30 min, and then washed in water and dehydrated in a series of methanol steps (25–50–75–100%), each lasting 1 h at 4°C. The samples went through critical point drying with methanol, undergoing an exchange for liquid CO₂ in an automatized critical point dryer (CPD300 AUTO; Leica Microsystems, Vienna, Austria) and were imaged with a cross-beam scanning electron microscope equipped with a Schottky field-emission cathode (Auriga 60; Carl Zeiss, Oberkochen, Germany) at 1.5 kV accelerating voltage. A non-coating approach was implemented within the LV-FESEM mode, whose low energies allow efficient interaction of electrons with native elements of the biological sample (typically low Z-number atoms). We applied the low-energy loss electron principle to generate a highly resolved chemical contrast, as we described in detail previously.²⁵ Images were acquired with an Everhart-Thornley electron detector (SE2 secondary electrons), the in-lens electron detector (SE1 secondary electrons) and the energy-selective back-scattered electron detector (EsB) directly from the sample surfaces with no coating or contrasting applied.^{24,25} The EsB detector grid potential was set to 1200 V, and brightness and contrast were adjusted to allow a distinction between the substratum (a polished silicon chip with a grey appearance), the biological sample (bacteria and their appendages, dark in appearance) and the nano-gold label (bright appearance). The sample imaging was performed in a dual-view mode enabling correlative imaging between 2 channels in parallel with pixel-to-pixel correlative accuracy.

Results

Purification of cytosolic enolase from *S. Typhimurium*

The method of *S. Typhimurium* enolase purification involved sonication, precipitation with ammonium sulfate, ion-exchange chromatography, gel filtration, and preparative electrophoresis. Preparative electrophoresis for the separation of cytosolic proteins permitted the purification of enzymatically active enolase with electrophoretic

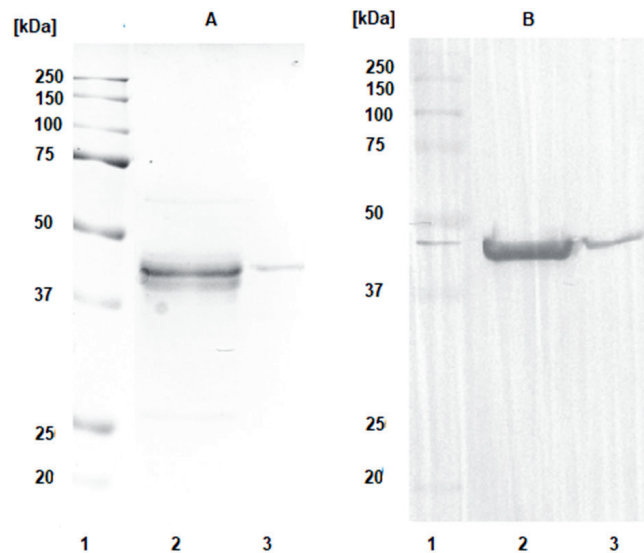


Fig. 1. Interaction of enolases with antibodies against *S. Typhimurium* cytosolic enolase. A. SDS-PAGE gel profile after Coomassie staining: 1. Molecular mass marker; 2. *Salmonella* OMPs; 3. *Salmonella* cytosolic enolase. B. Immunoblotting with anti-*S. Typhimurium* cytosolic enolase antibodies

mobility at about 45 kDa. Row 3 in Fig. 1A shows the homogeneity level of enolase that was used for rabbit immunization. The purification process resulted in pure protein with 15% efficiency (Table 1).

Purification of the enolase-like membrane protein from *S. Typhimurium*

The OMPs were extracted using CHAPS detergent and 4.4 mg was obtained as soluble micelles from 10 mg of membrane protein extract. The purification of enolase-like protein was performed using preparative SDS-PAGE with continuous elution. The OMPs with a molecular mass of 45–47 kDa were purified from the protein extract. The fraction of OMPs reactive with antibodies against *S. Typhimurium* cytosolic enolase (Fig. 1A, row 2) was selected for further testing on 2-DE.

Antibodies against *S. Typhimurium* cytosolic enolase cross-react with *S. Typhimurium* OMPs

Human α -enolase and β -enolase, like the OMPs and cytosolic enolases of *S. Typhimurium* used in the immunoblotting, reacted with antibodies from rabbit serum

Table 1. Purification of cytosolic enolase from *S. Typhimurium*

| Fractions | Total protein [mg] | Total activity [IU] | Specific activity [IU/mg] | Efficiency [%] |
|--|--------------------|---------------------|---------------------------|----------------|
| Crude extract | 717.7 | 409 | 0.57 | 100 |
| (30–80%) (NH ₄) ₂ SO ₄ | 435.7 | 314 | 0.72 | 77 |
| Q Sepharose Fast Flow | 102.04 | 202 | 1.98 | 49 |
| Sephadex G-100 | 17.88 | 123 | 6.88 | 30 |
| PrepCell | 2.94 | 61 | 20.9 | 15 |

immunized by cytosolic enolase (Fig. 1B). This observation corroborated that the 2 enolases could have similar antigenic properties.

S. Typhimurium enolase-like membrane protein binds to plasminogen

The OMPs that exhibited reactivity with anti-*S. Typhimurium* cytosolic enolase polyclonal antibodies also bound human plasminogen (Fig. 2A,B, row 2). However, no such interaction was observed for *Salmonella* cytosolic enolase (Fig. 2A,B, row 3). Denatured *Salmonella* cytosolic enolase showed no plasminogen binding capacity.

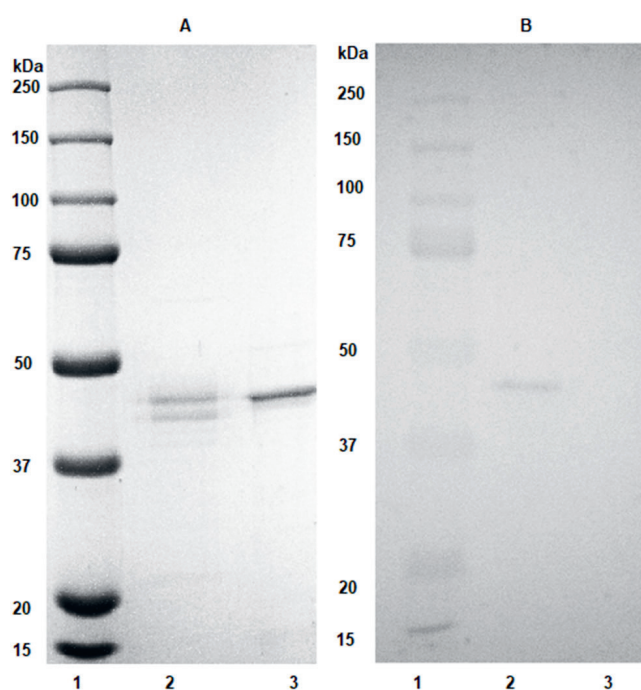


Fig. 2. Interaction of human plasminogen with membrane proteins and cytosolic enolase from *S. Typhimurium*. A. SDS-PAGE gel profile after Coomassie staining: 1. Molecular mass marker; 2. *Salmonella* OMPs; 3. *Salmonella* cytosolic enolase. B. Immunoblotting with human plasminogen

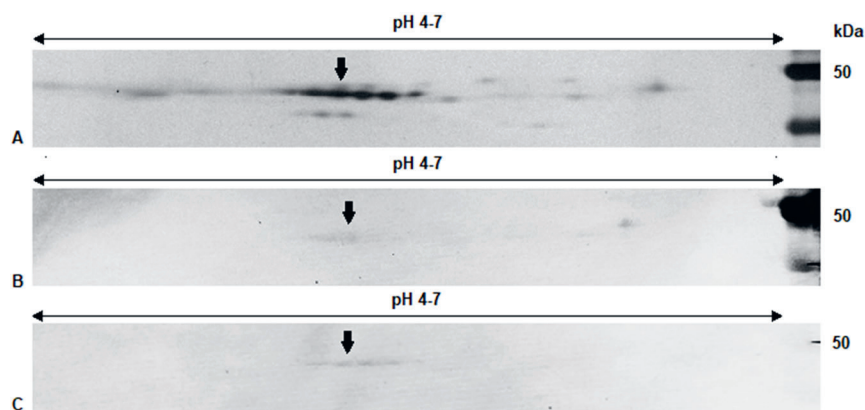


Fig. 3. Interaction of *S. Typhimurium* membrane proteins with antibodies against human enolases. A. Silver-stained 2-DE profile over pH 4–7 of *S. Typhimurium* OMPs isolated with CHAPS detergent after final purification using preparative electrophoresis. B. Immunoblotting of OMPs from *S. Typhimurium* with antibodies against human α -enolase. C. Immunoblotting of OMPs from *S. Typhimurium* with antibodies against human β -enolase. The spot identified by MS as enolase is indicated by the arrow

Enolase-like membrane protein from S. Typhimurium reacts with antibodies against human enolases

The OMPs exhibiting reactivity with anti-*S. Typhimurium* cytosolic enolase polyclonal antibodies were separated using 2-DE, and they bound antibodies against human α - and β -enolase. This revealed the serological similarity of epitopes of the enolase-like protein from *Salmonella* and from humans. The results of the immunoblotting assay are shown in Fig. 3B and 3C. Protein spots of interest were subsequently identified using liquid chromatography coupled with mass spectrometry. The OMP identification was achieved using the bioinformatics platform Mascot Search Engine to search the NCBI nr database. The protein identified was “Multispecies enolase (*Salmonella*); molecular weight: 45.627 kDa, pI: 5.25 Average sequence coverage: 65%”, score: 2625.

Scanning electron microscopy

Immunoelectron microscopy using anti-*S. Typhimurium* cytosolic enolase polyclonal antibodies confirmed the cell surface localization of enolase. On the outer membrane of the intact bacterial cell, reactivity was observed mostly at the flagella (Fig. 4A). In contrast, no labelling was observed in the negative control (Fig. 4B).

Discussion

Salmonella enolase has not previously been isolated and characterized. The procedure established in this study allowed us to obtain highly pure, enzymatically active enolase. The protein was purified and used to develop antibodies, which facilitated identification of the enolase-like protein on the bacterial outer membrane of *S. Typhimurium*. The efficiency of molecular biology methods and the ability to obtain recombinant proteins quickly gives these methods a greater advantage over long purification procedures developed to isolate native proteins.

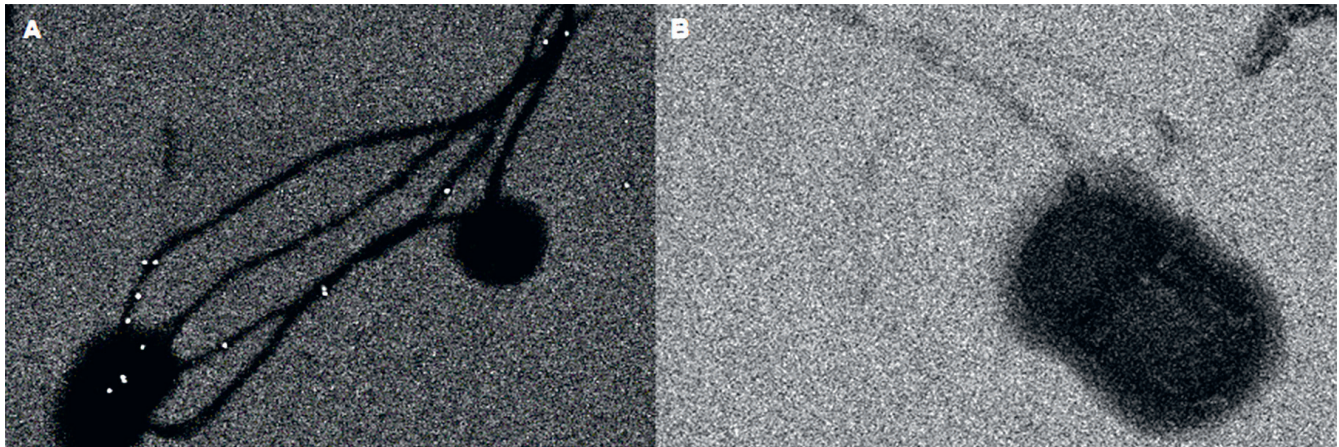


Fig. 4. Scanning electron microscopy localization of surface enolase on whole *S. Typhimurium* cells. A. Enolase detected with antibodies against bacterial cytosolic enolase and labeled with anti-rabbit antibodies coupled to 30 nm colloidal gold particles. B. Negative control with anti-rabbit antibodies coupled to 30 nm colloidal gold particles

Among the first microorganisms for which enolase isolation was described was Gram-positive *Brevibacterium fuscum*. Purification through salting and ion-exchange chromatography resulted in high protein losses and only 1.2% protein efficiency.²⁶ Chromatography affinity was used for the purification of *Streptococcus suis* enolase, leveraging the ability of the protein to bind to fibronectin.²⁷ *Escherichia coli* was the first Gram-negative bacterium for which the cytosolic enolase purification procedure was developed. Through desalting and the use of hydrophobic and ion exchange media, the purification of *E. coli* enolase yielded about 17%.²⁸ *Klebsiella pneumoniae* is another species of bacterium of the *Enterobacteriaceae* family for which an enolase purification procedure has been developed. After precipitation of the bacterial proteins with an 80–100% range of ammonium sulfate, gel filtration was performed, followed by ion exchange chromatography and preparative electrophoresis. The method developed in our laboratory yielded a 76-fold purification of cytosolic enolase with a total yield of 15%. This shows that preparative electrophoresis can be an effective purification method for an active enolase enzyme.¹⁷ The continuous development of chromatographic methods and media allowed us to improve the protein purification procedures and to reduce the number of steps. This minimized the loss of the active fraction of the enzyme, thus maintaining its biological properties.

We demonstrated that *S. Typhimurium* membrane proteins with a molecular mass of 45 kDa showed reactivity with antibodies against human α - and β -enolase, suggesting a serological similarity between epitopes. These observations indicate that *Salmonella* infections may cause the host immune system to produce antibodies against bacterial enolase and host enolase epitopes, resulting in the development of auto-aggressive diseases. There have been numerous examples of cross-reactivity between human and bacterial enolases. For example, cross-reactivity has been demonstrated between the enolase of the pathogen

causing periodontitis (*Treponema denticola*) and human α -enolase. Mice immunized with *T. denticola* enolase induced the production not only of antibodies against *T. dentolitic* enolase but also of antibodies against human α -enolase.²⁹ Similarly, antibodies against human α -enolase detected surface enolase on cells of *Borrelia burgdorferi*,³⁰ *Mycoplasma fermentans*³¹ and *Pseudomonas aeruginosa*.³² In studies of *Streptococcus agalactiae* immunogenic proteins, the bacterial enolase was identified as a protein that reacts with human antibodies from the sera of infected patients.³³ Lundberg et al. demonstrated that antibodies from the serum of rheumatoid arthritis (RA) patients showed cross-reactivity between citrullinated human α -enolase and recombinant citrullinated enolase from *Porphyromonas gingivalis*.³⁴ Moreover, Witkowska et al. demonstrated the immunoreactivity of the 45-kDa OMPs isolated from *K. pneumoniae*, *E. coli*, *Citrobacter*, and *Hafnia* membranes with patient antibodies and also with rabbit anti-human β -enolase antibodies.¹² Mass spectrometry analyses of *K. pneumoniae* enolase-like protein showed that several fragments of the 45-kDa protein were found to have sequences identical to the C-terminal domain of human β -enolase. Additionally, it has been reported that *Salmonella* membrane proteins with a range of 44–55 kDa were recognized by IgM antibodies from the serum samples of healthy patients and patients with Buerger's disease or psoriasis.¹² Among several *Enterobacteriaceae* species, only *Salmonella* protein of 44–55 kDa has been recognized by IgM antibodies. These results suggest that this protein may serve as a marker for the early phase of infection or recurrence as a result of a bacterial carrier state. The development of reactive arthritis is closely associated with infection of several Gram-negative enteric bacteria, including *Salmonella*.³⁵ Some patients with ulcerative colitis have higher odds of previous infection with *Salmonella* as well as *E. coli*, *Campylobacter* or *Clostridium difficile*.³⁶ Taken together, these results illustrate a potential link between autoimmune diseases and a history of food poisoning.

Scanning electron microscopy has corroborated the surface localization of membrane antigens that are reactive with anti-cytosolic enolase antibodies. It has also shown that enolase-like protein is present at the surface in low abundance, localized mostly to the flagella. The surface localization of *S. pneumoniae* enolase has also been confirmed using SEM.³⁷ Moreover, relatively low amounts of surface enolase have been proven to contribute to bacterial pathogenesis.¹¹ Enolase identified using SEM has been shown on the surface of *Streptococcus suis* and *Streptococcus pyogenes*.^{27,38} Enolase expressed on the surface could be recognized by the host immune system. The many reports of cross-reactivity between antibodies against human and bacterial enolases suggest that pathogen-related enolase may be involved in the development of autoimmune disease.

Our study showed that *Salmonella* membrane proteins with reactivity to antibodies against human α - and β -enolase also bound human plasminogen. Interestingly, the enolase isolated from the *Salmonella* cytosol had no plasminogen-binding capacity. The observed lack of affinity of the *S. Typhimurium* cytosolic enolase to human plasminogen, binding only to the enolase receptor located on the membrane of bacterial cells, suggests some structural differences between the 2 forms of enolase. This may be due to certain interactions of the enolase receptor protein with cell membrane components or to possible post-translational modification targeting the cell surface cytosolic protein. It is also important that the mechanisms leading to the transfer of this protein from the cytoplasm to the cell membrane and partial exposure to the cell surface are unknown. Koebnik et al. reported that the common structural β -barrel motif present in OMPs of Gram-negative bacteria is formed by a variable amount of transmembrane β -strands that expose the cell to a long loop available to the extracellular environment.⁷ It is interesting that in the three-dimensional structure of the cytosol, enolase is presented as C-terminal β -barrel domain with $\beta\beta\alpha(\beta\alpha)_6$ topology. As a classic cytosolic protein, enolase has no signal sequence, and no hydrophobic domain has been identified that would allow translocation to the cell membrane and anchoring in it. However, Redlitz et al. postulated that the hydrophobic domain splicing amino acids 33–44 near the N-terminus may serve as an internal signal sequence directing this protein to the cell membrane. Post-translational acylation through the addition of palmitic or myristic acid may be another explanation for the association of enolase with the cell membrane.³⁹

Plasminogen binding to enolase on the surface of bacterial cells has been demonstrated for bacteria such as *Borrelia burgdorferi*, *Mycoplasma fermentans* and *Pseudomonas aeruginosa*.^{30–32} However, there are studies that have shown plasminogen binding to the cytosolic fraction of Gram-positive bacteria.³⁷ Bacterial interaction with host plasminogen can elicit different effects. For example, in some commensals plasminogen plays a protective role

for the intestinal barrier by enhancing bacterial colonization; this mechanism has been described for bacteria from the *Bifidobacterium* genus.⁴⁰ Plasminogen can also promote invasion through the host tissue. Proteolytic activation of plasminogen results in the formation of plasmin, which degrades extracellular matrix proteins.³⁰ Further studies of the interaction between cytosol and membrane enolase obtained from Gram-negative bacteria with plasminogen are needed.

In conclusion, we have demonstrated for the first time the epitope similarity between *Salmonella* and human enolase. Additionally, we used electron microscopy to identify enolase-like protein on the surface of *S. Typhimurium*. This protein exhibits an affinity for human plasminogen, which indicates that *Salmonella* membrane enolase could play a role in interactions with host cells. The results of this study provide some insight into the interactions of *Salmonella* with the host and reveal new aspects of the role of glycolytic enzymes. It has become evident that the dual role of these enzymes is crucial to understanding the invasions and interactions of many pathogens with their hosts. The conservative structure of enolase may be a factor in autoimmune complications after bacterial infection. Further investigations may help to provide a comprehensive picture of these mechanisms.

ORCID iDs

Paweł Serek  <https://orcid.org/0000-0002-4685-4373>
 Iwona Bednarz-Misa  <https://orcid.org/0000-0001-7244-2017>
 Jadwiga Pietkiewicz  <https://orcid.org/0000-0001-5109-5618>
 Bartłomiej Dudek  <https://orcid.org/0000-0002-6181-3772>
 Magdalena Mierzchała-Pasierb  <https://orcid.org/0000-0001-9640-4883>
 Katarzyna Jermakow  <https://orcid.org/0000-0001-9889-4265>
 Marek Drab  <https://orcid.org/0000-0002-2771-1692>
 Andrzej Gamian  <https://orcid.org/0000-0002-2206-6591>

References

1. Cook J, Jeuland M, Whittington D, et al; DOMI Typhoid Economics Study Group. The cost-effectiveness of typhoid Vi vaccination programs: Calculations for four urban sites in four Asian countries. *Vaccine*. 2008;26(50):6305–6316. doi:10.1016/j.vaccine.2008.09.040
2. World Health Organization. Food safety. <https://www.who.int/news-room/fact-sheets/detail/food-safety>. Accessed June 30, 2020.
3. Popoff MY, Bockemuhl J, Gheesling LL. Supplement 2002 (No. 46) to the Kauffmann–White scheme. *Res Microbiol*. 2004;155(7):568–570. doi:10.1016/j.resmic.2004.04.005
4. World Health Organization. Salmonella (non-typhoidal). [https://www.who.int/en/news-room/fact-sheets/detail/salmonella-\(non-typhoidal\)](https://www.who.int/en/news-room/fact-sheets/detail/salmonella-(non-typhoidal)). Accessed June 30, 2020.
5. de Jong HK, Parry CM, van der Poll T, Wiersinga WJ. Host-pathogen interaction in invasive salmonellosis. *PLoS Pathog*. 2012;8(10):e1002933. doi:10.1371/journal.ppat.1002933
6. Alam J, Kim YC, Choi Y. Potential role of bacterial infection in autoimmune diseases: A new aspect of molecular mimicry. *Immune Netw*. 2014;14(1):7–13. doi:10.4110/in.2014.14.1.7
7. Koebnik R, Locher KP, Van Gelder P. Structure and function of bacterial outer membrane proteins: Barrels in a nutshell. *Mol Microbiol*. 2000;37(2):239–253. doi:10.1046/j.1365-2958.2000.01983.x
8. Pancholi V. Multifunctional α -enolase: Its role in diseases. *Cell Mol Life Sci*. 2001;58(7):902–920. doi:10.1007/PL00000910
9. López-Alemayn R, Longstaff C, Hawley S, et al. Inhibition of cell surface mediated plasminogen activation by a monoclonal antibody against alpha-enolase. *Am J Hematol*. 2003;72(4):234–242. doi:10.1002/ajh.10299

10. Díaz-Ramos À, Roig-Borrellas A, García-Melero A, López-Alemaný R. α -enolase, a multifunctional protein: Its role on pathophysiological situations. *J Biomed Biotechnol*. 2012;2012:156795. doi:10.1155/2012/156795
11. Kolberg J, Aase A, Bergmann S, et al. Streptococcus pneumoniae enolase is important for plasminogen binding despite low abundance of enolase protein on the bacterial cell surface. *Microbiology (Reading)*. 2006;152(Pt 5):1307–1317. doi:10.1099/mic.0.28747-0
12. Witkowska D, Pietkiewicz J, Szostko B, Danielewicz R, Masłowski L, Gamian A. Antibodies against human muscle enolase recognize a 45-kDa bacterial cell wall outer membrane enolase-like protein. *FEMS Immunol Med Microbiol*. 2005;45(1):53–62. doi:10.1016/j.femsim.2005.01.005
13. Lis J, Jarzab A, Witkowska D. Molecular mimicry in the etiology of autoimmune diseases. *Postepy Hig Med Dosw (Online)*. 2012;66:475–491. doi:10.5604/17322693.1003484
14. Lee KH, Chung HS, Kim HS, et al. Human alpha-enolase from endothelial cells as a target antigen of anti-endothelial cell antibody in Behçet's disease. *Arthritis Rheum*. 2003;48(7):2025–2035. doi:10.1002/art.11074
15. Fujii A, Yoneda M, Ito T, et al. Autoantibodies against the amino terminal of α -enolase are a useful diagnostic marker of Hashimoto's encephalopathy. *J Neuroimmunol*. 2005;162(1–2):130–136. doi:10.1016/j.jneuroim.2005.02.004
16. Nezos A, Cinoku I, Mavragani CP, Moutsopoulos HM. Antibodies against citrullinated alpha enolase peptides in primary Sjogren's syndrome. *Clin Immunol*. 2017;183:300–303. doi:10.1016/J.CLIM.2017.09.012
17. Bednarz-Misa I, Pietkiewicz J, Banaś T, Gamian A. Enolase from *Klebsiella pneumoniae* and human muscle cells. I. Purification and comparative molecular studies. *Adv Clin Exp Med*. 2009;18(1):71–78.
18. Wold F. Enolase. In: Boyer PD, ed. *The Enzymes*, 3rd edition, vol. V. New York, NY, USA: Academic Press; 1971: 499–538.
19. Baranowski T, Wolna E. Enolase from human muscle. *Methods Enzymol*. 1975;42(C):335–338. doi:10.1016/0076-6879(75)42137-1
20. Laemmli UK. Cleavage of structural proteins during the assembly of the head of bacteriophage T4. *Nature*. 1970;227(5259):680–685. doi:10.1038/227680a0
21. Bugla-Płoskońska G, Futoma-Kołoń B, Skwara A, Doroszkiewicz W. Use of zwitterionic type of detergent in isolation of *Escherichia coli* O56 outer membrane proteins improves their two-dimensional electrophoresis (2-DE). *Polish J Microbiol*. 2009;58(3):205–209.
22. Gromova I. Protein detection in gels by silver staining: A procedure compatible with mass spectrometry. *Cell Biol*. 2006;4:219–223. doi:10.1016/B978-012164730-8/50212-4
23. Malinowska A, Kistowski M, Bakun M, et al. Diffprot: Software for non-parametric statistical analysis of differential proteomics data. *J Proteomics*. 2012;75(13):4062–4073. doi:10.1016/J.JPROT.2012.05.030
24. Hodyra-Stefaniak K, Miernikiewicz P, Drapała J, et al. Mammalian host-versus-phage immune response determines phage fate in vivo. *Sci Rep*. 2015;5:14802. doi:10.1038/srep14802
25. Drab M, Krajniak J, Grzelakowski KP. The new methodology and chemical contrast observation by use of the energy-selective back-scattered electron detector. *Microsc Microanal*. 2016;22(6):1369–1373. doi:10.1017/S1431927616012514
26. Saito N. Purification and properties of bacterial phosphopyruvate hydratase. *J Biochem*. 1967;61(1):59–69. doi:10.1093/oxfordjournals.jbchem.a128521
27. Esgleas M, Li Y, Hancock MA, Harel J, Dubreuil JD, Gottschalk M. Isolation and characterization of α -enolase, a novel fibronectin-binding protein from *Streptococcus suis*. *Microbiology*. 2008;154(9):2668–2679. doi:10.1099/mic.0.2008/017145-0
28. Dannelly HK, Reeves HC. Purification and characterization of enolase from *Escherichia coli*. *Curr Microbiol*. 1988;17(5):265–268. doi:10.1007/BF01571326
29. Lee A, Kim YC, Baek K, et al. Treponema denticola enolase contributes to the production of antibodies against ENO1 but not to the progression of periodontitis. *Virulence*. 2018;9(1):1263–1272. doi:10.1080/21505594.2018.1496775
30. Floden AM, Watt JA, Brissette CA. Borrelia burgdorferi enolase is a surface-exposed plasminogen binding protein. *PLoS One*. 2011;6(11):e27502. doi:10.1371/journal.pone.0027502
31. Yavlovich A, Rechnitzer H, Rottem S. Alpha-enolase resides on the cell surface of *Mycoplasma fermentans* and binds plasminogen. *Infect Immun*. 2007;75(12):5716–5719. doi:10.1128/IAI.01049-07
32. Ceremuga I, Seweryn E, Bednarz-Misa I, et al. Enolase-like protein present on the outer membrane of *Pseudomonas aeruginosa* binds plasminogen. *Folia Microbiol (Praha)*. 2014;59(5):391–397. doi:10.1007/s12223-014-0311-9
33. Dobrut A, Brzozowska E, Górska S, et al. Epitopes of immunoreactive proteins of *Streptococcus agalactiae*: Enolase, inosine 5'-monophosphate dehydrogenase and molecular chaperone GroEL. *Front Cell Infect Microbiol*. 2018;8:349. doi:10.3389/fcimb.2018.00349
34. Lundberg K, Wegner N, Yucel-Lindberg T, Venables PJ. Periodontitis in RA: The citrullinated enolase connection. *Nat Rev Rheumatol*. 2010;6(12):727–730. doi:10.1038/nrrheum.2010.139
35. Rohekar S, Tsui FWL, Tsui HW, et al. Symptomatic acute reactive arthritis after an outbreak of salmonella. *J Rheumatol*. 2008;35(8):1599–1602. <http://www.ncbi.nlm.nih.gov/pubmed/18528961>. Accessed June 30, 2020.
36. Axelrad JE, Olén O, Askling J, et al. Gastrointestinal infection increases odds of inflammatory bowel disease in a nationwide case-control study. *Clin Gastroenterol Hepatol*. 2018. doi:10.1016/J.CGH.2018.09.034
37. Bergmann S, Rohde M, Chhatwal GS, Hammerschmidt S. Alpha-enolase of *Streptococcus pneumoniae* is a plasmin(ogen)-binding protein displayed on the bacterial cell surface. *Mol Microbiol*. 2001;40(6):1273–1287. doi:10.1046/j.1365-2958.2001.02448.x
38. Pancholi V, Fischetti VA. Alpha-enolase, a novel strong plasmin(ogen) binding protein on the surface of pathogenic streptococci. *J Biol Chem*. 1998;273(23):14503–14515. doi:10.1074/jbc.273.23.14503
39. Redlitz A, Fowler BJ, Plow EF, Miles LA. The role of an enolase-related molecule in plasminogen binding to cells. *Eur J Biochem*. 1995;227(1–2):407–415. doi:10.1111/j.1432-1033.1995.tb20403.x
40. Candela M, Biagi E, Centanni M, et al. Bifidobacterial enolase, a cell surface receptor for human plasminogen involved in the interaction with the host. *Microbiology (Reading)*. 2009;155(10):3294–3303. doi:10.1099/mic.0.028795-0

The true nature of P wave dispersion

Jacek Marcin Zawadzki^{1,A,C–F}, Katarzyna Zimmer^{2,A–C,E,F}, Wojciech Przywara^{3,A–C,E,F},
Dorota Zysko^{4,C,E,F}, Jadwiga Radziejewska^{1,B,C,F}, Agnieszka Sławuta^{5,B,C,E,F}, Jacek Gajek^{6,A–F}

¹ Department of Cardiology, Klodzko County Hospital, Poland

² Clinic and Department of Ophthalmology, Wrocław Medical University Hospital, Poland

³ Department of Dermatology, Regional Specialist Hospital in Wrocław, Poland

⁴ Department of Emergency Medicine, Wrocław Medical University, Poland

⁵ Department of Internal and Occupational Diseases, Hypertension and Clinical Oncology Wrocław Medical University, Poland

⁶ Department of Emergency Medical Service, Wrocław Medical University, Poland

A – research concept and design; B – collection and/or assembly of data; C – data analysis and interpretation;

D – writing the article; E – critical revision of the article; F – final approval of the article

Advances in Clinical and Experimental Medicine, ISSN 1899–5276 (print), ISSN 2451–2680 (online)

Adv Clin Exp Med. 2020;29(12):1443–1447

Address for correspondence

Jacek Zawadzki

E-mail: jacekzawadzki@gmail.com

Funding sources

None declared

Conflict of interest

None declared

Received on May 25, 2020

Reviewed on June 1, 2020

Accepted on October 8, 2020

Abstract

Background. The electrophysiological activity of the heart is recorded and presented in form of electrocardiography (ECG). In 1998, the concept of P wave dispersion as the risk factor for atrial fibrillation (AF) recurrence was introduced. It was calculated as the difference between the longest and the shortest P wave.

Objectives. To prove that the P wave dispersion is an artifact of low accuracy in P wave measurement.

Material and methods. The study included 104 patients (48 women, 56 men), aged 63 ± 14 years, undergoing various electrophysiological procedures. The P wave was measured twice – firstly at the paper speed of 50 mm/s, enhancement $\times 8$ (standard – imprecise), and secondly at 200 mm/s, $\times 64$ –256 (precise).

Results. The imprecise measurement method resulted in different duration of all P wave parameters in comparison with precise measurement. The longest P wave duration (Pmax) measured imprecisely was 105.1 ± 22.1 , the Pmax measured precisely was 134.0 ± 21.3 ($p < 0.001$). The P dispersion measured imprecisely was 44.1 ± 16.8 and the P dispersion measured precisely was 2.8 ± 3.4 ($p < 0.0001$). The correlation between imprecise Pmax and imprecise Pmin was $r = 0.664$ ($p < 0.05$). The correlation between imprecise Pmax and imprecise P wave dispersion was $r = 0.612$ ($p < 0.05$). The correlation between precise Pmax and Pmin was almost 1.0 ($r = 0.987$, $p < 0.05$).

Conclusions. The P wave dispersion does not exist. The measurements of the P wave have to be precise to assure the highest scientific and medical sincerity. The highest clinical value is related to the P wave duration.

Key words: P wave dispersion, P wave duration, total atrial activation time

Cite as

Zawadzki JM, Zimmer K, Przywara W, et al.

The true nature of P wave dispersion. *Adv Clin Exp Med.*

2020;29(12):1443–1447. doi:10.17219/acem/128232

DOI

10.17219/acem/128232

Copyright

© 2020 by Wrocław Medical University

This is an article distributed under the terms of the

Creative Commons Attribution 3.0 Unported (CC BY 3.0)

(<https://creativecommons.org/licenses/by/3.0/>)

Introduction

The electrophysiological activity of the working myocardium is recorded by the system of simultaneous leads of the electrocardiograph and presented in the form of electrocardiography (ECG).¹ The morphology of ECG recording in a specific lead is the result of the direction of the depolarization wave propagation and the range of spatial registration of the given lead.² The recording is performed simultaneously in all leads, i.e., the given phenomenon is recorded simultaneously by all leads of the electrocardiogram.³ In the case of a perpendicular activation vector in a bipolar lead and a parallel vector in the case of a unipolar lead, the isoelectric line is recorded by given lead.⁴

In 1998, Dilaveris et al. introduced the concept of P wave dispersion as ‘a marker of the nonuniform anisotropic inhomogeneous atrial conduction’ – cited from the original work – and the risk factor for atrial fibrillation (AF) recurrence.⁵ This P wave dispersion was determined as the difference between the longest and the shortest P wave duration (Pmax and Pmin), measured in 2 different ECG leads. The measurement methodology included simultaneously recording all 12 leads at the paper speed of 50 mm/s and the enhancement of 1 mV/cm as well as using a magnifying lens to increase measurement precision. In a group of 60 patients aged 59.0 ± 12.0 years with diagnosed idiopathic paroxysmal AF, the mentioned dispersion was 49 ± 15 ms (Pmax) and 28 ± 7 ms (Pmin) in the group of 40 healthy people, which was statistically significant. It should be emphasized that the compared groups were well matched according to the sociodemographic parameters, left atrial size, atrioventricular conduction time, and left ventricular ejection fraction (LVEF). In addition to the value of dispersion measured this way, the study groups also differed in the duration of the P wave (123 ± 16 ms compared to 101 ± 10 ms, $p < 0.0001$). Further statistical analysis showed that the risk of recurrent AF in patients was more related to the dispersion parameter exceeding 40 ms than the duration of the P wave above 110 ms.⁵ In the following years, many researchers reproduced the original results, using more or less the same flawed methodology in various groups of patients and reaching similar conclusions.^{6–8}

The research hypothesis of our study is to prove the non-existence of the P wave dispersion parameter, i.e., the defined parameter is an artifact of no accuracy in measuring the P wave (incorrect measurement methodology). The aim of our study was to assess the P wave parameters in the patient group undergoing different electrophysiological procedures.

Material and methods

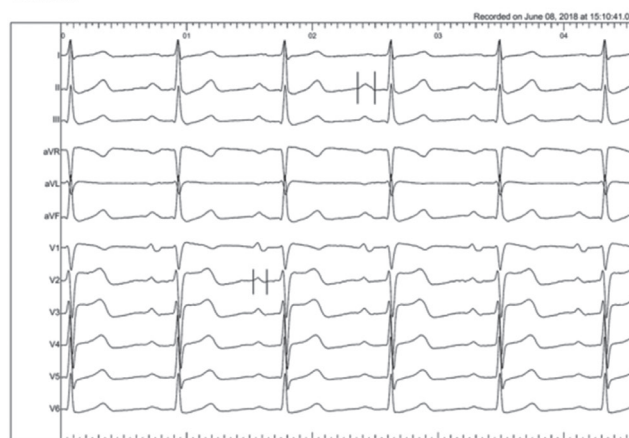
The study included 104 non-selected patients (48 women, 56 men), aged 63 ± 14 years (range: 21–89 years), undergoing various electrophysiological procedures using

LabSystem™ Pro EP Recording System (Boston Scientific, Boston, USA), (electrophysiological studies; AV-nodal reentrant tachycardia (AVNRT), atrioventricular reentrant tachycardia (AVRT), atrial flutter (AFL), right ventricular outflow tract (RVOT) arrhythmia ablations). The only inclusion criterion was the presence of sinus rhythm and the quality of the ECG tracings, which allowed us to measure the sinus P wave duration.

The P wave duration was measured in all leads twice: firstly time at the paper speed of 50 mm/s, enhancement $\times 8$ (basic measurement), and secondly at the paper speed of 200 mm/s, enhancement $\times 64$ – 256 (Fig. 1). The P wave dispersion was calculated as the difference between Pmax and Pmin in different leads for each measurements setting. The P wave measurements for every tracing were repeated 5 times for accuracy by 2 independent researches, who were unaware of each other's results and who were blinded to clinical data. The final value presented for each patient was their mean.

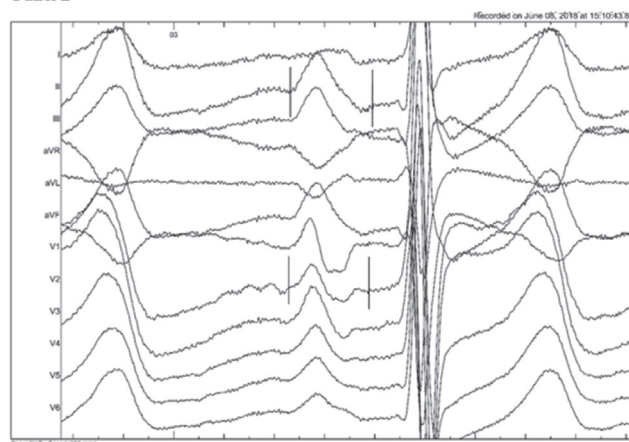
The study was approved by the local Bioethical Committee at Wroclaw Medical University, Poland.

Panel A



Lead II: 140 ms; Lead V2: 99 ms; Speed: 50 mm/s; Enhancement: 8x

Panel B



Lead II: 172 ms; Lead V2: 166 ms; Speed: 200 mm/s; Enhancement: 128x

Fig. 1. The methodology of P wave duration measurements and P wave dispersion calculations in different settings

A – imprecise measurement indicated the Pmax in lead II and Pmin in lead V2; B – the same was repeated in precise way in the same leads.

Statistical analysis

The continuous variables are presented as the means and standard deviations (SD) or medians and interquartile ranges (IQRs). The comparisons were performed with the parametrical Students-t test or non-parametrical Wilcoxon paired test for dependent variables. The correlations between the studied parameters were performed using Pearson’s correlations coefficient or Spearman’s rank correlation according to the statistical properties of the data. The p-values less than 0.05 were considered to be statistically significant.

Results

The results of the P wave parameters measurements using the standard method (basic measurements) and the precise method and their derivatives are presented in Table 1.

The use of the imprecise measurement method (basic measurement) resulted in significantly different duration of all P wave parameters taken, in comparison with precise measurement. What is more important, the difference between Δ Pmax and Δ Pmin indicated a much higher value for the latter parameter. The correlation between imprecise Pmax and imprecise Pmin is presented in Fig. 2. This presented relationship indicated a high correlation coefficient, amounting to 0.7. The correlation between imprecise Pmax and imprecise P wave dispersion is depicted in Fig. 3.

It was indicated that the imprecise P wave dispersion value correlated highly significantly with Pmax measured in a similar way. The correlation between precise Pmax and precise Pmin is shown in Fig. 4.

In contrast with the imprecise measurement method, Pmax and Pmin measured accurately were almost identical.

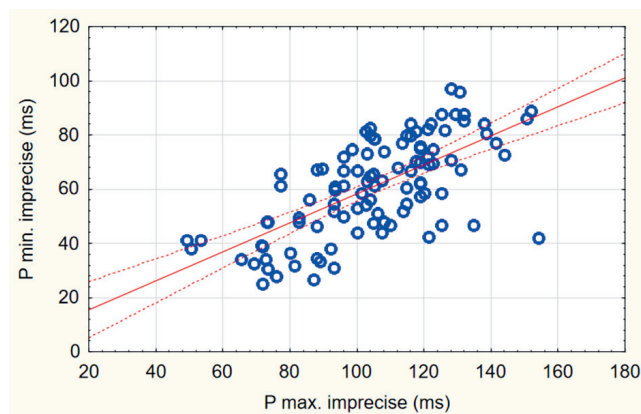


Fig. 2. The correlation between imprecise Pmax and imprecise Pmin ($r = 0.664, p < 0.05$)

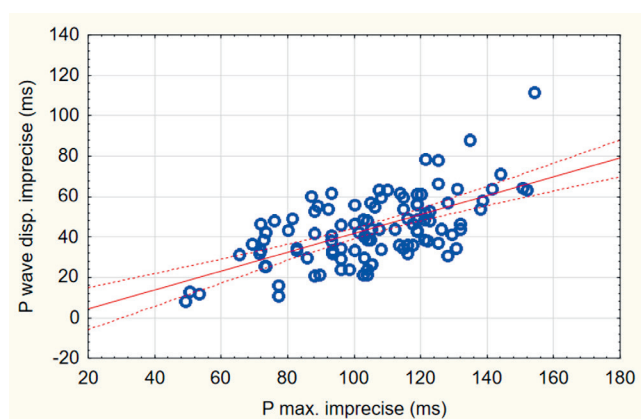


Fig. 3. The correlation between imprecise Pmax and imprecise P wave dispersion ($r = 0.612, p < 0.05$)

This resulted in correlation coefficient approaching 1.0. Figure 5 presents the contrast between the imprecise and precise Pmax measurements.

Table 1. Basic statistics of the P wave parameters

| Parameters [ms] | Basic statistics | | |
|---------------------|------------------|----------------------|------------|
| | M ±SD | Me [Q1, Q3] | Min–Max |
| Pmax | | | |
| Imprecise (n = 104) | 105.1 ±22.1* | 105.3 [90.7; 120.5] | 49.3–154.0 |
| Precise (n = 104) | 134.0 ±21.3* | 130.5 [120.8; 149.3] | 54.3–199.0 |
| Pmin | | | |
| Imprecise (n = 104) | 61.0 ±17.8# | 61.7 [47.3; 75] | 25.3–97.3 |
| Precise (n = 104) | 131.2 ±21.2# | 128.5 [118.0; 147.2] | 54.3–187.3 |
| P wave dispersion | | | |
| Imprecise (n = 104) | 44.1 ±16.8& | 43.3 [33.3; 55.3] | 8.0–112.0 |
| Precise (n = 104) | 2.8 ±3.4& | 1.4 [0.0; 5.4] | 0.0–11.7 |
| Pmax difference (Δ) | 29.0 ±26.3® | 22.3 [9.8; 42.6] | –6.7–108.3 |
| Pmin difference (Δ) | 70.2 ±28.0® | 67.4 [49.8; 88.4] | 13.0–147.0 |

*p < 0.001; #p < 0.001; &p < 0.0001; ®p < 0.001; M – mean; SD – standard deviation; Me – median; Q1 – lower quartile; Q3 – upper quartile; Min–Max – minimal–maximal range.

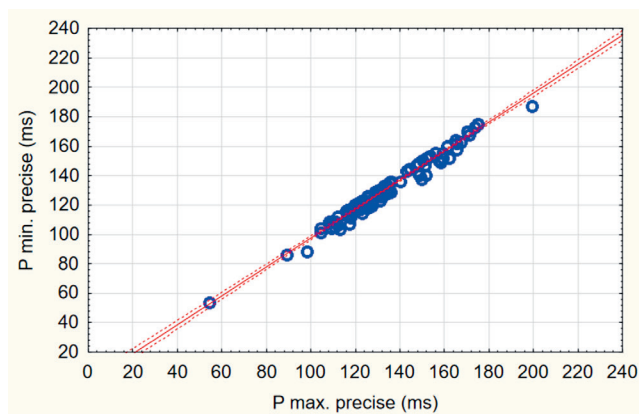


Fig. 4. The correlation between precise Pmax and precise Pmin ($r = 0.987$, $p < 0.05$)

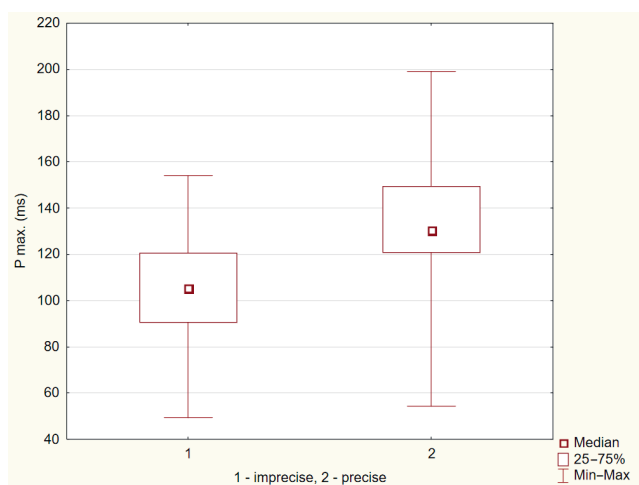


Fig. 5. The contrast between the imprecise and precise Pmax measurements ($p < 0.001$)

Discussion

One of the main principles of ECG is the simultaneous recording of an electrical signal in each lead. Therefore, if an event started in one lead, it continues in all others simultaneously. Similarly, if it is still present in any lead, it cannot be assumed that in the others it has already ended. The ECG signal – lead direction dependence mentioned in the introduction in the individual types of leads – results in the fact that some of them do not register a signal (isoelectric line) when the electric vector moves in a specific direction relative to the lead. In reality, however, we do not deal with 0/1 situations understood in this way and the isoelectric line in a given lead, in the face of an ongoing event in other leads, never occurs. At most, the voltage of the recorded signal in a given situation is beyond our perception.

The main result of our study, performed in an unselected group of patients undergoing electrophysiological procedure, disproves the existence of the so-called P wave dispersion. The use of an accurate method of the measurement

of the P wave duration eliminates the difference between the so-called Pmax and Pmin, i.e., the dispersion tends to 0. In fact, the difference of 0 ms was in the group of the studied patients in 46 out of 104 patients, up to 5 ms in 31 out of 104 patients, up to 10 ms in 24 out of 104 patients, and more than 10 ms in 3 patients. What is more, the high dispersion relationship of the P wave with Pmax, both measured using an imprecise method, clearly shows that the so-called dispersion is a derivative of the real length of the P wave and any of its incorrect (not precisely measured) minimum lengths. In addition, the correlation we have shown of Pmax and Pmin measured precisely, with a correlation coefficient tending to unity, confirms our conclusion.

It is not without reason that the precision of the P wave measurement, or rather the lack thereof, has been the subject of numerous studies over the past 2 decades, following the publication of the original publication on the P wave dispersion parameter.^{9,10} The authors were aware of the key importance of measurement accuracy and precision for proper clinical judgement. Even the author of the concept of the dispersion P wave pointed to such need relatively recently.¹¹ However, these voices always assumed the presence of the parameter itself and the methodology used (e.g., paper shifts 50 mm/s and gain 2 cm/1 mV, with the use of magnifying glasses) was far from perfect.^{12,13} In addition, no one indicated the key incompatibility of dispersion with the ECG principles mentioned previously.

Already in 2015, we pointed to the aforementioned problem, using the results on slightly more modest patient material. Based on similar results, we pointed out that the concept of P wave dispersion is based on incorrect methodology and in reality does not exist.¹⁴ Although this publication did not go unnoticed, in the meantime, numerous papers have been published that still describe the phenomenon of P wave dispersion,^{15–17} and an interesting interpretation of our study has appeared.⁶ Chávez-González and Donoiu, while citing our work, commented it like this: “Despite this, we continue to believe there is sufficient proof supporting the PWD (P wave dispersion) importance in the clinical practice and continuation of research.” The word ‘believe’ is crucial in this context.

In the perspective of our results, there is a need to reassess the initial brilliant idea of the relation between the P wave parameters and the risk of atrial arrhythmia, in particular AF. The already mentioned inaccuracy issues related to the P wave duration measurements are obviously caused by the small amplitude of P waves in some ECG leads. Low amplitude P wave signal is characteristic for advanced atrial muscle disease, which obviously will result in time in AF. There is a vast variety of scientific papers supporting this issue.^{18–20} Moreover, the interatrial conduction abnormalities introduced so successfully by Bayés de Luna et al. and other researchers could be also the causes of changes in amplitude and morphology of the P wave.^{21,22} In our opinion, the initial results

indicating the more relevant relation of AF with P wave dispersion than P duration is clearly the result of the discussed measurements inaccuracy.

In summary, in light of our results, we conclude that the so-called P wave dispersion is a measurement artefact, related to wrong methodology. The increase in measurement precision makes it simply disappear. Its clinical utility can be explained by its dependence on P wave duration, which reflects the left atrial muscle structural and functional disorders. The proper P wave duration parameter should be the ‘total atrial activation time’ already proposed by us, calculated in the simultaneously recorded 12-lead ECG, from the beginning of the earliest recorded P wave deflection, until the end of the latest P wave deflection recorded in any lead.¹⁴ This approach was recently supported by Bayés de Luna et al., explicitly advising that the P wave should be measured from its earliest beginning in any lead to the latest end in any lead.²³ Most probably the 21st century will require appropriate methodology and change of approach.

Study limitations

A serious limitation of our study is its single-center nature and relatively small study group. In addition, this is not a prospective study showing the relationship between ECG parameter and clinical prognosis. The influence of the human factor and the screen resolution of the monitors on the possibilities of limiting its impact on the obtained measurement results have not been discussed, and it should be emphasized that even with the precise measurement methodology, the differences in P wave duration were not 0 ms in all patients. Additionally, ECG tracing artifacts may influence even very precise measurements.

Conclusions

1. The P wave dispersion does not exist.
2. The measurements of the P wave and considerations of its doubtless clinical usefulness have to be precise to assure the highest scientific and medical sincerity.
3. The highest clinical value is related to the properly measured P wave duration.

ORCID iDs

Jacek Marcin Zawadzki  <https://orcid.org/0000-0003-4000-4164>
 Katarzyna Zimmer  <https://orcid.org/0000-0003-2300-8585>
 Wojciech Przywara  <https://orcid.org/0000-0002-1245-4785>
 Dorota Zyśko  <https://orcid.org/0000-0001-9190-0052>
 Jadwiga Radziejewska  <https://orcid.org/0000-0001-9153-9754>
 Agnieszka Sławuta  <https://orcid.org/0000-0001-5671-9864>
 Jacek Gajek  <https://orcid.org/0000-0002-0038-1750>

References

1. Becker ED. Fundamentals of electrocardiography interpretation. *Anesth Ed.* 2006;53(2):53–64.
2. Murthy ISN, Prasad GSSD. Analysis of ECG from pole-zero models. *IEEE Trans Biomed Eng.* 1992;39(7):741–751.
3. Bayés de Luna A. *Basic Electrocardiography: Normal and Abnormal ECG Patterns.* Hoboken, NJ: Blackwell Publishing; 2008. ISBN-13: 978-1405175708.
4. Grant RP. Spatial vector electrocardiography: A method for calculating the spatial electrical vectors of the heart from conventional leads. *Circulation.* 1950;2(5):676–695.
5. Dilaveris PE, Gialafos EJ, Sideris SK, et al. Simple electrocardiographic markers for the prediction of paroxysmal idiopathic atrial fibrillation. *Am Heart J.* 1998;135(5 Pt 1):733–738.
6. Chávez-González E, Donoio I. Utility of P-wave dispersion in the prediction of atrial fibrillation. *Curr Health Sci J.* 2017;43(1):5–11.
7. Aytémir K, Ozer N, Atalar E, et al. P wave dispersion on 12-lead electrocardiography in patients with paroxysmal atrial fibrillation. *Pacing Clin Electrophysiol.* 2000;23(7):1109–1112.
8. Gunduz H, Binak E, Arinc H, et al. The relationship between P wave dispersion and diastolic dysfunction. *Tex Heart Inst J.* 2005;32(2):163–167.
9. Darbar D, Jahangir A, Hammill SC, Gersh BJ. P wave signal-averaged electrocardiography to identify risk for atrial fibrillation. *Pacing Clin Electrophysiol.* 2002;25(10):1447–1453.
10. Nakatani Y, Sakamoto T, Yamaguchi Y, Tsujino Y, Kataoka N, Kinugawa K. Coefficient of variation of P-wave duration measured using an automated measurement system predicts recurrence of atrial fibrillation. *J Electrocardiol.* 2019;53:79–84.
11. Dilaveris P, Tousoulis D. P-wave dispersion measurement: Methodological considerations. *Indian Pacing Electrophysiol J.* 2017;17(3):89.
12. Dilaveris P, Stefanadis C. P-wave dispersion and atrial fibrillation risk: Methodological considerations. *Am J Cardiol.* 2011;107(9):1405.
13. Dilaveris PE, Gialafos JE. P-wave duration and dispersion analysis: Methodological considerations. *Circulation.* 2001;103(21):E111-1.
14. Zimmer K, Przywara W, Zyśko D, Sławuta A, Gajek J. The nature of P-wave dispersion: A clinically useful parameter that does not exist. *Int J Cardiol.* 2016;212:59–60.
15. Yolbaş S, Yıldırım A, Düzenci D, Karakaya B, Necati Dağlı M, Serdar Koca S. QT dispersion and P wave dispersion in patients with fibromyalgia. *Eur J Rheumatol.* 2016;3(4):165–168.
16. Pérez-Riera AR, de Abreu LC, Barbosa-Barros R, Grindler J, Fernandes-Cardoso A, Baranchuk A. P-wave dispersion: An update. *Indian Pacing Electrophysiol J.* 2016;16(4):126–133.
17. Demirci S, Arslan A, Yürekli VA, Kutluhan S, Rifat Koyuncuoğlu H, Demirci S. P-wave dispersion in patients with Guillain-Barré syndrome. *Acta Neurol Belg.* 2017;117:289–293.
18. Park JK, Park J, Uhm JS, Joung B, Lee MH, Pak HN. Low P-wave amplitude (<0.1 mV) in lead I is associated with displaced inter-atrial conduction and clinical recurrence of paroxysmal atrial fibrillation after radiofrequency catheter ablation. *Europace.* 2016;18(3):384–391.
19. Schreiber T, Kähler N, Tscholl V, et al. Correlation of P-wave properties with the size of left atrial low voltage areas in patients with atrial fibrillation. *J Electrocardiol.* 2019;56:38–42.
20. Ooie T, Wakisaka O, Hujita T, et al. A specific combination of P wave duration and morphology accurately predicts the presence of left atrial low voltage area in patients with atrial fibrillation. *J Electrocardiol.* 2019;2019:S0022-0736(19)30549-7.
21. Bayés de Luna A, Fort de Ribot R, Trilla E, et al. Electrocardiographic and vectorcardiographic study of interatrial conduction disturbances with left atrial retrograde activation. *J Electrocardiol.* 1985;18(1):1–13.
22. Holmqvist F, Platonov PG, Carlson J, Zareba W, Moss AJ; MADIT II Investigators. Altered interatrial conduction detected in MADIT II patients bound to develop atrial fibrillation. *Ann Noninvasive Electrocardiol.* 2009;1(3):4:268–275.
23. Bayés de Luna A, Baranchuk A, Escobar Robledo AL, Massó van Roessel A, Martínez-Sellés M. Diagnosis of interatrial block. *J Geriatr Cardiol.* 2017;14(3):161–165.

Does image file transfer, exposure time and optimization algorithm affect digital intraoral radiographs?

Wojciech Grzebieluch^{1,A–D}, Urszula Kaczmarek^{2,D–F}, Tomasz Staniowski^{2,B–D}, Marcin Mikulewicz^{3,D–F}

¹ Laboratory for Digital Dentistry, Department of Conservative Dentistry and Pedodontics, Wrocław Medical University, Poland

² Department of Conservative Dentistry and Pedodontics, Wrocław Medical University, Poland

³ Division of Facial Abnormalities, Department of Maxillofacial Orthopedics and Orthodontics, Wrocław Medical University, Poland

A – research concept and design; B – collection and/or assembly of data; C – data analysis and interpretation;

D – writing the article; E – critical revision of the article; F – final approval of the article

Advances in Clinical and Experimental Medicine, ISSN 1899–5276 (print), ISSN 2451–2680 (online)

Adv Clin Exp Med. 2020;29(12):1449–1458

Address for correspondence

Wojciech Grzebieluch

E-mail: dentysta@poczta.fm

Funding sources

None declared

Conflict of interest

None declared

Received on July 21, 2020

Reviewed on July 24, 2020

Accepted on October 8, 2020

Abstract

Background. The transfer of digital radiographic images is widely practiced. Digital image processing can influence the perception of image quality. The question arises as to how exposure, internal image adjusting algorithms and image file transfer affect the optical density of digital radiographs.

Objectives. To evaluate the influence of exposure time, optimization and file transfer on digital radiographs.

Material and methods. Calibration patterns were formed and a series of digital radiograms were recorded under standardized conditions. The radiographs were exported and then imported into the same software. Three groups of radiographs were analyzed: A – images originally performed and recorded in the software; B – images imported after exporting an optimized image; and C – images imported after exporting an image without optimization but with measurements of the density of the marked regions of interest.

Results. An increase of the exposure time decreases optical density. The optimization algorithm increases contrast and decreases differences between exposure times. Long exposures affect the visibility of objects with low optical density. After importing the images in Group B, there was a risk of using the optimization algorithm twice. When optimization was not performed, there were no differences between Groups B and A. In Group C, there was no risk of doubling the optimization algorithm.

Conclusions. The transfer of digital radiographs can exert an influence on the optical density values. To avoid the risk of image distortion, files should be exported without image optimization.

Key words: image analysis, digital radiography, image transfer

Cite as

Grzebieluch W, Kaczmarek U, Staniowski T, Mikulewicz M. Does image file transfer, exposure time and optimization algorithm affect digital intraoral radiographs? *Adv Clin Exp Med.* 2020;29(12):1449–1458. doi:10.17219/acem/128231

DOI

10.17219/acem/128231

Copyright

© 2020 by Wrocław Medical University

This is an article distributed under the terms of the Creative Commons Attribution 3.0 Unported (CC BY 3.0) (<https://creativecommons.org/licenses/by/3.0/>)

Introduction

The traditional technology using X-ray films is being replaced by digital radiography and other digital technologies. Images recorded on radiographs are black and white and individual pixels possess a specific lightness ranging from 0 to 255 (256-grade 8-bit grayscale – the scale of optical density). The brighter the area appears on radiographs, the higher the optical density. The software (the internal algorithms of image processing) compensates for changes in exposure time and allows the images to have suitable brightness and contrast; therefore, “lighted” (dark) or “under-exposed” (bright) images are uncommon.^{1,2} Digital processing of image parameters such as brightness, contrast, sharpening, smoothing, and zooming can correct the visibility of certain regions, making the image more accessible to the human eye. However, digital image processing can produce artefacts that may resemble pathologies.^{3–5} The software also makes it possible to measure the length, angle and optical density of selected areas of the image.^{6,7} In the case of measuring the length of an object, the picture can be calibrated; however, in case of the optical density measurements (radiodensitometry and radioabsorption), this is not possible. The transfer of digital radiographs and the scanning of conventional radiographs to obtain a digital image is practiced widely, but digital processing of an image can have some impact on both the diagnostic value of the X-ray image and the subjective perception of the image quality.⁸

The advantage of digital images lies in the ease of storage and transferring. However, it should be also remembered that most dental software uses an internal, integrated optimization algorithm to compensate for the exposure conditions and sensor properties. Therefore, the question arises as to how the exposure conditions, internal image adjusting algorithms and image file transfer affect the optical density of digital radiographs. There is a lack of data in the available literature on this topic.

The purpose of the study was to evaluate the impact that file transfer, exposure time and the optimization algorithm have on the optical density of dental radiographs.

Material and methods

A pattern containing 2 separate stepped-wedge patterns for digital radiographs was produced. Pattern 1 was formed from aluminum and consisted of 5 steps: 0.7 mm, 1.3 mm, 1.9 mm, 2.5 mm, and 3.1 mm. Pattern 2, showing lower radiolucency, was made from lead foil that originated from radiographic film (Foton Dental DX-D 3–4 cm ANSI 1. ISO W2 Emulsion No. 00905.3; Foton, Warsaw, Poland) and consisted of 4 steps formed by 1–4 foil layers (Fig. 1). Radiographs were taken with a digital radiography Dixi 3-CCD sensor (Planmeca, Helsinki, Finland), Planmeca Intra X-ray apparatus (Planmeca) and Dimaxis Classic

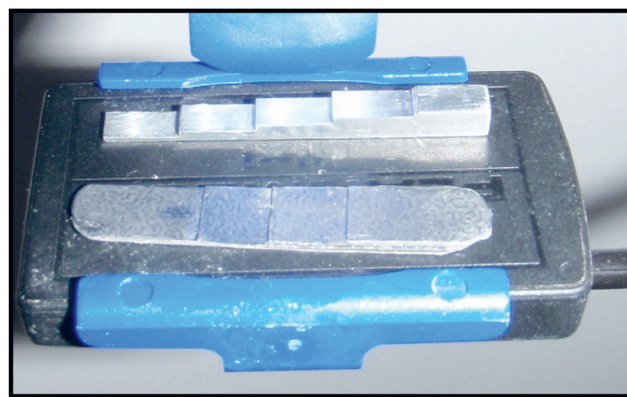


Fig. 1. The phantom consisting of two stepwages patterns placed on the receptor Dixi 3 (upper from aluminium, and bottom from lead)

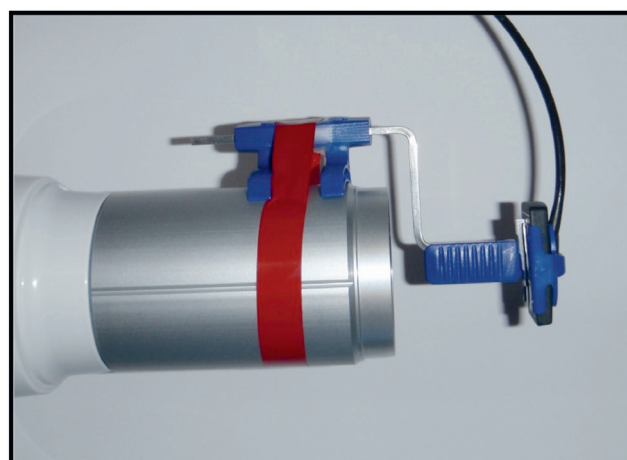


Fig. 2. The setting of the tube, the holder and the receptor during exposure

v. 4.2.0 (Planmeca). The Dimaxis Classic software was also used for image analysis export and import. The images were recorded after fastening the receptor and a holder to a 30-cm-long tube. The abovementioned patterns were located on the sensor surface (Fig. 2).

A distance of 4 cm between the tube of the Planmeca Intra and the Dixi 3 sensor was kept constant. Likewise, the position of the patterns on the surface of the sensor was constant. The selected parameters of the exposure were 60 kV and 8 mA, whereas the exposure time was the only variable.

A series of 7 images were recorded (256-grade 8-bit grayscale) with exposure times of 0.05 s, 0.064 s, 0.08 s, 0.1 s, 0.125 s, 0.16 s, and 0.2 s, at the maximum resolution and equivalent software settings (Group A). Radiographs captured with exposure times of 0.05 s and 0.125 s, without any manual image correction, were exported from the software using 2 different file export options. The 1st one exported the image relying on default software settings with the automated picture adjustment algorithm turned on (the “export” function), whereas the 2nd one exported “the clear” image without an automated picture

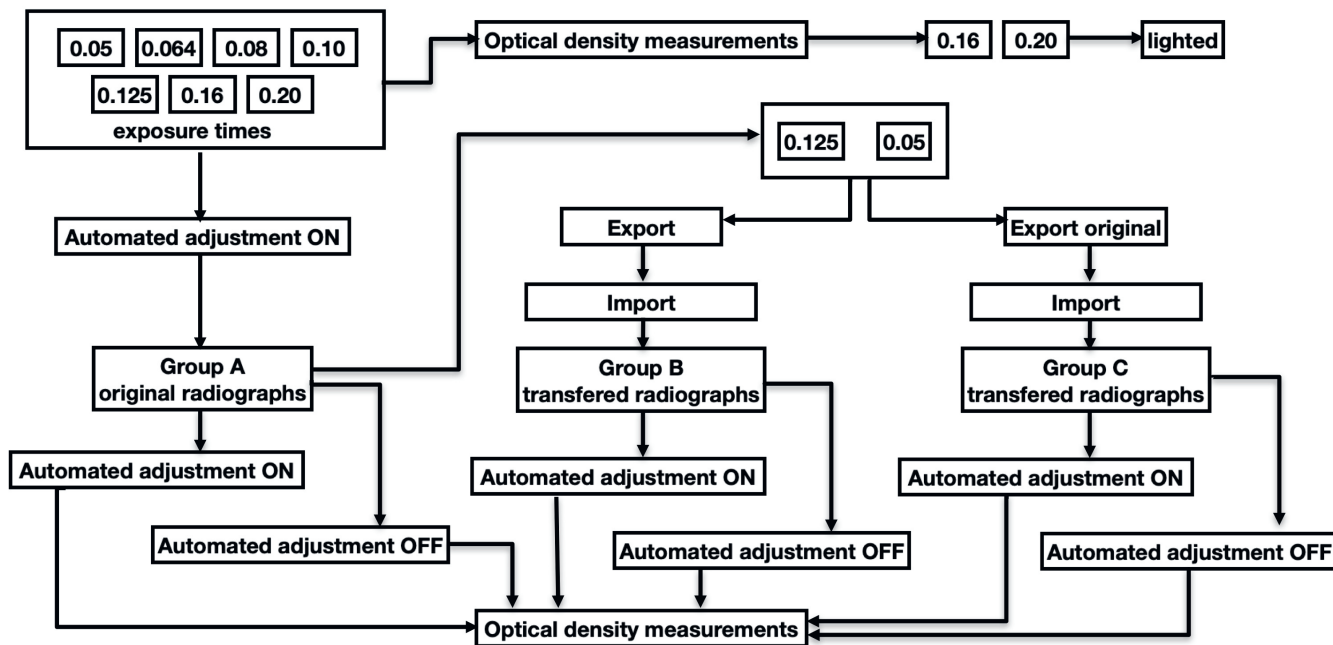


Fig. 3. Diagram of the procedures of export, import and optical density measurement during research

adjustment algorithm (the “original export” function). The exported files were saved in the lossless TIFF format. Then, the resulting radiograph files were imported into the Dimaxis software. In this way, 3 groups of radiographs were received. The 1st group of radiographs (Group A) included those which were originally made and recorded in the database of the Dimaxis software, whereas the 2nd one (Group B) comprised of radiographs imported after having been exported with optimization performed by the software (the “export” option); the 3rd one (Group C) comprised of radiographs imported after having been exported without optimization performed by the software, which is called “original export”. A diagram of the procedures of export, import and optical density measurements used in the study are presented in Fig. 3.

All radiographs were analyzed according to the same scheme, where the regions of interest (ROIs) were marked on the pattern-free background (marked as 0) and on particular steps of the 1st and 2nd patterns. The parts of the 1st pattern (the aluminum one) were marked in steps 1–5 and the parts of the 2nd pattern (the lead one) in steps 6–9. Higher figures refer to a higher degree of radioabsorption. The optical density for each of the ROIs was expressed by the software as an average value, together with standard deviation (SD) (Fig. 4). The mean value and SD of each ROI (in a 256-grade scale of grayness from 0 to 255) were recorded. The blackened areas have low values, whereas the light ones have high values because they show high radioabsorption. The number of pixels in the ROIs ranged from 18,500 to 20,000 (the size differences between the ROIs did not exceed 1,500 ppx).

Additionally, to evaluate the effect that the changes in exposure time, the internal image adjusting algorithms,

and the transfer of the image files had on the optical density of the bone structure, a series of dry human jaw bone radiographs were performed with the aluminum pattern as described above. The images were analyzed by 2 observers with general dental knowledge about X-ray image evaluation.

Results

According to the study design, the 1st stage consisted in collecting values of optical density for all exposure times after image registration in the patients’ charts and without the image corrections being subjected to analysis on the PC connected to the Dixi3 sensor (Group A). The values of optical density in Group A are presented in Table 1 and Fig. 5. The data (Group A) showed the influence of exposure time on optical density when the image optimization algorithm was active (default software setting). When the exposure times ranged from 0.05 s to 0.125 s, the optical density values measured along all phantom steps decreased with an increase in exposure time. The largest optical density decrease was observed for step 1 – 31.7% (14.2 ± 2.2 at 0.05 compared to 9.7 ± 1.4 at 0.125) – and the smallest was for step 9: 0.8% (234.0 ± 1.9 at 0.05 compared to 232.1 ± 1.2 at 0.125). At exposure times of 0.05–0.125 s and over the whole optical density range, the differences between the degrees of the pattern were sufficient, i.e., the images had sufficient contrast. The Group A radiographs of bone specimen captured with exposure times of 0.125 s and 0.2 s are presented in Fig. 6. The excessive exposure time caused image disturbances of the objects with an optical density of less than 50. On the images captured with an exposure

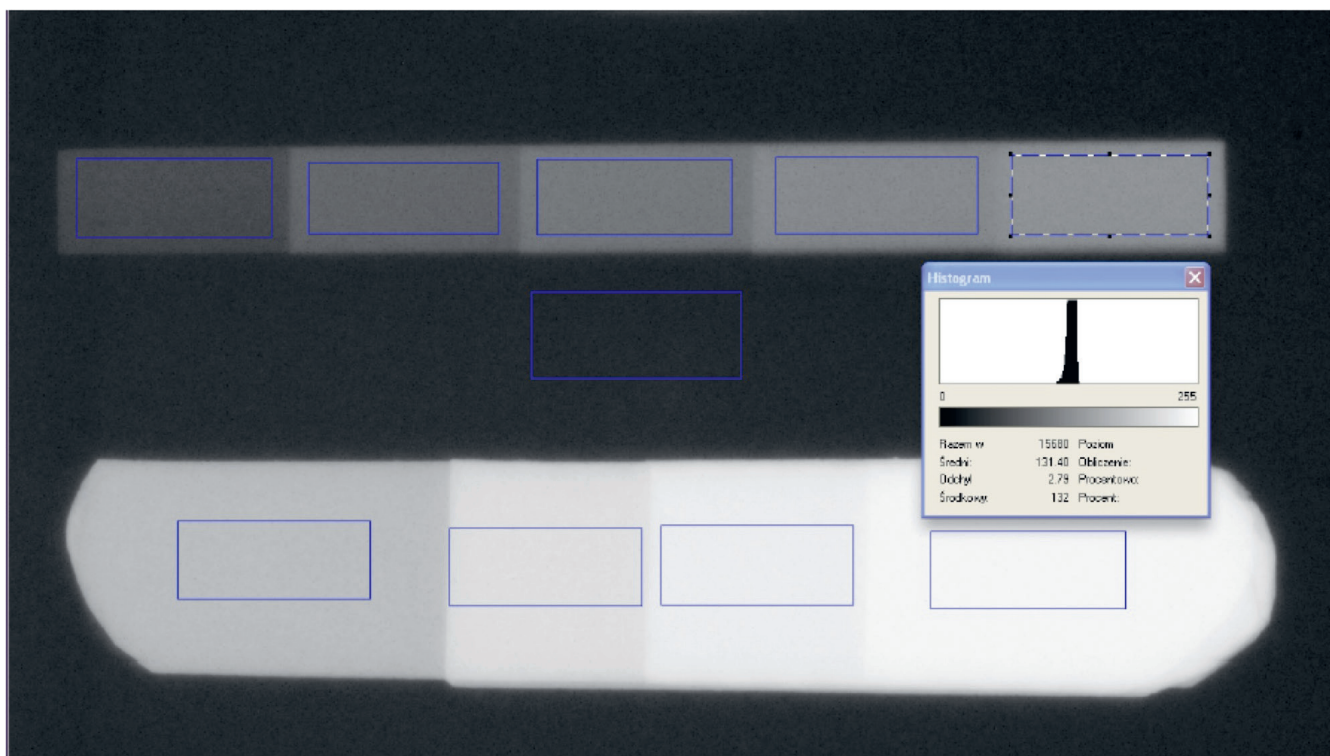


Fig. 4. The analyzed radiograph with the marked region of interest (ROI) and histogram of optical density

Table 1. The optical density values at different exposure times (Group A)

| Exposure time [s] | Degrees of the phantom | | | | | | | | | |
|-------------------|------------------------|-----------|-----------|-----------|-----------|-----------|------------|------------|------------|------------|
| | 0 | 1 | 2 | 3 | 4 | 5 | 6 | 7 | 8 | 9 |
| | x ±SD | x ±SD | x ±SD | x ±SD | x ±SD | x ±SD | x ±SD | x ±SD | x ±SD | x ±SD |
| 0.05 | 3.5 ±1.1 | 14.2 ±2.2 | 28.7 ±2.8 | 42.2 ±3.1 | 57.9 ±3.4 | 66.9 ±3.6 | 127.6 ±3.5 | 189.1 ±3.1 | 218.7 ±2.3 | 234.0 ±1.9 |
| 0.64 | 2.9 ±1.0 | 13.0 ±2.0 | 27.5 ±2.5 | 40.7 ±2.8 | 54.5 ±3.1 | 65.4 ±3.3 | 126.3 ±3.2 | 188.6 ±2.7 | 218.8 ±2.0 | 234.4 ±1.6 |
| 0.80 | 2.0 ±0.8 | 11.1 ±1.7 | 24.8 ±2.1 | 37.8 ±2.4 | 51.3 ±2.8 | 62.4 ±2.9 | 122.8 ±2.8 | 185.7 ±2.7 | 216.4 ±1.8 | 232.5 ±1.3 |
| 0.10 | 1.0 ±0.8 | 11.1 ±1.7 | 24.8 ±2.1 | 37.8 ±2.4 | 51.2 ±2.8 | 62.3 ±2.9 | 122.8 ±2.8 | 185.7 ±2.4 | 216.0 ±1.9 | 232.4 ±1.4 |
| 0.125 | 3.2 ±0.5 | 9.7 ±1.4 | 22.8 ±2.0 | 35.6 ±2.3 | 49.0 ±2.4 | 59.9 ±2.6 | 120.9 ±2.4 | 184.8 ±2.3 | 215.9 ±1.6 | 232.1 ±1.2 |
| 0.16 | 18.8 ±0.8 | 18.9 ±0.9 | 22.7 ±1.1 | 33.0 ±2.0 | 45.9 ±2.3 | 56.6 ±2.6 | 118.2 ±2.4 | 183.1 ±2.3 | 214.8 ±1.5 | 231.1 ±1.2 |
| 0.20 | 45.0 ±1.2 | 46.6 ±0.9 | 47.4 ±0.8 | 47.0 ±0.9 | 48.0 ±1.6 | 56.2 ±2.5 | 118.0 ±2.3 | 182.6 ±2.6 | 214.8 ±1.5 | 231.6 ±1.0 |

0 – the measurement area beyond the area of the density phantoms (the X-ray beam is directed to the receptor); SD – standard deviation.

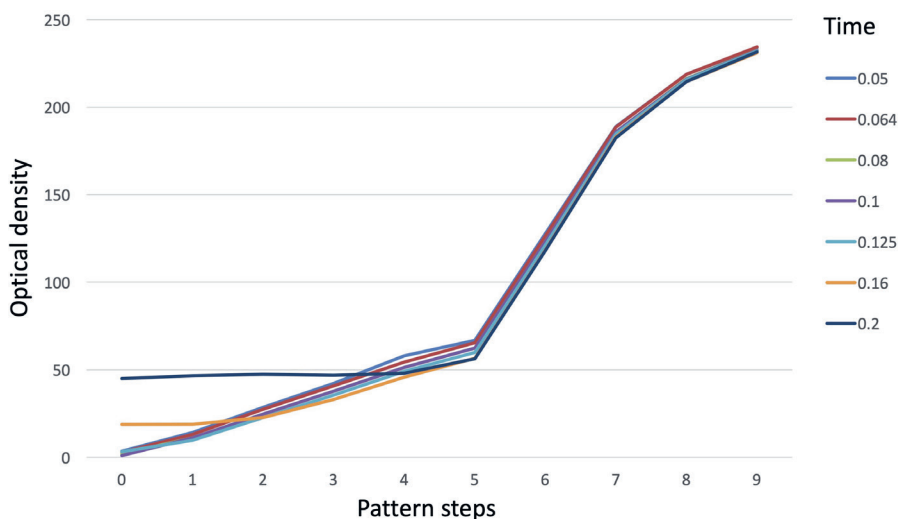


Fig. 5. The optical density values of Group A radiographs at different exposure times, automated adjustment turned on

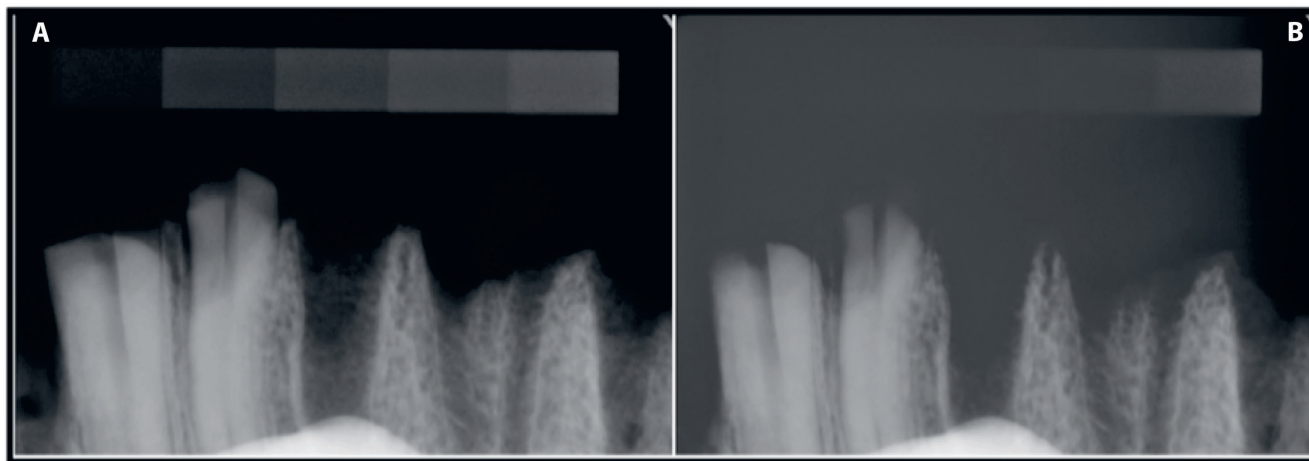


Fig. 6. Radiographs (Group A) performed at exposure time: A – 0.125 s; B – 0.2 s (overexposed)

Table 2. The optical density values at selected exposure times (Group A), with automated adjustment function on or off

| Exposure time [s] | Automated adjustment | Degrees of the phantom | | | | | | | | | |
|-------------------|----------------------|------------------------|-----------|-----------|------------|------------|------------|------------|------------|------------|------------|
| | | 0 | 1 | 2 | 3 | 4 | 5 | 6 | 7 | 8 | 9 |
| | | x ±SD | x ±SD | x ±SD | x ±SD | x ±SD | x ±SD | x ±SD | x ±SD | x ±SD | x ±SD |
| 0.05 | off | 45.6 ±4.5 | 72.5 ±4.3 | 96.0 ±3.9 | 113.0 ±3.6 | 127.5 ±3.5 | 137.6 ±4.2 | 184.9 ±2.3 | 221.5 ±1.7 | 237.1 ±1.2 | 244.7 ±1.0 |
| | on | 3.5 ±1.1 | 14.2 ±2.2 | 28.7 ±2.8 | 42.2 ±3.1 | 57.9 ±3.4 | 66.9 ±3.6 | 127.6 ±3.5 | 189.0 ±3.1 | 218.7 ±2.3 | 234.0 ±1.9 |
| | difference | 92.2% | 80.5% | 70.1% | 62.7% | 54.6% | 51.4% | 31.0% | 14.6% | 7.7% | 4.3% |
| 0.125 | off | 37.4 ±1.7 | 57.2 ±3.4 | 82.3 ±3.2 | 100.7 ±3.0 | 116.5 ±2.7 | 127.6 ±2.8 | 178.1 ±1.9 | 218.2 ±1.4 | 235.2 ±1.0 | 243.7 ±0.7 |
| | on | 3.2 ±0.5 | 9.7 ±1.4 | 22.8 ±2.0 | 35.6 ±2.3 | 49.0 ±2.4 | 59.9 ±2.6 | 120.9 ±2.4 | 184.8 ±2.3 | 215.9 ±1.6 | 232.1 ±1.2 |
| | difference | 91.1% | 83.1% | 72.3% | 64.6% | 57.9% | 53.1% | 32.1% | 15.3% | 8.2% | 4.8% |

0 – the measurement area beyond the area of the density phantom (X-ray beam is directed to the receptor); SD – standard deviation.

time of 0.16 s, the differences between the background and steps 1 and 2 of the pattern were blurred and no considerable differences between these ROIs were noticed. With an exposure time of 0.2 s, the differences were blurred not only between the background and steps 1 and 2, but also between the background and steps 3 and 4. Therefore, it can be stated that an object with low radioabsorption becomes imperceptible at exposure times of 0.16 s or 0.2 s. A comparison of the bone specimen radiographs that were captured with exposure times of 0.125 s and 0.2 s displayed a blurred difference between the background and the object at a longer exposure time (Fig. 5).

The impact of the optimization algorithm on the Group A radiographs, which were captured at exposure times of 0.05 s and 0.125 s, are presented in Table 2 and Fig. 7. The radiographs of the bone specimen captured with an exposure time of 0.125 s – with and without the automated adjustment option – are presented in Fig. 8.

The results demonstrate that the algorithm causes a reduction in the difference between particular exposure times as well as a reduction in optical density. The lower the optical density, the larger the decrease in optical density was recorded (Fig. 7). The decrease in optical density recorded for the exposure times of 0.05 s and 0.125 s at step 1 amounted to 80.5% and 83.1%, respectively, and

at step 9 it was 4.3% and 4.8%, respectively. A detailed analysis of step 2 of the imaging phantom showed the difference between the optical density value for exposures of 0.05 s and 0.125 s to be 13.7 (96.0 ±3.9 compared to 82.3 ±3.2) with the automated adjustment function switched off, and only 5.9 (2.3 times lower) (28.7 ±2.8 compared to 22.8 ±2.0) when the function was on. These changes can be seen in the radiographs of bone specimen (Fig. 7).

The use of automated adjustment resulted in the image becoming darker and more contrastive in areas with an optical density higher than 50 (phantom steps 5–9). The higher image contrast displaying the clearer structure of the object. However ROI's with low optical density became blurred (decrease of contrasts between steps 1 and 2, 2 and 3, 4 and 5) in comparison with the radiographs without the automated adjustment option. The algorithm made the 1st degree of the pattern and a thin alveolar plate invisible to the observers (Fig. 7).

The optical density values of Group B and Group A images captured with exposure times of 0.05 s and 0.125 s are presented in Table 3 and Fig. 9. Radiographs of Group B with a bone specimen recorded with an exposure time of 0.125 s are presented in Fig. 10. The analysis of the Group B images transferred after exporting with

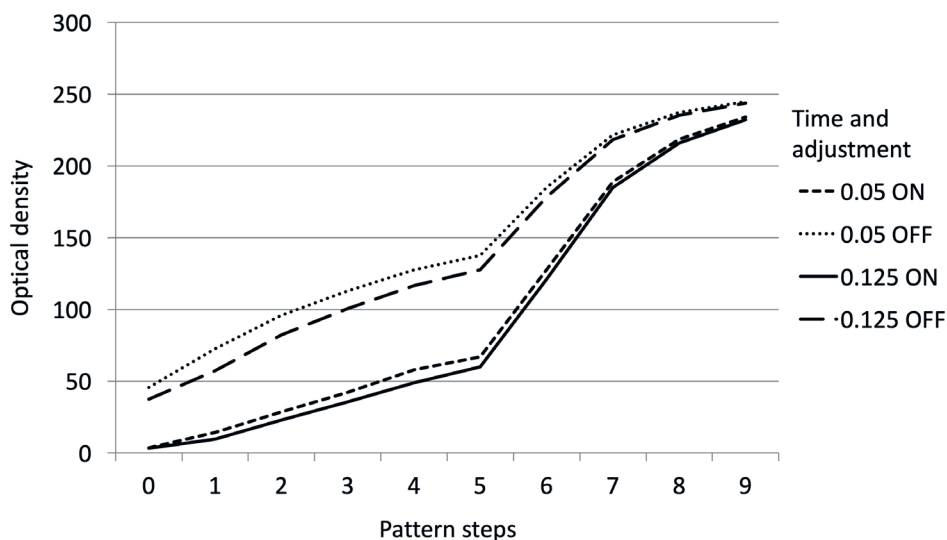


Fig. 7. The optical density values for the selected exposure times (Group A) automated adjustment turned on and off

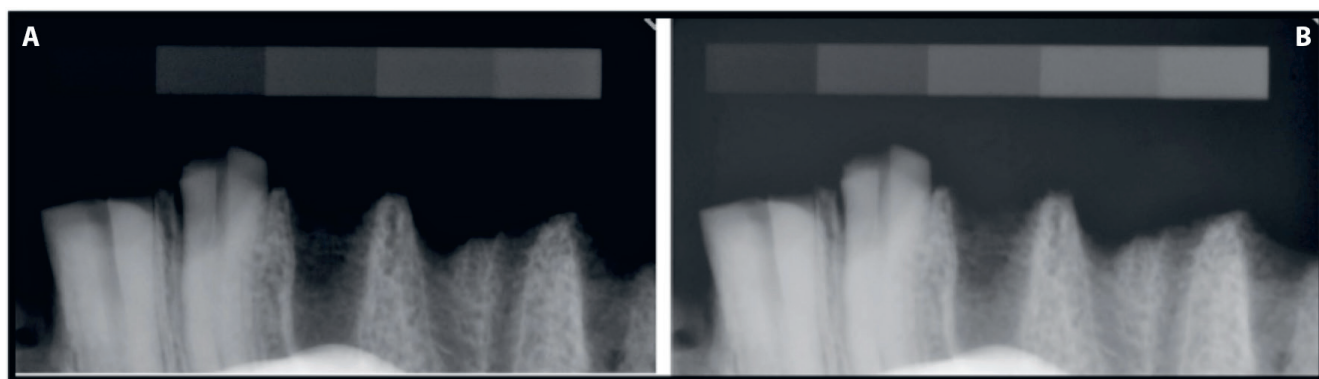


Fig. 8. Radiographs performed at exposure time 0.125 s (Group A), automated image adjustment: A – on; B – off.

Table 3. The optical density values after importing Group B files with selected exposure times, with automated adjustment function on or off

| Exposure time [s] | Automated adjustment | Degrees of the phantom | | | | | | | | | |
|-------------------|----------------------|------------------------|-----------|-----------|-----------|-----------|-----------|------------|------------|------------|------------|
| | | 0 | 1 | 2 | 3 | 4 | 5 | 6 | 7 | 8 | 9 |
| | | x ±SD | x ±SD | x ±SD | x ±SD | x ±SD | x ±SD | x ±SD | x ±SD | x ±SD | x ±SD |
| 0.05 | on | 0 | 0.6 ±0.6 | 3.4 ±1.2 | 7.8 ±1.9 | 13.9 ±2.6 | 20.1 ±3.2 | 73.2 ±6.4 | 160.6 ±7.8 | 214.2 ±7.2 | 244.6 ±6.2 |
| | off | 3.7 ±1.8 | 14.6 ±3.4 | 29.1 ±4.4 | 42.6 ±4.9 | 56.2 ±5.7 | 67.4 ±5.7 | 128.3 ±5.7 | 189.3 ±4.7 | 219.0 ±3.7 | 234.2 ±3.1 |
| | difference | 100% | 95.9% | 88.3% | 81.7% | 75.3% | 70.2% | 42.9% | 15.2% | 2.2% | -4.4% |
| | original | 3.5 ±1.1 | 14.2 ±2.2 | 28.7 ±2.8 | 42.2 ±3.1 | 57.9 ±3.4 | 66.9 ±3.6 | 127.6 ±3.5 | 189.0 ±3.1 | 218.7 ±2.3 | 234.0 ±1.9 |
| 0.125 | on | 0 | 0.3 ±0.7 | 2.3 ±1.1 | 5.6 ±1.3 | 10.9 ±1.8 | 16.4 ±2.3 | 67.7 ±4.8 | 158.2 ±5.6 | 215.7 ±5.0 | 249.3 ±3.9 |
| | off | 3.3 ±0.7 | 9.8 ±2.2 | 22.9 ±3.1 | 35.7 ±3.7 | 48.9 ±4.1 | 59.9 ±4.3 | 121.4 ±4.3 | 185.0 ±3.3 | 216.0 ±2.5 | 232.3 ±1.9 |
| | difference | 100% | 96.9% | 89.9% | 84.3% | 77.7% | 72.6% | 44.2% | 14.5% | 0.14% | -7.3% |
| | original | 3.2 ±0.5 | 9.7 ±1.4 | 22.8 ±2.0 | 35.6 ±2.3 | 49.0 ±2.4 | 59.9 ±2.7 | 120.9 ±2.4 | 184.8 ±2.3 | 215.9 ±1.6 | 232.1 ±1.2 |

0 – the measurement area beyond the area of the density phantom (X-ray beam is directed to the receptor); original – with automated adjustment turned on (Group A); SD – standard deviation.

the “export” option (after optimization) revealed that after importing, some structures of the spongy bone (density equivalent to steps 1, 2 and 3 of the phantom) may become undetectable. The use of automated adjustment, after file import, reduced the optical density values of the phantom radiographs from degree 1 to 8, at exposure times of both 0.05 s (from 95.9% to 2.2%) and 0.125 s (from 96.9%

to 0.14%) – with the exception of degree 9. The observed ROIs were black and steps 1 and 2 of the phantom also became invisible at shorter (0.05 s) and longer (0.125 s) exposure times. The image background achieves the optical density equal 0 and is totally black. The structures with higher radioabsorption remained visible and the optical density was reduced for steps 6 and 7 of the phantom.

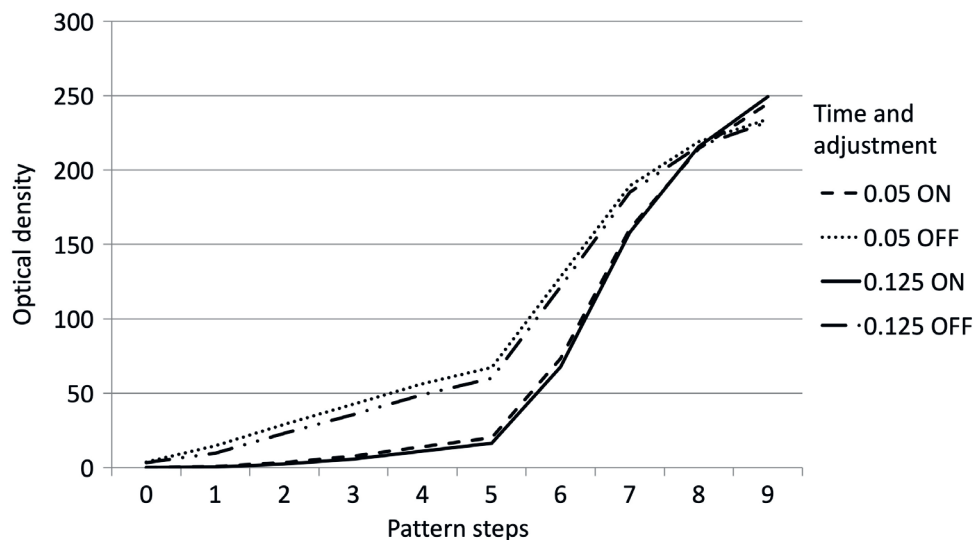


Fig. 9. The optical density values of Group B radiographs, exposure time 0.05 and 0.125 s, automated adjustment turned on and off

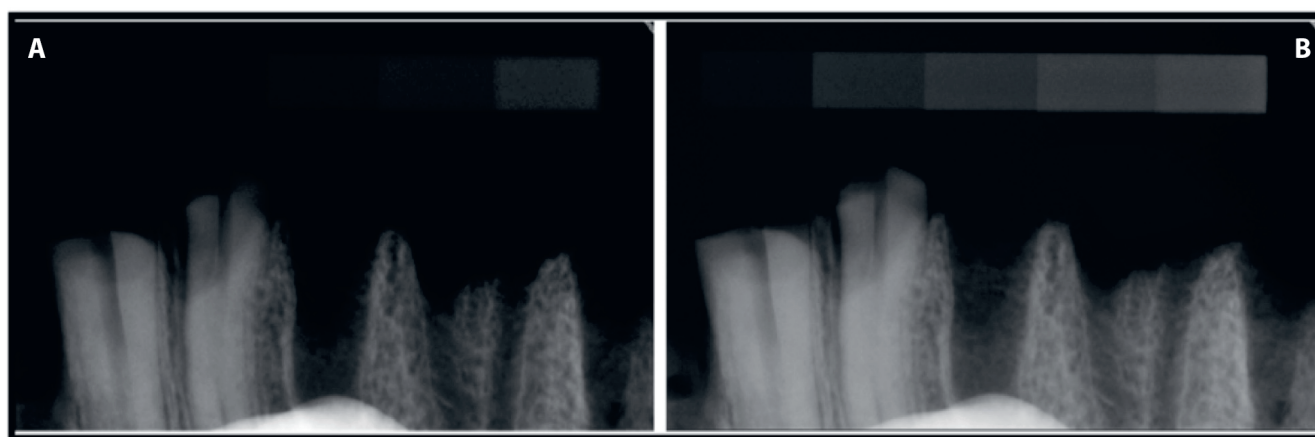


Fig. 10. Group B radiographs after import to Dimaxis software, automated image adjustment: A – on (“digital” underexposure) and B – off

It did not change in the case of step 8 and grew in the case of step 9 at both exposure times. The observed problems with the image were the result of using the optimization algorithm repeatedly. In this case, the algorithm should be turned off. Deactivating the optimization algorithm resulted in an optical density that was comparable (identical) with the original one at both exposure times and images that were less dark, displaying the object details more precisely (Fig. 9).

The recorded optical density values of the Group C radiographs captured at exposure times of 0.05 s and 0.125 s and the original images are presented in Table 4 and Fig. 11. The Group C radiograph of bone specimen captured at an exposure time of 0.125 s is presented in Fig. 12. The analysis of the Group C images (export without optimization) revealed that not applying the automated adjustment function after file import yielded an increase in the optical density values of the radiographs of all the phantom degrees over the original images (enhanced with the optimization algorithm). The increase was independent of exposure time (at 0.05 s the value changed from 80.2% to 4.4% and at 0.125 s from 82.9% to 4.7%). However,

activating this function (after import) provided an optical density almost identical to the original radiographs of all phantom degrees at both exposure times. Similarly Group C radiographs of the bone samples appears identical to those of Group A. (Fig. 7 and 11).

Discussion

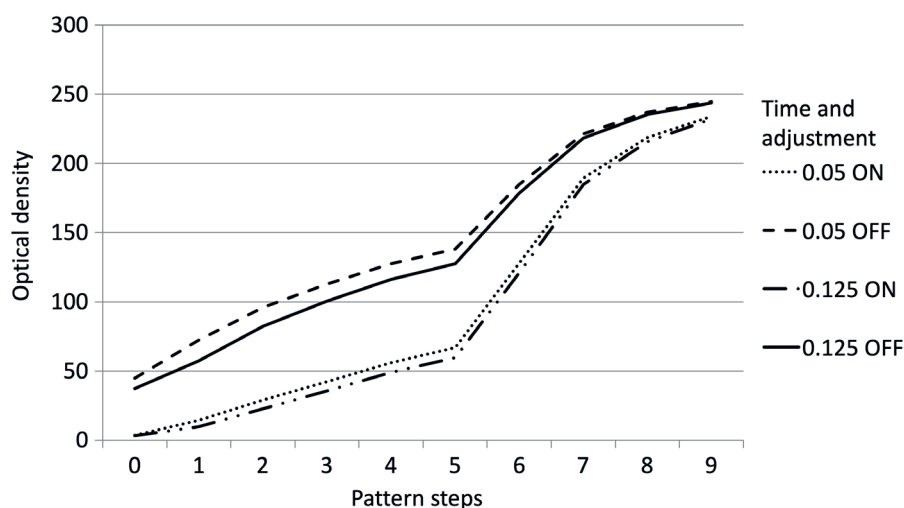
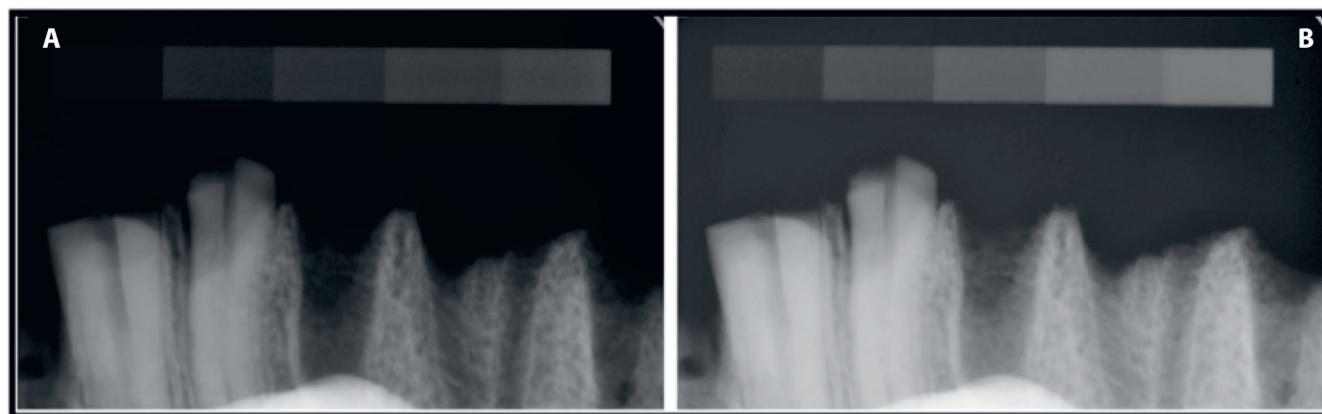
Every image stored in the form of a file can be transferred, duplicated and changed digitally. Each adjustment which restores, improves, analyzes, or in some way changes a digital image is a form of image processing, e.g., image enhancement – brightness and contrast, sharpening and smoothening, or zooming in – or image analysis – measurement, segmentation, proportion finding, object classification, image synthesis, or compression.^{3,5}

This type of processing does not alter the content of the image but does improve (or change) the visual perception to enable a better diagnosis.^{9,10} That is why understanding the individual of functions and their appropriate applications is extremely important in professional

Table 4. The optical density values after importing Group C files with selected exposure times, with automated adjustment on or off

| Exposure time [s] | Automated adjustment | Degrees of the phantom | | | | | | | | | |
|-------------------|----------------------|------------------------|-----------|-----------|------------|------------|------------|------------|------------|------------|------------|
| | | 0 | 1 | 2 | 3 | 4 | 5 | 6 | 7 | 8 | 9 |
| | | x ±SD | x ±SD | x ±SD | x ±SD | x ±SD | x ±SD | x ±SD | x ±SD | x ±SD | x ±SD |
| 0.05 | on | 3.5 ±1.1 | 14.3 ±2.2 | 29.0 ±2.8 | 42.2 ±3.1 | 55.9 ±3.3 | 66.9 ±3.6 | 127.9 ±3.5 | 189.3 ±2.9 | 218.7 ±2.3 | 234.0 ±2.0 |
| | off | 44.8 ±4.4 | 72.4 ±4.3 | 96.0 ±3.9 | 113.0 ±3.6 | 127.6 ±3.4 | 138.1 ±3.3 | 184.8 ±2.4 | 221.5 ±1.7 | 237.0 ±1.2 | 244.7 ±1.0 |
| | difference | 92.2% | 80.2% | 69.8% | 62.6% | 56.2% | 51.5% | 30.8% | 14.5% | 7.7% | 4.4% |
| | original | 3.5 ±1.1 | 14.2 ±2.2 | 28.7 ±2.8 | 42.2 ±3.1 | 57.9 ±3.4 | 67.0 ±3.6 | 127.6 ±3.5 | 189.1 ±3.1 | 218.7 ±2.3 | 234.0 ±1.9 |
| 0.125 | on | 3.2 ±0.5 | 9.8 ±1.4 | 22.7 ±2.0 | 35.6 ±2.3 | 48.9 ±2.5 | 59.7 ±2.7 | 120.8 ±2.6 | 184.6 ±2.4 | 215.7 ±1.6 | 232.1 ±1.3 |
| | off | 37.3 ±1.7 | 57.2 ±3.4 | 82.3 ±3.2 | 100.5 ±3.1 | 116.2 ±2.8 | 127.5 ±2.8 | 178.3 ±1.9 | 218.2 ±1.3 | 235.3 ±0.9 | 243.7 ±0.7 |
| | difference | 91.4% | 82.9% | 72.4% | 64.6% | 57.9% | 53.2% | 32.2% | 15.4% | 8.3% | 4.7% |
| | original | 3.2 ±0.5 | 9.7 ±1.4 | 22.8 ±2.0 | 35.6 ±2.3 | 49.0 ±2.4 | 59.9 ±2.6 | 120.9 ±2.4 | 184.7 ±2.3 | 215.9 ±1.6 | 232.1 ±1.2 |

0 – the measurement area beyond the area of the density patterns (X-ray beam is directed to the receptor); original – with automated adjustment turned on (Group A); SD – standard deviation.

**Fig. 11.** The optical density values of Group C radiographs, exposure time 0.05 and 0.125 s, automated adjustment turned on and off**Fig. 12.** Group C radiographs after import to Dimaxis software, automated image adjustment: A – on; B – off

work, regardless of the X-ray detector type.¹¹ On the other hand, the exporting of digital radiographs to a file format that is compatible with commercial graphic software can cause some changes in the original digital information.⁴ For the purpose of this study, a simple pattern consisting of aluminum and lead steps with graded thicknesses were prepared. The use of the pattern allows exposure

differences to be compensated for (and/or detected), the optical density to be calibrated, and finally, for different exposure conditions to be compared objectively. The use of an imaging phantom to measure bone optical density provides accurate and reproducible results and allows the impact of file transfers on qualitative and quantitative image changes to be measured.¹²

A similar device with fixed degrees of absorbed X-ray radiation was successfully used as a phantom by Yang et al. to measure the density of the jaw bone.¹³ The repeatability of projection and exposure is an important factor when digital images are compared.^{14,15} The use of a pattern simplifies the objective detection of and compensation for differences between objects with identical radioabsorption, as well as image calibration. On the other hand, the pattern covers a significant area of the small intraoral sensor or plate. Therefore, in clinical conditions, the use of a pattern is difficult or even impossible, especially when other structures overlap the image of the pattern. In most software used for dental radiography, instead of a phantom, some optimization algorithms are used to compensate for differences between the exposures. In clinical conditions, when it is difficult to maintain repeatability, the proper functioning of optimization algorithms is crucial.

The tools for measuring the optical density of bone radiographs and improving the image contrast are widely used during the evaluation of digital radiographs. Image manipulations, as well as the use of inappropriate monitors, affect perceptions; therefore, attention should be paid to the appropriate selection of exposure parameters and image correction tools.¹⁶ However, thoughtful and skillful application of these tools to detect root resorption can be applied according to the observer's preferences without affecting the diagnostic accuracy.¹⁷ The use of appropriate filters in digital radiology allows for a more accurate assessment of radiographs when dealing with inflammatory conditions of periapical tissues.¹⁸ Some filters, like the reverse of the grayscale, allows the image to be evaluated from a different aspect. However, it does not always have significant influence, e.g., in assessing the length of root canal instruments radiographically.¹⁹ Optical density measurement with the use of cone-beam computed tomography (CBCT) was also used to compare bone density around the impacted canines, which allowed a higher optical density of the bone surrounding the impacted teeth to be shown.²⁰ The use of appropriate software may also help in the detection of general diseases such as osteoporosis based on dental X-ray radiographs.^{21,22} The correlation between the measurement of the bone density of alveolar bone and spinal bone indicates the importance of dentists being the first to pay attention to bone density disorders.^{23,24}

When analyzing and comparing images, it should not be forgotten that the software usually compensates for variations in exposure parameters with automated optimizing algorithms. The option (algorithm) of automated adjustment, which corrects a digital image, is also included in the Dimaxis software that was used in this study. The default application of an optimization algorithm significantly reduces the differences between exposure times if they are in the range of 0.05–0.125 s. The use of longer exposure times (0.16 s and 0.2 s) highlights the limitations of the software and the sensor used in this study,

as it caused image disturbances of objects with an optical density of less than 50. Because an object with low radioabsorption becomes imperceptible at exposure times of 0.16 s or 0.2 s, those radiographs were recognized as “lighted.” A similar selection was made in the article by Morea et al. due to the ghost images which were produced by an exposure time beyond the latitude of the sensor.¹⁶ Overexposure of the 0.16-second and 0.2-second images can also be caused by the lack of a soft-tissue-equivalent absorbing part of the radiation between the X-ray beam and sensor. The soft tissue model was not included in the current study. This assumption is confirmed in Fig. 7, where the operation of the algorithm is visible and makes the first-degree pattern and a thin alveolar plate invisible.

Suryani et al. presented the importance of post-processing the digital panoramic radiographs for a more accurate visualization of anatomical structures in children.⁹ Image quality processing techniques affect the quality of the image in various ways depending on the diagnostic purpose (caries, periapical lesion or root canal treatment) and must be properly selected. Based on the optical density of the ROIs, the use of automated image adjustment should be considered unfavorable because some structures may become invisible.

Bone density measurement to assess bone tissue and the images after importing is used in various studies.²⁵ Measuring and comparing the density of selected jaw fragments is important when the healing or inflammation processes are compared over time.²⁶ The efficacy of this method of testing the optical density of rat bones after the administration of ketoprofen was found by Martins et al.²⁷ Disturbances in the readout of X-ray image parameters during transfer, such as optical density measurements or contrast differences, may be important in diagnosis. This was confirmed in studies in which the contrast change significantly changed the possibilities of measuring the length of small root canal instruments.²⁸ However, accurate measurement of the optical density of bones is also important and may be a complement to CT analysis before implantation in the mandible.²⁶ The results of the current study suggest that the automated adjustment function can disturb the process of image transfer (exporting from the raw data and importing to another database), and that in some cases, it can cause considerable differences in the recorded values of optical density. The analysis of Group B images revealed problems associated with the repeated use of image optimization, when areas with low radioabsorption become completely invisible. Importing files that have not been subjected to the optimization algorithm (Group C) seems to be safer, as there is no risk of image darkening or blurring of structures. In the era of digital radiology, the clinician assessing an imported radiograph should be aware of the possibility of such interference. In this study, a specific sensor and software were used, so the resulting limitations should be considered when analyzing the results.

Conclusions

Within the limitations of this study, it can be concluded that 1) the transfer of digital radiographs can exert an influence on the recorded values of optical density, and thus on a comparative assessment, so the same (or a similar) algorithm of image processing should be used; 2) automated contrast enhancement and exposure compensation may blur the image of low-density structures; and 3) the radiogram files should be exported without image optimization. This way the risk of image distortion can be eliminated and the perception of low-density structures will not be distorted.

ORCID iDs

Wojciech Grzebieluch  <https://orcid.org/0000-0003-0725-4620>
 Urszula Kaczmarek  <https://orcid.org/0000-0002-9692-283X>
 Tomasz Staniowski  <https://orcid.org/0000-0001-5333-7289>
 Marcin Mikulewicz  <https://orcid.org/0000-0001-5754-0284>

References

- Maschtakow PS, Moraes ME, Soares MG, Santos LR, Moraes LC, Castilho JC. Assessment of manipulation accuracy of digitized occlusal radiographic images-sub and over exposure. *Acta Odontol Latinoam*. 2009; 22(2):113–117.
- Yoshiura K, Nakayama E, Shimizu M, et al. Effects of the automatic exposure compensation on the proximal caries diagnosis. *Dentomaxillofac Radiol*. 2005;34(3):140–144.
- Brettle D, Carmichael F. The impact of digital image processing artefacts mimicking pathological features associated with restorations. *Br Dent J*. 2011;211(4):167–170.
- Calberson FL, Hommez GM, De Moor RJ. Fraudulent use of digital radiography: Methods to detect and protect digital radiographs. *J Endod*. 2008;34(5):530–536.
- Gormez O, Yilmaz HH. Image post-processing in dental practice. *Eur J Dent*. 2009;3(4):343–347.
- Shah N, Bansal N, Logani A. Recent advances in imaging technologies in dentistry. *World J Radiol*. 2014;6(10):794–807.
- Piepenbring ME, Potter BJ, Weller N, Robert J, Loushine RJ. Measurement of endodontic file lengths: A density profile plot analysis. *J Endod*. 2000;26(10):615–618.
- Butt A, Mahoney M, Savage NW. The impact of computer display performance on the quality of digital radiographs: A review. *Aust Dent J*. 2012;57(Suppl 1):16–23.
- Suryani IR, Villegas NS, Shujaat S, et al. Image quality assessment of pre-processed and post-processed digital panoramic radiographs in paediatric patients with mixed dentition. *Imaging Sci Dent*. 2018; 48(4):261–268.
- Svenson B, Larsson L, Båth M. Optimization of exposure in panoramic radiography while maintaining image quality using adaptive filtering. *Acta Odontol Scand*. 2016;74(3):229–235.
- Farman AG, Farman TT. A comparison of 18 different detectors currently used in dentistry. *Oral Surg Oral Med Oral Pathol Oral Radiol Endod*. 2005;99(4):485–489.
- Nackaerts O, Jacobs R, Horner K, et al. Bone density measurements in intra-oral radiographs. *Clin Oral Invest*. 2007;11(3):225–229.
- Yang J, Chiou R, Ruprecht A, Vicario J, MacPhail LA, Rams TE. A new device for measuring density of jaw bones. *Dentomaxillofac Radiol*. 2002;31(5):313–316.
- Li G. Comparative investigation of subjective image quality of digital intraoral radiographs processed with 3 image-processing algorithms. *Oral Surg Oral Med Oral Pathol Oral Radiol Endod*. 2004;97(6):762–767.
- Southard TE, Wunderle DM, Southard KA, Jakobsen JR. Geometric and densitometric standardization of intraoral radiography through use of a modified XCP system. *Oral Surg Oral Med Oral Pathol Oral Radiol Endod*. 1999;87(2):253–257.
- Morea C, Dominguez GC, Coutinho A, Chilvarquer I. Quantitative analysis of bone density in direct digital radiographs evaluated by means of computerized analysis of digital images. *Dentomaxillofac Radiol*. 2010;39(6):356–361.
- Nascimento EHL, Gaêta-Araujo H, Galvão NS, Moreira-Souza L, Oliveira-Santos C, Freitas DQ. Effect of brightness and contrast variation for detectability of root resorption lesions in digital intraoral radiographs. *Clin Oral Investig*. 2019;23(8):3379–3386.
- Yalcinkaya S, Kunzel A, Willers R, Thoms M, Becker J. Subjective image quality of digitally filtered radiographs acquired by the Dürr Vistascan system compared with conventional radiographs. *Oral Surg Oral Med Oral Pathol Oral Radiol Endod*. 2006;101(5):643–651.
- Oliveira ML, Vieira ML, Cruz AD, Bóscolo FN, de Almeida SM. Gray scale inversion in digital image for measurement of tooth length. *Braz Dent J*. 2012;23(6):703–706.
- Servais JA, Gaalaas L, Lunos S, Beiraghi S, Larson BE, Leon-Salazar V. Alternative cone-beam computed tomography method for the analysis of bone density around impacted maxillary canines. *Am J Orthod Dentofacial Orthop*. 2018;154(3):442–449.
- Lee JS, Adhikari S, Liu L, Jeong HG, Kim H, Yoon SJ. Osteoporosis detection in panoramic radiographs using a deep convolutional neural network-based computer-assisted diagnosis system: A preliminary study. *Dentomaxillofac Radiol*. 2018;48(1):20170344. doi:10.1259/dmfr.20170344
- Ayed MS, Shafiq SS, Diab HM, Alahmari AD, Divakar DD. Assessing periapical dental radiographs as a screening parameter for early indications of osteoporosis in postmenopausal periodontal patients and root surface evaluation using spectrochemical analysis. *Saudi Med J*. 2018;39(7):719–724.
- Takaishi Y, Arita S, Honda M, et al. Assessment of alveolar bone mineral density as a predictor of lumbar fracture probability. *Adv Ther*. 2013;30(5):487–502.
- Jin-Woo C, Won-Jeong H, Eun-Kyung K. Image enhancement of digital periapical radiographs according to diagnostic tasks. *Imaging Sci Dent*. 2014;44(1):31–35.
- Kaczmarek U, Matthews-Brzozowska T, Mikulewicz M, Grzebieluch W. Evaluation of alveolar process bone density using digital radiography Digora: Experimental studies. *Dent Med Probl*. 2002;39:237–239.
- Homolka P, Beer A, Birkfellner W, Gahnleitner A, Novotny R, Bergmann H. Local calibrated bone mineral density in the mandible presented using a color coding scheme. *Med Eng Phys*. 2001;23(9): 673–677.
- Martins MV, da Silva MA, Medici Filho E, de Moraes LC, Castilho JC, da Rocha RF. Evaluation of digital optical density of bone repair in rats medicated with ketoprofen. *Braz Dent J*. 2005;16(3):207–212.
- Farhadi N, Shokraneh A, Mehdizadeh M. Effect of contrast inversion enhancement on the accuracy of endodontic file length determination in digital radiography. *J Clin Diagn Res*. 2015;9(5):ZC102–ZC105.

Assessment of dietary habits and lifestyle among people with HIV

Paweł Duda^{1,A–F}, Brygida Knysz^{2,B,D,E}, Jacek Gąsiorowski^{2,A,B}, Bartosz Szetela^{2,A–C}, Ewa Piotrowska^{1,B,C,E}, Monika Bronkowska^{1,A–F}

¹ Department of Human Nutrition, Wrocław University of Environmental and Life Sciences, Poland

² Department of Infectious Diseases, Liver Diseases and Acquired Immune Deficiencies, Wrocław Medical University, Poland

A – research concept and design; B – collection and/or assembly of data; C – data analysis and interpretation;

D – writing the article; E – critical revision of the article; F – final approval of the article

Advances in Clinical and Experimental Medicine, ISSN 1899–5276 (print), ISSN 2451–2680 (online)

Adv Clin Exp Med. 2020;29(12):1459–1467

Address for correspondence

Monika Bronkowska

E-mail: monika.bronkowska@upwr.edu.pl

Funding sources

None declared

Conflict of interest

None declared

Received on September 1, 2020

Reviewed on September 19, 2020

Accepted on October 8, 2020

Abstract

Background. The aim of this study was to determine the consumption of specific food groups by people with HIV and to determine the quality of their diets.

Objectives. To assess the relationship between selected eating habits and lifestyles of people infected with HIV. The research was conducted at the HIV/AIDS Preventative and Therapeutic Clinic of the Infectious Disease Prevention and Therapy Center at Wrocław Health Center (SPZOZ Wrocław), Poland.

Material and methods. The study was conducted in 2019 among 31 patients of a counselling center in Wrocław. To determine the frequency of food consumption and eating habits, the KomPAN[®] questionnaire, prepared by employees of the Polish Academy of Sciences, was used.

Results. All study participants were characterized by a small degree of unhealthy features in their diets; 87% of the respondents also demonstrated a small degree of healthy features in their diets, although the responses they gave showed that they assessed their nutritional knowledge and diet highly. Consumption of sweet snacks and adding salt to cooked meals were prevalent. The respondents took part in moderate physical activity and rarely consumed highly processed fast food products, though they ate fish and legumes – an important part of the diet – with similar frequency.

Conclusions. More attention should be given to the nutritional issues of patients treated for HIV, and emphasis should be placed on promoting healthy eating habits among this population. In the scientific literature, few such studies are available that address issues related to the diet of HIV-infected people.

Key words: lifestyle, quality index, eating behavior, nutrition in HIV, KomPAN

Cite as

Duda P, Knysz B, Gąsiorowski J, Szetela B, Piotrowska E, Bronkowska M. Assessment of dietary habits and lifestyle among people with HIV. *Adv Clin Exp Med.* 2020;29(12):1459–1467. doi:10.17219/acem/128234

DOI

10.17219/acem/128234

Copyright

© 2020 by Wrocław Medical University

This is an article distributed under the terms of the Creative Commons Attribution 3.0 Unported (CC BY 3.0) (<https://creativecommons.org/licenses/by/3.0/>)

Introduction

Researchers eagerly use nutritional questionnaires to assess subjects' eating habits, due to the low cost and simplicity.¹ Their convenience is obvious, especially for the respondents: they can answer the questions at any time. Therefore, such questionnaires are a very useful tool for studying the lifestyles of populations who for various reasons try to minimize contact with others, as in the case of patients with human immunodeficiency virus (HIV). It is a retrovirus and a type of lentivirus (*Lentiviridae*) which causes long-term infections, leading to chronic diseases and, consequently, to death.²

Until now, it has not been possible to find a drug that would definitively terminate the development of this infection in the human body; however, the antiretroviral treatment (ARV) significantly reduces the multiplication of the virus, halting the weakening of the immune system and – in the case of people who follow ARV treatment – slowly rebuilding its functioning. At the very beginning, HIV infection presents with very uncharacteristic symptoms, so it is very rarely diagnosed during primary HIV infection. Only after the “window period” has passed, i.e., the period from infection to the formation of anti-HIV antibodies in the blood – which usually lasts about 3 months – can the infection be diagnosed. If started early enough, ARV therapy prevents the occurrence of AIDS, so that the infected person can enjoy a long life (as long as an uninfected person), if only the daily medication intake regime is strictly followed.³

The HIV infection does not require a complete change in eating habits. However, paying attention to rational nutrition and the supply of essential nutrients is important. Meals should be varied and provide sufficient energy. The main aim of nutritional therapy should be to determine the amounts and variety of the foods consumed, which, apart from satisfying nutritional needs, should provide an adequate supply of the vitamins and minerals that benefit patient's health.¹¹ It has been confirmed that the recommendation of a higher intake of certain nutrients is justified, because it reduces the risk of full-blown AIDS. Such ingredients include vitamins A, B6, B12, C, and E, magnesium, iron, selenium, and zinc.⁴

Currently in Poland, the care of a patient with HIV is mainly focused on pharmacotherapy, marginalizing the issues related to proper nutrition.^{5,6} However, several studies have confirmed that nutrition impacts the absorption and metabolism of drugs; therefore, the nutrition issue should receive more interest.⁶ In Poland, only few studies and some time ago have been carried out on the diets of people with HIV.^{7,8} More recent research frequently focuses on only one issue, without assessing the intake of various food groups.⁹ There are recommendations for increasing the consumption of some product groups and limiting the consumption of others. However, due to the lack of control over patients' diets, it cannot be clearly stated

whether those with HIV are aware of the nutritional recommendations made for them.^{4,10} The aim of the study was to conduct a survey among seropositive people aged 16–65 years using a questionnaire (KomPAN v. 1.2¹¹) to study their nutritional views and habits. The results of this study would determine the consumption of specific food groups and assess diet quality using diet quality indicators, according to the data development procedure,¹² and also help determine whether patients present proper eating habits and which most common mistakes they make in terms of consuming specific food groups.

Material and methods

Material

The study involved 31 patients of the HIV/AIDS Preventative and Therapeutic Clinic of the Infectious Disease Prevention and Therapy Center at Wrocław Health Center (SPZOZ Wrocław) in Poland. The consent to conduct the research was issued by the Bioethics Committee at the Wrocław Medical University (approval No. KB-326/2019). The study group consisted of men ($n = 31$) who had been infected with HIV through sexual contact with other men. Recruitment was performed at the Outpatient Clinic during patients' conversations with the doctors working there. During their periodic visits, the patients were informed about the purpose and scope of the tests, the voluntary nature of their participation and the possibility of resigning from the research at any time. In order to ensure anonymity, each study participant received their own code consisting of the letters “GB” and numbers ranging from 1 to 250. The research was conducted in March–May 2019. The participants were asked to fill out the nutritional questionnaire and return it in pre-addressed envelopes.

The KomPAN questionnaire

The questionnaire used to assess patients' views and eating habits had 2 versions – one was used by the interviewer for questioning and the other was adapted for the participant to complete on his own. The questionnaire consisted of 4 parts:

- Part A, with questions about eating habits;
- Part B, with questions about the frequency in which individual food groups were consumed;
- Part C, regarding the participant's views on food and nutrition; and
- Part D, with questions about lifestyle and patient data.¹²

The participants were asked to complete the KomPAN questionnaire given to them, stating that they did not have to fill in Part C, since the scope of the research did not cover the respondents' views on food.

Based on the responses, it was possible to develop 2 dietary quality indicators: the healthy diet-10 index (pHDI-10) and the unhealthy diet-14 index (nHDI-14). The healthy

Table 1. Combining the 2 questions regarding physical activity¹²

| Physical activity at work/school | Physical activity in free time | | |
|--|---|--|---|
| | low (predominantly sitting, watching TV, reading newspapers or books, light housework, or walking; 1–2 h a week) | moderate (walking, cycling, gymnastics, or other light physical activity; 2–3 h a week) | high (cycling, jogging, and other recreational sports activities requiring physical effort; over 3 h a week) |
| Low (more than 70% of the time sitting) | low | low | moderate |
| Moderate (about 50% of the time sitting and about 50% of the time moving) | low | moderate | moderate |
| High (about 70% of the time moving or doing physical work requiring heavy effort) | moderate | moderate | high |

diet index included questions regarding the consumption of the following food groups: whole-meal bread, buckwheat, oatmeal, whole-grain pasta, or other coarse cereals, milk (including flavored milk, cocoa, and coffee with milk), fermented dairy drinks, cottage cheese (including homogenized cheese and cottage cheese desserts), poultry, fish, legumes, and fruit and vegetables.¹²

The nHDI-14 index was calculated based on the frequency in which the following product groups were consumed: light bread (e.g., wheat, rye, mixed wheat-rye, toasted bread, rolls, croissants, white rice, plain pasta, or small groats), fast food, meat- or flour-based fried foods, butter as an addition to bread or dishes for frying, baking, etc., lard as an addition to bread or dishes for frying, baking, etc., cheese (including processed cheese and blue cheese), cold cuts, processed sausages or frankfurters, red meat, sweets and other confectionery, canned meat, sweetened carbonated or non-carbonated drinks, energy drinks, and alcoholic beverages.¹²

Individual responses to the questionnaire were assigned the following values: 0 – never, 0.06 – 1–3 times a month, 0.14 – once a week, 0.5 – several times a week, 1 – once daily, and 2 – several times a day. The range of results for the pHDI-10 was 0–20 points, while for the nHDI-14 it was 0–28 points. In order to unify the 2 indices and facilitate comparisons (interpretation), it was decided to recalculate the total frequency of consumption and to express the result on a scale of 0–100. A division into 3 categories of nutritional trait intensity was used: low (0–33), moderate (34–66) and high (67–100) intensity.¹²

The questionnaire also included questions about physical activity, both at work/school and in free time. Three answers could be given to these 2 questions: low, moderate or high activity.¹² Table 1 presents the method of combining the 2 variants of physical activity.

Statistical analysis

The statistical analysis was performed using STATISTICA v. 13.1 software (StatSoft Inc., Tulsa, USA). The normality of the distribution was checked using the Shapiro–Wilk test.

The table also used cardinality tables and multi-tier tables. In order to check the interdependence of 2 variables, the χ^2 test was used, assuming $p < 0.05$.

Results

Participant characteristics

The study was conducted among 31 patients, whose average age was 42 years. The youngest respondent was 26 years old, while the oldest was 65 years old. Most respondents lived in a city with at least 100,000 inhabitants. There were no participants with only a basic education. Almost half (48.3%) of the respondents had a university degree. The same percentage of people described their financial situation as good. The largest group of respondents were diagnosed with HIV in the years 2016–2019 (35.5%). However, the differences in the number of people between individual years were insignificant.³⁴ Two patients did not specify the time when they learned about their infection. The characteristics of the study group are shown in Table 2.

Eating habits and lifestyle

Almost half (45.2%) of the respondents ate 3 meals a day. A small percentage (9.7%) reported consuming only 2 meals daily; others ate 4 or 5. All ate between meals, usually several times a week (41.9%), although there were those who snacked several times a day (29%). Most willingly declared that they ate fruit and sweet snacks between meals (87% and 64.5%, respectively). Vegetables, sweetened beverages and dairy desserts were least preferred as snacks (both variants 22.6%). For spread, they usually used butter (32.3%), although a large group did not use any fat when making sandwiches (22.6%). For frying, most chose vegetable oil (51.6%). The respondents generally did not sweeten hot drinks (41.9%), though they added salt to cooked meals and sandwiches (58.1%). Most ate out 1–3 times a month (51.6%), although there were those who ate in bars,

Table 2. Participant characteristics

| Variable | Number of people (n) | % |
|--|----------------------|-------|
| Sex | | |
| Male | 31 | 100.0 |
| Age [years] | | |
| 15–24 | 0 | 0.0 |
| 25–44 | 17 | 54.8 |
| 45–69 | 14 | 45.2 |
| Place of residence | | |
| Village | 8 | 25.8 |
| Small town (<20,000 inhabitants) | 3 | 9.7 |
| Town (20,000–100,000 inhabitants) | 9 | 29.0 |
| City (>100,000 inhabitants) | 11 | 35.5 |
| Financial situation of household | | |
| We live modestly or very modestly | 0 | 0.0 |
| We live modestly | 3 | 9.7 |
| We live normally | 10 | 32.3 |
| We are relatively wealthy | 15 | 48.3 |
| We are very wealthy | 3 | 9.7 |
| Educational level | | |
| Primary | 0 | 0.0 |
| Lower secondary | 4 | 12.9 |
| Upper secondary | 12 | 38.8 |
| Higher | 15 | 48.3 |
| Time from detection of infection [years] | | |
| 0–3 | 11 | 35.5 |
| 4–9 | 9 | 29.0 |
| >10 | 9 | 29.0 |
| No data | 2 | 6.5 |

restaurants or canteens once a day or more often (13% in total). Twenty-two people were smokers, while 4 had quit smoking. Low physical activity at work or school was declared by 32.4%; moderate activity was declared by 48.4%, and high activity by 19.4%. Taking into account physical activity in free time, the percentage of those who reported moderate physical activity decreased (41.9%), while the number who assessed their activity as high was a few percentage points higher (22.6%) (Table 5). Only 1 person rated their nutritional knowledge as very good; the majority

of respondents described it as good (61.3%). Others rated it as satisfactory (25.8%) or insufficient (9.7%). Seventy-one percent of people rated their diet as good, 25.8% as bad and 3.2% as very good (Table 6).

In analyzing the results concerning the influence of age, time since the initiation of treatment and time since diagnosis on the self-assessment of the patients' nutritional knowledge, a relationship was found between the time since diagnosis and the assessment of nutritional knowledge ($p = 0.03$).

When comparing the assessment of diets among the patients, no significant relationships were observed between age, time since the infection was detected and time since the start of treatment.

Light bread was chosen more often as the bread consumed daily or more than once a week in comparison to whole-meal bread (Table 3). A similar tendency was observed in the case of white rice, plain pasta, and small groats: 38.7% of respondents ate these products more than once a week, while whole-grain products and coarse cereals were eaten only by ¼ of respondents. Most frequently they consumed the latter group of products 1–3 times a month (42%). Over 1/10 of the participants (12.9%) never consumed whole grains or whole-meal bread (19.4%). Fast food was not popular among the respondents – no one reported consuming this type of food more than once a week, and more than half (51.6%) had it just 1–3 times a month. As many as 35.5% did not eat such food at all. A similar frequency of consumption as that of burgers, pizzas, fries, casseroles, and hot dogs was observed for fish – here as well 51.6% most frequently ate fish 1–3 times a month, while 6.5% did not eat it at all and 16.1% did so more than once a week.

Fruit and vegetable consumption several times a day was reported by 22.6% and 19.4% of respondents, respectively. As many as 54.8% consumed fruit once a week, and 38.7% ate vegetables that often. With the same frequency as fruit (once a day), 22.6% reached for sweets. However, most declared that they ate food from this group more than once a week. Cheese and cottage cheese were consumed once a week by 38.7% and 41.9%, respectively, but the participants were more likely to choose yellow cheese on a daily basis. Eggs were most often consumed once a week or several times a week (48.4% and 32.3%), appearing on the menu every day for one respondent. Potatoes

Table 3. Anthropometric parameters of the study group

| Factor | Min | Max | M | ±SD | Me |
|---------------------|------|-------|------|------|------|
| Body height | 1.7 | 1.93 | 1.77 | 0.05 | – |
| Body weight | 60 | 103 | 75.3 | 13.1 | – |
| WHR | 0.86 | 1.06 | 0.96 | 0.05 | – |
| Hip circumference | 80.0 | 112.0 | – | – | 90.0 |
| Waist circumference | 74.0 | 115.0 | – | – | 85.5 |
| BMI | 19.6 | 33.3 | – | – | 22.4 |

WHR – waist-to-hip ratio; BMI – body mass index; Min – minimum; Max – maximum; M – mean; SD – standard deviation; Me – median.

Table 4. Frequency (%) of selected food consumption among participants

| Food | Never | 1–3 times a month | Once a week | More than once a week | Once a day | More than once a day |
|--|-------|-------------------|-------------|-----------------------|------------|----------------------|
| White bread | 3.2 | 19.4 | 0 | 32.2 | 22.6 | 22.6 |
| Wholemeal bread | 19.4 | 22.6 | 12.9 | 25.8 | 12.9 | 6.4 |
| White rice, white pasta, or fine-ground groats | 0 | 29.0 | 32.3 | 38.7 | 0 | 0 |
| Buckwheat, oats, wholegrain pasta, or other coarse-ground groats | 12.9 | 42.0 | 16.1 | 25.8 | 3.2 | 0 |
| Fried foods | 12.9 | 35.5 | 19.4 | 29.0 | 3.2 | 0 |
| Fast foods | 35.5 | 51.6 | 12.9 | 0 | 0 | 0 |
| Fish | 6.5 | 51.6 | 25.8 | 16.1 | 0 | 0 |
| Fruits | 0 | 3.2 | 9.7 | 54.8 | 12.9 | 19.4 |
| Vegetables | 0 | 6.5 | 6.5 | 38.6 | 25.8 | 22.6 |
| Sweets | 3.2 | 9.7 | 9.7 | 48.4 | 22.6 | 6.4 |
| Cheese | 3.2 | 25.8 | 12.9 | 38.7 | 16.2 | 3.2 |
| Eggs | 0 | 16.1 | 48.4 | 32.3 | 3.2 | 0 |
| Potatoes (excluding chips and fries) | 3.2 | 25.8 | 19.4 | 41.9 | 9.7 | 0 |
| Fruit juices, vegetable | 6.4 | 25.8 | 9.7 | 51.6 | 0 | 6.5 |
| Juices, fruit and vegetable juices | 19.4 | 38.7 | 12.9 | 29.0 | 0 | 0 |
| Poultry meat | 3.2 | 12.9 | 16.1 | 67.8 | 0 | 0 |
| Milk | 25.8 | 22.6 | 6.4 | 22.6 | 6.5 | 16.1 |
| Fermented milk beverages | 3.2 | 29.0 | 16.1 | 35.5 | 9.7 | 6.5 |
| Fresh cheese curd products | 6.5 | 29.0 | 19.4 | 41.9 | 3.2 | 0 |
| Cold meats, smoked sausages, and hot dogs | 6.5 | 3.2 | 6.5 | 64.4 | 9.7 | 9.7 |
| Red meat | 12.9 | 35.5 | 19.4 | 29.0 | 3.2 | 0 |
| Legume dishes | 9.7 | 58.0 | 25.8 | 6.5 | 0 | 0 |
| Canned meat | 45.2 | 48.4 | 3.2 | 3.2 | 0 | 0 |
| Sweetened hot beverages | 29.0 | 6.5 | 0 | 9.7 | 6.5 | 48.3 |
| Sweetened beverages | 22.6 | 41.9 | 16.1 | 9.7 | 3.2 | 6.5 |
| Energy drinks | 80.6 | 19.4 | 0 | 0 | 0 | 0 |
| Water | 3.2 | 12.9 | 0 | 22.6 | 12.9 | 48.4 |
| Alcoholic beverages | 29.0 | 38.6 | 16.1 | 16.1 | 0 | 0 |

Table 5. Physical activity (% of people)

| Physical activity | Low | Moderate | High |
|-------------------|------|----------|------|
| At work or school | 32.3 | 48.4 | 19.4 |
| During free time | 35.5 | 41.9 | 22.6 |

Free-time physical activity did not depend on the time since detection of the infection ($p = 0.38$), but it did depend on the age of the respondents ($p = 0.045$). There was no significant effect of the above times on physical activity at work or at school.

Table 6. The respondents’ assessment of their own nutritional knowledge and diet

| Parameter | Very good | Good | Bad | Very bad |
|-----------------------|-----------|------|------|----------|
| Nutritional knowledge | 3.2 | 61.3 | 25.8 | 9.7 |
| Diet | 3.2 | 71.0 | 25.8 | 0.0 |

were also consumed more often than once a week, in a form other than chips or fries, although a large group (25.8%) consumed them 1–3 times a month.

Vegetable and vegetable–fruit juices were not very popular among the study participants – 19.4% never consumed

them compared to 6.4% who never consumed fruit juices. The latter were most often consumed once a week (51.6%). Most often, the respondents had vegetable juices 1–3 times a month (38.7%), while nobody drank this type of drink more than several times a week.

As many as 67.8% ate poultry meat several times a week, nobody more often. Only one person gave up white meat completely. With similar frequency, the study participants declared consuming sausages, and frankfurters (64.5%). In the case of red meat, 12.9% of respondents never consumed it, 35.5% did so 1–3 times a month, and 29.0% several times a week. A total of 9.7% consumed it daily or several times a day, slightly less (6.5%) once a week.

In the case of milk, cocoa or flavored milk, 25.8% declared that they did not consume these products at all, 22.6% several times a week and 16.1% several times a day. Fermented dairy drinks such as yogurt and kefir, both plain and flavored, were quite popular among the respondents. It was observed that 35.5% of people consumed them several times a week, 9.7% once a day and 6.5% several times a day.

Over half of the respondents (58.1%) ate legumes and dishes containing them only 1–3 times a month; 25.8% reported eating legumes once a week, while 9.7% did not eat them at all. Canned meats were not very popular – as many as 93.6% consumed them 1–3 times a month or never. Overall, 80.6% did not consume energy drinks and nobody consumed them more often than 1–3 times a month.

Water and sweetened hot drinks such as tea, coffee or fruit/herbal teas were the most common daily drinks: both types of drinks were consumed several times a week by almost half of the respondents (48.4%). A significant number did not consume sweetened hot drinks at all (29%). Sweetened carbonated drinks were not very popular among this group of people, since 41.9% consumed them 1–3 times a month and 22.6% not at all. Alcohol was consumed most often 1–3 times a month by 38.7%; whereas 29.0% did not drink it at all. People who consumed alcohol most often reported drinking beer (45.2%).

Diet quality indices

Table 7 shows the values for the healthy and unhealthy diet indices. The average pHDI-10 result for the whole study group (21.1%) means that they show a small degree

of dietary health features. On the other hand, in the case of the average nHDI-14 result, the mean value of 15.5% places them in the category of a small degree of unhealthy features. Only 4 patients had a healthy diet index above 33 points, which means their diet can be described as having a moderate degree of healthy features. None of the participants had a diet with a large degree of pro-health features. In the case of nHDI-14, the diets of all participants were qualified as diets with a small degree of unhealthy traits, i.e., none of the participants scored more than 33 points.

Using the χ^2 test, it can be observed that the time since diagnosis does not significantly affect the value of the healthy diet index ($p = 0.06$). However, the time since the start of treatment significantly affects the value of the pHDI-10 index ($p = 0.02$) (Table 8).

In the breakdown into individual periods since the detection of the infection, the highest index of a healthy diet was observed in patients who were diagnosed 10 years ago or earlier, while the lowest pHDI-10 belonged to patients with HIV diagnoses 4–9 years ago. Patients with an infection detected more than 10 years ago or earlier are also characterized by the lowest index of an unhealthy diet; this means that their diet has the smallest degree of unhealthy dietary features among all the respondents. The highest nHDI-14 index was observed among people with recent diagnoses (Table 8).

Discussion

The topic of HIV infection is currently being discussed by scientists and doctors in Poland. Along with the development of medicine around the world, research is underway whose results are supposed to provide an improvement in the nutritional status of HIV-infected patients and positively affect the functioning of their immune systems. The role of nutritional intervention is also to prevent weight loss or excessive weight gain.¹³ The role of this study

Table 7. Dietary quality indices (%)

| Diet index | N | M | Min | Max | Q1 | Q3 | SD |
|------------|----|------|-----|------|------|------|------|
| pHDI-10 | 31 | 21.1 | 3.8 | 48.5 | 12.3 | 30.6 | 11.8 |
| nHDI-14 | 31 | 15.5 | 3.1 | 27.7 | 10.9 | 20.9 | 6.5 |

N – number; M – mean; Min – minimum; Max – maximum; Q1 – 1st quartile; Q3 – 3rd quartile.

Table 8. The value of dietary quality indicators depending on the time of the infection detection

| Time since the infection was detected [years] | N | pHDI-10 | nHDI-14 |
|---|----|---------|---------|
| 0–3 | 11 | 22.5 | 18.3 |
| 4–9 | 9 | 15.3 | 17.9 |
| >10 | 9 | 23.4 | 12.9 |
| No data | 2 | 25.3 | 5.9 |

N – number.

was to identify the dietary habits and frequency which with individual food groups are consumed, so that in the future – in cooperation between doctors, patients and dietitians – the best solutions can be worked out, resulting in the best care for the patient not only from the attending physician, but also from representatives of other disciplines. Knowing the frequency of food intake will also shed light on the current nutritional trends of patients and, if necessary, enable undertaking nutritional intervention.

According to the currently adopted recommendations for patients infected with HIV, it is recommended to eat 4–6 meals a day, which stems from the need for a steady supply of basic nutrients from the diet.⁵ Our analysis of the results shows that respondents usually eat 3 meals a day. In addition, frequent snacking between meals was observed. Snacking between meals may be caused by the low caloric value of the meals consumed or an uneven distribution throughout the day, which further confirms the belief that the recommendation of 4–6 meals a day in the diet of seropositive patients should be followed. A low number of meals is one of the basic mistakes related to nutrition, while it is worth noting here that over 61% of people described their nutritional knowledge as good or very good.

Usually, when snacking, subjects reach for fruit, but a large group of people also declared that they choose sweets. Almost half of the respondents consumed sweets several times a week, and almost 1/3 do so daily or several times a day. Therefore, the risk of not only obesity, but also other diseases such as caries, type 2 diabetes and cardiovascular diseases is higher.^{14–17} Sugar consumption should be limited not only because of the abovementioned diseases, but also because ARV therapy alone causes weight gain in 30–50% of patients.⁵ A large group of people add salt to cooked meals. Without recording the exact amounts of salt they add to dishes, it cannot be clearly determined whether these people consume significant amounts of salt, but taking into account the trends of Poles in the consumption of salt,¹⁸ the addition of salt to dishes should be limited.

In the area of cereal consumption, there are no clear guidelines in Poland regarding the quantity and type of such products for people with HIV, but considering that this type of food is on one of the basic levels of the Pyramid of Healthy Nutrition and Physical Activity,¹⁹ the selection of these products should be adapted to the recommendations of the Institute of Food and Nutrition, i.e., they should be mainly whole grains, containing more B vitamins and fiber than white bread or plain pasta.²⁰ It is worth mentioning that the intake of vitamins and minerals by HIV-infected patients is recommended to be 100–150% of the recommended daily intake for other adults.^{5,34} In view of these recommendations, unfavorable trends can be observed among the respondents in that they consume much more white bread and processed products, such as white rice and plain pasta, than products from so-called full milling.

One very positive aspect is the subjects' avoidance or very rare consumption of fast food. In view of the generally

high proportion of fats in the diet and the risk of lipid disorders in people with HIV,^{21,22} it is a good sign that the respondents are limiting highly-processed fast foods. Considering the current recommendations in terms of fish consumption for healthy people,^{20,33} it is worth focusing on problem of how rarely of these products are consumed. Patients should be advised to increase their fish intake due to the documented benefits of reducing low-density-lipoprotein (LDL) cholesterol and improving the overall lipoprotein profile.^{22,32}

The consumption of fruit and vegetables was very low for the respondents in comparison with the current recommendations.^{19,20,35} Only 1/5 of participants consumed fruit and vegetables several times a day; most reported consuming them several times a week. This is significant because vitamins and minerals have been proven many times^{24,25,29} to have a positive influence on the defense mechanisms of the body. This study shows that fruit and vegetable juices were a substitute for fruit and vegetables in the daily diet of the respondents – both types were consumed several times a week, but not every day. The good news is that there was minimal consumption of energy drinks – only 1/5 consumed them 1–3 times a month, the rest never. However, the high consumption of sweetened hot drinks may be worrying. Alcoholic beverages were consumed by a total of 71%, of which over half did so 1–3 times a month. Various studies and recommendations require that virtually all alcohol be eliminated from the diet of HIV-positive patients, due to possible adverse interactions with ARV drugs.^{4,5,28}

In accordance with the principles of healthy eating, adults should consume at least 2 large glasses of milk every day or replace them with fermented milk beverages. Research shows that almost a quarter do not consume milk at all, while only slightly over 21% consume milk once or several times a day. Fermented milk drinks were consumed with the same frequency by about 15% of respondents. As many as 22.6% and 29% of subjects reported consuming milk and dairy drinks only 1–3 times a month, respectively. It has been proven that people with HIV have a higher risk of bone disease: for osteopenia, the risk ranges from 22% to even 77%. Increased catabolism of vitamin D occurs with some drugs.^{5,25,26,30} Therefore, dairy products should feature in the daily diet as a good source of calcium, although some scientists note that fermented dairy beverages (and raw eggs) should be limited because of the possibility of bacterial growth and their negative impact on a weakened immune system.^{4,27,31}

Proper nutrition helps improve not only health, but also the quality of life of HIV-positive people. It can eliminate the occurrence of significant malnutrition in infected people as well as a deficit of minerals and vitamins with immunostimulating properties (vitamins B, A, C, and E). Proper nutrition also reduces the undesirable effects of ARV therapy (hyperglycemia and hypercholesterolemia).⁵

Although patients rated their nutritional knowledge and diet highly, this did not translate into the dietary quality

as calculated in the study. The fact that all participants displayed a small degree of unhealthy dietary features is encouraging, as it may indicate that they actually have nutritional knowledge about restricting certain products which are not recommended for their daily diet. However, the patients' own nutritional assessment does not transfer into their diet having strong features of a healthy diet. In this aspect, one should strive to make patients more aware about the importance of products included in the diet as components of a healthy dietary index.

Conclusions

Patients appraise their nutritional knowledge highly, although this does not always translate into the quality of their diet. People with a newly diagnosed infection do not pay as much attention to what they eat, which makes the average unhealthy diet index in this group much higher than in the other groups. Eating habits change with the passage of time after diagnosis, which translates into a decrease in nHDI-14 values and an increase in the proportion of products classified as having pro-health properties. Eating fruit and vegetables too rarely is also a noticeable problem, though it is satisfactory that HIV-positive people rarely eat highly processed foods.

ORCID iDs

Paweł Duda  <https://orcid.org/0000-0002-7907-5974>
 Brygida Knysz  <https://orcid.org/0000-0003-2605-1079>
 Jacek Gašiorowski  <https://orcid.org/0000-0001-5039-4579>
 Bartosz Szetela  <https://orcid.org/0000-0001-7178-9801>
 Ewa Piotrowska  <https://orcid.org/0000-0002-8899-2010>
 Monika Bronkowska  <https://orcid.org/0000-0003-2960-6981>

References

- Cade HE, Burley VJ, Warm DL, Thompson RL, Margetts BM. Food-frequency questionnaires: A review of their design, validation and utilization. *Nutr Res Rev.* 2004;17(1):5–22.
- Gładysz A, Knysz B. Zakażenia HIV i AIDS – poradnik dla lekarzy. Wrocław Poland: Wydawnictwo Continuo; 2014.
- Horban A, Podlasiński R, Cholewińska G, et al., eds. Zasady opieki nad osobami zakażonymi wirusem HIV. Zalecenia Polskiego Towarzystwa Naukowego AIDS 2018. Warszawa–Szczecin, Poland: Polskie Towarzystwo Naukowe AIDS; 2018.
- Lebiedzińska A, Bierzycka N, Lemańska M, et al. Assessment of energy value of daily food rations of HIV-positive adults. *Rocz Panstw Zakł Hig.* 2009;2(60):191–194.
- Tomaszewska-Olijarczyk A, Rozpłochowski B, Kierepa A, Mozer-Lisewska I, Kowala-Piaskowska A. Dietary management in people infected with HIV. In: Parczewski M, Bociąga-Jasik M, eds. Rules for the Care of People Infected with HIV: PTN AIDS Recommendations 2019. 2nd ed. Warszawa, Poland: Polskie Towarzystwo Naukowe AIDS; 2019:356–363.
- Stojanović D, Marković D, Kocić G. Nutrition and patients with HIV/AIDS. *Acta Medica Mediana.* 2011;50(3):63–68. doi:10.5633/amm.2011.0312
- Maksymowicz-Jaroszuk J, Grzeszczuk A, Filon J, Karczewski J. Assessment of nutrition and nutritional status of patients infected with HIV from the Podlasie area. *Probl Hig Epidemiol.* 2013;94(4):919–922.
- Lebiedzińska A, Bierzycka N, Lemańska M, et al. Assessment of energy value of daily food rations of HIV-positive adults. *Rocz Panstw Zakł Hig.* 2009;2(60):191–199.
- Labban L. The implications of HIV/AIDS on the nutritional status and the MNT for its patients. *EC Nutrition.* 2016;3(4):680–686.
- Stradling C. HIV. In: Payne A, Barker H, eds. *Dietetics and Clinical Nutrition.* 2nd ed. Wrocław, Poland: Urban & Partner Medical Publishing; 2010:159–180.
- Jeżewska-Zychowicz M, Gawecki J, Wadolowska L, et al. Dietary habits and nutrition beliefs questionnaire for people 15–65 years old, version 1.2 – self-administered questionnaire. In: Gawecki J, ed. *Dietary Habits and Nutrition Beliefs Questionnaire and the Manual for Developing of Nutritional Data.* The Committee of Human Nutrition, Polish Academy of Sciences: Olsztyn, Poland; 2018:21–33.
- Wadolowska L, Krusinska B. The manual for developing nutritional data from the KomPAN[®] questionnaire. In: Gawecki J, ed. *Dietary Habits and Nutrition Beliefs Questionnaire and the Manual for Developing Nutritional Data.* The Committee of Human Nutrition, Polish Academy of Sciences: Olsztyn, Poland; 2018:34–52.
- Kourkouta L, Monios A, Mihalache A, Iliadis C, Ouzounakis P, Dimitriadou A. AIDS and nutrition in patients. *Prog Health Sci.* 2017;7(1):182–186.
- Delli Bovi AP, Di Michele L, Laino G, Vajro P. Obesity and obesity related diseases, sugar consumption and bad oral health: A fatal epidemic mixtures: the pediatric and odontologist point of view. *Transl Med UniSa.* 2017;16:11–16.
- Te Morenga L, Mallard S, Mann J. Dietary sugars and body weight: Systemic review and meta-analyses of randomized controlled trials and cohort studies. *BMJ.* 2012;346:e7492. doi:https://doi.org/10.1136/bmj.e7492
- Kapczuk P, Komorniak N, Rogulska K, Bosiacki M, Chlubek D. Highly processed foods and its impact on the health of children and adults. *Biochem Adv.* 2020;1(66):23–29. doi:https://doi.org/10.18388/pb.2020_309
- Kłósiewicz-Latoszek L, Cybulska B. Sugar and the risk of obesity, diabetes and cardiovascular disease [in Polish]. *Probl Hig Epidemiol.* 2011;92(2):181–186.
- Narodowe Centrum Edukacji Żywności i Żywienia Instytutu Żywności i Żywienia. <https://ncez.pl/abc-zywienia-fakty-i-mity/dieta-polakow-a-zalecenia-za-tlusto-za-slono-za-slodko->. Warszawa, Poland: NCEZ IŻŻ; 2020. Accessed on March 28, 2020.
- Narodowe Centrum Edukacji Żywności i Żywienia Instytutu Żywności i Żywienia. <https://ncez.pl/abc-zywienia-zasady-zdrowego-zywienia-piramida-zdrowego-zywienia- and physical-activity-for-adults>. Warszawa, Poland: NCEZ IŻŻ; 2020. Accessed on March 28, 2020.
- Narodowe Centrum Edukacji Żywności i Żywienia Instytutu Żywności i Żywienia. <https://ncez.pl/abc-zywienia-zasady-zdrowego-zywienia-podstawowe-zasady-zdrowego-zywienia>. Warszawa, Poland: NCEZ IŻŻ; 2020. Accessed on March 28, 2020.
- Drelichowska J, Kwiatkowska W, Knysz B, et al. Lipodystrophy syndrome in HIV-infected patients: A cohort study in Lower Silesia, Poland. *HIV AIDS Rev.* 2017;16(1):40–49. doi:10.5114/hivar.2017.65114
- Jackiewicz A, Czarnecki M, Knysz B. Effect of diet on lipid profile in HIV-infected patients. *HIV AIDS Rev.* 2018;17(3):159–163.
- Wytyczne ESC/EAS dotyczące leczenia zaburzeń lipidowych w 2016 roku. Grupa Robocza Europejskiego Towarzystwa Kardiologicznego (ESC) i Europejskiego Towarzystwa Miażdżycowego (EAS) do spraw leczenia zaburzeń lipidowych. *Kardiologia Pol.* 2016;74(11):1234–1318. doi:10.5603/KP.2016.0157.
- Lebiedzińska A, Bierzycka N, Lemańska M, et al. Vitamins in the diet of HIV-positive people [in Polish]. *Bromatology and Toxicological Chemistry.* 2009;42(3):672–677.
- Grygiel-Górniak B, Puszczewicz M. Vitamin D: A new view in medicine and rheumatology [in Polish]. *Postepy Hig Med Dosw (Online).* 2014;68:359–368.
- Pezzotti P, Napoli P, Acciai S. Increasing survival time after AIDS in Italy: The role of new combination antiretroviral therapies. Tuscany AIDS Study Group. *AIDS.* 1999;13(2):249–255.
- Hendricks M, Eley B, Bourne L. Nutrition and HIV/AIDS in infants and children in South Africa: Implications for food-based dietary guidelines. *Matern Child Nutr.* 2007;3(4):322–333.
- Knox TA, Zafonte-Sanders M, Fields-Gardner C, Moen K, Johansen D, Paton N. Assessment of nutritional status, body composition, and human immunodeficiency virus associated morphologic changes. *Clin Infect Dis.* 2003;36(Suppl 2):63–66.

29. Capili B, Anastasi JK. Body mass index and nutritional intake in patients with HIV and chronic diarrhea: A secondary analysis. *J Am Acad Nurse Pract.* 2008;20(9):463–470.
30. Baum MK, Shor-Posner G, Bonvehi P, et al. Influence of HIV infection on vitamin status and requirements. *Ann NY Acad Sci.* 1992;669:165–174.
31. Beach RS, Mantero-Atienza E, Shor-Posner G, et al. Specific nutrient abnormalities in asymptomatic HIV-1 infection. *AIDS.* 1992;6(7):701–708.
32. Kotler D. Antioxidant therapy and HIV infection. *Am J Clin Nutr.* 1998; 67:7–9.
33. Hughes S, Kelly P. Interactions of malnutrition and immune impairment, with specific reference to immunity against parasites. *Parasite Immunol.* 2006;18(11):577–588.
34. Pribram V, Childs K, Poulton M. A nutritional screening audit of new adult out-patients with HIV. *J Hum Nutr Diet.* 2008;21(4):373–406.
35. Topping CM, Humm DC, Fischer RB, Brayer KM. A community-based, interagency approach by dietitians to provide meals, medical nutrition therapy, and education to clients with HIV/AIDS. *J Am Diet Assoc.* 1995;95(6):683–686.
36. Crofford S, Cashman L, Bush R, Moreland, K. Nutrition knowledge of persons with HIV/AIDS who use a Food Assistance Program. *J Am Diet Assoc.* 1999;9(99 Suppl):A92.
37. World Health Organization. Global Summary of the HIV/AIDS Epidemic. <https://www.who.int/news-room/fact-sheets/detail/hiv-aids>. Geneva, Switzerland: WHO; 2018.

The impact of environmental air pollution on the prevalence of molar incisor hypomineralization in schoolchildren: A cross-sectional study

Natalia Głódkowska^{A–D,F}, Katarzyna Emerich^{A,E,F}

Department of Pediatric Dentistry, Medical University of Gdańsk, Poland

A – research concept and design; B – collection and/or assembly of data; C – data analysis and interpretation; D – writing the article; E – critical revision of the article; F – final approval of the article

Advances in Clinical and Experimental Medicine, ISSN 1899–5276 (print), ISSN 2451–2680 (online)

Adv Clin Exp Med. 2020;29(12):1469–1477

Address for correspondence

Katarzyna Emerich
E-mail: emerich@gumed.edu.pl

Funding sources

This work was supported by funds from the Polish Ministry of Science and Higher Education, granted to maintain statutory activities.

Conflict of interest

None declared

Acknowledgements

The authors wish to thank Dr. Jan Kaczmarek for his enthusiastic and tireless help and his encouragement during the preparation of the manuscript.

Received on April 15, 2020

Reviewed on May 20, 2020

Accepted on October 8, 2020

Cite as

Głódkowska N, Emerich K. The impact of environmental air pollution on the prevalence of molar incisor hypomineralization in schoolchildren: A cross-sectional study. *Adv Clin Exp Med.* 2020;29(12):1469–1477. doi:10.17219/acem/128227

DOI

10.17219/acem/128227

Copyright

© 2020 by Wrocław Medical University
This is an article distributed under the terms of the Creative Commons Attribution 3.0 Unported (CC BY 3.0) (<https://creativecommons.org/licenses/by/3.0/>)

Abstract

Background. Molar incisor hypomineralization (MIH) is a common condition that causes considerable pain to children and distress to their parents. Clinically it is manifested by demarcated opacities of tooth enamel with reduced mineralization. The mean global incidence of this disorder has been estimated at around 13–14%. Environmental pollution is one of the suspected etiological factors, but the impact of air pollutant components on MIH has yet to be studied.

Objectives. To assess whether the level of air pollution components has an impact on the prevalence of MIH.

Material and methods. This cross-sectional study included 2354 children, aged 6–12 years, attending schools in 2 voivodeships (regions) of Poland with best and worst air quality. Smog alarms are announced more than 50 times a year in the Silesian voivodeship, while in the Pomeranian voivodeship, consistently low levels of air pollution are observed. Our air quality assessment was carried out on the basis of average annual results from measuring stations located in the 2 voivodeships. Dental examinations of teeth were conducted using the European Academy of Paediatric Dentistry (EAPD) criteria for the diagnosis of MIH.

Results. Levels of air pollution components over time were notably higher in the Silesian voivodeship, especially sulfur dioxide (SO₂), particulate matter (PM10) and polycyclic aromatic hydrocarbons (PAH). The MIH was diagnosed more often in children in the Silesian voivodeship (13.7%) than in the Pomeranian (6.4%). In the Pomeranian voivodeship, MIH was most often diagnosed in children aged 6 (14.53%).

Conclusions. This study shows a correlation between higher concentrations of air pollutants and the occurrence of enamel developmental disorder in the form of MIH. Future research is required to assess whether this is related to the presence of a specific component or to the more frequent occurrence and treatment of air pollution-related general diseases, such as respiratory illnesses.

Key words: children, air pollution, prevalence, enamel defects, molar incisor hypomineralization

Introduction

Due to increasing awareness as well as a decline in the incidence of dental caries, researchers have been focusing on developmental disorders of the teeth. One developmental disorder of enamel, first described in 2001, is molar incisor hypomineralization (MIH).¹ It involves reduced mineralization and increased porosity of the tooth enamel, and involves the first permanent molars (FPM) and often the permanent incisors (PI).¹ Clinically the changes are manifested as white, cream-yellow or brown opacities, clearly demarcated from healthy enamel (Fig. 1). The affected enamel has a disturbed structure and, due to the effects of chewing forces, it may break down soon



Fig. 1. Demarcated opacities on first permanent molar



Fig. 2. Posteruptive breakdown (PEB) of first permanent molar

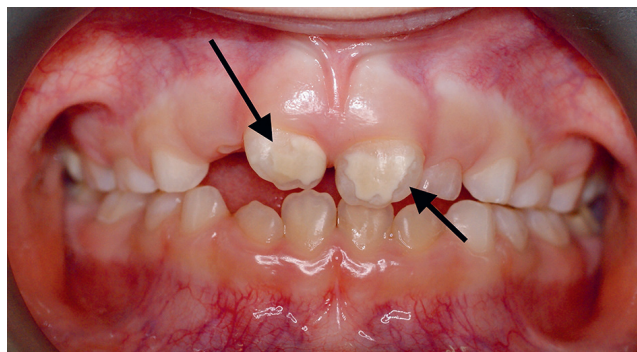


Fig. 3. Demarcated opacities on permanent incisors

after eruption, resulting in a significant loss of mineralized tooth structure (Fig. 2).²

The MIH is a public health problem whose consequences are not only health-related but also economic. For the patient, these teeth are the cause of discomfort and sometimes pain (even during brushing), and often require advanced treatment at a very young age. Furthermore, when the disorder also includes incisors – visible when smiling – it can create a major esthetic problem (Fig. 3). Visible patches can negatively affect the patient's well-being and their contact with peers.³

For a dentist, treating children with MIH represents a significant challenge.⁴ The affected teeth cause pain and hypersensitivity, and often do not undergo sufficient anesthesia, compromising the child's cooperation. Children with MIH are more prone to suffer from dental phobia than healthy ones. Furthermore, the incorrect enamel structure does not allow for the effective adhesion of materials, and fillings often chip off, necessitating repeated treatment. Studies show that children with MIH require more frequent treatment than children without MIH.⁵ Treatment mainly concentrates on prevention of post-eruptive enamel fractures and reduction of tooth sensitivity. However, in more advanced cases – where there is a loss of hard tooth tissues – tooth reconstruction is required; sometimes it is even necessary to extract teeth at a very young age. The MIH is considered to be the second biggest cause of permanent molar loss after caries, emphasizing the need for deeper understanding of this disorder and the possibility of its prevention.⁶

In the last few years, several papers have been published on the prevalence of MIH.⁷ In 2 recent meta-analyses, the average prevalence was estimated at 14.2% and 13.1% (range: 2–40%), with statistically significant differences between macroregions, regions and countries.^{8–10} These studies confirm that the number of MIH cases is still growing, with the highest prevalence being in high-income countries.⁹

Despite many attempts to establish the etiology of this disorder, no single specific factor responsible for the occurrence of MIH has been identified. Determining a specific etiological factor is difficult because the research conducted is often retrospective. First permanent molar

disorders can be diagnosed only following their eruption, i.e., around 6–7 years of age, while the amelogenesis of these teeth occurs much earlier, i.e., in the perinatal period and the first years of a child's life, so the causative factor must work at that time. Parents often do not remember the history of illnesses and the medicines taken a few years ago.¹⁰ In the literature, the following suspected factors are presented, among the others: childhood illness, prematurity, fevers, otitis media, hypoxia at birth, pneumonia, and drugs taken, including antibiotics.^{11–15} Scientists are also trying to find a genetic predisposition for this disorder, but there is still no clear evidence of one.^{15,16} At present, the etiology is considered multifactorial, without indicating any single specific causal factor.¹⁷

Researchers' hypotheses also increasingly point to environmental pollution as a predisposing factor for MIH. Due to the toxic effects on human health even many years after exposure, dioxins have been considered a predisposing factor for dental development disorders. They belong to the group of persistent organic pollutants (POPs) that are still a considerable component of environmental pollution.¹⁸ Studies have shown a correlation between exposure to dioxins (mainly due to their excretion in breast milk), prolonged breastfeeding and the occurrence of MIH,¹⁹ although other researchers have rejected this hypothesis.²⁰ In the literature, one can also find a link between exposure to polychlorinated biphenyls (PCBs) and their impact on enamel development, including hypomineralization.²¹ Other contaminants, such as polycyclic aromatic hydrocarbons and respirable particulate matter with a diameter of up to 10 µm (PM10), also pose a threat to human health.

There is still little evidence that can unequivocally confirm or rule out a link between environmental pollution and the occurrence of MIH. To our knowledge, the relationship between MIH and the level of common air pollutant components other than PCBs has yet to be studied. The aim of this study is thus to determine the prevalence of MIH in 2 different regions of Poland – the Pomeranian and Silesian voivodeships – which, due to their location and industrialization, differ substantially in the intensity of air pollutants. Based on previous research, it can be hypothesized that air quality influences the prevalence of MIH.

Methods

Study design and sampling procedures

The study was conducted in primary schools in 2 voivodeships in Poland: Pomeranian and Silesian. The research group was made up of children residing in the Silesian voivodeship, while children from Pomeranian voivodeship were assigned to the negative control group. There are 719 primary schools in the Pomeranian voivodeship and 1,454 in the Silesian. Special care schools, penal institutions,

correctional schools, and schools in hospitals were excluded, leaving 553 schools in the Pomeranian voivodeship and 1,324 in the Silesian voivodeship qualified for the study. According to the latest data, 150,372 children aged 6–12 attend primary schools in the Pomeranian voivodeship and 260,789 in the Silesian voivodeship, so assuming a 95% confidence level, 383 children in Pomerania and 384 in Silesia should be examined for the group to be representative. According to recommendations from Elfrink et al.,⁷ for assessing the prevalence of MIH estimated at 5%, a minimum group of 300 children is required, and a minimum number of 1,000 children is recommended to evaluate a possible MIH etiological factor.

We selected 30 schools from the Pomeranian voivodeship and 15 from the Silesian voivodeship, and sent letters to the school heads inviting them to participate in the study.

Ethical considerations

The Independent Bioethics Committee for Scientific Research at the Medical University of Gdańsk gave their approval (No. NKBBN/182/2013) to conduct the study. Permission was obtained to conduct the study in 15 schools in the Pomeranian voivodeship and 7 in the Silesian. Information regarding the study and consent forms for participation in the study was sent to the parents or legal guardians of children aged 6–12. On the day of the study, children without a parent's or guardian's permission, children with general medical diseases, and children who were uncooperative or did not assent to the examination were excluded from the study.

Study location and air pollution measurement methods

The Pomeranian voivodeship is located in the north of the country, on the Baltic Sea coast, while Silesia is located in the south of the country, about 600 km away. Smog alarms are announced more than 50 times a year in the Silesian voivodeship; in the Pomeranian voivodeship, constantly low levels of air pollution are observed. In both voivodeships, stations measuring the level of air pollution are located in various cities. The number of stations has changed over time; there are currently 20 in the Pomeranian voivodeship and 30 in Silesian. The stations perform hourly or 24-hour tests. The archived results are posted on the website of the Chief Inspectorate for Environmental Protection in Poland at <http://powietrze.gios.gov.pl/pjp/current>.

The enamel mineralization of FPM and PI starts in the perinatal period and ends at the age of about 3 years. Given that the study was conducted in the years 2016–2019, studied children aged 6–12 were born between 2004 and 2012. Therefore, the air pollution levels from 2004 to 2013 were taken into account for the study. In order to assess air quality in those years, archive data on the level of pollution

were averaged for each year. The available measurements for air pollutant components comprise:

- inorganic gas pollutants: sulfur dioxide (SO₂), nitrogen dioxide (NO₂), nitrogen oxides (NO_x), ozone (O₃), and carbon monoxide (CO);
- particulate matter (PM₁₀);
- heavy metals in PM₁₀: lead (Pb; PM₁₀), arsenic (As; PM₁₀), cadmium (Cd; PM₁₀) and nickel (Ni; PM₁₀);
- volatile organic compounds: benzene (C₆H₆);
- polycyclic aromatic hydrocarbons (PAHs) in PM₁₀: benzo(a)pyrene (BaP; PM₁₀), benzo(a)anthracene (BaA; PM₁₀), benzo(b)fluorantene (BbF; PM₁₀), benzo(k)fluorantene (BkF; PM₁₀), and benzo(j)fluorantene (BjF; PM₁₀).

Study settings

Each child's dental examination was carried out at school using a dental probe, an oral mirror and a head lamp. The teeth were not cleaned or dried before examination. When necessary, cotton rolls were used to remove food debris. All the surfaces of the index teeth were examined, and MIH was diagnosed according to the criteria published by Weerheijm et al.²² (Table 1). Only defects greater than 1 mm in diameter were reported. All the examinations of all the children were performed by the same investigator (NG), who was trained and calibrated before the process commenced. The reliability of that examiner was also assessed by re-examination of every 10th child.

Statistical analyses

Descriptive statistics of the data were generated using standard statistical parameters: percentage, mean (M) and standard deviation (SD), median, and minimum and maximum (min and max). Correlations between pairs of numerical parameters were studied using the χ^2 test. The air quality was compared using Student's t-test for independent samples. A p-value <0.05 was considered statistically significant for all tests. The data were organized into files (Microsoft Excel 2013; Microsoft Inc., Redmond, USA) and statistically processed using STATISTICA v. 13.1 software (StatSoft Inc., Tulsa, USA).

Results

Characteristics of the surveyed population

The study involved 2,354 children (a response rate of 67.3%) aged 6–12 (M = 8.80, SD = 1.89), of whom 50% were girls and 50% were boys. Most of the children (61%) came from the Pomeranian voivodeship, while over a third (39%) were from the Silesian voivodeship. Over 75% lived in cities, while 23% lived in rural areas. We excluded 79 children from the study because they had no erupted permanent molars. A total of 96.7% (n = 2275) of the examined children had at least 1 erupted FPM and were included in the study, so assuming a 95% confidence level, the statistical error can be assessed as 2% for the entire population.

Characteristics of air pollution

The annual average air pollutants for both voivodeships are presented in Table 2. The statistical analysis of the data showed significantly higher levels of most of the pollutants measured in the Silesian voivodeship than in the Pomeranian. The greatest differences were observed in the cases of SO₂ and PAH, especially BaP (PM₁₀). The concentrations of these substances in the south of Poland were almost 4 times higher than in the north of the country. In terms of PM₁₀, C₆H₆, NO₂ and CO the levels were almost double in Silesian voivodeship than in Pomeranian. In the group of heavy metals in PM₁₀, the mean values of lead, cadmium and arsenic were also significantly higher in the Silesian voivodeship. The level of Ni (PM₁₀) turned out to be higher in the Pomeranian voivodeship, but the difference was not statistically significant. The only statistically significant higher level in the Pomeranian voivodeship was the O₃ concentration.

Distribution and dissemination of MIH depending on the voivodeship

The MIH was diagnosed in 212 children, representing 9.32% of the study population. The χ^2 analysis revealed statistically significant differences between the prevalence

Table 1. MIH diagnostic criteria according to Weerheijm et al.²²

| | |
|--------------------------------------|--|
| Demarcated opacity | A demarcated defect involving an alteration in the translucency of the enamel, variable in degree. The defective enamel is of normal thickness with a smooth surface and can be white, yellow or brown in color. |
| Post-eruptive enamel breakdown (PEB) | A defect that indicates deficiency of the surface after eruption of the tooth. Loss of initially formed surface enamel after tooth eruption. The loss is often associated with a pre-existing demarcated opacity. |
| Atypical restoration | The size and shape of restoration do not conform to the temporary caries picture. In most cases, in molars these are restorations extended to the buccal or palatal smooth surface. At the border of the restorations frequently opacity can be noticed. In incisors, a buccal restoration can be noticed not related to a trauma. |
| Extracted molar due to MIH | The absence of a first permanent molar should be assessed in relation to other teeth. Reasons for considering extraction due to MIH are: Opacities or atypical restorations in the other first permanent molars combined with absence of a first permanent molar. The absence of first permanent molars in sound dentition in combination with demarcated opacities on the incisors is likely to be due to MIH. It is not likely that incisors will be extracted due to MIH. |
| Unerupted | The first permanent molar or the incisor to be examined are not yet erupted. |

Table 2. Annual average air pollutants for both voivodeships

| Year | Voivode-ship | SO ₂ [µg/m ³] | | NO ₂ [µg/m ³] | | NO _x [µg/m ³] | | O ₃ [µg/m ³] | | CO [mg/m ³] | | PM10 [µg/m ³] | | Pb (PM10) [µg/m ³] | | As (PM10) [ng/m ³] | |
|----------------|--------------|--------------------------------------|--------|--------------------------------------|--------|--------------------------------------|--------|-------------------------------------|--------|-------------------------|-------|---------------------------|--------|--------------------------------|-------|--------------------------------|-------|
| | | Avg. | SD | Avg. | SD | Avg. | SD | Avg. | SD | Avg. | SD | Avg. | SD | Avg. | SD | Avg. | SD |
| 2013 | Silesian | 13.595 | 15.654 | 24.407 | 17.822 | 42.987 | 59.033 | 48.352 | 31.393 | 0.52 | 0.367 | 44.183 | 31.877 | 0.039 | 0.035 | 1.719 | 1.058 |
| | Pomeranian | 5.009 | 4.573 | 14.581 | 11.766 | 22.229 | 26.469 | 53.094 | 24.611 | 0.394 | 0.241 | 24.057 | 15.318 | 0.009 | 0.006 | 1.027 | 0.202 |
| 2012 | Silesian | 11.959 | 15.074 | 21.343 | 11.161 | 48.806 | 73.254 | 50.644 | 33.394 | 0.632 | 0.646 | 45.318 | 43.757 | 0.038 | 0.034 | 1.866 | 1.828 |
| | Pomeranian | 5.113 | 9.678 | 7.611 | 7.763 | 24.351 | 28.666 | 47.903 | 24.183 | 0.377 | 0.257 | 25.032 | 19.437 | 0.013 | 0.015 | 1.358 | 1.479 |
| 2011 | Silesian | 11.052 | 12.61 | 25.241 | 12.032 | 57.017 | 87.628 | 48.153 | 31.581 | 0.614 | 0.584 | 48.526 | 41.945 | 0.036 | 0.031 | 2.214 | 2.326 |
| | Pomeranian | 3.838 | 6.795 | 8.646 | 9.461 | 28.472 | 41.571 | 49.674 | 25.972 | 0.381 | 0.305 | 25.61 | 20.758 | 0.026 | 0.105 | 1.174 | 0.519 |
| 2010 | Silesian | 17.087 | 19.671 | 22.836 | 13.413 | 50.082 | 64.894 | 43.266 | 30.438 | 0.648 | 0.619 | 51.888 | 47.679 | 0.04 | 0.047 | 4.845 | 5.341 |
| | Pomeranian | 3.746 | 5.274 | 8.841 | 8.378 | 30.646 | 39.695 | 51.617 | 24.521 | 0.429 | 0.354 | 28.223 | 22.643 | 0.015 | 0.015 | 1.076 | 0.471 |
| 2009 | Silesian | 14.548 | 12.381 | 24.176 | 18.807 | 43.651 | 58.273 | 46.133 | 32.278 | 0.553 | 0.483 | 41.974 | 36.845 | 0.037 | 0.033 | 3.348 | 2.329 |
| | Pomeranian | 3.878 | 4.482 | 18.042 | 15.303 | 27.96 | 35.716 | 47.42 | 26.024 | 0.39 | 0.306 | 25.611 | 19.903 | 0.044 | 0.081 | 2.927 | 2.789 |
| 2008 | Silesian | 11.421 | 9.186 | 26.002 | 18.696 | 45.282 | 57.854 | 45.0 | 32.375 | 0.561 | 0.456 | 38.43 | 34.091 | n/d | n/d | n/d | n/d |
| | Pomeranian | 3.413 | 4.707 | 17.134 | 13.611 | 23.692 | 27.544 | 53.077 | 19.064 | 0.367 | 0.238 | 22.923 | 16.689 | 0.031 | 0.039 | 1.46 | 1.976 |
| 2007 | Silesian | 11.444 | 10.769 | 24.092 | 11.34 | 19.484 | 14.662 | 45.196 | 31.646 | 0.601 | 0.498 | 35.457 | 33.874 | n/d | n/d | n/d | n/d |
| | Pomeranian | 2.105 | 1.813 | 5.259 | 3.604 | 19.358 | 22.223 | 55.77 | 24.474 | 0.327 | 0.197 | 23.684 | 15.387 | 0.016 | 0.022 | n/d | n/d |
| 2006 | Silesian | 22.45 | 34.733 | 31.134 | 23.624 | 18.339 | 14.786 | 47.389 | 32.877 | 0.815 | 0.767 | 48.567 | 60.14 | n/d | n/d | n/d | n/d |
| | Pomeranian | 6.009 | 10.599 | 17.8 | 14.079 | 25.216 | 28.504 | 58.937 | 28.38 | 0.399 | 0.287 | 28.831 | 25.126 | n/d | n/d | n/d | n/d |
| 2005 | Silesian | 19.767 | 15.432 | 27.289 | 19.84 | 18.658 | 12.382 | 50.467 | 32.708 | 0.683 | 0.519 | 45.932 | 40.154 | n/d | n/d | n/d | n/d |
| | Pomeranian | 2.473 | 2.571 | 15.77 | 12.403 | 23.77 | 24.626 | 51.379 | 25.598 | 0.364 | 0.201 | 26.667 | 18.859 | n/d | n/d | n/d | n/d |
| 2004 | Silesian | 31.349 | 24.51 | 24.803 | 14.518 | 17.274 | 8.218 | 43.96 | 30.924 | 0.76 | 0.567 | 39.413 | 36.524 | 0.093 | 0.099 | n/d | n/d |
| | Pomeranian | 5.088 | 5.603 | 14.71 | 13.852 | 20.215 | 20.501 | 53.206 | 23.52 | 0.375 | 0.268 | 26.542 | 23.06 | n/d | n/d | n/d | n/d |
| Mean 2004–2013 | Silesian | 16.467 | 6.505 | 25.132 | 2.660 | 36.158 | 15.753 | 46.856 | 2.573 | 0.639 | 0.093 | 43.969 | 5.145 | 0.047 | 0.022 | 2.798 | 1.310 |
| | Pomeranian | 4.067 | 1.238 | 12.839 | 4.756 | 24.591 | 3.607 | 52.208 | 3.487 | 0.38 | 0.027 | 25.718 | 1.908 | 0.022 | 0.012 | 1.504 | 0.717 |
| t | | 3.8891 | | 7.1329 | | 2.2634 | | 3.9053 | | 8.4723 | | 10.5185 | | 2.5554 | | 2.0884 | |
| p-value | | <0.05* | | <0.05* | | <0.05* | | <0.05* | | <0.05* | | <0.05* | | <0.05* | | >0.05 | |

Avg. – average; SD – standard deviation; t – Student’s t-test result; * statistically significant; n/d – no data.

of MIH in the 2 voivodeships. The MIH was observed more than twice as often in children in the Silesian voivodeship (13.7%) than in the Pomeranian (6.4%). Furthermore, in children from the Silesian voivodeship, MIH was significantly more often diagnosed on PIs than in their counterparts from the Pomeranian voivodeship (4.9% compared to 3.2%). The results are presented in Table 3.

Distribution and prevalence of MIH depending on gender, age and year of birth

The MIH was diagnosed more often in boys than in girls (54.2% compared to 45.8%), but the gender difference was not statistically significant in either of the voivodeships; nor did the genders differ in terms of the presence of lesions on incisors. In the Pomeranian voivodeship, MIH was diagnosed more often in children aged 6 (14.53%) than in older children, which was statistically significant. In the Silesian voivodeship, there were no significant differences between the age groups. A comparison of the occurrence of MIH in children born in different years is shown

in Table 4. There was a gradual increase in the incidence of MIH in children born in later years, but none of the differences were statistically significant (Fig. 4).

Discussion

According to reports from the European Environment Agency (EEA),²³ air quality in many cities in Poland falls below European Union (EU) pollution standards. The reports also show differences in the intensity of pollution depending on the region of Poland, with higher concentrations of hazardous substances observed in the south of the country, including the Silesian voivodeship. As many as 3 cities in this voivodeship are in the top 10 European cities with the largest number of days per year in which the permissible concentration of 24-hour PM10 was exceeded. The problem of pollution increases significantly during the heating season. Adverse meteorological conditions (low rainfall or wind) in this area are also contributing factors. The components of air pollution analyzed in this study are those commonly used to assess air quality in EU countries.²³

Table 2, cont. Annual average air pollutants for both voivodeships

| Year | Voivodeship | Cd (PM10) [ng/m ³] | | Ni (PM10) [ng/m ³] | | C ₆ H ₆ [µg/m ³] | | BaP (PM10) [ng/m ³] | | BaA (PM10) [ng/m ³] | | BbF (PM10) [ng/m ³] | | BkF (PM10) [ng/m ³] | | BjF (PM10) [ng/m ³] | |
|----------------|-------------|--------------------------------|-------|--------------------------------|-------|--|-------|---------------------------------|--------|---------------------------------|--------|---------------------------------|--------|---------------------------------|-------|---------------------------------|--------|
| | | Avg. | SD | Avg. | SD | Avg. | SD | Avg. | SD | Avg. | SD | Avg. | SD | Avg. | SD | Avg. | SD |
| 2013 | Silesian | 1.171 | 1.32 | 2.54 | 3.399 | 2.006 | 1.961 | 6.77 | 7.074 | 5.376 | 5.682 | 4.97 | 4.494 | 2.542 | 2.332 | 4.25 | 3.873 |
| | Pomeranian | 0.249 | 0.165 | 2.293 | 2.308 | 0.658 | 0.951 | 2.589 | 3.956 | 2.101 | 3.573 | 2.82 | 3.92 | 1.126 | 1.553 | 0.728 | 1.177 |
| 2012 | Silesian | 0.976 | 1.319 | 1.619 | 1.276 | 2.444 | 3.287 | 8.314 | 11.692 | 8.911 | 14.527 | 7.748 | 10.643 | 4.136 | 6.065 | 5.224 | 7.422 |
| | Pomeranian | 0.421 | 0.609 | 6.146 | 8.847 | 0.689 | 1.159 | 3.038 | 5.194 | 2.799 | 7.164 | 2.263 | 3.563 | 0.848 | 1.313 | 3.218 | 8.36 |
| 2011 | Silesian | 1.351 | 1.448 | 1.775 | 1.414 | 2.047 | 3.02 | 8.908 | 11.069 | 7.012 | 7.972 | 7.763 | 7.515 | 3.849 | 3.779 | 4.746 | 4.485 |
| | Pomeranian | 0.45 | 0.523 | 5.429 | 5.581 | 0.782 | 1.175 | 2.75 | 4.999 | 2.45 | 4.94 | 1.929 | 3.3 | 0.801 | 1.606 | 6.513 | 13.764 |
| 2010 | Silesian | 1.183 | 1.274 | 2.583 | 2.756 | 1.867 | 3.225 | 9.272 | 11.121 | 10.289 | 12.84 | 9.168 | 10.283 | 3.995 | 4.088 | 5.104 | 5.121 |
| | Pomeranian | 0.446 | 0.492 | 4.194 | 4.342 | 0.684 | 1.272 | 4.683 | 6.91 | 8.885 | 14.144 | 3.856 | 5.121 | 2.63 | 3.655 | 13.285 | 18.491 |
| 2009 | Silesian | 1.246 | 0.882 | 5.436 | 7.108 | 1.894 | 2.547 | 8.685 | 10.812 | 8.024 | 12.003 | 8.476 | 11.466 | 3.775 | 4.383 | 7.545 | 8.954 |
| | Pomeranian | 0.74 | 0.774 | 3.628 | 5.248 | 1.762 | 2.19 | 3.111 | 3.893 | 3.035 | 3.599 | 2.006 | 2.315 | 1.594 | 1.579 | 5.032 | 5.902 |
| 2008 | Silesian | n/d | n/d | n/d | n/d | 2.31 | 3.141 | n/d | n/d | n/d | n/d | n/d | n/d | n/d | n/d | n/d | n/d |
| | Pomeranian | 0.703 | 0.755 | 3.397 | 5.081 | 1.401 | 1.625 | 2.152 | 3.179 | n/d | n/d | n/d | n/d | n/d | n/d | n/d | n/d |
| 2007 | Silesian | n/d | n/d | n/d | n/d | 2.918 | 3.838 | n/d | n/d | n/d | n/d | n/d | n/d | n/d | n/d | n/d | n/d |
| | Pomeranian | n/d | n/d | n/d | n/d | 2.402 | 1.652 | 0.925 | 1.574 | n/d | n/d | n/d | n/d | n/d | n/d | n/d | n/d |
| 2006 | Silesian | n/d | n/d | n/d | n/d | 2.679 | 4.951 | n/d | n/d | n/d | n/d | n/d | n/d | n/d | n/d | n/d | n/d |
| | Pomeranian | n/d | n/d | n/d | n/d | n/d | n/d | n/d | n/d | n/d | n/d | n/d | n/d | n/d | n/d | n/d | n/d |
| 2005 | Silesian | n/d | n/d | n/d | n/d | 3.572 | 4.004 | n/d | n/d | n/d | n/d | n/d | n/d | n/d | n/d | n/d | n/d |
| | Pomeranian | n/d | n/d | n/d | n/d | n/d | n/d | n/d | n/d | n/d | n/d | n/d | n/d | n/d | n/d | n/d | n/d |
| 2004 | Silesian | n/d | n/d | n/d | n/d | n/d | n/d | n/d | n/d | n/d | n/d | n/d | n/d | n/d | n/d | n/d | n/d |
| | Pomeranian | n/d | n/d | n/d | n/d | n/d | n/d | n/d | n/d | n/d | n/d | n/d | n/d | n/d | n/d | n/d | n/d |
| Mean 2004–2013 | Silesian | 1.185 | 0.137 | 2.791 | 1.542 | 2.373 | 0.587 | 8.390 | 0.970 | 7.922 | 1.864 | 7.625 | 1.596 | 3.659 | 0.640 | 5.373 | 1.271 |
| | Pomeranian | 0.502 | 0.186 | 4.181 | 1.407 | 1.197 | 0.683 | 2.750 | 1.130 | 3.854 | 2.835 | 2.575 | 0.797 | 1.4 | 0.756 | 5.755 | 4.730 |
| t | | 6.7955 | | 1.5637 | | 3.7051 | | 9.0107 | | 2.6814 | | 6.3307 | | 5.0995 | | 0.1741 | |
| p-value | | <0.05* | | >0.05 | | <0.05* | | <0.05* | | <0.05* | | <0.05* | | <0.05* | | >0.05 | |

Avg. – average; SD – standard deviation; t – Student's t-test result; * statistically significant; n/d – no data.

Table 3. Occurrence of MIH in Pomeranian and Silesian voivodeships

| Children | Voivodeship | | Total n (%) | χ ² | p-value |
|---|------------------|----------------|--------------|----------------|---------|
| | Pomeranian n (%) | Silesian n (%) | | | |
| With MIH diagnosis; FPM and PI affected | 88 (6.43) | 124 (13.69) | 212 (9.32) | | |
| Without MIH | 1281 (93.57) | 782 (86.31) | 2063 (90.68) | 33.99 | <0.001* |
| PI affected | 44 (3.21) | 44 (4.86) | 88 (3.87) | | |
| Non-PI affected | 1325 (96.79) | 862 (95.14) | 2187 (96.13) | 3.96 | 0.047* |
| Total | 1369 (100) | 906 (100) | 2275 (100) | – | – |

* statistically significant; FPM – first permanent molars; PI – permanent incisors; MIH – molar incisor hypomineralization.

This study has attempted to assess whether environmental air quality has an impact on the prevalence of MIH in a given population. It has been shown that in the Silesian voivodeship, where it can be objectively concluded that air quality is inferior, based on measurements of pollution levels and data published by the EEA, the prevalence of MIH was over twice as high as in the Pomeranian voivodeship. Particular differences pertained to the concentration of SO₂, the level of which in the south of Poland was 4 times higher than in the north. Concentrations about

twice as high were also observed for PM10 NO₂, lead and cadmium.

A study assessing the prevalence of MIH in children from 2 regions of Turkey that significantly differ in terms of industrialization showed no association between MIH prevalence and the levels of polychlorinated dibenzo-p-dioxins (PCDDs) and polychlorinated dibenzofurans (PCDFs) in the environment. The measurements of the concentration of the substances were carried out on the basis of soil samples in a given region.²⁴ However, other air-polluting

Table 4. Occurrence of MIH depending on the age of the respondents

| Region | Children | Age [years] | | | | | | | χ ² | p-value |
|------------|-------------|-------------|-------------|-------------|-------------|-------------|-------------|-------------|----------------|---------|
| | | 6 n (%) | 7 n (%) | 8 n (%) | 9 n (%) | 10 n (%) | 11 n (%) | 12 n (%) | | |
| Pomeranian | with MIH | 17 (14.53)* | 21 (7.95) | 21 (7.17) | 12 (5.58) | 5 (2.73) | 8 (5.33) | 3 (2.65) | 21.15* | 0.002* |
| | without MIH | 100 (85.47) | 243 (92.05) | 272 (92.83) | 203 (94.42) | 178 (97.27) | 142 (94.67) | 110 (97.35) | | |
| | total | 117 (100) | 264 (100) | 293 (100) | 215 (100) | 183 (100) | 150 (100) | 113 (100) | | |
| Silesia | with MIH | 4 (16) | 35 (19.13) | 28 (15.3) | 17 (9.77) | 22 (15.94) | 7 (8.33) | 8 (8.70) | 11.77 | 0.06 |
| | without MIH | 21 (84) | 148 (80.87) | 155 (84.70) | 157 (90.23) | 116 (84.06) | 77 (91.67) | 84 (91.30) | | |
| | total | 25 (100) | 183 (100) | 183 (100) | 174 (100) | 138 (100) | 84 (100) | 92 (100) | | |

* statistically significant; MIH – molar incisor hypomineralization.

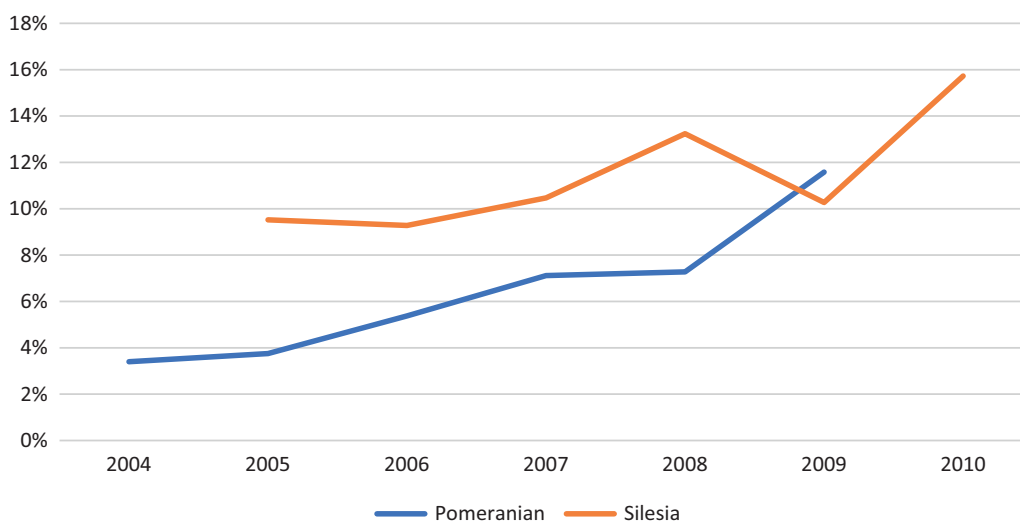


Fig. 4. The prevalence of MIH in various birth years in the Pomeranian and Silesian voivodeships

Pomeranian - (χ² (8, n = 1369) = 12.94; ni), p = 0.095; Silesia - (χ² (8, n = 906) = 10.47; ni), p = 0.202

substances were not taken into account, and given their negative impact on health, they can undoubtedly have an equally negative effect on tooth development. Apart from the worst effects of pollution described in the literature, such as premature mortality and shortened life expectancy,²⁵ air-polluting substances are also responsible for the occurrence of diseases considered in the etiology of MIH, such as otitis media and respiratory diseases, which in children are mainly manifested as irritations, acute infections and asthma attacks.^{26,27} Acute or chronic action of the air polluting substances depends on the time of exposure to a given factor and its concentration and accumulation in the human body. Undoubtedly, the negative impact of pollution on children, in both the prenatal and postnatal periods, is more dangerous and cannot be compared with the effects on adults. The lungs develop throughout childhood and their sensitivity to airborne contaminants at different stages of puberty can vary.²⁸ Even if air pollution is not directly responsible for the occurrence of MIH, it can act indirectly, leading to disease and therefore a need to take various medications. Recently, evidence of a relationship between prenatal exposure to air pollution and autism spectrum disorders and cognitive dysfunction has also been identified.²⁹

In our study, six-year-old children in the Pomeranian voivodeship displayed a significantly more frequent occurrence of MIH than did children from other age groups. Research in the Pomeranian voivodeship was carried out in 2016 and 2017, so six-year-old children were born in 2010 and 2011. Interestingly, in these years, the highest concentrations of NO₂ and CO in the Pomeranian voivodeship were recorded in the years being analyzed. However, the largest difference and clearly higher concentrations in these years were observed in the case of PAHs, mainly benzo(a)anthracene BaA (PM10) and benzo(j)fluoranthene BfF (PM10). The PAHs are organic compounds consisting of 2 or more fused benzene rings arranged in different configurations. The literature has highlighted their mutagenic and carcinogenic effects.³⁰ They are also thought to be detrimental to the nervous system, heart, brain vessels, and respiratory system.³¹ In addition, exposure during the prenatal period is harmful to the developing brain and may thus instigate cognitive dysfunction.³² The PAHs arise as a result of incomplete combustion of organic materials (e.g., coal, wood, oil), mainly related to anthropogenic activities but also from natural sources, such as open combustion or volcanic eruptions. Moreover, their presence in the environment leads to their presence in numerous types of food. Processed food

is considered to be their main source, because cooking processes and techniques such as baking, smoking or drying contribute to their formation. Their presence can be detected in dairy products, nuts, drinks, and meat products (mainly pork), among others.³³ The PAHs are highly soluble in fats, so they are easily absorbed from the digestive tract and mostly accumulate in adipose tissue.³⁰ Further research is certainly needed, but based on the results obtained in this study, a link between PAHs exposure during the prenatal period as well as during the first years of life cannot be excluded from the etiology of the occurrence of MIH.

Recently, bisphenol A and its analogs, used worldwide in plastic containers, have been mentioned among the potential etiological factors of enamel disorders.³⁴ Researchers who have found evidence of the presence of MIH in ancient populations are questioning the impact of modern factors such as antibiotics, bisphenol A or dioxin on the occurrence of MIH. These factors were not present in ancient times because they relate to industries that only appeared in the 20th century. Therefore, it has been suggested that MIH etiologies can be found among factors that have been present for centuries.³⁵ Still, many components of air pollution have existed since the emergence of human beings and the use of open fire. There is evidence of the presence of, for example, lead, soot and PAHs in ancient times.³⁶

The importance of air quality in the etiology of MIH can additionally be demonstrated by the difference in occurrence in different regions of the country. Problems during pregnancy, childhood diseases and other medical factors occur in children around the world, so MIH etiology should be researched comprehensively in specific local environmental conditions. In line with global trends, another study has found that the number of MIH cases is increasing.⁹


Given the difficulties associated with treatment, MIH is a challenge for both dentists and patients. It is important to establish the etiology of the disorder to discover possible interventions, highlight risk groups and prevent severe complications.⁵

Conclusions

The results of this study suggest the impact of air pollution on the higher incidence of MIH in a given population. Further research is necessary to determine the specific pollutant. Therefore, although our research points in a specific direction, further research in various regions of different countries is required to confirm these findings.

ORCID iDs

Natalia Głódkowska  <https://orcid.org/0000-0002-9876-6703>

Katarzyna Emerich  <https://orcid.org/0000-0003-3175-0931>

References

- Weerheijm KL, Jälevik B, Alaluusua S. Molar-incisor hypomineralisation. *Caries Res.* 2001;35(5):390–391. doi:10.1159/000047479
- Weerheijm KL. Molar incisor hypomineralization (MIH): Clinical presentation, etiology and management. *Dent Update.* 2004;31(1):9–12. doi:10.12968/denu.2004.31.1.9
- Leal SC, Oliveira TRM, Ribeiro APD. Do parents and children perceive molar-incisor hypomineralization as oral health problem? *Int J Paediatr Dent.* 2017;27(5):372–379. doi:10.1111/ipd.12271
- Silva M, Kilpatrick N, Crombie F, Ghanim A, Manton DJ. What's new in molar incisor hypomineralization? *Dent Update.* 2017;44(2):100–106. doi:10.12968/denu.2017.44.2.100
- Jälevik B, Klingberg G. Dental treatment, dental fear and behaviour management problems in children with severe enamel hypomineralization of their permanent first molars. *Int J Paediatr Dent.* 2002;12(1):24–32. doi:10.1046/j.0960-7439.2001.00318.x
- Albadri S, Zaitoun H, McDonnell ST, Davidson LE. Extraction of first permanent molar teeth: Results from three dental hospitals. *Br Dent J.* 2007;203(7):E14. doi:10.1038/bdj.2007.679
- Elfrink ME, Ghanim A, Manton DJ, Weerheijm KL. Standardised studies on molar incisor hypomineralisation (MIH) and hypomineralised second primary molars (HSPM): A need. *Eur Arch Paediatr Dent.* 2015; 16(3):247–255. doi:10.1007/s40368-015-0179-7
- Zhao D, Dong B, Yu D, Ren Q, Sun Y. The prevalence of molar incisor hypomineralization: Evidence from 70 studies. *Int J Paediatr Dent.* 2017;28(2):170–179. doi:10.1111/ipd.12323
- Schwendicke F, Elhennawy K, Reda S, Bekes K, Manton DJ, Krois J. Global burden of molar incisor hypomineralization. *J Dent.* 2018;68: 10–18. doi:10.1016/j.jdent.2017.12.002
- Crombie F, Manton D, Kilpatrick N. Aetiology of molar-incisor hypomineralization: A critical review. *Int J Paediatr Dent.* 2009;19(2):73–83. doi:10.1111/j.1365-263X.2008.00966.x
- Arrow P. Risk factors in the occurrence of enamel defects of the first permanent molars among schoolchildren in Western Australia. *Community Dent Oral Epidemiol.* 2009;37(5):405–415. doi:10.1111/j.1600-0528.2009.00480.x
- Garot E, Manton D, Rouas P. Peripartum events and molar-incisor hypomineralisation (MIH) amongst young patients in southwest France. *Eur Arch Paediatr Dent* 2016;17(4):245–250. doi: 10.1007/s40368-016-0235-y
- Ghanim A, Manton D, Bailey D, Mariño R, Morgan M. Risk factors in the occurrence of molar-incisor hypomineralization amongst a group of Iraqi children. *Int J Paediatr Dent.* 2013;23(3):197–206. doi:10.1111/j.1365-263X.2012.01244.x
- Serna C, Vicente A, Finke C, Ortiz AJ. Drugs related to the etiology of molar incisor hypomineralization: A systematic review. *J Am Dent Assoc.* 2016;147(2):120–130. doi:10.1016/j.adaj.2015.08.011
- Vieira A, Kup E. On the etiology of molar-incisor hypomineralization. *Caries Res.* 2016;50(2):166–169. doi:10.1159/000445128
- Jeremias F, Koruyucu M, Küchler EC, et al. Genes expressed in dental enamel development are associated with molar-incisor hypomineralization. *Arch Oral Biol* 2013;58(10):1434–1442. doi:10.1016/j.archoralbio.2013.05.005
- Alaluusua S. Aetiology of molar-incisor hypomineralisation: A systematic review. *Eur Arch Paediatr Dent.* 2010;11(2):53–58. doi:10.1007/BF03262713
- Alaluusua S, Calderara P, Gerthoux PM, et al. Developmental dental aberrations after the dioxin accident in Seveso. *Environ Health Perspect.* 2004;112(13):1313–1318. doi:10.1289/ehp.6920
- Fagrell TG, Ludvigsson J, Ullbro C, Lundin SA, Koch G. Aetiology of severe demarcated enamel opacities – an evaluation based on prospective medical and social data from 17,000 children. *Swed Dent J.* 2011;35(2):57–67.
- Laisi S, Kiviranta H, Lukinmaa PL, Vartiainen T, Alaluusua S. Molar-incisor-hypomineralisation and dioxins: New findings. *Eur Arch Paediatr Dent.* 2008;9(4):224–227. doi:10.1007/BF03262639
- Jan J, Sovcikova E, Kocan A, Wsolova L, Trnovec T. Developmental dental defects in children exposed to PCBs in eastern Slovakia. *Chemosphere.* 2007;67(9):S350–S354. doi:10.1016/j.chemosphere.2006.05.148

22. Weerheijm KL, Duggal M, Mejàre I, et al. Judgement criteria for molar incisor hypomineralisation (MIH) in epidemiologic studies: A summary of the European meeting on MIH held in Athens, 2003. *Eur J Paediatr Dent*. 2003;4(3):110–113.
23. European Environment Agency (EEA). *Air Quality in Europe – 2016 Report*. Copenhagen, Denmark: EEA; 2016. doi:10.2800/413142
24. Kuscu OO, Çağlar E, Aslan S, Durmusoglu E, Karademir A, Sandalli N. The prevalence of molar incisor hypomineralization (MIH) in a group of children in a highly polluted urban region and a windfarm-green energy island. *Int J Paediatr Dent*. 2000;19(3):176–185. doi:10.1111/j.1365-263X.2008.00945.x
25. Lelieveld J, Evans JS, Fnais M, Giannadaki D, Pozzer A. The contribution of outdoor air pollution sources to premature mortality on a global scale. *Nature*. 2015;525(7569):367–371. doi:10.1038/nature15371
26. Bowatte G, Tham R, Perret JL, et al. Air pollution and otitis media in children: A systematic review of literature. *Int J Environ Res Public Health*. 2018;15(2):e257. doi:10.3390/ijerph15020257
27. Kurt OK, Zhang J, Pinkerton KE. Pulmonary health effects of air pollution. *Curr Opin Pulm Med*. 2016;22(2):138–144. doi:10.1097/MCP.0000000000000248
28. Pinkerton KE, Joad JP. Influence of air pollution on respiratory health during perinatal development. *Clin Exp Pharmacol Physiol*. 2006;33(3):269–272. doi:10.1111/j.1440-1681.2006.04357.x
29. Oudin A, Frondelius K, Haglund N, et al. Prenatal exposure to air pollution as a potential risk factor for autism and ADHD. *Environ Int*. 2019;133(Pt A):105149. doi:10.1016/j.envint.2019.105149
30. Abdel-Shafy HI, Mansour MSM. A review on polycyclic aromatic hydrocarbons: Source, environmental impact, effect on human health and remediation. *Egyptian Journal of Petroleum*. 2016;25(1):107–123. doi:10.1016/j.ejpe.2015.03.011
31. Li X, Yang Y, Xu X, Xu C, Hong J. Air pollution from polycyclic aromatic hydrocarbons generated by human activities and their health effects in China. *Journal of Cleaner Production*. 2016;112(2):1360–1367. doi:10.1016/j.jclepro.2015.05.077
32. Jedrychowski WA, Perera FP, Camann D, et al. Prenatal exposure to polycyclic aromatic hydrocarbons and cognitive dysfunction in children. *Environ Sci Pollut Res Int*. 2015;22(5):3631–3639. doi:10.1007/s11356-014-3627-8
33. Singh L, Varshney JG, Agarwal T. Polycyclic aromatic hydrocarbons' formation and occurrence in processed food. *Food Chem*. 2016;199:768–781. doi:10.1016/j.foodchem.2015.12.074
34. Jedeon K, De la Dure-Molla M, Brookes SJ, et al. Enamel defects reflect perinatal exposure to bisphenol A. *Am J Pathol*. 2013;183(1):108–118. doi:10.1016/j.ajpath.2013.04.004
35. Garot E, Couture-Veschambre C, Manton D, Beauval C, Rouas P. Analytical evidence of enamel hypomineralisation on permanent and primary molars amongst past populations. *Sci Rep*. 2017;7(1):1712. doi:10.1038/s41598-017-01745-w
36. Borsos E, Makra L, Béczi R, Vitányi B, Szentpéteri M. Anthropogenic air pollution in the ancient times. *Acta Climatologica et Chorologica*. 2003;36-37:5–15.

Analysis of how obtaining melanocytes by magnetic cell separation contributes to autoepidermal transplantation technology in treating leucoderma

Xingyu Mei^{A-E}, Jie Huang^{B,E}, Yue Sun^B, Zhouwei Wu^B, Weimin Shi^F

Shanghai General Hospital, Shanghai Jiao Tong University School of Medicine, China

A – research concept and design; B – collection and/or assembly of data; C – data analysis and interpretation; D – writing the article; E – critical revision of the article; F – final approval of the article

Advances in Clinical and Experimental Medicine, ISSN 1899–5276 (print), ISSN 2451–2680 (online)

Adv Clin Exp Med. 2020;29(12):1479–1486

Address for correspondence

Weimin Shi
E-mail: shi128_1@tom.com

Funding sources

This study was funded by the National Natural Science Foundation of China (grant No. 81703140).

Conflict of interest

None declared

Received on August 8, 2018
Reviewed on August 27, 2018
Accepted on November 18, 2019

Cite as

Mei X, Huang J, Sun Y, Wu Z, Shi W. Analysis of how obtaining melanocytes by magnetic cell separation contributes to autoepidermal transplantation technology in treating leukoderma. *Adv Clin Exp Med.* 2020;29(12):1479–1486. doi:10.17219/acem/114339

DOI

10.17219/acem/114339

Copyright

© 2020 by Wrocław Medical University
This is an article distributed under the terms of the Creative Commons Attribution 3.0 Unported (CC BY 3.0) (<https://creativecommons.org/licenses/by/3.0/>)

Abstract

Background. Leucoderma, a depigmentation of the skin, is a common disease in humans, and has been observed in cattle, horses and buffalo as well.

Objectives. To analyze the correlation between melanin stem cells and the differentiation and proliferation of melanocytes (MCs).

Material and methods. Magnetic cell separation was used to separate melan-A+ cells and PAX3+ cells, which were cultured in vitro. The L-DOPA staining was used to observe cell morphology; Cell Counting Kit-8 (CCK8) was used to determine the cell proliferation rate; and flow cytometry (FCM) was used to determine cell cycle changes. The relative mRNA levels of melanocyte-inducing transcription factor (MITF), dopachrome tautomerase (DCT) and melan-A in cells were determined with reverse-transcription polymerase chain reaction (RT-PCR).

Results. The number of MC dendrites increased and extended continually during in vitro culture following magnetic cell separation. The proportion of positive L-DOPA staining cells increased from a baseline 40.70% to 82.03%, and the cell proliferation rate increased from 335.0% at D3 to 1577.4% at D20. The results of FCM showed that the cell proportion at the G1 stage in the D20 group was significantly lower than the D3 group; the cell proportion at the G2/M stage also decreased significantly. The expression of MITF and melan-A increased as the culture time increased, while the expression of DCT decreased.

Conclusions. The number of MC stem cells decreased and mature MCs increased gradually, indicating that MC stem cells can gradually differentiate into mature MCs during in vitro culture following magnetic cell separation.

Key words: MSCs, MCs, magnetic cell separation, leucoderma

Introduction

Leucoderma, a depigmentation of the skin, is a common disease in humans, and has been observed in cattle, horses and buffalo as well. Its main characteristic is the appearance of limited or extensive discoloration of areas of the skin, with distinct boundaries. Most of the patients are teenagers. Leucoderma affects nearly 2% of the world population.¹ The causes of leucoderma are complex and its pathogenesis can be divided into neurosexual theory, immunology theory, oxidation and reduction theory, transformation theory, among others.² The mechanisms causing melanocyte (MC) destruction or dysfunction are an important part of the pathogenesis of leucoderma. Leucoderma causing large areas of depigmentation that affect patients' appearance and quality of life is especially difficult to treat. The main treatments are external hormones, calcineurin inhibitors, photosensitizers, phototherapy, and surgical transplantation.³ Surgical transplantation includes epidermal transplantation and melanoma cell transplantation. Therefore, the cultivation of MCs is important in autologous epidermal transplantation technology.

Melanocytes are phenotypically prominent but histologically inconspicuous skin cells. They are responsible for the pigmentation of skin and hair, and thereby contribute to the appearance of the skin.⁴ Mutations of the function or number of MCs can lead to a series of refractory pigmentation diseases, such as leucoderma and chloasma. The surface dependent antigens of MCs have melanoma antigen recognized by T cells-1 (melan-A), melanocyte-inducing transcription factor (MITF), tyrosinase (TYR), and tyrosinase-related protein-2 (TRP-1).⁵ Melan-A is synthesized by the melanosomes and endoplasmic reticulum of MCs, and has been identified as a marker antigen for mature MCs.⁶ Research shows that the cultivation of MCs is difficult. As compared with the other main types of skin cells, the percentage of MCs in epidermis cells is low, as is mitotic activity, which leads to the rapid growth of other cells, such as keratinocytes (KCs) and fibroblasts (FBs).⁷ Reports have shown that MC stem cells (MSCs) can differentiate into mature MCs in leucoderma patients.⁸ Most MSCs stay in the resting stage and can turn into MCs when stimulated by the related cytokines, which induces the formation of melanin. Current research on the mechanisms of MCs and the proliferation and differentiation of MSCs is mainly based on mice, while research on human MCs and MSCs is rarer.⁹ At the same time, regarding the co-culture of MCs, few reports in the literature have discussed whether MSCs participate in the differentiation of MCs. Therefore, further study of MSCs on changes in pigment and the mechanisms and treatment of related diseases has major significance. Since foreskins contain a relatively high density of MCs,¹⁰ they are the main cell type for the cultivation of MCs.

In this study, the enzyme digestion method was used to isolate and obtain skin cells in normal human foreskin

tissue. Magnetic cell sorting (MACS) was used to isolate PAX3+ MSCs and mature melan-A+ MCs from primary hybrid cells. The L-DOPA staining was used to determine the cell proliferation rate, cell cycle and related specific markers.

Material and methods

Obtaining tissue to culture

Normal skin tissues were obtained from men aged 20–50 years who underwent circumcision in the Urinary Surgery Department of Shanghai First People's Hospital (China) between February 2017 and December 2017. All the participants signed informed consent forms. Patients with a chronic skin history, type 2 diabetes, cardiovascular disease (CVD), chronic gastritis, any history of leucoderma, hyperthyroidism, systemic lupus erythematosus, or other autoimmune-related diseases were excluded.

Tissue cell culture

The prepuce tissues were washed 3 times in 30 mL of phosphate-buffered saline (PBS). Then, they were cut into approx. 2 × 2 mm squares with sterile scissors, put in 40 mL of 0.05% trypsin-EDTA (8 mL of 0.25% trypsin-EDTA + 32 mL of PBS) and refrigerated overnight at 4°C to digest. Then, 40 mL of 0.05% collagenase was added to the digested tissues and stirred with a magnetic stirrer for 2 h to digest. Afterwards, the samples were filtered and centrifuged at 1800 rpm for 5 min. Cells were resuspended in 1% human melanocyte growth supplement-2 (HMGS-2) and 0.04 µg/mL of amikacin keratinocyte serum-free medium. Following this, 100 µL of the re-suspending solution was taken out and 25 µL of trypan blue was added to the mix for cell counting. Cell concentration was adjusted and inoculated to T75 culture flasks at a density of 1 × 10⁶ per flask, and then the cells were put in an incubator with 5% CO₂ at 37°C.

After 24 h, the primary cell culture dish was taken out of the incubator and washed with 15 mL of PBS. The cells were put back in the incubator with 5% CO₂ at 37°C and the cell morphology was observed regularly under an inverted microscope. A subculture was performed when cell growth density reached 60~70%.

Magnetic beads

Twenty microliters of magnetic beads marked with biotin, 20 µL of PAX-3 antibody marked with biotin and 20 µL of melan-A antibody marked with biotin were refrigerated overnight at 4°C. The previously separated skin-cell mixes were taken out of the incubator and pancreatin was added until the cells became round under the microscope. The cell solution was transferred to a 15 mL centrifuge

tube and centrifuged at 1000 rpm for 10 min. Five hundred microliters of PBS was used to suspend cells, and biotin magnetic bead with PAX-3 and melan-A antibody was added to the cells for 90 min. Cells were obtained by centrifugation and put in the MS separation column (Miltenyi Biotec Technology & Trading; Shanghai, China). Magnetic bead-marked cells were obtained and cryopreserved at -80°C .

Hematoxylin staining

A histological evaluation was performed after 3 weeks. The hydrogels were fixed overnight in 4% paraformaldehyde at 4°C and transferred to 70% ethanol until embedded in paraffin according to standard histological techniques. Sections were stained with hematoxylin and eosin (H&E) for general cell morphology and using the von Kossa method to characterize the mineralization.

L-DOPA staining

Cells adhering to the wall were washed in PBS, and 4% triformol was added for fixation at room temperature for 10 min. After washing 3 times with PBS, 10 mL of 0.1M phosphate buffer (PB) was added and the cells soaked for 10 min. The supernatant was discarded, 0.1% L-DOPA was added and the cells were put in an electric heat blower drier to stain for 4 h. Four fields were selected under a microscope, and the number of cells in each field was calculated.

Cell proliferation

Cell growth was analyzed using a WST-8 Cell Counting Kit-8 (CCK-8; Beyotime, Nanking, China). Cells (7.5×10^3) suspended in 100 μL of RPMI 1640 medium containing 10% fetal bovine serum (FBS) were seeded in 96-well plates and incubated for 2 days. The CCK-8 solution (10 μL) was added to each well and the cultures were incubated at 37°C for 90 min. Absorbance at 450 nm was measured using an immunoreader C10066-50 (Hamamatsu Photonics; Hamamatsu, Japan). The results were plotted as means \pm standard deviation (SD) of 3 separate tests, with 4 measurements per test for each of the experimental conditions.

Cell cycle

Cell cycle distribution was analyzed using flow cytometry (FCM). After the treatments outlined above, the cells were trypsinized, rinsed with PBS, fixed with 70% ethanol at 4°C overnight, and then treated with RNaseA (0.02 mg/mL) in the dark at room temperature for 30 min. The cells were resuspended in 0.05 mg/mL propidium iodide and analyzed with a flow cytometer (Becton, Dickinson, Franklin Lakes, USA). DNA histograms were analyzed using ModFit

LT v. 2.0 software (Verity Software House, Topsham, USA). For each sample, at least 104 events were recorded.

Tyrosinase activity determination

Cultured cells that had undergone magnetic cell separation were inoculated on 96-well plates with 1×10^5 cells/well and incubated with 5% CO_2 at 37°C for cultivation. After 24 h, the supernatant was discarded and the precipitate was washed twice with PBS. To each well, 500 μL of culture medium was added; after magnetic bead separation, D3 cells were taken as the control. Next, 160 μL of 10g/L Triton X-100 (pH 7.5) was added to each well, and the culture plate was put in -80°C refrigerator for 30 min. Then, the cells were split at 37°C for 4 h with 100 μL of 0.1% L-DOPA solution added to each well. After 4 h, the absorbance value in each well was determined. Tyrosinase relative activity was calculated as „(eq. 1):

$$\text{tyrosinase relative activity} = \frac{(\text{average absorbance of the experimental group} - \text{average absorbance of the blank group})}{(\text{average absorbance of the control group} - \text{average absorbance of the blank group})}$$

RNA isolation and quantitative RT-PCR

Based on the manufacturer's instructions, we extracted total mRNA from the retinal samples using TRIzol Reagent (Life Technologies, Grand Island, USA). A pipette was used mix the samples and then transfer them to 1.5 mL Eppendorf (EP) tubes, and the samples were kept standing for 5 min to separate the nucleic acid protein complex. To each EP tube, 1 mL of Trizol and 200 μL of pre-cooled chloroform was added. The tubes were shaken for 15 s and centrifuged at 4°C , 12,000 rpm, for 15 min. We drew the aqueous phase into fresh 1.5 mL EP tubes and added 0.5 mL of isopropanol. The mixture was centrifuged at 4°C , 12,000 rpm, for 15 min. After removing the supernatant, 1 mL of pre-cooled 75% ethanol was added to wash the RNA precipitate; this procedure was repeated 3 times. Then, the RNA precipitate was dried in a vacuum and its concentration was determined with a NanoDrop 1000 spectrophotometer (NanoDrop Technologies, Wilmington, USA). One microliter of Ologo dT (0.5 $\mu\text{g}/\mu\text{L}$), 2 μg of total RNA and 12 μL of diethylpyrocarbonate (DEPC) were added to polymerase chain reaction (PCR) tubes. After being mixed evenly, the tubes were placed in a 65°C water bath for 5 min, and then immediately placed on ice. Reverse transcription was performed at 55°C for 30 min, with initial activation for 15 min at 95°C ; next, 40 cycles of denaturation were conducted at 94°C for 15 s, then annealing for 30 s at 55°C and extension for 30 s at 72°C were performed. The expression level was normalized using U6 small nuclear RNA using the $2^{-\Delta\text{Ct}}$ method. The ΔCt values were normalized to GAPDH level.

Statistical analysis

The statistical analyses were performed using SPSS software v. 20.0 (SPSS Inc., Chicago, USA). All the data was expressed as means \pm SD. Student's t-test or a one-way analysis of variance (ANOVA) test was performed to determine significant differences. $P < 0.05$ was considered statistically significant.

Results

Cell morphology

Cell morphology was observed before and after magnetic cell separation; the results are shown in Fig. 1. As can be

seen, after digested separated skin cells were inoculated for 24 h, some cells stuck to the wall; the cells were round, triangular or oval; and a lot of floating cells could be seen. After 3 days, the cells gradually formed into small colonies (Fig. 1A). After magnetic bead separation, melan-A+ and PAX3+ cells comprise 10.26% of the total. After separation for 24 h, some cells adhered to the wall, and most of them grew in bipolar or multi-stage dendrites. Most of the MC cells had 2 or 3 dendrites and no obvious KCs were observed (Fig. 1B). Before the 1st transmission, multiple dendritic cells could be seen but they grew slowly. Melanocytes also grew slowly. However, multi-stage dendritic processes and slender axons were obvious and there were no obvious KCs. After a few generations, MCs grew fast and multi-stage dendritic growth appeared with 3 to 4 dendrites, and no obvious KC growth was seen (Fig. 1C). After the 2nd transmission, the lens is covered with dendritic cells, the slender axis is prominent and no obvious KC growth was seen (Fig. 1D). In conclusion, the number of MCs increased as the incubation time increased, reaching a maximum on the 20th day of culture.

Absolute cell count and morphology after magnetic bead separation

The number of mixed cells in the primary skin was approx. 2.0×10^7 . After separation, the number of PAX3+ and melan-A+ cell was about 1.9×10^6 . Cell passage cultivation was carried out on the 3rd day after magnetic bead separation and the number of cells was 2.5×10^6 (Fig. 2A). The cells were inoculated into T75 culture flasks at the density of $1 \times 10^6/T75 \times 2$ bottles in vitro and cell morphology was observed under a microscope. As can be seen, the MC cells were lightly dyed, had a bipolar or tripolar form, and part of the extension was dendritic (Fig. 2B). Cell passage cultivation was carried out on the 10th day after magnetic bead separation and the number of cells was 5.8×10^6 . A large number of L-DOPA-stained positive cells were observed under a microscope. The cell bodies were larger than before, the dendrites were obvious and the length varied (Fig. 2C). Cell passage cultivation was carried out on the 20th day

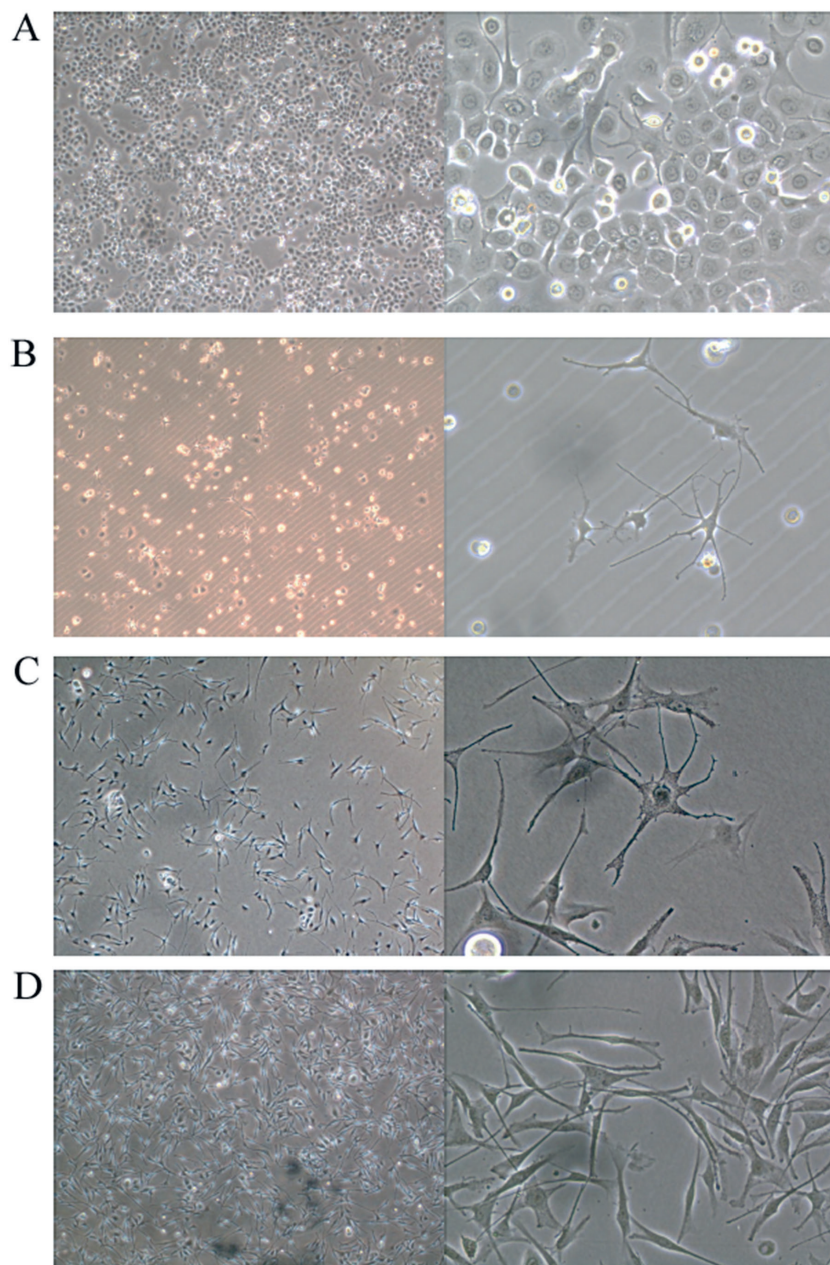


Fig. 1. Cell growth situation before and after magnetic cell separation

A. Digested isolated skin cell growth after adherence to the wall of the culture flask for 3 days. Melan-A+ and PAX3+ cell growth after magnetic cell separation for (B) 1 day, (C) 10 days and (D) 20 days

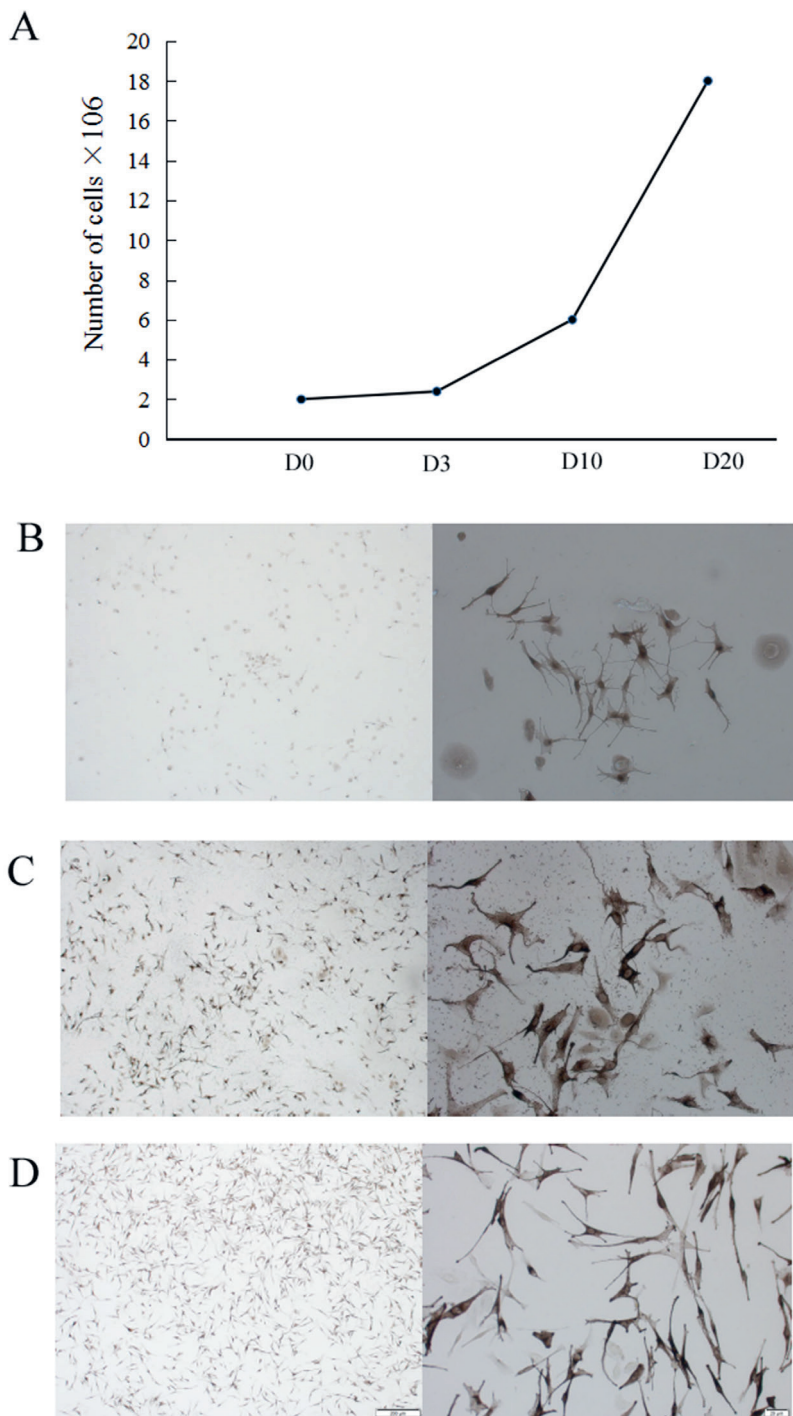


Fig. 2. The counts and morphology of melan-A+ and PAX3+ cells after magnetic cell separation

A – absolute cell counts at different times after magnetic cell separation. L-DOPA staining of melan-A+ and PAX3+ cells observed under a microscope after magnetic cell separation for (B) 1 day, (C) 10 days and (D) 20 days

separation, the optical density (OD) value was 0.316 ± 0.002 ; it was 0.469 ± 0.012 on the 3rd day; 0.723 ± 0.008 on the 5th day; and 1.222 ± 0.009 on the 7th day. This indicated that the proliferative capacity of the cells increased with time after magnetic bead separation.

Flow cytometry was used to determine the proportion of cells in the cell cycle stages at different times, and results are shown in Fig. 3B. On day 3, the ratio of cells at the G1 stage was 71.30 ± 0.27 ; the ratio at the S stage was 12.81 ± 0.40 ; and at the G2/M stage the ratio was 15.9 ± 0.13 . On day 10, the ratio of cells at the G1 stage was 68.19 ± 0.80 ; the ratio at the S stage was 20.88 ± 0.75 ; and at the G2/M stage it was 10.93 ± 0.11 . On day 20, the ratio of cells at the G1 stage was 63.83 ± 0.20 ; the ratio S stage was 29.83 ± 0.41 ; and the ratio at the G2/M stage was 6.27 ± 0.30 . Compared with the control (day 3), the G2/M phase of cells was significantly decreased after magnetic bead separation, the percentage of cells at the S stage increased and the percentage of cells at the G1 stage decreased slightly.

Changes in tyrosinase activity

Tyrosinase activity in cells was determined at different times after magnetic cell separation, and the results are shown in Fig. 4. As shown, the OD value after separation for 3 days was 0.295 ± 0.008 ; on the 10th day the value was 0.486 ± 0.007 ; and on the 20th day it was 1.038 ± 0.002 . The ratio of tyrosinase activity (D10) to tyrosinase activity (D3) was 2.0, and the ratio of tyrosinase activity (D20) to tyrosinase activity (D3) was 4.91.

after magnetic bead separation and the number of cells was 1.83×10^7 . Under a microscope, a large number of heavily dyed MCs were observed; the dendrites were obvious and fully extended (Fig. 2D).

Changes in cell proliferation and the cell cycle

A CCK-8 assay was used to determine the cell proliferation rate at different times; the results are shown in Fig. 3A. As can be seen, after 1 day of magnetic bead

MITF, DCT and melan-A expression

The MITF is the main regulator of melanogenesis and a key regulatory enzyme in the biosynthesis of melanin, while DCT can be regarded as a specific MSC surface antigen, but it can also be expressed in MCs. Melan-A is a major protein involved in the formation and maturation of melanosomes, and is a specific antigen on the surface of MCs. We determined the mRNA levels of MITF, DCT and melan-A at different times after magnetic cell separation using reverse-transcription PCR (RT-PCR); the results are shown

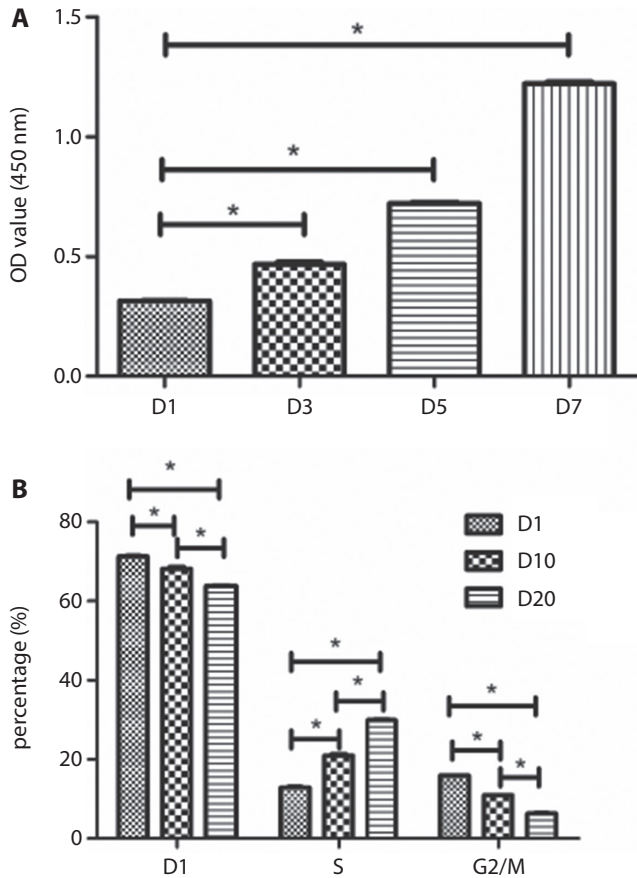


Fig. 3. Changes in melan-A+/PAX3+ cell proliferation and cell cycle after magnetic cell separation

A. Cell proliferation at different times after magnetic cell separation using CCK-8; B. Cell cycle variations at different times after magnetic cell separation using FCM; * p < 0.05; ** p < 0.01.

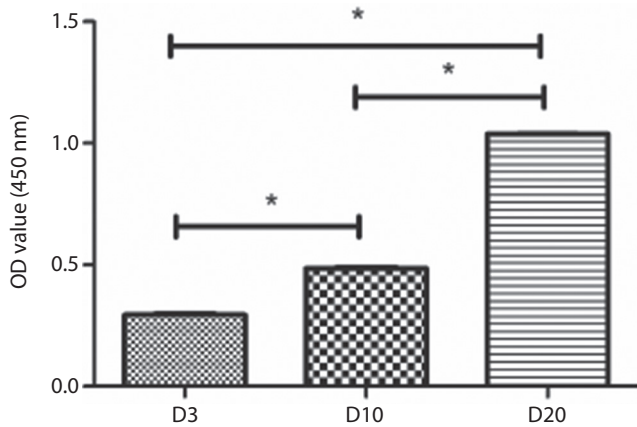


Fig. 4. Tyrosinase activity in cells at different times after magnetic cell separation by L-DOPA staining method

* p < 0.05; ** p < 0.01.

in Fig. 5. As can be seen, the relative level of MITF and melan-A increased significantly over time, while the relative level of DCT decreased significantly (p < 0.05). This indicated that the expression of MITF and melan-A is positively correlated with the number of days, while the expression of DCT is negatively correlated with the number of days.

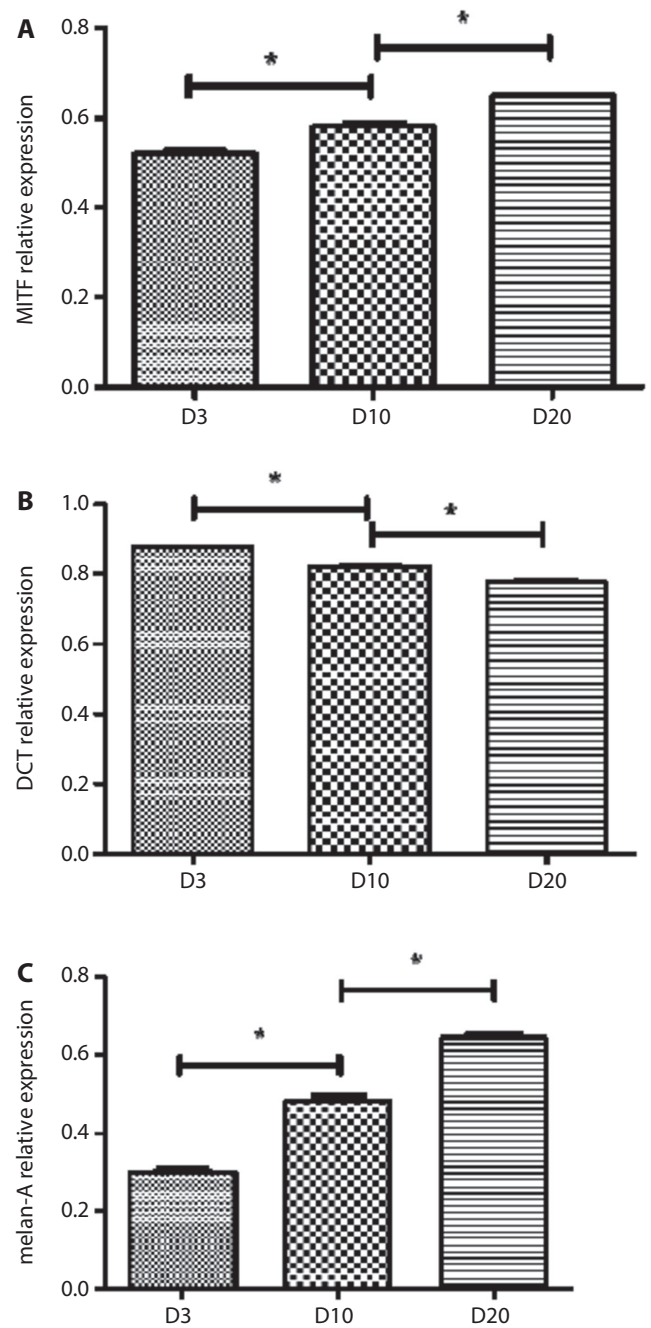


Fig. 5. The relative mRNA levels of (A) MITF, (B) DCT and (C) melan-A+ in cells cultured in vitro and magnetic cell separation for 3, 10 and 20 days

* p < 0.05; ** p < 0.01.

Discussion

At present, in vitro culture of MCs has been widely used in the experimental and clinical research of various tryptophan diseases, such as leucoderma and chloasma. Melanocytes, the main group of cells in the skin and hair coloring of vertebrates, are present in the epidermal basal layer and a small part of the hair follicle. The mammalian follicle contains a variety of cell lines and has great potential for development. Active melanin stem cells differentiate into hair follicles melanocyte (hf-mc) precursors, which

are then generated by mature hf-mcs, whose main function is to synthesize melanin. The technique of culturing hf-mcs in vitro has opened up new research pathways and solutions for the treatment of pigmentary diseases. Melanocytes cultured in vitro can also be used to study the etiology and pathology of malignant melanoma, and to examine the efficacy and toxicity of drugs that remove pigmentation. The regulation of pigmentation involves the development, heterogeneity, regeneration, and aging of MCs and their precursors. Some studies have reported that immature MCs and MSCs could be activated to differentiate into mature MCs in leucoderma patients.¹¹ Therefore, we believe that MSCs are involved in the differentiation and proliferation of MCs, and have therapeutic value for pigmentation disorders, trauma and melanoma.

Melanocyte surface antigens include melan-A, MITF, TYR, DCT, and others.^{12,13} Melan-A is one of the most important MC markers and can be expressed in melanosome and the endoplasmic reticulum of MCs. It also participates in the formation and maturation of melanosome, which as a lysosomal organelle can synthesize, store and transport melanin. Melan-A can combine with the major structural protein Pmel17 of melanosome to form a complex to participate in the transport and processing of melanosome.¹⁴ Melan-A can be expressed in mature MCs, but not on the surface of MSCs. Therefore, in this study, melan-A was selected as a marker antigen of mature MCs for MC screening in mixed cells. The MITF is a key transcription factor that encodes MC development. It plays an important role in the various processes of MC development, including neural crest differentiation, melanoblast growth and terminal MC differentiation.¹⁵ The *DCT*, also named *TRP-2*, is a mouse gene. The carboxyl terminal and membrane domain of DCT play a key role in the formation of melanosome. The DCT can form into a tyrosinase complex with TYR and TRP-1. DCT and TRP-1 mutations can induce pigment changes rather than depigmentation. Therefore, DCT and TRP-1 play a modifying role in melanogenesis. The DCT can be expressed not only in embryonic MCs, but also in mature MCs. The surface of MSCs lacks MC surface-related antigens such as TYR, MITF, melan-a, SOX10, KIT, and others, and only expresses PAX3 and DCT.^{16,17} PAX3 is an important transcription factor in the neuroectoderm of embryo development and is first expressed in anterior neural crest cells during the embryonic period.¹⁸ The pairing domain and homologous domain of PAX3 can promote the binding of PAX3 to DNA by recognizing the common sequences of DNA, which activates the transcription of target genes.¹⁹ In the embryonic stage, PAX3 can inhibit cell apoptosis by targeting p53 to make sure the cells are fully developed.²⁰ It can promote the migration of MCs from neural crest cells and promote the migration of MSCs from hair follicles to dermal papillae.²¹ Therefore, in this study, PAX3 was used as a marker to analyze and detect MSCs.

In this study, melan-A⁺ and PAX3⁺ MSCs were isolated from mixed cells digested from skin and cultured in vitro

to establish MC and MSC in vitro culture models. The key to culturing MCs is the selection of culture conditions and preparation of the culture medium, since the growth of MCs is negligible under standard cell culture conditions. In this experiment, we used a medium containing HMGS-2 and endothelin (ET), without 12-O-tetradecanoylphorbol-13-acetate (TPA) or cholera toxin (CT). HMGS-2 can reduce the possibility of cell mutagenesis, and is usually used to culture neonatal MCs or MSCs,²² increasing the availability of cultured cells for clinical use. At different stages of the culture process, we observed that dendrites of separated MCs constantly increased over time and no obvious KCs or other cell growth was observed. This means that magnetic cell separation can separate MCs from other cells in mixed skin cells and maintain MC characteristics during the culture process. However, during the culture stage, we found that some cells with large amounts of cytoplasm had no obvious dendrites. To verify whether these cells are PAX3⁺ MSC cells and whether they participate in the differentiation and maturation of MCs, we performed L-DOPA staining on the cells at different stages of the culture, counted the L-DOPA-positive cells and calculated their proportion in the cultured cells. The L-DOPA staining is a classic method for identifying active MCs and positive staining indicates the existence of active tyrosinase in melanosomes.²³ Both MSCs and differentiated MCs lack functional tyrosinase and cannot produce melanin; only mature MCs produce melanin.²⁴ Therefore, as primitive cells unable to synthesize melanin particles, L-DOPA staining of MSCs should be negative, while the L-DOPA staining of MCs with active tyrosinase is positive. Our results showed that the number of positive L-DOPA stained PAX3⁺ and melan-A⁺ cells increased, and most cells gradually differentiated into mature MCs. This provides a cellular biological model for further study of the process and mechanism of human MC differentiation and maturation.

In order to further study cell growth after magnetic cell separation, a proliferation curve was plotted using CCK-8 and the cell cycle was studied with FCM. The results of CCK-8 showed that the number of cells increased as the duration of the culture increased. The results of FCM showed that after magnetic cell separation, the cells in G1 phase decreased with the extension of the culture time, indicating that cells in the static phase decreased and MSCs develop into mature MCs. Cells in S phase increased and cells in the G2/M phase decreased, which indicates that the DNA replication period is prolonged and MC proliferation is active. Therefore, we inferred that cell proliferation capacity increased; the cells in the stationary phase gradually reduced; and cells in the inactive phase gradually increased after in vitro culturing and magnetic cell separation.

In order to study the biological function of cells after separation, we examined the tyrosinase activity and gene expression of the cells. Tyrosinase, as a key enzyme in melanin metabolism, mainly exists in mature MCs and cannot be detected in MSCs.²⁵ Our study showed that tyrosinase

activity increased with the duration of the culture, which indicated that the ability to secrete melanin was significantly improved and the content of melanin in MCs increased. Both MSCs and differentiated MCs lack functional tyrosinase and could not produce melanin; only mature MCs can produce melanin. The MITF is the main regulator of melanogenesis and the key regulator of melanin biosynthesis. The DCT can be used as a specific surface antigen of MSCs and can also be expressed in MCs. Melan-A is a major protein involved in the formation and maturation of melanosomes, and a specific surface antigen of MCs. Therefore, we mainly studied the relative mRNA levels of MITF, DCT and melan-A in cells cultured in vitro after magnetic cell separation. Our study showed that the relative expression levels of MITF and melan-A in cells increased with culture time, while the relative mRNA levels of DCT decreased over time. Therefore, we believe that after magnetic bead separation, the cells have the characteristics of MSCs and MCs, and that MSCs constantly differentiate into mature MCs.

ORCID iDs

Weimin Shi  <https://orcid.org/0000-0003-2305-3503>
 Xingyu Mei  <https://orcid.org/0000-0003-1515-6916>
 Jie Huang  <https://orcid.org/0000-0002-2981-2403>
 Yue Sun  <https://orcid.org/0000-0002-6638-5850>
 Zhouwei Wu  <https://orcid.org/0000-0002-7247-1560>

References

- Basha, K, Anjaneyulu E, Gopi Krishna S, Niaz Parveen DD, Gudivada S. Plants used in the treatment of leucoderma by the tribals of Yerramalai Forest of Kurnool District, Andhra Pradesh, India. *Journal of Ethnobiology and Traditional Medicine*. 2014;121:761–766.
- Szczurko O, Boon HS. A systematic review of natural health product treatment for vitiligo. *BMC Dermatol*. 2008;8:2.
- Usha SS, Narain A. Traditional treatment of leucoderma by Kol tribes of Vindhyan region of Uttar Pradesh. *Indian Journal of Traditional Knowledge*. 2010;9(1):173–174.
- Ali SA, Naaz I. Biochemical aspects of mammalian melanocytes and the emerging role of melanocyte stem cells in dermatological therapies. *Int J Health Sci (Qassim)*. 2018;12(1):69–76.
- Imokawa G. Autocrine and paracrine regulation of melanocytes in human skin and in pigmentary disorders. *Pigment Cell Res*. 2004;17(2):96–110.
- Moussa R. Immunohistochemical expression of melan-A in canine melanocytic tumors. *Bulletin of the University of Agricultural Sciences & Veterinary Medicine Cluj-Napoca*. 2011;68(1):260–267.
- Sandu C, Dumas M, Malan A, et al. Human skin keratinocytes, melanocytes, and fibroblasts contain distinct circadian clock machineries. *Cell Mol Life Sci*. 2012;69(19):3329–3339.
- Birlea SA, Costin GE, Roop DR, Norris DA. Trends in Regenerative Medicine: Repigmentation in Vitiligo Through Melanocyte Stem Cell Mobilization. *Med Res Rev*. 2017;37(4):907–935. doi:10.1002/med.21426
- Hoerter JD, Bradley P, Casillas A, et al. Extrafollicular dermal melanocyte stem cells and melanoma. *Stem Cells Int*. 2012;2012:407079.
- Sextius P, Betts R, Benkhalifa I, et al. Polygonum multiflorum Radix extract protects human foreskin melanocytes from oxidative stress in vitro and potentiates hair follicle pigmentation ex vivo. *Int J Cosmet Sci*. 2017;39(4):419–425.
- Nishimura EK. Melanocyte stem cells: A melanocyte reservoir in hair follicles for hair and skin pigmentation. *Pigment Cell Melanoma Res*. 2011;24(3):401–410.
- Zhang P, Liu W, Yuan X, Li D, Gu W, Gao T. Endothelin-1 enhances the melanogenesis via MITF-GPNMB pathway. *BMB Rep*. 2013;46(7):364–369.
- Hwang JA, Park NH, Na YN, et al. Coumestrol downregulates melanin production in melan-a murine melanocytes through degradation of tyrosinase. *Biol Pharm Bull*. 2017;40(4):535–539.
- Hoashi T, Tamaki K, Hearing VJ. The secreted form of a melanocyte membrane-bound glycoprotein (Pmel17/gp100) is released by ectodomain shedding. *FASEB J*. 2010;24(3):916–930.
- Seberg HE, Van OE, Cornell RA. Beyond MITF: Multiple transcription factors directly regulate the cellular phenotype in melanocytes and melanoma. *Pigment Cell Melanoma Res*. 2017;30(5):454–466.
- Garbuzov A, Pech MF, Hasegawa K, et al. Purification of GFRα1+ and GFRα1- spermatogonial stem cells reveals a niche-dependent mechanism for fate determination. *Stem Cell Rep*. 2018;10(2):553–567.
- Negro S, Imsland F, Valera M, Molina A, Solé M, Andersson L. Association analysis of KIT, MITF, and PAX3 variants with white markings in Spanish horses. *Anim Genet*. 2017;48(3):349–352.
- Xiao J, Li Q, Qu P, et al. Isolation of bovine skin-derived precursor cells and their developmental potential after nuclear transfer. *Cellular Reprogram*. 2016;18(6):411–418.
- Moore S, Ribes V, Terriente V, Wilkinson D, Relaix F, Briscoe J. Distinct regulatory mechanisms act to establish and maintain Pax3 expression in the developing neural tube. *PLoS Genet*. 2013;9(10):e1003811.
- Wang L, Lin S, Yi D, et al. Apoptosis, expression of PAX3 and P53, and caspase signal in fetuses with neural tube defects. *Birth Defects Res*. 2017;109(19):1596–1604.
- Choi H, Jin SH, Han MH, et al. Human melanocytes form a PAX3-expressing melanocyte cluster on Matrigel by the cell migration process. *J Dermatol Sci*. 2014;76(1):60–66.
- Hirobe T. Endothelins are involved in regulating the proliferation and differentiation of mouse epidermal melanocytes in serum-free primary culture. *J Invest Dermatol Symp Proc*. 2001;6(1):25–31.
- Muñoz-Muñoz JL, Acosta-Motosa JR, Garcia-Molina F, et al. Tyrosinase inactivation in its action on dopa. *Biochim Biophys Acta Proteins Proteom*. 2010;1804(7):1467–1475.
- Tang J, Cheng B, Jing L. Primary culture of human face skin melanocytes for the study of hyperpigmentation. *Cytotechnology*. 2014;66(6):891–898.
- Şohretoglu D, Sari S, Barut B, Ozel A. Tyrosinase inhibition by some flavonoids: Inhibitory activity, mechanism by in vitro and in silico studies. *Bioorg Chem*. 2018;15(81):168–174.

Foreskin healing after distal hypospadias repair: Does stenting affect the outcome?

Ireneusz Honkisz^{1,A–D,F}, Janusz Sulisławski^{1,B,E,F}, Barbara Dobrowolska-Glazar^{1,B,E,F},
Caroline F. Kuijper^{2,A,E,F}, Rafał Chrzan^{1,A,B,E,F}

¹ Department of Pediatric Urology, Jagiellonian University Medical College, Kraków, Poland

² Department of Pediatric Urology, Amsterdam University Medical Center, Amsterdam, the Netherlands

A – research concept and design; B – collection and/or assembly of data; C – data analysis and interpretation;
D – writing the article; E – critical revision of the article; F – final approval of the article

Advances in Clinical and Experimental Medicine, ISSN 1899–5276 (print), ISSN 2451–2680 (online)

Adv Clin Exp Med. 2020;29(12):1487–1490

Address for correspondence

Rafał Chrzan

E-mail: rafal.chrzan@uj.edu.pl

Funding sources

None declared

Conflict of interest

None declared

Acknowledgements

We are grateful to Prof. Tom P.V.M. de Jong for his continuous stimulation and the critical feedback that helped improve the outcomes; to Mr. Mirosław Witkowski for the statistical support; and to Dr. M. Wolnicki who operated on some cases.

Received on May 23, 2020

Reviewed on June 7, 2020

Accepted on September 20, 2020

Cite as

Honkisz I, Sulisławski J, Dobrowolska-Glazar B, Kuijper CF, Chrzan R. Foreskin healing after distal hypospadias repair: Does stenting affect the outcome? *Adv Clin Exp Med.* 2020;29(12):1487–1490. doi:10.17219/acem/127677

DOI

10.17219/acem/127677

Copyright

© 2020 by Wrocław Medical University

This is an article distributed under the terms of the Creative Commons Attribution 3.0 Unported (CC BY 3.0) (<https://creativecommons.org/licenses/by/3.0/>)

Abstract

Background. Distal penile hypospadias account for about 70% of all cases of hypospadias. There is a variety of operative techniques that could be performed when foreskin reconstruction is an option. The urethral stent is left in the urethra to prevent complications.

Objectives. To determine whether the duration of stenting influences the healing of foreskin after distal hypospadias repair.

Material and methods. Data from 2 institutions was retrospectively analyzed. Inclusion criteria were as follows: 1) a modified meatal advancement glanuloplasty without tubularization of the urethral plate, 2) foreskin reconstruction and 3) follow-up – 12 months. All other types of reconstruction and re-do procedures were excluded. The period of urethral stenting was determined intraoperatively depending on the surgeon's preferences. Mean age at operation was 23.3 months. The cohort was divided into 3 groups. In Group I (G-I), no catheter was left or it was removed the next day after surgery. In Group II, the catheter was left for more than 5 days. In those 2 groups, the surgery was done by different surgeons. Group III consisted of 35 patients who had a stent for <2 days, and the procedure was performed by the same surgeon. The χ^2 with Yates's correction and Pearson's χ^2 tests were used for the statistical analysis.

Results. Overall, 11 patients had foreskin dehiscence and needed re-do surgery. None of the patients required operation because of foreskin stenosis. Complications occurred in 3 out of 33 patients (9%) in Group I, 2 out of 27 in Group II (7.4%) and 6 out of 35 in Group III (17%). There was no statistically significant difference between Groups I and II ($p = 0.8144$), nor between Groups I and III ($p = 0.5344$). In the non-parametric Pearson's χ^2 test, no significant difference was found in such grouped data ($p = 0.4239$).

Conclusions. Prolonged urethral stenting does not reduce the risk of a re-do foreskin surgery after hypospadias repair.

Key words: complication, hypospadias, foreskin, preputioplasty, stenting

Introduction

The meatal advancement and glanuloplasty procedure (MAGPI) and its modifications are commonly used for distal hypospadias repair (Fig. 1). Deep, lateral mobilization of the distal part of the urethra is done in our institution for distal/coronal hypospadias followed by its advancement and glanuloplasty. This procedure is called an advanced-MAPGI (aMAGPI). With this method, suturing of the urethra is avoided, which might reduce the risk of such urethra-related complications as a fistula and/or dehiscence. Originally, MAGPI procedure was combined with circumcision.¹ Preservation of the foreskin is an option that can be offered to the patient/caregivers, providing it is technically feasible (the foreskin is well developed for closure). Nevertheless, preputioplasty itself comes with some specific complications such as fistula/dehiscence of the foreskin or phimosis.² The normal-looking meatus in a male is located slightly proximal to the tip of the glans. After hypospadias and foreskin repair, a slightly ventral position of the meatus results in deflection of the urinary stream towards the reconstructed prepuce. In order to allow for adequate wound healing and reduce the risk of complications, a catheter is often left in the bladder. In the past, the catheter was left for many days after any type of hypospadias correction. Currently, there is a common trend to perform hypospadias repair as a one-day procedure, with or without urinary diversion.

The goal of this study was to assess the impact of duration of urethra stenting on the healing of the foreskin after distal hypospadias repair using the aMAGPI procedure.



Fig. 1. Intraoperative view of the distal hypospadias and sufficient foreskin

Material and methods

A retrospective analysis of the distal hypospadias repairs performed at 2 institutions was undertaken. The inclusion criteria were: 1) a modified aMAGPI procedure, 2) foreskin reconstruction, 3) follow-up >12 months. All other types of reconstruction and the re-do procedures were excluded.

The duration of urethral stenting was determined intraoperatively depending on the surgeon's preferences.

At the University Children's Hospital in Kraków, Poland, the surgical corrections were performed by different surgeons. From October 2016, the duration of urethral stenting was significantly shortened to meet the international standards. The cohort from this institution was divided into 2 groups. In Group I (G-I), no catheter was left or it was removed the next day after surgery. In Group II (G-II), the catheter was left for more than 5 days. Group III (G-III) consisted of patients operated at the University Children's Hospital in Amsterdam, and the aMPGPI procedure with preputioplasty was performed by 1 surgeon (RC). In this group, no catheter was left or it was removed the next day after surgery.

Surgical techniques

A polypropylene traction suture is positioned through the glans. The transverse lip (bridge) of tissue distal to the meatus, if present, is divided by a longitudinal incision and the free edges of the wound are sutured together transversally. A catheter is then placed into the bladder.

A U-like incision is made around the meatus and then prolonged towards the top of the glans. The distal part (ca. 8–10 mm long) of the urethra is dissected free from the skin and corpora cavernosa and then advanced to the top of the glans. The glanular wings are approximated in the midline around the urethra by interrupted sutures (5/0 polyglactin). The ventral edge of the meatus is attached to the glans.

The major steps of foreskin reconstruction were the same in all cases. An U-like incision was made along the free margins of foreskin. The 2 layers were separated, and then the free edges were brought together with interrupted sutures (6/0 polyglactin) in 2 layers. A 10 Fr tube was left in the urethra and in the bladder (Fig. 2). In G-III, the dartos was approximated with 2–3 interrupted stitches whenever possible to identify and mobilize. Antibiotics (amoxicillin/clavulanic acid or cefuroxime depending on the local protocols) were administered perioperatively.



Fig. 2. Intraoperative view after foreskin reconstruction

Follow-up

Each patient was assessed at the outpatient clinic between 6 and 12 months after the operation. Any distal foreskin dehiscence or a foreskin fistula requiring re-do surgery was defined as a failure.

Statistical analysis was performed using Dell Statistica, v. 13 (Dell Inc, USA). The χ^2 test with Yates's correction was used to assess differences between G-I and G-II, G-I and G-III, as well as G-II and G-III. Additionally, Pearson's χ^2 test was used to assess the relationship between the groups. A p-value <0.05 was considered significant.

Results

There were 33 patients aged from 5 to 81 months in G-I, 27 patients aged from 10 to 95 months in G-II and 35 patients aged from 4 to 22 months in G-III (Table 1). No intraoperative complications were encountered. In G-I, 3 of the 33 patients (9%) developed foreskin dehiscence. In G-II, a catheter was kept for 5–9 days (mean time 7 days) and 2 out of 27 (7.4%) had foreskin dehiscence. In G-III, 6 out of the 35 patients (17%) developed foreskin dehiscence. The χ^2 test with Yates's correction was used to check differences between G-I and G-II, as well as G-I and G-III. There was no statistically significant difference in the incidence of complications between Groups I and II ($p = 0.8144$), or between Groups I and III ($p = 0.5344$). Also, in the non-parametric Pearson's χ^2 test, the difference was not significant in such grouped data ($p = 0.4239$).

Discussion

Distal penile hypospadias accounts for about 70% of all cases of hypospadias. There is a variety of operative techniques for distal hypospadias repairs, and most of them are combined with circumcision. However, in many cases, foreskin reconstruction can be offered as an option whenever technically possible.^{3–6}

In this study, we focused only on the foreskin complications to find out whether the duration of stenting might affect the outcome. Many factors can influence the outcome of preputioplasty, such as suture material, the technique used, duration of stenting, as well as the experience of the surgeon. Under a few circumstances, the foreskin cannot be preserved, e.g., when needed for urethroplasty

or when it is underdeveloped, making its reconstruction impossible.

The MAGPI procedure was devised by Duckett in 1981 for glandular hypospadias.¹ When the meatus is located at the level of the corona, a simple MAGPI procedure might not be the optimal solution. Several other methods have been proposed for this type of hypospadias. Among the most commonly performed are the TIPU – tubularized incised urethral plate urethroplasty – and the Mathieu procedure.^{5–8} In our institution, a modified MAGPI procedure is used, which consists of an extensive mobilization of the urethral walls and its advancement.

Foreskin preservation was first described by Righini in 1961, and the principle of this procedure remained consistent.⁹ However, many surgeons still prefer circumcision because some prior studies showed an increase in complications of urethroplasty when combined with preputioplasty.⁴ In 1989, Frey and Cohen performed foreskin reconstruction in combination with a MAGPI procedure in 46 patients and experienced foreskin dehiscence in 10 patients (21.7%).¹⁰

The reported foreskin related complication rate in the other types of hypospadias repair ranged from 2.5% to 34.8%.^{11–13} In our cohort, 11.6% of the patients developed foreskin dehiscence requiring re-do surgery. No significant foreskin stenosis occurred in our study population.

Some recent studies demonstrated a satisfactory outcome of the prepuce without an increase in the rate of urethroplasty or skin complications in patients undergoing TIPU repair.^{5,6,14} Moreover, it has been suggested that the reconstructed prepuce might act as a protective “layer” reducing the risk of the urethral fistulae.³

The prepuce reconstruction can be performed in 2 or 3 layers. The intermediate layer (dartos) is a thin connective tissue layer that can play an essential role in proper sliding between the inner and outer layers of the skin after reconstruction.¹² In the majority of our cases, the repair was performed in 2 layers (6/0 polyglactin); however, in some patients, a few interrupted stiches were placed to approximate the dartos layer of the prepuce. This maneuver seems not to reduce the complication rate.

Also, suturing material has been considered to influence the outcome. Antao et al. reported an increased risk of foreskin-related complications (dehiscence and fistula) when the wound was closed in a running way (polyglactin rapid breakdown) in comparison to an interrupted manner (polyglactin).¹¹ In our cohort, interrupted stiches were used (polyglactin).

Table 1. Patient data

| Group of patients | Catheterization | Range of age (average, median) in months | Foreskin dehiscence |
|---|-----------------|--|---------------------|
| G-I – 33 patients (different surgeons) | 0 or 1 day | 5–81 (22, 16) | 3 patients (9%) |
| G-II – 27 patients (different surgeons) | > 5 days | 10–95 (36, 29) | 2 patients (7.4%) |
| G-III – 35 patients (the same surgeon) | 0 or 1 day | 4–22 (12, 12) | 6 patients (17%) |

The role of the use of urethral stenting in distal hypospadias surgery is controversial, and usually, only the urethra-related complications are analyzed in this aspect.^{14–17} The foreskin is preferably used as an interposing layer to cover the urethroplasty.^{18,19} The impact of duration of stenting on the healing of the prepuce has not been studied yet.

We hypothesized that the urinary stream directed towards the reconstructed foreskin could increase the incidence of foreskin-related complication when there is no catheter left after reconstruction or when the catheter is removed shortly after the procedure. In the past, some surgeons have tended to leave the catheter for a long time even after distal hypospadias repair. Catheter placement has an impact on patients' postoperative comfort, which means it should be removed as soon as possible. In this study, different pediatric urologists were involved in the surgical treatment of the patients in G-I and G-II. The duration of stenting varied depending on the surgeon's preference, which might have affected the outcome. Group III was included in the analysis to minimize the surgeon-related bias. The patients had been operated by the same pediatric urologist, and the catheter was removed shortly after the procedure. Although the complication rate in G-III was higher than in G-I and G-II, the difference was statistically insignificant.

Limitations

We realize that there are many different factors that might affect the final outcome of any surgical procedure. The inclusion criteria of our study were very strict to minimize any bias. For this reason, the outcome of urethroplasty was not taken into consideration. The main concern was the number of surgeons performing surgery in G-I and G-II. The human-related bias was reduced by adding G-III analysis. The operating surgeons might likely have tended to leave a catheter a bit longer in older children, as the average age of patients in G-II was higher than in the other groups. No conclusion should be drawn from this as today the majority of patients are scheduled for this surgery between 6 and 18 months of life.

The small number of participants is another limitation of this study. Nevertheless, proper statistical methods have been chosen to compare the samples. Retrospective analysis has its limitations for the assessment of the outcome, but the endpoint of the study was clearly defined – partial (fistula) or total foreskin dehiscence requiring re-do surgery.

Conclusions

Prolonged urethral stenting does not reduce the risk of re-do foreskin surgery after hypospadias repair.

ORCID iDs

Ireneusz Honkisz  <https://orcid.org/0000-0002-7448-9908>
 Janusz Sulislawski  <https://orcid.org/0000-0002-4802-5210>
 Barbara Dobrowolska-Glazar  <https://orcid.org/0000-0002-0192-9263>
 Caroline F. Kuijper  <https://orcid.org/0000-0001-9668-5339>
 Rafal Chrzan  <https://orcid.org/0000-0001-8620-1898>

References

- Duckett JW. MAGPI (meatoplasty and glanuloplasty): A procedure for subcoronal hypospadias. *Urol Clin North Am.* 1981;8(3):513–519.
- Kallampallil J, Hennayake S. Foreskin retractility following hypospadias repair with preputioplasty: Medium term outcomes. *J Pediatr Urol.* 2013;9(6):1204–1209. doi:10.1016/j.jpuro.2013.05.022
- Dewan PA. Distal hypospadias repair with preputial reconstruction. *J Pediatr Child Health.* 1993;29(3):183–184.
- Suoub M, Dave S, El-Hout Y, Braga LH, Farhat WA. Distal hypospadias repair with or without foreskin reconstruction: A single-surgeon experience. *J Pediatr Urol.* 2008;4(5):377–380. doi:10.1016/j.jpuro.2008.01.215
- Snodgrass W, Dajusta D, Villanueva C, Bush N. Foreskin reconstruction does not increase urethroplasty or skin complications after distal TIP hypospadias repair. *J Pediatr Urol.* 2013;9(4):401–406. doi:10.1016/j.jpuro.2012.06.008
- Esposito C, Savanelli A, Escolino M, et al. Preputioplasty associated with urethroplasty for correction of distal hypospadias: A prospective study and proposition of a new objective scoring system for evaluation of esthetic and functional outcome. *J Pediatr Urol.* 2014;10(2):294–299. doi:10.1016/j.jpuro.2013.09.003
- Subramaniam R, Spinoit AF, Hoebeke P. Hypospadias repair: An overview of the actual techniques. *Semin Plast Surg.* 2011;25(3):206–212. doi:10.1055/s-0031-1281490
- El-Ganainy EO, Hameed DA, Abdelsalam YM, Abdelaziz MA. Prepuce preserving versus conventional Mathieu urethroplasty for distal hypospadias: A prospective randomized study. *J Pediatr Urol.* 2012; 8(3):264–267. doi:10.1016/j.jpuro.2011.05.004
- Righini A. Symposium sur l'hypospadias. *Ann Chir Infant.* 1969;10:314.
- Frey P, Cohen SJ. Reconstruction of foreskin in distal hypospadias repair. *Prog Pediatr Surg.* 1989;23:192–200.
- Antao B, Lansdale N, Roberts J, Mackinnon E. Factors affecting the outcome of foreskin reconstruction in hypospadias surgery. *J Pediatr Urol.* 2007;3(2):127–131. doi:10.1016/j.jpuro.2006.06.003
- Castagnetti M, Bagnara V, Rigamonti W, Cimador M, Esposito C. Preputial reconstruction in hypospadias repair. *J Pediatr Urol.* 2017;13(1): 102–109. doi:10.1016/j.jpuro.2016.07.018
- Klijn AJ, Dik P, de Jong TP. Results of preputial reconstruction in 77 boys with distal hypospadias. *J Urol.* 2001;165(4):1255–1257.
- Castagnetti M, Gnech M, Angelini L, Rigamonti W, Bagnara V, Esposito C. Does preputial reconstruction increase complication rate of hypospadias repair? 20-year systematic review and meta-analysis. *Front Pediatr.* 2016;28(4):41. doi:10.3389/fped.2016.00041
- Buson H, Smiley D, Reinberg Y, Gonzales R. Distal hypospadias repair without stents: Is it better? *J Urol.* 1994;151(4):1059–1060.
- Chalmers DJ, Siparsky GL, Wiedel CA, Wilcox DT. Distal hypospadias repair in infants without a postoperative stent. *Pediatr Surg Int.* 2015; 31(3):287–290. doi:10.1007/s00383-014-3647-y
- Leclair MD, Camby C, Battisti S, Renaud G, Plattner V, Heloury Y. Unstented tubularized incised plate urethroplasty combined with foreskin reconstruction for distal hypospadias. *Eur Urol.* 2004;46(4): 526–530.
- El-Karamany TM, Al-Adi AM, Omar RG, Abdel Aal AM, Eldakhkhny AS, Abdelbaki SA. A critical analysis of stented and unstented tubularized incised plate urethroplasty through a prospective randomised study and assessment of factors influencing the functional and cosmetic outcomes. *Urology.* 2017;107:202–208. doi:10.1016/j.urology.2017.04.056
- El-Kassaby AW, Al-Kandari AM, Elzayat T, Shoekeir AA. Modified tubularized incised plate urethroplasty for hypospadias repair: A long-term results of 764 patients. *Urology.* 2008;71(4):611–615. doi:10.1016/j.urology.2007.11.121

Infectious diseases of the skin in contact sports

Danuta Nowicka^{1,B–D,F}, Marta Bagłaj-Oleszczuk^{1,B,D,F}, Joanna Maj^{2,A,E,F}

¹ Department of Dermatology, Venereology and Allergology, Wrocław Medical University, Poland

² Institute of Health Sciences, University of Opole, Poland

A – research concept and design; B – collection and/or assembly of data; C – data analysis and interpretation;

D – writing the article; E – critical revision of the article; F – final approval of the article

Advances in Clinical and Experimental Medicine, ISSN 1899–5276 (print), ISSN 2451–2680 (online)

Adv Clin Exp Med. 2020;29(12):1491–1495

Address for correspondence

Danuta Nowicka

E-mail: danuta.nowicka@umed.wroc.pl

Funding sources

None declared

Conflict of interest

None declared

Received on October 17, 2020

Reviewed on October 19, 2020

Accepted on October 28, 2020

Abstract

Although the benefits of practicing sports are unquestionable, it can contribute to the spread of skin diseases. Mechanical trauma, exposure to environmental and infectious agents, and contact with the skin of other athletes increase the chances of getting an infection. In contact sports, skin infections are responsible for up to 20% of lost training and competition time. In the USA, skin infections, with an incidence of 8.5–20.9%, are the 2nd cause (following upper respiratory infections) of all medical consultations among young wrestlers. The high morbidity of skin diseases poses a great challenge for the diagnosis and treatment of skin infections in athletes practicing contact sports, for whom recommendations may differ from those in the general population. In this review paper, we summarize and discuss the management of infectious diseases of the skin in contact sports. The review shows that the most frequent among athletes are bacterial infections, including folliculitis, erysipelas, furuncles and inflammation of the subcutaneous tissue; viral infections caused by herpes simplex virus, human papilloma virus and molluscum contagiosum virus; fungal infections such as tinea; and infestations, including pediculosis and scabies. Preventing the spread of the infection is the 2nd most important aspect of treatment, following pharmacotherapy. This includes avoiding contact with other athletes, protection or removal of lesions, disinfection of common sports equipment, not sharing towels or other personal equipment. We conclude that protecting against infection and transmission of pathogens in sports teams is crucial in avoiding unnecessary morbidity and minimizing disruption to the training and competition schedule.

Key words: contact sport, skin infection, wrestling, sports

Cite as

Nowicka D, Bagłaj-Oleszczuk M, Maj J. Infectious diseases of the skin in contact sports. *Adv Clin Exp Med.* 2020;29(12):1491–1495. doi:10.17219/acem/129022

DOI

10.17219/acem/129022

Copyright

© 2020 by Wrocław Medical University

This is an article distributed under the terms of the Creative Commons Attribution 3.0 Unported (CC BY 3.0) (<https://creativecommons.org/licenses/by/3.0/>)

Background

Physical activity and sports have become part of current life, even among amateur athletes. Although the benefits of sports are unquestionable,¹ participating in sports can be associated with several skin problems. Mechanical trauma, exposure to environmental and infectious agents, as well as contact with various other factors and with the skin of other athletes increase the chances of getting an infection. Furthermore, physical effort often exacerbates existing dermatological lesions.² Contact sports seem to be the disciplines with the most frequent occurrence of skin problems, the majority of which are skin infections.³ According to data from the literature, up to 20% of wrestlers lose training or competition time each year due to skin infections. Of those infections, over 22% have a recurrent nature.⁴ An epidemiology study conducted in the USA showed that skin infections are the 2nd most frequent cause (following upper respiratory infections) of medical consultations among high school and college wrestlers, with an incidence of 8.5–20.9%.⁵ The recommended treatment of skin infections in athletes practicing contact sports may differ from the management of skin infections in the general population. The recommendations are summarized in Table 1 and discussed further in the present review.

Diagnosing specific sports dermatoses can be challenging. In this review, we discuss and highlight some of the typical skin problems associated with practicing sports.

Bacterial infections

Infections with *Staphylococcus* and *Streptococcus* species are the most frequently seen skin and soft tissue infections in humans. In clinical practice, impetigo contagious, erysipelas, panniculitis, and furuncles are the most frequent; however, a superficial bacterial infection of the skin that causes vesicle-purulent lesions including blisters and open lesions that leave honey-yellow scabs dominates over other skin infections. Due to the superficial nature of such conditions, systemic treatment is rarely necessary.³

Folliculitis is manifested by small pustules around hair follicles. In people using tight-fitting workout clothes, folliculitis may take the form of so-called “bikini bottom”. In such cases, the lesions are localized in the areas where the clothes fit. It can be treated with topical and oral antibiotics. This disease usually causes no problems in diagnosis and treatment. Although folliculitis is considered highly contagious, it is rarely the cause of lost training time.⁴ Nevertheless, it is advisable to reduce the intensity of training and to avoid contact with other athletes for at least 72 h from the start of the treatment. Body shaving may contribute to increased frequency of folliculitis.⁶

Deep bacterial infections such as erysipelas, furuncles or inflammations of the subcutaneous tissue have been reported to occur equally often in contact and in group sports such as football and basketball.^{7,8} Direct contact seems to be crucial for contracting these contagious diseases; however, some of the authors highlight the role of mats and equipment in spreading infections.⁹ What

Table 1. Skin infections: Recommendations and treatment for athletes practicing contact sports

| Disease | Recommendations | Treatment |
|---------------------------|---|---|
| Bacterial infections | Avoid contact with other athletes for at least 72 h from the start of the treatment or if new lesions appeared during 48 h or if moist exudative lesions are present. Avoid body shaving. | Antibiotics |
| HSV viral infection | Before a competition, all lesions must be dry and covered with crusts. Avoid contact with other athletes if new lesions appeared for during last 72 h or systemic symptoms are present or for at least 120 h from the start of antivirals. | Topical antivirals for skin lesions; systemic antivirals for massive skin lesions and systemic symptoms. |
| MCV viral infection | Participation is allowed immediately after removal of lesions. Treated sites must be covered with a bio-occlusive dressing. | Removal of lesions (curettage, cryotherapy). |
| Fungal infections: Tinea | Participation is allowed after 72 h from the start of treatment in case of skin tinea and 14 days in case of tinea capitis. | Topical antifungal cream twice daily; cover a lesion and 2 cm surrounding skin. For tinea capitis, systemic antifungal treatment plus 2% ketoconazole shampoo. Followed by maintenance treatment. Relapse prevention – shampoo 1–2 times a week. |
| Infestations: Pediculosis | Participation is allowed after 24 h from the start of treatment unless active infestation is present. | 1% permethrin shampoo once and repeated 3–7 days after if pediculosis persists. |
| Infestations: Scabies | Participation is allowed after 24 h from the start of treatment if no evidence of active infestation in skin scrapings. | One application of 5% permethrin topical cream. |

HSV – herpes simplex virus; MCV – molluscum contagiosum virus.

seems to be necessary for stopping the spread of an infection is quick diagnosis, treatment and isolation of the sick athlete. If the infection spreads, it also seems necessary to identify the carriers, e.g., by collecting and testing bacteriological swabs from body cavities. The treatment of deep bacterial infections may be challenging, due to much higher skin colonization rates with methicillin-resistant *Staphylococcus aureus* among athletes. In wrestlers, carriage may reach 76% in comparison to 18% in people who do not practice any sport.¹⁰

Viral infections of the skin and mucosa

Common viral infections that afflict athletes include those caused by herpes simplex virus (HSV), human papilloma virus (HPV) and molluscum contagiosum virus (MCV). Herpes simplex can occur in any location, especially in contact sports. The HSV infection can be easily contracted, resulting in massive outbreaks during athletic training camps.^{11–13} In this context it is called herpes gladiatorum, a term which was used as early as the 1960s, but which came into widespread use in 1989,¹⁴ when 60 of 175 participants of a Minnesota (USA) high-school wrestling camp presented with signs of HSV infection, forcing the US Department of Public Health to disband the camp.¹¹ The clinical picture of HSV infection often includes massive, painful follicular lesions in groups or a rash of blisters at the site of infection. In the literature, facial presentation is the most common (up to 70%). Lesions located on the fingers or thumbs, on the extremities and the trunk constitute the remaining 30% of cases.^{11,15}

Coexisting dermatoses, mainly atopic dermatitis or contact eczema, may increase the risk of HSV skin infection. Involvement of the eye is also possible. Herpetic keratitis (involvement of the cornea) can lead to scarring, and with repeated lesions, it can lead to permanent corneal opacity, requiring a corneal transplant to maintain good vision. Retinal necrosis leading to blindness may also occur. Retinal necrosis due to HSV infection is the most common cause of blindness of contagious origin in the USA.^{16–18} The treatment of HSV infection is based on antivirals (e.g., acyclovir, ganciclovir) given in cases of high intensity of general symptoms. In cases of eye involvement, an ophthalmologic consultation is required. Antibiotic therapy may become necessary after secondary bacterial infection.

The MCV is highly infectious and spreads through contact with the content of skin lesions. As in the case of herpes, atopic diseases increase the risk of contracting the infection. In most cases, active treatment is not necessary. Extensive and complicated lesions, as well as those causing esthetic problems, may be subjected to mechanical, chemical or pharmacological treatment.¹⁹ In sports, it should be treated as early as possible using mechanical methods to reduce the chances of the infection spreading among

the athletes.²⁰ Warts are lesions caused by MCV types 1, 2 and 3, as well as 6, 11, 16 and 18. Lesions such as papules can appear all over the skin, with a predilection for the dorsal surface of the hand, the soles of the feet and the face. The source of infection can be direct contact with other infected persons, but also through uneven, moist surfaces (shower floors, sauna benches, exercise mats). Studies show that MCV spreads easily among swimmers through shared use of towels and wet surfaces, and is a cause of frequent outbreaks of molluscum contagiosum in athletes practicing water sports.^{7,21} The management of MCV infections should be focused primarily on prophylaxis (wearing protective shoes) as well as on the destruction of the lesions (e.g., with laser surgery or cryotherapy), or application of imiquimod, salicylic acid or podophyllin.¹⁹ Propagation of good hygienic practice is recommended as well, e.g., avoiding sharing towel and personal equipment, and using only disinfected mats.^{7,21,22}

Fungal infections

Athletes are at high risk of fungal infections caused by dermatophytes due to increased exposure to pathogens (e.g., swimmers through contact with water, wrestlers through using mats) and repeated exposure to mechanical factors (e.g., microinjuries of the skin of runners' feet). In disciplines involving close contact during competitions, particularly in wrestlers and judokas, anthropophilic infections with *Trichophyton tonsurans* (tinea gladiatorum) play the greatest role. Some studies report that infections with *T. tonsurans* were detected in at least 1 athlete in up to 84% of the wrestling teams in the USA.²³ Tinea gladiatorum is highly contagious and often causes minor epidemics, especially if the primary source of infection is not quickly identified. The sports environment (e.g., mats) and asymptomatic carriers may be involved in the further spread of this disease. In sumo wrestlers, for example, the scalp often serves as the reservoir of the pathogen.³ It seems that tinea pedis is often underdiagnosed and undertreated. Colonization of the environment by fungal spores may be responsible for the much higher level of fungal infections of the feet in children and adolescents who practice sports. Infections of the toenails (onychomycosis) are more frequent than fingernail infections. They may result in the separation of the nail from the nail bed and pave the way for secondary bacterial or mold infections. On the other hand, zoophilic and geophilic dermatophytes are rarely transmitted to athletes who have contact with animals, e.g., equestrians.²⁴

Dermatophytes infect the stratum corneum (tinea corporis), but also the hair and hair follicles in the scalp area (tinea capitis). In children and adolescents involved in contact sports, the infection leads to endothrix on the scalp, with parasitic spores visible within the hair shaft and undamaged hair cuticle, often called black-dot ringworm.

In contrast, in adults, it leads to asymptomatic carriage.²⁵ Transmitting pathogens and contracting the disease depend not only on contact with an infected person, but also on other factors, such as the occurrence of sports-related abrasions, an unfavorable indoor climate, the intensity of sweating, and the time between competition and shower. Majocchi granuloma may also develop in cases of local or systemic immunosuppression.²⁶

In contact sports, tinea corporis presents with pruritic and annular plaques, often with vesicles at their periphery. This infection has been widely reported in wrestlers and is often referred to as tinea gladiatorum, trichophytosis gladiatorum and tinea corporis gladiatorum. Several studies have examined the epidemiology of tinea corporis gladiatorum in wrestlers. It was found that the rate of affected wrestlers in wrestling teams varies from 24% to 77%. Another study on teams of asymptomatic wrestlers found that about 24% of athletes were carriers.^{27–30}

Tinea capitis is less common in athletes. This condition mostly affects people who practice sports that entail close contact among the athletes and those using protective equipment, e.g., jockeys and hockey players.^{31–33}

Tinea versicolor, a condition caused by a fungus (*Malassezia furfur*), is another relatively frequent superficial skin infection.³⁴ Its occurrence is associated with individual predisposition, excessive sweating, humidity, and close-fitting clothing. Recurrences of the disease are frequent among athletes.

Infestations: Scabies and head lice

Scabies and pediculosis of the head, torso and pubic area are parasitic diseases caused by ectoparasites that live on or in the skin of the host. These infestations may be challenging to diagnose; however, their treatment is easy. Ectoparasitoses are highly contagious by a direct head-to-head or body-to-body contact. Symptoms may appear 3–4 weeks after infection, which hampers the diagnosis, delays treatment and facilitates the spread of the parasites.³

The most common sign of pediculosis is intense itching on the scalp, torso or in the pubic area – parts of the body covered by hairy skin. The diagnosis is based on clinical examination and detection of live lice or viable nits. Using sticky tape over the infected area to collect lice for a microscope examination can be helpful. If only nits are found on the hair shafts, in the absence of nymphs or adult lice, then a recent infestation can be suspected, but active disease cannot be confirmed.³⁵ Medicinal shampoos with permethrin, phenothrin or carbaryl are effective therapeutic agents.³⁶

Symptoms of scabies include an itchy, lumpy rash, often with vesicles, pustules or lumps. It is caused by the mite *Sarcoptes scabiei*, which burrows into the skin. Scabies can be suspected when the characteristic skin appearance and distribution of lesions are seen; however, a proper

diagnosis can be confirmed by identifying the mite or mite eggs in skin scrapings under a low-power microscope. The treatment of choice is a topical permethrin cream.³⁷


When combating scabies and pediculosis, maintaining clean bed linens and towels is important. Textiles should be washed in hot water with a regular laundry detergent to reduce the risk of re-infestation. In the case of fabrics that are difficult to wash at high temperatures, it is helpful to put them in plastic bags and keep them for 7 days at a low room temperature or freezer. The basis of epidemiological treatment is the simultaneous treatment of all the people who have close contact with the infected individual.³⁸

Conclusions

Skin infections and related skin lesions are a common problem among people who practice sports disciplines, especially those with direct skin-to-skin contact. Protecting against infections and the transmission of pathogens in sports teams is crucial in avoiding unnecessary morbidity and minimizing any disruption to the training and competition schedule.

ORCID iDs

Danuta Nowicka  <https://orcid.org/0000-0002-1717-4280>

Marta Bagłaj-Oleszczuk  <https://orcid.org/0000-0002-4554-7603>

Joanna Maj  <https://orcid.org/0000-0001-8300-8208>

References

- Warburton DER, Nicol CW, Bredin SSD. Health benefits of physical activity: The evidence. *CMAJ*. 2006;174(6):801–809.
- Derya A, Ilgen E, Metin E. Characteristics of sports-related dermatoses for different types of sports: A cross-sectional study. *J Dermatol*. 2005;32(8):620–625.
- Peterson AR, Nash E, Anderson BJ. Infectious diseases in contact sports. *Sports Health*. 2019;11(1):47–58.
- Herzog MM, Fraser MA, Register-Mihalik JK, Kerr ZY. Epidemiology of skin infections in men's wrestling: Analysis of 2009–2010 through 2013–2014 National Collegiate Athletic Association surveillance data. *J Athl Train*. 2017;52(5):457–463.
- Yard EE, Collins CL, Dick RW, Comstock RD. An epidemiologic comparison of high school and college wrestling injuries. *Am J Sports Med*. 2008;36(1):57–64.
- Börjesson M, Arvidsson D, Rensburg CJV, Schweltnus M. Return to play after infectious disease. In: Musahl V, Karlsson J, Krutsch W, Mandelbaum BR, Espregueira-Mendes J, d'Hooghe P, eds. *Return to Play in Football*. Berlin-Heidelberg: Springer Verlag; 2017:755–769.
- Kirkland R, Adams BB. Dermatological problems in the football player. *Int J Dermatol*. 2006;45(8):927–932.
- Sosin DM, Gunn RA, Ford WL, Skaggs JW. An outbreak of furunculosis among high school athletes. *Am J Sports Med*. 1989;17(6):828–832.
- Young LM, Motz VA, Markey ER, Young SC, Beaschler RE. Recommendations for best disinfectant practices to reduce the spread of infection via wrestling mats. *J Athl Train*. 2017;52(2):82–88.
- Champion AE, Goodwin TA, Brolinson PG, Werre SR, Prater MR, Inzana TJ. Prevalence and characterization of methicillin-resistant *Staphylococcus aureus* isolates from healthy university student athletes. *Ann Clin Microbiol Antimicrob*. 2014;13:33.
- Belongia EA, Goodman JL, Holland EJ, et al. An outbreak of herpes gladiatorum at a high-school wrestling camp. *N Eng J Med*. 1991; 325(13):906–910.
- Freeman MJ, Bergfeld WF. Skin diseases of football and wrestling participants. *Cutis*. 1977;20(3):333–341.

13. Bergfeld WF, Taylor JS. Trauma, sports, and the skin. *Am J Ind Med.* 1985;8(4–5):403–413.
14. Selling B, Kibrick S. An outbreak of herpes simplex among wrestlers (herpes gladiatorum). *N Engl J Med.* 1964;270:979–982.
15. Anderson BJ. The epidemiology and clinical analysis of several outbreaks of herpes gladiatorum. *Med Sci Sports Exerc.* 2003;35(11):1809–1814.
16. Usatine RP, Tinitigan R. Nongenital herpes simplex virus. *Am Fam Physician.* 2010;82(9):1075–1082.
17. Jefferis J, Perera R, Everitt H, et al. Acute infective conjunctivitis in primary care: Who needs antibiotics? An individual patient data meta-analysis. *Br J Gen Pract.* 2011;61(590):e542–e548.
18. Johnson R. Herpes gladiatorum and other skin diseases. *Clin Sports Med.* 2004;23(3):473–484.
19. Meza-Romero R, Navarrete-Dechent C, Downey C. Molluscum contagiosum: An update and review of new perspectives in etiology, diagnosis, and treatment. *Clin Cosmet Investig Dermatol.* 2019;12:373–381.
20. Adams BB. Which skin infections are transmitted between athletes? *West J Med.* 2001;174(5):352–353.
21. Freiman A, Barankin B, Elpern DJ. Sports dermatology part 1: Common dermatoses. *CMAJ.* 2004;171(8):851–853.
22. Choong KY, Roberts LJ. Molluscum contagiosum, swimming and bathing: A clinical analysis. *Australas J Dermatol.* 1999;40(2):89–92.
23. Bassiri-Jahromi S, Sadeghi G, Asghari Paskiaee F. Evaluation of the association of superficial dermatophytosis and athletic activities with special reference to its prevention and control. *Int J Dermatol.* 2010;49(10):1159–1164.
24. Gnat S, Łagowski D, Nowakiewicz A, Dyląg M. Tinea corporis caused by *Trichophyton equinum* transmitted from asymptomatic dogs to two siblings. *Braz J Microbiol.* 2020;51(3):1433–1438.
25. Peixoto RRGB, Meneses OMS, da Silva FO, Donati A, Veasey JV. Tinea capitis: Correlation of clinical aspects, findings on direct mycological examination, and agents isolated from fungal culture. *Int J Trichology.* 2019;11(6):232–235.
26. Grosset-Janin A, Nicolas X, Saraux A. Sport and infectious risk: A systematic review of the literature over 20 years. *Med Mal Infect.* 2012;42(11):533–544.
27. Beller M, Gessner BD. An outbreak of tinea corporis gladiatorum on a high school wrestling team. *J Am Acad Dermatol.* 1994;31(2 Pt 1):197–201.
28. Adams BB. Tinea corporis gladiatorum: A cross-sectional study. *J Am Acad Dermatol.* 2000;43(6):1039–1041.
29. Ilkit M, Saracli M, Kurdak H, et al. Clonal outbreak of *Trichophyton tonsurans* tinea capitis gladiatorum among wrestlers in Adana, Turkey. *Med Mycol.* 2009;48(3):480–485.
30. Kaushik N, Pujalte GG, Reese ST. Superficial fungal infections. *Prim Care.* 2015;42(4):501–516.
31. John AM, Schwartz RA, Janniger CK. The kerion: An angry tinea capitis. *Int J Dermatol.* 2018;57(1):3–9.
32. Hay RJ. Tinea capitis: Current status. *Mycopathologia.* 2017;182(1–2):87–93.
33. Auchus IC, Ward KM, Brodell RT, Brents MJ, Jackson JD. Tinea capitis in adults. *Dermatol Online J.* 2016;22(3):13030/qt4dm9s3fh.
34. Renati S, Cukras A, Bigby M. Pityriasis versicolor. *BMJ.* 2015;350:h1394.
35. Hatam-Nahavandi K, Ahmadpour E, Pashazadeh F, et al. Pediculosis capitis among school-age students worldwide as an emerging public health concern: A systematic review and meta-analysis of past five decades. *Parasitol Res.* 2020;119(10):3125–3143.
36. Verma P, Namdeo C. Treatment of pediculosis capitis. *Indian J Dermatol.* 2015;60(3):238–247.
37. Flinders DC, De Schweinitz P. Pediculosis and scabies. *Am Fam Physician.* 2004;69(2):341–348.
38. Gunning K, Pippitt K, Kiraly B, Saylor M. Pediculosis and scabies: Treatment update. *Am Fam Physician.* 2012;86(6):535–541.

Applications for graphene and its derivatives in medical devices: Current knowledge and future applications

Jacek Arkowski^{1,A,B,D}, Marta Obremska^{1,E}, Kamil Kędzierski^{2,B,D}, Agnieszka Sławuta^{3,D}, Magdalena Wawrzyńska^{1,A,E,F}

¹ Department of Preclinical Studies, Wrocław Medical University, Poland

² Department of Emergency Medical Services, Wrocław Medical University, Poland

³ Department of Internal and Occupational Diseases, Hypertension and Clinical Oncology, Wrocław Medical University, Poland

A – research concept and design; B – collection and/or assembly of data; C – data analysis and interpretation;

D – writing the article; E – critical revision of the article; F – final approval of the article

Advances in Clinical and Experimental Medicine, ISSN 1899–5276 (print), ISSN 2451–2680 (online)

Adv Clin Exp Med. 2020;29(12):1497–1504

Address for correspondence

Magdalena Wawrzyńska

E-mail: magdalena.wawrzyńska@umed.wroc.pl

Funding sources

None declared

Conflict of interest

None declared

Received on September 23, 2020

Reviewed on November 2, 2020

Accepted on November 18, 2020

Abstract

Graphene is a novel carbon-based material with unique crystal nanostructure and extraordinary physical and chemical properties. Several biomedical applications of graphene and graphene-derived materials have been proposed. Its antimicrobial properties might be useful in all areas of medicine where antiseptics are required. On the other hand, the safe limits of graphene concentration for human cells have not been clearly established yet. The possibility to attach various chemically active groups to the basic lattice structure allows researchers to build graphene-based sensors for detecting biochemical molecules (and ultimately – selected cells). Sensors for physical signals, such as cardiac electrical activity, have also been proposed. The unique nanostructure of the material and the resulting physical properties (mechanical strength, elasticity and large surface area) make it a very promising material for scaffolds used in tissue regeneration. Several studies have investigated the potential advantages of a graphene coating for endovascular implants, such as stents or valves. Most of them indicate an advantage of graphene coating over other currently available solutions in terms of better hemocompatibility and facilitating endothelialization. Many of the results published so far are from in vitro studies. Promising as they might be, more data, preferably from experiments on more sophisticated animal models, must be obtained before any valid conclusions as to potential uses of graphene in medicine can be drawn.

Key words: graphene, medical devices, biocompatibility, cardiovascular

Cite as

Arkowski J, Obremska M, Kędzierski K, Sławuta A, Wawrzyńska M. Applications for graphene and its derivatives in medical devices: Current knowledge and future applications. *Adv Clin Exp Med.* 2020;29(12):1497–1504. doi:10.17219/acem/130601

DOI

10.17219/acem/130601

Copyright

© 2020 by Wrocław Medical University

This is an article distributed under the terms of the Creative Commons Attribution 3.0 Unported (CC BY 3.0) (<https://creativecommons.org/licenses/by/3.0/>)

Introduction

Graphene is a novel nanomaterial composed of sp² carbon atoms arranged in a two-dimensional hexagonal honeycomb crystal lattice. Its unique spatial structure results in extraordinary physical and chemical properties. Some of the most important properties are high mechanical strength, excellent conductivity, a large surface-to-volume ratio, and the potential to bind different types of chemically active groups. As a consequence, several possible uses of graphene in biomedicine have been proposed and tested. The most promising applications of graphene include its use as an antimicrobial agent, a scaffold in regenerative medicine, a material for sensors of both biochemical and biophysical signals, and as a coating for endovascular implants. In this review, we present the biomedical, diagnostic and therapeutic applications of graphene-based nanomaterials in various fields of medicine. The most recent interest is the potential use of graphene coatings in medical devices for cardiovascular applications.

Synthesis, modification, and chemical properties

Graphene was created for the first time in 2004 by being stripped from graphite. There are several methods for preparing graphene: mechanical stripping, redox methods, orientation epitaxy, chemical vapor deposition, graphitization, solvothermal methods, organic synthesis, graphite exfoliation, and reduction of graphene oxide (GO).¹

Graphene-based materials can be classified according to the number and spatial arrangement of the sheets, the oxygen content, and chemical modification. Several sheets stacked on top of each other form graphite, a single rolled sheet forms a carbon nanotube, and spherically wrapped "closed" sheet builds a fullerene. A single layer of pure graphene is hard to synthesize and difficult to suspend in solution. Therefore, GO or reduced GO (rGO) is used more often in biomedical applications. Sheets of GO display several types of chemically active groups (such as carboxylate, epoxide and hydroxyl) which, together with the capacity to build π - π and hydrogen bonds, are responsible for interactions and bonds with other particles. The physical and chemical properties of graphene, GO and rGO can be imagined on a scale with graphene at one end (the best electrical conductivity, hydrophobic, and the least chemically reactive), GO on the other end (reactive, hydrophilic, and poor conductivity) and rGO in between the two.²

Many covalent and non-covalent modifications of graphene have been described. In general, the covalent modifications are more stable and offer higher binding capacity – an important distinction for drug carrier applications.

Graphene and graphene-based materials have already found many applications in areas as diverse as fuel cells, electrochemistry and catalysis.

Safety and potential cytotoxicity

As with every new material, concerns have been raised about its biocompatibility and potential interactions with living cells. Obviously, safety issues must be clarified before any serious biomedical applications of a substance can be considered.

It has been found that graphene interacts with proteins and nucleic acids – molecules essential for key cell functions.^{3–5} There have been a number of studies where the influence of graphene and graphene-related materials on cell viability have been tested. At this point, it is somewhat difficult to draw any general conclusions from these experiments. Different cell lines (both human and non-human) were used with graphene-related materials modified in various ways. It may tentatively be concluded that GO in concentrations on the order of 100 $\mu\text{g}/\text{mL}$ might exert negative effects (reduced viability) on cell lines (both murine and human). Most researchers have concluded that the effect is dose-dependent, with some evidence pointing towards a higher toxicity for pristine graphene than for GO.⁶ It was found that articulate state, particle size and surface charge/oxygen content of the graphene all had a strong impact on the toxicological and biological responses to human red blood cells.⁷ Interestingly, Sasidharan et al. showed that pristine graphene accumulated in the cell membrane, which leads to apoptosis due to the high oxidative stress, whereas its carboxyl-functionalized derivative internalized in the cells without any cytotoxicity.⁸ Additionally, the method of administration might play an important role, as shown by 1 study, where orally administered PEG-functionalized GO sheets led to no tissue uptake while intraperitoneal injection resulted in accumulation in the spleen and liver.⁹ Several mechanisms of these effects have been proposed. In a study by Luan et al., it was found that hydrophobic protein–protein interactions can be interrupted by graphene. The researchers attributed this effect to the separation of 2-deoxyribose-5-phosphate aldolase and phosphoglucose isomerase.¹⁰ Another study showed that GO provokes oxidative stress in A549 cells, which may decrease cell viability.¹¹

There have been some attempts to investigate the effect of graphene on a whole multicellular organism. In a systematic evaluation of graphene quantum dots in mice, toxicity was found to be low overall in terms of the influence on reproduction and cell viability.¹²

It seems that especially low concentrations of graphene do not provoke any measurable noxious effects. For instance, in a study by Jiang et al., a low concentration of graphene quantum dots showed a relatively weak influence on the morphology, viability, membrane integrity, internal cellular reactive oxygen species level, and mortality of HeLa cells. Similarly, small amounts of graphene quantum dots brought little harm to the cardiovascular system of zebrafish embryos.¹³ The authors concluded that at least this particular graphene derivative demonstrates

good biocompatibility and that, thanks to its high quantum yield and strong photoluminescence, it might be a promising material for cell imaging, biolabeling and other biomedical applications.

Antibacterial activity

The potential antibacterial activity of graphene materials has been proposed as another, more favorable aspect of graphene–cell interactions. The researchers who studied the issue found that the effect depends on the lattice size and shape and the number of layers and surface modifications.^{14–16} In particular, a reduction in cell viability was reported for *Escherichia coli* and *Staphylococcus aureus* in contact with GO and rGO. Cell membrane damage was proposed as the underlying mechanism.¹⁷ At the molecular level, the antimicrobial effects were associated with protein disruption, lipid extraction, and reactive oxygen species (ROS) production.^{10,18–20}

Even more convincing results were observed when graphene was functionalized with known antimicrobial agents, such as silver nanoparticles, other metals or metal ions/oxides, polymers and enzymes.²¹

On the one hand, these findings present an opportunity of using graphene-based materials as antibacterial agents. On the other hand, great care must be taken to investigate and quantify any potential undesirable effects on cells and the human body before these materials can find widespread application that puts them in contact with living human cells.

Detecting biomolecules

Due to its high surface-to-volume ratio (allowing the attachment of a large amount of the required ligand) and very good conductivity, graphene may be very useful for building sensitive electrical and electrochemical sensors. A receptor (such as an antibody or enzyme) bound to graphene can interact with ions, organic molecules or even whole cells. The chemical signal of interaction between the receptor and target molecule may be converted to electricity.

As an example, at least 2 types of graphene-based glucose sensors have been developed. One of them uses glucose oxidase attached to graphene,²² and the other is based on competitive binding of glucose or a graphene-based molecule to the sensor.²³ The high prevalence and often asymptomatic onset of type II diabetes and the serious consequences of inadequate treatment make any improvements in early detection and accurate monitoring very important for the large number of patients suffering from this disease.

An accurate and reliable detection of biomarker molecules is similarly crucial in diagnosing other many diseases (such as cancers or inflammatory syndromes). Graphene-based biosensors have been shown to successfully detect

specific proteins, for example, glial fibrillary acidic protein (a marker of central nervous system injury).²⁴ Graphene-based systems for detecting cancer cells have been also developed, using optical biosensors²⁵ or magnetic fluorescent biosensors.²⁶ A very good level of sensitivity has been achieved in both cases.

Another example is the use of graphene quantum dots modified with annexin V antibody to label apoptotic cells in live zebrafish. Graphene quantum dots have also been used in the imaging of human breast adenocarcinoma cell line (MCF-7 cells), human cervical cancer cell line (HeLa cells) and normal human mammary epithelial cell line (MCF-10A). The toxicity of graphene quantum dots has also been investigated; they were found to have high biocompatibility because they did not affect significantly the growth of zebrafish.²⁷

In cardiovascular medicine, as in oncology, the identification of at-risk patients might bring substantial advantages, as many life-threatening conditions develop suddenly, without clear pre-existing symptoms. Such is often the case with myocardial infarction and ischemic stroke. High levels of circulating platelet-derived microparticles are an associated risk of those events. A GO-based sensor highly specific for platelet-derived microparticles has been tested by Kailashiya et al.²⁸ The proposed sensor is postulated to be a convenient tool for identifying individuals at a high risk of such incidents.

In another study, a platinum nanoparticle-decorated rGO field effect transistor biosensor was used for highly sensitive detection of BNP – a molecule widely accepted as a marker of heart failure – in whole blood.²⁹

Detecting physical signals: Wearable sensors and ECG

It seems that the unique properties of graphene, such as its large specific surface area, outstanding mechanical flexibility, excellent thermal and electrical conductivity, high optical transmittance, and ultrahigh carrier mobility, make it a very promising material for the development of wearable sensors and implantable devices in health monitoring in all cases where detection of a physical signal is required.

Graphene on-skin wearable electrodes are characterized by high stretchability and durability.³⁰ The excellent air permeability of some designs is an improvement over the current electronic sensors, where constrained perspiration and inflammation risk remain issues.

The potential applications of such wearable sensors are not limited to strictly medical uses. The market demand for wearable electric devices is growing rapidly, especially with the ever-increasing popularity of exercise devices (heart rate monitors, etc.); the comfort of prolonged use and resistance to humidity, abrasion and tension are all very important features of sensors for such devices.

As opposed to wearable sensors, other designs make it possible to acquire the electrical signal directly from the heart and other tissues.

A flexible graphene-based microprobe developed using microelectromechanical technology was demonstrated to enable high-resolution detection of electrophysiological signals (including ECG) in zebrafish models. A special hydrophilization treatment was used to improve the signal-to-noise ratio of the device.³¹

The biocompatibility and suitability of graphene microelectrodes for extracellular recordings were also tested by measuring electrical activities from acute heart tissue and cardiac muscle cells. The recordings showed encouraging signal-to-noise ratios of 65:15 for heart tissue recordings and 20:10 for HL-1 cells. Due to low noise and excellent robustness, those sensor arrays might be suitable for diverse and biologically relevant applications.³²

Targeted therapy: Delivering drugs to selected cells

The successful treatment of many malignant tumors requires high concentrations of anti-tumor agents that are also lethal for healthy tissues. Several methods have been developed to facilitate only localized release (i.e., only to the tumor cells) of those potent drugs or physical impulses. In photothermal therapy, a light-controlled release of heat is used. Graphene nanomaterials are characterized by strong near-infrared absorbance and a large surface area (which can be functionalized with active molecules). Therefore, several groups have reported graphene-based methods of photothermal therapy, in some case coupled with photodynamic therapy and targeted chemotherapy.^{33,34} When treating solid tumors where penetration deep below the surface is required, an ultrasound rather than a light signal is used to provoke the desired effect (the release of the active substance or physical impulse). This approach is called sonodynamic therapy.³⁵ In each case, graphene-based materials were functionalized with photosensitizers, sonosensitizers, or anticancer drugs. Applications in photothermally controlled gene delivery have also been reported,³⁶ as has intracellular probing for specific proteins.³⁷

Regenerative medicine: Potential applications in orthopedics, neurology and cardiology

In the case of tissue loss or damage, traditional treatments use the patient's own tissue (autograft) or tissues from donors (allograft). Both methods have limitations, mainly a lack of sufficient "spare" healthy tissue in the case of autografts and a limited number of donors, technical

limitations of organ transplantation, and the need for immunosuppressive medication in the case of allografts. In contrast to those traditional methods, tissue engineering uses scaffold materials to control cell proliferation, differentiation, migration, and adhesion, as well as the growth of suitable extracellular matrix. Graphene and graphene-delivered materials have been proposed in tissue engineering techniques for bone, nervous and cardiac tissues.³⁸

In several *in vitro* studies, graphene-based materials have been shown to promote growth and osteogenic differentiation of mesenchymal stem cells.³⁹ In some studies, a special matrix composed of poly (L-lactic-co-glycolic acid), hydroxyapatite and GO was built, where GO increased the tensile strength of the material.⁴⁰ The matrix promoted protein adsorption, induced osteogenic function, and accelerated the proliferation and differentiation of human mesenchymal stem cells.

The incapacitating nature of many degenerative neurological diseases (such as Alzheimer's, Parkinson's, Huntington's, or amyotrophic lateral sclerosis) makes the potential regeneration of central nervous system cells and tissues a very interesting area of study. The effective differentiation of neural stem cells into uniaxially arranged neurons remains a substantial challenge. Nevertheless, some studies have reported promising results. As an example, a novel composite scaffold structure including aligned electrospun silk nanofibers and conductive reduced graphene paper enhanced the directional growth and differentiation of neurons.⁴¹ The presence of neuron marking proteins was confirmed in this study as well as the alignment and conductivity of the axons. In another study, a graphene-based hybrid nanofibrous scaffold promoted differentiation into oligodendrocytes.⁴²

Muscle tissue engineering has great potential value for treating damage and degeneration of skeletal muscles and many internal organs in which smooth muscle cells constitute an important part. Differentiation of murine myoblasts into myotubes on a graphene-containing platform was reported in 2 studies.^{43,44}

Given the prevalence of cardiovascular disease and its significant impact as one of the leading causes of mortality and morbidity in modern industrialized societies, any new treatment modality could have a huge impact on the healthcare system. Advanced heart failure is often associated with poor prognosis. This is mainly due to the fact that damage to cardiac tissue is irreversible in adults. Therefore, any progress in cardiac tissue engineering would be eagerly welcomed by cardiologists. Some interesting results in this area have been achieved with the use of graphene-derived materials. Biocompatibility and conductivity remain an important challenge for any cardiomyocyte scaffold. Such scaffolds using reduced GO were built by 2 groups and proved to be a satisfactory microenvironment for cardiomyocyte culturing.^{45,46} It was also found that GO improves the engraftment

of mesenchymal stem cells used to repair ischemia–reperfusion injury of the heart.⁴⁷

However, in another experiment on mouse embryos, graphene decreased the stem cell proliferation, probably by accelerating cell differentiation. The graphene also enhanced the mechanical properties and electrical conductivity of the tissue. Interestingly, the cardiac differentiation of the embryonic bodies with graphene was significantly greater than for those without graphene applied. The result was confirmed by high-throughput gene analysis.⁴⁸

In a study by Norahan et al., a collagen–GO composite cardiac patch showed angiogenic activity. Such a property might be useful when the patch is applied in the area of post-infarction injury.⁴⁹

In a rat model (both in vivo and in an isolated heart), a polymer chitosan scaffold containing GO was implanted in an infarcted heart. It was characterized by better (two-fold) conductivity than conventional chitosan scaffolds. It supported cell attachment and growth and showed no signs of toxicity; improved conductivity and contractility were also demonstrated.⁵⁰

An interesting effect was found by Ray et al.: GO interacted favorably with the His118 residue of NDPK to potentially prevent it from binding with adenosine triphosphate (ATP). As ATP would otherwise trigger the phosphorylation of the mutated G protein, the observed effect might eventually lead to increased cAMP levels during heart failure.⁵¹

Applications in cardiology: Electrotherapy

Modern electrotherapy is based on the presence of leads in the vascular system. Lead failure, infections and tricuspid valve insufficiency are the most common complications that arise. In patients with heart failure, the outcome of such infections may even be fatal, hence the different concepts of leadless pacing methods and the need to research new materials. Graphene and its derivatives, with known antimicrobial properties, might be considered interesting candidate materials for electrotherapy devices (both electrodes and device cans).

Graphene has been successfully used for sensors, including devices that provide a real-time electrocardiogram (ECG) signal.⁴⁵ On a zebrafish model, Chen et al. proved the concept of using a graphene microprobe to obtain high-resolution electrophysiological signals, including ECG, in vivo.³¹ This result provides a strong incentive for further research.

Park et al.⁴⁷ presented an extremely interesting concept that could become a form of electrotherapy in the treatment of heart failure. An epicardial mesh made of mechanically elastic and electrically conductive material was integrated with the heart and acted as a structural element with elastic properties similar to those of epicardial tissue.

The mesh detected the electrical signals of the moving rat heart and synchronized electrical stimulation over the ventricles. This design shortened total ventricular activation time, reduced wall stress and improved several indices of systolic functioning. The mesh was also successfully used to deliver a shock in order to terminate ventricular tachycardia. The features of this design constitute a comprehensive form of electrotherapy, currently a standard in heart failure treatment. The concept was very a sophisticated form of cardiomyoplasty – an idea of externally stabilizing cardiac muscle to prevent post-infarction remodeling.

Another potentially very promising field of research is the attempt to fabricate implantable protein-based bio-electrochemical capacitors (bECs) employing new nanocomposite heterostructures. In this model, 2D reduced GO sheets were interlayered with chemically modified mammalian proteins.⁵² The GO nanocomposite material showed no toxicity to mouse embryo fibroblasts. These unique capacitors, being protein-based devices, use serum as an electrolyte. They may be the first step in developing bio-friendly, protein-based batteries or supercapacitors using human bodily fluids as electrolytes. In the future, such solutions might eliminate the need to replace the electrotherapy devices when the battery is drained.

Applications in cardiology: Endovascular implants

As many disorders of the cardiovascular system are primarily caused by atherosclerosis, endovascular therapy remains crucially important in cardiology. The state-of-the-art coronary stents are characterized by very satisfactory mechanical properties and their biocompatibility is much better than that of the first bare-metal stents and the first drug-eluting stents designed almost 2 decades ago. Nevertheless, even after what seems to be a successful angioplasty, late complications such as restenosis and thrombosis may eventually lead to life-threatening events. The current understanding is that interactions between the stent surface, the cells of the vascular wall, and circulating blood are the underlying causes of these events. The quest for a perfect stent material and coating remains a leading research topic in interventional cardiology. Given the very structure of graphene itself (very thin sheets) and its chemical dissimilarity from both metal and the polymers so far investigated as stent materials, it seems logical to study the performance of graphene-related materials as coatings for cardiovascular stents.

A method of coating a stainless steel stent with graphene and graphene with TiO₂ was developed by ElSawy et al. The researchers examined the hemocompatibility of such coated stents and found neither platelet adhesion nor an adverse effect on erythrocytes or leukocytes.⁵³

In a study by Yang et al. a composite stent coating including GO performed better than other composite coatings – it had lower platelet adsorption and induced longer activated partial thromboplastin times (APTT) than other designs.⁵⁴

In another experiment, a novel composite drug-eluting coating was composed from magnetic mesoporous silica nanoparticles and carbon nanotubes. The nanostructured coating proved to be mechanically flexible and biocompatible with blood as well as offering very good drug release and loading properties. In vivo studies showed rapid endothelialization.⁵⁵

Pro-healing properties of GO coatings have also been investigated on a titanium stent. The coating enhanced endothelial cell adhesion and proliferation as compared with a polydopamine coating and the titanium blank. Loading heparin onto the GO coating significantly reduced platelet adhesion and prolonged the APTT, but it did not influence endothelial cell adhesion and proliferation. It was concluded by the authors that the heparin-loaded GO coating can simultaneously enhance the cytocompatibility to endothelial cells and blood compatibility of the biomaterials.⁵⁶

Another interesting design was evaluated by Ge et al. They covered a stainless steel stent with graphene and an antiproliferative drug. The stents were successfully implanted into rabbit carotid arteries. Several weeks after implantation, there were significantly fewer smooth muscle cells and less fibrin on the study stents than on the uncovered control stents. Most likely, the observed effect was due to the action of the antiproliferative drug, but the experiment demonstrates the feasibility of a graphene-coated drug-eluting stent. It is also worth noting that no toxic effects of the GO were observed on histological examination of the rabbit organs.⁵⁷

In a study performed by authors of this review, it was shown that graphene coating on 316L stainless steel supported the adhesion and proliferation of human primary coronary artery endothelial cells to a greater extent than the uncoated substrate. It was also proven that the coated surface has a unique potential to affect the endothelial cell phenotype by diminishing the endothelial-to-mesenchymal transition, thus possibly reducing the risk of in-stent restenosis.⁵⁸

As an example of a different approach, Misra et al. attempted to use graphene and similar materials, not as a coating but as a scaffold. A personalized 3D-printed cardiovascular stent was built from a biodegradable polymer carbon composite doped with graphene nanoplatelets (which ensured the controlled release of 2 types of drugs – antiproliferative and antirestenotic).⁵⁹

Artificial heart valves represent another type of intravascular implants where limited biocompatibility may lead to adverse events. Graphene oxide was tested as a potential coating for heart valves in a study by Wilczek et al. Platelet adhesion and activation was found to be similar to that of the control materials.⁶⁰

All those examples show that endovascular implant coating with graphene-derived materials is feasible and can offer satisfactory biocompatibility. Some results suggest that graphene promotes vascular healing and prevents both restenosis and thrombosis.

Summary

As this concise review indicates, graphene is a novel material with unique physical and chemical properties. Its biocompatibility has not yet been thoroughly investigated, but it seems that at least low concentrations are well-tolerated by cells and multicellular organisms. There are many biomedical applications proposed for graphene and its derivatives. They include areas as diverse as antimicrobial materials, physical and chemical sensors, targeted therapy and drug delivery, regeneration-promoting tissue scaffolds, and endovascular implant coatings. Many studies have demonstrated that at least basic conceptions of potential use of graphene-derived materials seem to be correct and reproducible on cellular and tissue scales. Nevertheless, only experiments involving whole multicellular organisms (of which very few have been conducted so far) will yield valid conclusions on the potential use of graphene in future diagnostics and therapy.

ORCID iDs

Jacek Arkowski  <https://orcid.org/0000-0003-2761-7580>
 Marta Obremska  <https://orcid.org/0000-0003-1937-1891>
 Kamil Kędzierski  <https://orcid.org/0000-0003-1340-7021>
 Agnieszka Sławuta  <https://orcid.org/0000-0001-5671-9864>
 Magdalena Wawrzyńska  <https://orcid.org/0000-0001-6855-5510>

References

1. Han S, Sun J, He S, Tang M, Chai R. The application of graphene-based biomaterials in biomedicine. *Am J Transl Res*. 2019;11(6):3246–3260.
2. Zhang B, Wang Y, Zhai G. Biomedical applications of the graphene-based materials. *Mater Sci Eng C Mater Biol Appl*. 2016;61:953–964. doi:10.1016/j.msec.2015.12.073
3. Jung JH, Cheon DS, Liu F, Lee KB, Seo TS. A graphene oxide based immuno-biosensor for pathogen detection. *Angew Chem Int Ed Engl*. 2010;49(33):5708–5711.
4. Gan S, Zhong L, Han D, Niu L, Chi Q. Probing bio–nano interactions between blood proteins and monolayer-stabilized graphene sheets. *Small*. 2015;11(43):5814–5825.
5. Tan X, Feng L, Zhang J, et al. Functionalization of graphene oxide generates a unique interface for selective serum protein interactions. *ACS Appl Mater Interfaces*. 2013;5(4):1370–1377.
6. Wang K, Ruan J, Song H, et al. Biocompatibility of graphene oxide. *Nanoscale Res Lett*. 2010;6(1):8.
7. Liao KH, Lin YS, Macosko CW, Haynes CL. Cytotoxicity of graphene oxide and graphene in human erythrocytes and skin fibroblasts. *ACS Appl Mater Interfaces*. 2011;3(7):2607–2615.
8. Sasiharan A, Panchakarla L, Chandran P, et al. Differential nano-bio interactions and toxicity effects of pristine versus functionalized graphene. *Nanoscale*. 2011;3(6):2461–2464.
9. Yang K, Gong H, Shi X, Wan J, Zhang Y, Liu Z. In vivo biodistribution and toxicology of functionalized nano-graphene oxide in mice after oral and intraperitoneal administration. *Biomaterials*. 2013;34(11):2787–2795.
10. Luan B, Huynh T, Zhao L, Zhou R. Potential toxicity of graphene to cell functions via disrupting protein-protein interactions. *ACS Nano*. 2015;9(1):663–669.

11. Chang Y, Yang S, Liu J, et al. In vitro toxicity evaluation of graphene oxide on A549 cells. *Toxicol Lett.* 2011;200(3):201–210.
12. Zhang D, Zhang Z, Wu Y, et al. Systematic evaluation of graphene quantum dot toxicity to male mouse sexual behaviors, reproductive and offspring health. *Biomaterials.* 2019;194:215–232.
13. Jiang D, Chen Y, Li N, et al. Synthesis of luminescent graphene quantum dots with high quantum yield and their toxicity study. *PLoS One.* 2015;10(12):e0144906. doi:10.1371/journal.pone.0144906
14. Perreault F, de Faria AF, Nejadi S, Elimelech M. Antimicrobial properties of graphene oxide nanosheets: Why size matters. *ACS Nano.* 2015;9(7):7226–7336.
15. Wang J, Wei Y, Shi X, Gao H. Cellular entry of graphene nanosheets: The role of thickness, oxidation and surface adsorption. *RSC Adv.* 2013;3(36):15776.
16. Sadhukhan S, Ghosh TK, Roy I, et al. Green synthesis of cadmium oxide decorated reduced graphene oxide nanocomposites and its electrical and antibacterial properties. *Mater Sci Eng C.* 2019;99:696–709.
17. Akhavan O, Ghaderi E. Toxicity of graphene and graphene oxide nanowalls against bacteria. *ACS Nano.* 2010;4(10):5731–5736.
18. Tu Y, Lv M, Xiu P, et al. Destructive extraction of phospholipids from *Escherichia coli* membranes by graphene nanosheets. *Nat Nanotechnol.* 2013;8(8):594–601.
19. Ullaha S, Ahmada A, Subhanb F, et al. Tobramycin mediated silver nanospheres/graphene oxide composite for synergistic therapy of bacterial infection. *J Photochem Photobiol B.* 2018;183:342–348.
20. Gurunathan S, Han JW, Abdal Dayem A, Eppakayala V, Kim JH. Oxidative stress-mediated antibacterial activity of graphene oxide and reduced graphene oxide in *Pseudomonas aeruginosa*. *Int J Nanomedicine.* 2012;7:5901–5914.
21. Some S, Ho SM, Dua P, et al. Dual functions of highly potent graphene derivative-poly-L-lysine composites to inhibit bacteria and support human cells. *ACS Nano.* 2012;6(8):7151–7161.
22. Jiang B, Zhou K, Wang C, et al. Label-free glucose biosensor based on enzymatic graphene oxide-functionalized tilted fiber grating. *Sensor Actuat B.* 2018;254:1033–1039.
23. Li B, Yu A, Lai G. Self-assembly of phenoxyl-dextran on electrochemically reduced graphene oxide for nonenzymatic biosensing of glucose. *Carbon.* 2018;127:202–208.
24. Khetani S, Kollath VO, Kundra V, et al. Polyethylenimine modified graphene-oxide electrochemical immunosensor for the detection of glial fibrillary acidic protein in central nervous system injury. *ACS Sens.* 2018;3(4):844–851.
25. Wang Y, Zhang S, Xu T, et al. Ultra-sensitive and ultra-fast detection of whole unlabeled living cancer cell responses to paclitaxel with a graphene-based biosensor. *Sensor Actuat B.* 2018;263:417–425.
26. Cui F, Ji J, Sun J, et al. A novel magnetic fluorescent biosensor based on graphene quantum dots for rapid, efficient, and sensitive separation and detection of circulating tumor cells. *Anal Bioanal Chem.* 2019;411(5):985–995.
27. Roy P, Periasamy AP, Lin CY, et al. Photoluminescent graphene quantum dots for in vivo imaging of apoptotic cells. *Nanoscale.* 2015;7(6):2504–2510. doi:10.1039/c4nr07005d
28. Kailashiya J, Singh N, Singh SK, Agrawal V, Dash D. Graphene oxide-based biosensor for detection of platelet-derived microparticles: A potential tool for thrombus risk identification. *Biosens Bioelectron.* 2015;65:274–280. doi:10.1016/j.bios.2014.10.056
29. Lei YM, Xiao MM, Li YT, et al. Detection of heart failure-related biomarker in whole blood with graphene field effect transistor biosensor. *Biosens Bioelectron.* 2017;91:1–7. doi:10.1016/j.bios.2016.12.018
30. Sun B, McCay RN, Goswami S, et al. Gas-permeable, multifunctional on-skin electronics based on laser-induced porous graphene and sugar-templated elastomer sponges. *Adv Mater.* 2018;30(50):e1804327. doi:10.1002/adma.201804327
31. Chen CH, Lin CT, Hsu WL, et al. A flexible hydrophilic-modified graphene microprobe for neural and cardiac recording. *Nanomedicine.* 2013;9(5):600–604. doi:10.1016/j.nano.2012.12.004
32. Kireev D, Seyock S, Ernst M, Maybeck V, Wolfrum B, Offenhäusser A. Versatile flexible graphene multielectrode arrays. *Biosensors (Basel).* 2016;7(1):1. doi:10.3390/bios7010001
33. Yang K, Zhang S, Zhang G, Sun X, Lee ST, Liu Z. Graphene in mice: Ultrahigh in vivo tumor uptake and efficient photothermal therapy. *Nano Lett.* 2010;10(9):3318–3323.
34. Zhang L, Xia J, Zhao Q, Liu L, Zhang Z. Functional graphene oxide as a nanocarrier for controlled loading and targeted delivery of mixed anticancer drugs. *Small.* 2010;6(4):537–544.
35. Chen Y, Liu T, Chang P, et al. A theranostic nrGO@MSN-ION nanocarrier developed to enhance the combination effect of sonodynamic therapy and ultrasound hyperthermia for treating tumor. *Nanoscale.* 2016;8(25):12648–12657.
36. Kim H, Kim WJ. Photothermally controlled gene delivery by reduced graphene oxide-polyethylenimine nanocomposite. *Small.* 2014;10(1):117–126.
37. Wang Y, Li Z, Hu D, Lin CT, Li J, Lin Y. Aptamer/graphene oxide nanocomplex for in situ molecular probing in living cells. *J Am Chem Soc.* 2010;132(27):9274–9276.
38. Kim TH, Lee T, El-Said WA, Choi JW. Graphene-based materials for stem cell applications. *Materials (Basel).* 2015;8(12):8674–8690. doi:10.3390/ma8125481
39. Elkhenany H, Amelse L, Lafont A, et al. Graphene supports in vitro proliferation and osteogenic differentiation of goat adult mesenchymal stem cells: Potential for bone tissue engineering. *J Appl Toxicol.* 2015;35(4):367–374.
40. Fu C, Bai H, Zhu J, et al. Enhanced cell proliferation and osteogenic differentiation in electrospun PLGA/hydroxyapatite nanofiber scaffolds incorporated with graphene oxide. *PLoS One.* 2017;12(11):e0188352. doi:10.1371/journal.pone.0188352
41. Qing H, Jin G, Zhao G, et al. Heterostructured silk-nanofiber-reduced graphene oxide composite scaffold for sh-sy5y cell alignment and differentiation. *ACS Appl Mater Interfaces.* 2018;10(45):39228–39237.
42. Shah S, Yin PT, Uehara TM, Chueng SD, Yang L, Lee K. Guiding stem cell differentiation into oligodendrocytes using graphene-nanofiber hybrid scaffolds. *Adv Mater.* 2014;26(22):3673–3680.
43. Ku SH, Park CB. Myoblast differentiation on graphene oxide. *Biomaterials.* 2013;34(8):2017–2023.
44. Krueger E, Chang AN, Brown D, et al. Graphene foam as a three-dimensional platform for myotube growth. *ACS Biomater Sci Eng.* 2016;2(8):1234–1241.
45. Ameri SK, Singh PK, D'Angelo R, Stoppel W, Black L, Sonkusale SR. Three dimensional graphene scaffold for cardiac tissue engineering and in-situ electrical recording. *Annu Int Conf Proc IEEE Eng Med Biol Soc.* 2016;2016:4201–4203.
46. Shin SR, Zihlmann C, Akbari M, et al. Reduced graphene oxide-gelMA hybrid hydrogels as scaffolds for cardiac tissue engineering. *Small.* 2016;12(27):3677–3689.
47. Park J, Kim B, Han J, et al. Graphene oxide flakes as a cellular adhesive: Prevention of reactive oxygen species mediated death of implanted cells for cardiac repair. *ACS Nano.* 2015;9(5):4987–4999. doi:10.1021/nn507149w
48. Ahadian S, Zhou Y, Yamada S, et al. Graphene induces spontaneous cardiac differentiation in embryoid bodies. *Nanoscale.* 2016;8(13):7075–7084. doi:10.1039/c5nr07059g
49. Norahan MH, Amroon M, Hahremanzadeh R, Mahmoodi M, Baheiraei N. Electroactive graphene oxide-incorporated collagen assisting vascularization for cardiac tissue engineering. *J Biomed Mater Res A.* 2019;107(1):204–219. doi:10.1002/jbm.a.36555
50. Saravanan S, Sareen N, Abu-El-Rub E, et al. Graphene oxide-gold nanosheets containing chitosan scaffold improves ventricular contractility and function after implantation into infarcted heart. *Sci Rep.* 2018;8(1):15069. doi:10.1038/s41598-018-33144-0
51. Ray A, Macwan I, Singh S, Silwal S, Patra P. A computational approach for understanding the interactions between graphene oxide and nucleoside diphosphate kinase with implications for heart failure. *Nanomaterials (Basel).* 2018;8(2):57. doi:10.3390/nano8020057
52. Mosa IM, Pattammattel A, Kadimisetty K, et al. Ultrathin graphene-protein supercapacitors for miniaturized bioelectronics. *Adv Energy Mater.* 2017;7(17):1700358.
53. ElSawy AM, Attia NF, Mohamed HI, Mohsen M, Talaat MH. Innovative coating based on graphene and their decorated nanoparticles for medical stent applications. *Mater Sci Eng C Mater Biol Appl.* 2019;96:708–715. doi:10.1016/j.msec.2018.11.084
54. Yang MC, Tsou HM, Hsiao YS, et al. Electrochemical polymerization of PEDOT-graphene oxide-heparin composite coating for anti-fouling and anti-clotting of cardiovascular stents. *Polymers (Basel).* 2019;11(9):1520. doi:10.3390/polym11091520

55. Wang Y, Zhang W, Zhang J, Sun W, Zhang R, Gu H. Fabrication of a novel polymer-free nanostructured drug-eluting coating for cardiovascular stents. *ACS Appl Mater Interfaces*. 2013;5(20):10337–10345.
56. Pan CJ, Pang LQ, Gao F, et al. Anticoagulation and endothelial cell behaviors of heparin-loaded graphene oxide coating on titanium surface. *Mater Sci Eng C Mater Biol Appl*. 2016;63:333–340. doi:10.1016/j.msec.2016.03.001
57. Ge S, Xi Y, Du R, et al. Inhibition of in-stent restenosis after graphene oxide double-layer drug coating with good biocompatibility. *Regen Biomater*. 2019;6(5):299–309. doi:10.1093/rb/rbz010
58. Wawrzyńska M, Bil-Lula I, Krzywonos-Zawadzka A, et al. Biocompatible carbon-based coating as potential endovascular material for stent surface. *Biomed Res Int*. 2018;2018:2758347. doi:10.1155/2018/2758347
59. Misra SK, Ostadhossein F, Babu R, et al. 3D-printed multidrug-eluting stent from graphenenanoplatelet-doped biodegradable polymer composite. *Adv Healthc Mater*. 2017;6(11). doi:10.1002/adhm.201700008
60. Wilczek P, Major R, Lipinska L, Lackner J, Mzyk A. Thrombogenicity and biocompatibility studies of reduced graphene oxide modified acellular pulmonary valve tissue. *Mater Sci Eng C Mater Biol Appl*. 2015;53:310–321. doi:10.1016/j.msec.2015.04.044

The emerging role of mood disorders in inflammatory bowel diseases

Paweł Kuźnicki^{A–F}, Radosław Kempniński^{D–F}, Katarzyna Neubauer^{A–F}

Department of Gastroenterology and Hepatology, Wrocław Medical University, Poland

A – research concept and design; B – collection and/or assembly of data; C – data analysis and interpretation;

D – writing the article; E – critical revision of the article; F – final approval of the article

Advances in Clinical and Experimental Medicine, ISSN 1899–5276 (print), ISSN 2451–2680 (online)

Adv Clin Exp Med. 2020;29(12):1505–1510

Address for correspondence

Paweł Kuźnicki

E-mail: pawel.kuznicki@student.umed.wroc.pl

Funding sources

The article processing charge was funded by Wrocław Medical University, Poland.

Conflict of interest

None declared

Received on June 17, 2020

Reviewed on June 24, 2020

Accepted on September 2, 2020

Abstract

Inflammatory bowel diseases (IBD) are chronic, devastating conditions of the gastrointestinal tract characterized by a complex pathogenesis, increasing worldwide prevalence, a wide spectrum of extraintestinal manifestations, and a reduced health-related quality of life (HRQoL). Furthermore, mood disorders, specifically anxiety and depression, are more prevalent among IBD patients compared to the general population. The connection between mental disorders and IBD is compound, bidirectional and still not fully understood. The IBD may impact psychological health, whereas anxiety and depression are associated with a more aggressive course of IBD. The inflammation process, gut microbiota alterations and drug side effects are factors that influence the mental state of patients with IBD. Importantly, despite the high prevalence of depression and anxiety in IBD, many of the current guidelines do not include clear recommendation for assessment of mental problems in patients and further management. Therefore, monitoring for mood disorders should become a part of the multi-disciplinary and holistic approach to patients with IBD. This review is based on current literature searched in PubMed, mainly considering publications from the last 10 years.

Key words: depression, anxiety, inflammatory bowel disease, ulcerative colitis, Crohn's disease

Cite as

Kuźnicki P, Kempniński R, Neubauer K. The emerging role of mood disorders in inflammatory bowel diseases.

Adv Clin Exp Med. 2020;29(12):1505–1510.

doi:10.17219/acem/127676

DOI

10.17219/acem/127676

Copyright

© 2020 by Wrocław Medical University

This is an article distributed under the terms of the Creative Commons Attribution 3.0 Unported (CC BY 3.0)

(<https://creativecommons.org/licenses/by/3.0/>)

Introduction

Inflammatory bowel diseases (IBD), encompassing ulcerative colitis (UC) and Crohn's disease (CD), are chronic, devastating conditions of the gastrointestinal tract, characterized by a relapsing course with periods of flares and remissions and the presence of the wide spectrum of extraintestinal manifestations (EMs).¹ The prevalence of IBD is increasing worldwide, especially in highly developed countries, where about 0.3% of the population is already suffering from them, and in newly industrialized regions of the world.² For instance, in Canada, one of the countries with the highest incidence of IBD, it is estimated that 0.9% of the population will be affected in 2025, whereas in China there will be over 1.5 million cases of IBD by that time.^{3,4} Furthermore, the etiopathogenesis of IBD has not been fully elucidated. The key role in the development of the disease is played by the interaction of genetic, immunological, microbiological, and environmental factors. Consequently, there are no single diagnostic tests, and despite the introduction of novel biological treatment strategies, effective therapy remains unavailable. Additionally, it has repeatedly been demonstrated that the health-related quality of life (HRQoL) of IBD patients is significantly reduced. For example, a recently published meta-analysis, which encompassed 7154 patients, demonstrated that in all 19 studies included, the QoL levels in IBD patients compared to healthy controls were poorer in at least 1 aspect.⁵ Furthermore, almost 40% of IBD patients in remission suffer from fatigue, which has a negative impact on HRQoL⁶ independently of disease activity. Last of all, anxiety and depression disorders are more prevalent in IBD patients compared to the general population, and the interrelation between the conditions is unclear. The gut–brain axis and interference of numerous agents in communication between the gut and the brain seem to play a crucial role. Among the suggested mechanisms are activation of the inflammatory response in the brain, compromised blood–brain barrier integrity and the impact of gut microbiota.⁷ The results of studies on the impact of mental disorders on IBD onset and course are inconclusive. Additionally, in a recently published study it was demonstrated that patients with anxiety, depression and immune-mediated disorders (including IBD, multiple sclerosis and rheumatoid arthritis) had reduced cognitive function.⁸ Moreover, 1/3 of IBD patients with depression and 2/3 of those with anxiety remained undiagnosed.⁹ It also has to be emphasized that all the aforementioned factors, along with the fact that the onset of IBD is associated with young age, indicate not only the necessity of further research, but above all the importance of including the mental aspects in IBD patients' care.

Epidemiology of depression and anxiety disorders in patients with IBD

Patients with IBD have a 2- to 4-fold greater risk of developing depressive disorders and a 3- to 5-fold of greater risk of developing anxiety disorders than the general population.¹⁰ Many cases of psychiatric disorders remain undiagnosed.¹¹ Many studies have repeatedly demonstrated that psychological problems are more common in patients with active disease compared to those in remission; that patients with CD are at higher risk than those with UC; and that women are affected more often than men.^{12,13} However, the occurrence of depression and anxiety in IBD is similar or even less frequent than their occurrence with other chronic disorders (Table 1).^{14,15}

Table 1. Factors related to the prevalence of anxiety and depression disorders in IBD patients

| Depression and anxiety in IBD patients | | |
|--|---|------------------------|
| IBD | > | general population |
| IBD | ≤ | other chronic diseases |
| CD | > | UC |
| flare | > | remission |
| woman | > | man |

IBD – inflammatory bowel diseases; CD – Crohn's disease; UC – ulcerative colitis.

Furthermore, in a large study conducted in Canada, the prevalence and incidence of depression, anxiety, bipolar disorders, and schizophrenia were higher in IBD individuals than in a matched cohort of the general population. The study, comprising more than 6000 IBD patients, showed that women were more often affected by depression and anxiety than men. However, the authors also observed that the incidence of psychiatric disorders was higher in individuals aged 18–24 years, in urbanites and in individuals of lower socioeconomic status.¹⁶ There is a growing body of evidence that the prevalence of mental health problems in IBD patients is increasing. For instance, in a cohort of more than 60,000 US veterans with IBD, the annual age-standardized prevalence rates of depression and anxiety increased respectively 3.75-fold and 5-fold in the years 2001–2015.¹⁷

Selected studies evaluating the prevalence of anxiety and depression disorders and associated factors among IBD patients are presented in Table 2.

Gut microbiota

Gut microbiota is involved in IBD pathogenesis and is simultaneously among the crucial factors interfering with the gut–brain axis. Therefore, the gut microbiome can be a link between IBD and mental disorders. Characteristic

Table 2. Prevalence of anxiety and depression disorders in IBD patients

| Author, year | Number of IBD patients | Prevalence of anxiety | Prevalence of depression | Associated factors |
|--|------------------------|----------------------------|--------------------------|--|
| van den Brink et al., 2020 ¹⁸ | 374 | 28.3% | 2.9% | female sex, disease activity, disease duration |
| Choi et al., 2019 ¹⁹ | 15569 | CD – 11.5%* UC – 16.7%* | CD – 8%* UC – 10.8%* | medication use, comorbid medical conditions |
| Lewis et al., 2019 ⁹ | 242 | 40.1% | 30.6% | female sex for depression |
| Bhamre et al., 2018 ²⁰ | 70 | 18.6% | 34.3% | disease activity |
| Navabi et al., 2018 ²¹ | 432 | 39.4% | 25% | female sex, extra-intestinal manifestations of IBD, prior IBD-related surgery, tobacco use in CD |
| Byrne et al., 2017 ²² | 327 | 21.2% | 25.8% | female sex, disease activity |
| Chan et al., 2017 ²³ | 200 | 27% | | |
| Bennebroek Evertsz' et al., 2012 ²⁴ | 231 | 42.6% | | disease activity |

*6 years after diagnosis; IBD – inflammatory bowel diseases; CD – Crohn's disease.

differences in the abundance of individual microbiota species in IBD patients with associated anxiety and depression disorders as well as reduced HRQoL have been identified.²⁵ Dysbiosis is associated with abnormal metabolism of tryptophan, which under normal conditions passes through the blood–brain barrier and becomes a precursor of serotonin. In an alternative pathway, especially intensified in the case of intestinal inflammation, tryptophan can be metabolized to kynurenine and its derivatives, leading to the development of depressive disorders both by the direct action of these substances on neuronal transmission and indirectly by decreasing serotonin levels.²⁶ In addition, through fermentation of dietary fibers, gut microbiota is responsible for the production of short chain fatty acids (SCFAs), which control the inflammation process of the intestines. In IBD, the amount of SCFAs is reduced, so the concentration of some of their metabolites is also reduced. One of them, gamma-aminobutyric acid, is inhibitory neurotransmitter involved in the development of anxiety and depression.^{27,28} This connection may be the starting point for creating a future therapeutic strategy based on selective manipulation of microbiota species to modify the course of both IBD and associated mental disorders. However, even if the results of preliminary studies on the influence of gut microbiota modulation on depression and anxiety in IBD patients are promising, there is not enough evidence to apply it in clinical practice.²⁹

Ingesting certain microorganisms can influence human brain activity in specific regions modifying behavior, emotions and cognition. Additionally, it can lead to decreases in the concentration of stress hormones. These findings mean that some probiotic species, which in this context are termed 'psychobiotics', may be usable as a treatment option. Interestingly, microbiome alterations may be significant in psychiatric pharmacotherapy, because some drugs currently prescribed by psychiatrists or neurologists

were used as antibacterial agents in the past. However, as already mentioned, scientific evidence is still insufficient to recommend psychobiotics as a form of therapy.^{30,31}

The impact of depression and anxiety disorders on IBD onset

The influence of mental disorders on the development of IBD remains unclear. It is suggested that abnormalities in mental functioning may occur several years before the diagnosis of intestinal disease. For instance, a Canadian study demonstrated that anxiety disorders and mood disorders were diagnosed in respectively 80% and 54% of patients with IBD on average 2 years before the IBD diagnosis. Additionally, patients with depression and anxiety disorders were diagnosed with the disease earlier (34.9 years on average) than those without these disorders (37.8 years on average).¹³ In subsequent studies, it was found that the interval between the deterioration of mental functioning and the diagnosis of intestinal disease may be even longer, and could be up to 5 years.³²

Impact of anxiety and depression disorders on the course of IBD

Depression and anxiety associated with IBD may directly affect its course. The correlation between intestinal disease activity and worsened mental condition is particularly evident in patients who believe that psychological stress contributes to exacerbations.³³ It was observed that IBD patients with accompanying mental disorders have increased likelihoods of surgical interventions, extended diagnostics with additional examinations, such as computer tomography (CT) or multiple colonoscopies, as well as a need for

corticosteroids, immunomodulators or anti-tumor necrosis factor (TNF) therapy.³⁴ The presence of depressive symptoms can worsen the course of IBD and may be considered a predictor of aggressive, recurrent disease.^{35,36}

One of the suggested mechanisms explaining how depression can influence the activity and severity of IBD is its impact on the inflammatory process. For instance, in about 80% of severely depressed patients, hyperactivity of the hypothalamic-pituitary-adrenal (HPA) axis is observed. The resulting chronic hypercortisolemia leads to elevation of pro-inflammatory mediators.³⁷ Moreover, depression is associated with decreased parasympathetic activity of the autonomic nervous system (ANS), which causes inhibition of macrophage activation through the cholinergic anti-inflammatory pathway. As a result, depression clearly influences the Crohn's Disease Activity Index score in CD patients, can lead to exacerbations of IBD and increases the rate of failure during infliximab treatment. In a study of 100 people with CD, it turned out that patients with major depressive disorder (MDD) found it harder to achieve remission. Persistent MDD after adequate treatment of CD with infliximab is a risk factor for the need of early retreatment.^{38,39}

Interestingly, a study of a small group of women with depression showed that treating them with behavioral-cognitive therapy resulted in a decrease in the concentration of interleukin 6 (IL-6), which is one of the major pro-inflammatory cytokines in IBD.⁴⁰ According to another meta-analysis, behavioral-cognitive therapy in patients with IBD has limited and short-term effectiveness in treating depressive symptoms and improving HRQoL, without affecting anxiety, stress levels or disease activity.⁴¹

Regarding pharmacotherapy of depression and anxiety disorders in IBD, although antidepressants are commonly used by these patients with (based on previous research) apparently beneficial effects, it is not possible to determine conclusively whether pharmacotherapy affects the course of IBD.⁴² Central neuromodulators may be used in painful IBD as supplements to peripheral agents, like in the management of functional disorders. In cases of major psychiatric problems, consulting with a psychiatrist to optimize therapy is recommended.⁴³ The previously described potential benefits of using antidepressants may be associated with a reduction in inflammatory processes or simply with mood improvement.⁴⁴ For now, it is only known that the use of certain antidepressants reduces the risk of intestinal disease in the future.⁴⁵ Properly conducted randomized controlled trials are necessary to accurately define their efficacy.

The impact of IBD on anxiety and mental disorders

Depressive disorders are accompanied by elevated concentrations of pro-inflammatory mediators such as C-reactive protein (CRP), IL-6, IL-1, IL-12, and TNF- α .^{38,46} It has

been suggested that CRP levels might be used to predict the severity and recurrence of depression.⁴⁷ Consequently, patients with CD who received anti-inflammatory therapy with anti-TNF agents (infliximab or adalimumab) reported rapid improvement in depressive disorders. Most importantly, this was not associated solely with clinical improvement of their IBD.^{48–50}

Sleep disorders observed in patients with IBD, which are closely related to depression, may be a marker of subclinical inflammation or persistent histologic disease activity. It has been suggested that elevated levels of circulating cytokines contribute to sleep disturbances, even in clinical remission. Injection of pro-inflammatory IL-1 or TNF in animal models suppresses rapid-eye movement (REM) sleep and alters sleep patterns. Additionally, administration of IL-6 increases non-rapid eye movement (NREM) sleep and reduces slow-wave sleep during the 1st half of the sleep cycle.⁵¹ Interestingly, some studies have shown that CD patients who have impaired sleep quality while in clinical remission have a greater risk of disease flare-ups. This is why sleep disturbances, potentially modifiable risk factors for IBD relapse, should be considered for routine assessment in patients.^{52–54}

Depression as a side effect of IBD treatment

Drugs used in the treatment of IBD may also influence the occurrence of depression and anxiety disorders. It is known that long-term use of glucocorticosteroids negatively affects the mood of patients.⁵⁵ Interestingly, in previous randomized clinical trials and observational studies, adverse psychiatric effects (APE) during biological treatment were very rare or absent. However, the exact frequency of them among biologically treated patients is difficult to assess, because many studies do not consider adverse effects of the drug on the patient's psychological state. It is not known whether the authors did not observe such effects or whether they did not collect data related to this aspect.⁵⁶

Depression and anxiety disorders in the guidelines

In the recent guidelines of the European Crohn's and Colitis Organization (ECCO) regarding the management of CD (2019) and UC (2017), there are no recommendations concerning assessment of the patients' mental state and possible therapeutic interventions.^{57,58} Such recommendations appeared in the 2018 Nurses' European Crohn's and Colitis Organization (N-ECCO) consensus regarding the role of nurses in caring for patients with IBD. According to this document, nurses should be aware of more frequent depression and anxiety disorders among


the patients than in the general population, and, if necessary, should refer selected patients to a specialist.⁵⁹ The British Gastroenterology Association also took a position on this matter in guidelines issued in 2019. The British recommendations suggest supportive behavioral therapy, hypnotherapy or mindfulness meditation for interested patients. Similarly, the German Clinical Practice Guideline on IBD emphasizes the significance of accompanying psychiatric symptoms. So far, no reliable studies have been conducted in patients with IBD and depression or anxiety disorders that may provide a basis for recommending antidepressants.^{60,61}


Conclusions

The risk of depression and anxiety disorders in patients with IBD is significantly higher than in the general population, so both family physicians and gastroenterologists should consider them in patients under their care, as they can negatively impact the course of the disease. Nevertheless, the current guidelines refer to this problem only to a limited extent at best. Considering the close relationship between depression and anxiety and the degree of disease activity, optimization of IBD treatment should include psychiatric, psychological and social support. Due to the steadily increasing incidence of IBD, a holistic approach is needed, both to avoid the development of depression-related disabilities and to improve HRQoL and patient–doctor compliance.

ORCID iDs

Paweł Kuźnicki  <https://orcid.org/0000-0003-2190-3754>

Radosław Kempniński  <https://orcid.org/0000-0002-6030-2700>

Katarzyna Neubauer  <https://orcid.org/0000-0003-3650-9311>

References

- Vavricka SR, Schoepfer A, Scharl M, Lakatos PL, Navarini A, Rogler G. Extraintestinal manifestations of inflammatory bowel disease. *Inflamm Bowel Dis*. 2015;21(8):1982–1992. doi:10.1097/MIB.0000000000000392
- Ng SC, Shi HY, Hamidi N, et al. Worldwide incidence and prevalence of inflammatory bowel disease in the 21st century: A systematic review of population-based studies. *Lancet*. 2017;390(10114):2769–2778. doi:10.1016/S0140-6736(17)32448-0
- Coward S, Clement F, Williamson T, et al. The rising burden of inflammatory bowel disease in North America from 2015 to 2025: A predictive model. *Am J Gastroenterol*. 2015;110:S829.
- Kaplan GG. The global burden of IBD: From 2015 to 2025. *Nat Rev Gastroenterol Hepatol*. 2015;12(12):720–727. doi:10.1038/nrgastro.2015.150
- Knowles SR, Graff LA, Wilding H, Hewitt C, Keefer L, Mikocka-Walus A. Quality of life in inflammatory bowel disease: A systematic review and meta-analyses – Part I. *Inflamm Bowel Dis*. 2018;24(4):742–751. doi:10.1093/ibd/izx100
- Romberg-Camps MJL, Bol Y, Dagnelie PC, et al. Fatigue and health-related quality of life in inflammatory bowel disease. Results from a population-based study in the Netherlands: The IBD-South Limburg cohort. *Inflamm Bowel Dis*. 2010;16(12):2137–2147. doi:10.1002/ibd.21285
- Abautret-Daly Á, Dempsey E, Parra-Blanco A, Medina C, Harkin A. Gut–brain actions underlying comorbid anxiety and depression associated with inflammatory bowel disease. *Acta Neuropsychiatr*. 2018;30(5):275–296. doi:10.1017/neu.2017.3
- Whitehouse CE, Fisk JD, Bernstein CN, et al. Comorbid anxiety, depression and cognition in MS and other immune-mediated disorders. *Neurology*. 2019;92(5):e406–e417. doi:10.1212/WNL.0000000000006854
- Lewis K, Marrie RA, Bernstein CN, et al; CIHR Team in Defining the Burden and Managing the Effects of Immune-Mediated Inflammatory Disease. The prevalence and risk factors of undiagnosed depression and anxiety disorders among patients with inflammatory bowel disease. *Inflamm Bowel Dis*. 2019;25(10):1674–1680. doi:10.1093/ibd/izz045
- Graff LA, Walker JR, Bernstein CN. Depression and anxiety in inflammatory bowel disease: A review of comorbidity and management. *Inflamm Bowel Dis*. 2009;5(7):1105–1118. doi:10.1002/ibd.20873
- Marafini I, Longo L, Lavasani DM, et al. High frequency of undiagnosed psychiatric disorders in inflammatory bowel diseases. *J Clin Med*. 2020;9(5):1387. doi:10.3390/jcm9051387
- Panara AJ, Yarur AJ, Rieders B, et al. The incidence and risk factors for developing depression after being diagnosed with inflammatory bowel disease: A cohort study. *Aliment Pharmacol Ther*. 2014;39(8):802–810. doi:10.1111/apt.12669
- Walker JR, Ediger JP, Graff LA, et al. The Manitoba IBD cohort study: A population-based study of the prevalence of lifetime and 12-month anxiety and mood disorders. *Am J Gastroenterol*. 2008;103(8):1989–1997. doi:10.1111/j.1572-0241.2008.01980.x
- Mikocka-Walus A, Knowles SR, Keefer L, Graff L. Controversies revisited: A systematic review of the comorbidity of depression and anxiety with inflammatory bowel diseases. *Inflamm Bowel Dis*. 2015;22(3):752–762. doi:10.1097/MIB.0000000000000620
- Zhang CK, Hewett J, Hemming J, et al. The influence of depression on quality of life in patients with inflammatory bowel disease. *Inflamm Bowel Dis*. 2013;19(8):1732–1739. doi:10.1097/MIB.0b013e318281f395
- Bernstein CN, Hitchon CA, Walld R, et al. Increased burden of psychiatric disorders in inflammatory bowel disease. *Inflamm Bowel Dis*. 2019;25(2):360–368. doi:10.1093/ibd/izy235
- Thakur ER, Sangsriy S, Kramer JR, et al. The incidence and prevalence of anxiety, depression and post-traumatic stress disorder in a national cohort of US veterans with inflammatory bowel disease. *Inflamm Bowel Dis*. 2019;26(9):1423–1428. doi:10.1093/ibd/izz280
- van den Brink G, Stapersma L, Vlug LE, et al. Clinical disease activity is associated with anxiety and depressive symptoms in adolescents and young adults with inflammatory bowel disease. *Aliment Pharmacol Ther*. 2018;48(3):358–369. doi:10.1111/apt.14832
- Choi K, Chun J, Han K, et al. Risk of anxiety and depression in patients with inflammatory bowel disease: A nationwide, population-based study. *J Clin Med*. 2019;8(5):654. doi:10.3390/jcm8050654
- Bhamre R, Sawrav S, Adarkar S, Sakaria R, J Bhatia S. Psychiatric comorbidities in patients with inflammatory bowel disease. *Indian J Gastroenterol*. 2018;37(4):307–312. doi:10.1007/s12664-018-0870-9
- Navabi S, Gorrepati VS, Yadav S, et al. Influences and impact of anxiety and depression in the setting of inflammatory bowel disease. *Inflamm Bowel Dis*. 2018;24(11):2303–2308. doi:10.1093/IBD/IZY143
- Byrne G, Rosenfeld G, Leung Y, et al. Prevalence of anxiety and depression in patients with inflammatory bowel disease. *Can J Gastroenterol Hepatol*. 2017;2017:6496727. doi:10.1155/2017/6496727
- Chan W, Shim HH, Lim MS, et al. Symptoms of anxiety and depression are independently associated with inflammatory bowel disease-related disability. *Dig Liver Dis*. 2017;49(12):1314–1319. doi:10.1016/j.dld.2017.08.020
- Bennebroek Evertsz' F, Thijssens NAM, Stokkers PCF, et al. Do inflammatory bowel disease patients with anxiety and depressive symptoms receive the care they need? *J Crohns Colitis*. 2012;6(1):68–76. doi:10.1016/j.crohns.2011.07.006
- Humbel F, Rieder JH, Franc Y, et al; Swiss IBD Cohort Study Group. Association of alterations in intestinal microbiota with impaired psychological function in patients with inflammatory bowel diseases in remission. *Clin Gastroenterol Hepatol*. 2019;18(9):2019–2029.e11. doi:10.1016/j.cgh.2019.09.022
- Waclawiková B, El Aidy S. Role of microbiota and tryptophan metabolites in the remote effect of intestinal inflammation on brain and depression. *Pharmaceuticals (Basel)*. 2018;11(3):63. doi:10.3390/ph11030063
- Oligschlaeger Y, Yadati T, Houben T, Condello Oliván CM, Shiri-Sverdlov R. Inflammatory bowel disease: A stressed “gut/feeling.” *Cells*. 2019;8(7):659. doi:10.3390/cells8070659

28. Lydiard RB. The role of GABA in anxiety disorders. *J Clin Psychiatry*. 2003;64(Suppl 3):21–27.
29. Kilincarslan S, Evrensel A. The effect of fecal microbiota transplantation on psychiatric symptoms among patients with inflammatory bowel disease: An experimental study. *Actas Esp Psiquiatr*. 2020;48(1):1–7.
30. Skonieczna-Żydecka K, Marlicz W, Misera A, Koulaouzidis A, Łoniewski I. Microbiome: The missing link in the gut-brain axis. Focus on its role in gastrointestinal and mental health. *J Clin Med*. 2018;7(12):521. doi:10.3390/jcm7120521
31. Jacobs JP, Mayer EA. Psychobiotics: Shaping the mind with gut bacteria. *Am J Gastroenterol*. 2019;114(7):1034–1035.
32. Marrie RA, Walld R, Bolton JM, et al; CIHR Team in Defining the Burden and Managing the Effects of Psychiatric Comorbidity in Chronic Immunoinflammatory Disease. Rising incidence of psychiatric disorders before diagnosis of immune-mediated inflammatory disease. *Epidemiol Psychiatr Sci*. 2019;28(3):333–342. doi:10.1017/S2045796017000579
33. Araki M, Shinzaki S, Yamada T, et al. Psychologic stress and disease activity in patients with inflammatory bowel disease: A multicenter cross-sectional study. *PLoS One*. 2020;15(5):e0233365. doi:10.1371/journal.pone.0233365
34. Ananthakrishnan AN, Gainer VS, Perez RG, et al. Psychiatric co-morbidity is associated with increased risk of surgery in Crohn's disease. *Aliment Pharmacol Ther*. 2013;37(4):445–454. doi:10.1111/apt.12195
35. Kochar B, Barnes EL, Long MD, et al. Depression is associated with more aggressive inflammatory bowel disease. *Am J Gastroenterol*. 2018;113(1):80–85. doi:10.1038/ajg.2017.423
36. Moulton CD, Pavlidis P, Norton C, et al. Depressive symptoms in inflammatory bowel disease: An extraintestinal manifestation of inflammation? *Clin Exp Immunol*. 2019;197(3):308–318. doi:10.1111/cei.13276
37. Leonard BE. Inflammation and depression: A causal or coincidental link to the pathophysiology? *Acta Neuropsychiatr*. 2018;30(1):1–16. doi:10.1017/neu.2016.69
38. Howren MB, Lamkin DM, Suls J. Associations of depression with C-reactive protein, IL-1, and IL-6: A meta-analysis. *Psychosom Med*. 2009;71(2):171–186. doi:10.1097/PSY.0b013e3181907c1b
39. Persoons P, Vermeire S, Demyttenaere K, et al. The impact of major depressive disorder on the short- and long-term outcome of Crohn's disease treatment with infliximab. *Aliment Pharmacol Ther*. 2005;22(2):101–110. doi:10.1111/j.1365-2036.2005.02535.x
40. Gazal M, Souza LD, Fucolo BA, et al. The impact of cognitive behavioral therapy on IL-6 levels in unmedicated women experiencing the first episode of depression: A pilot study. *Psychiatry Res*. 2013;209(3):742–745. doi:10.1016/j.psychres.2013.03.002
41. Gracie DJ, Irvine AJ, Sood R, Mikocka-Walus A, Hamlin PJ, Ford AC. Effect of psychological therapy on disease activity, psychological comorbidity and quality of life in inflammatory bowel disease: A systematic review and meta-analysis. *Lancet Gastroenterol Hepatol*. 2017;2(3):189–199. doi:10.1016/S2468-1253(16)30206-0
42. Macer BJD, Prady SL, Mikocka-Walus A. Antidepressants in inflammatory bowel disease: A systematic review. *Inflamm Bowel Dis*. 2017;23(4):534–550. doi:10.1097/MIB.0000000000001059
43. Sobin WH, Heinrich TW, Drossman DA. Central neuromodulators for treating functional GI disorders: A primer. *Am J Gastroenterol*. 2017;112(5):693–702. doi:10.1038/ajg.2017.57
44. Tynan RJ, Weidenhofer J, Hinwood M, Cairns MJ, Day TA, Walker FR. A comparative examination of the anti-inflammatory effects of SSRI and SNRI antidepressants on LPS stimulated microglia. *Brain Behav Immun*. 2012;26(3):469–479. doi:10.1016/j.bbi.2011.12.011
45. Frolkis AD, Vallerand IA, Shaheen AA, et al. Depression increases the risk of inflammatory bowel disease, which may be mitigated by the use of antidepressants in the treatment of depression. *Gut*. 2019;68(9):1606–1612. doi:10.1136/gutjnl-2018-317182
46. Anisman H, Merali Z. Cytokines, stress and depressive illness: Brain-immune interactions. *Ann Med*. 2003;35(1):2–11. doi:10.1080/07853890310004075
47. Liukkonen T, Silvennoinen-Kassinen S, Jokelainen J, et al. The association between C-reactive protein levels and depression: Results from the Northern Finland 1966 Birth Cohort Study. *Biol Psychiatry*. 2006;60(8):825–830. doi:10.1016/j.biopsych.2006.02.016
48. Minderhoud IM, Samsom M, Oldenburg B. Crohn's disease, fatigue, and infliximab: Is there a role for cytokines in the pathogenesis of fatigue? *World J Gastroenterol*. 2007;13(14):2089–2093. doi:10.3748/wjg.v13.i14.2089
49. Loftus EV, Feagan BG, Colombel JF, et al. Effects of adalimumab maintenance therapy on health-related quality of life of patients with Crohn's disease: Patient-reported outcomes of the CHARM trial. *Am J Gastroenterol*. 2008;103(12):3132–3141. doi:10.1111/j.1572-0241.2008.02175.x
50. Guloksuz S, Wichers M, Kenis G, et al. Depressive symptoms in Crohn's disease: Relationship with immune activation and tryptophan availability. *PLoS One*. 2013;8(3):e60435. doi:10.1371/journal.pone.0060435
51. Rohleder N, Aringer M, Boentert M. Role of interleukin-6 in stress, sleep and fatigue. *Ann N Y Acad Sci*. 2012;1261:88–96. doi:10.1111/j.1749-6632.2012.06634.x
52. Ananthakrishnan AN, Long MD, Martin CF, Sandler RS, Kappelman MD. Sleep disturbance and risk of active disease in patients with Crohn's disease and ulcerative colitis. *Clin Gastroenterol Hepatol*. 2013;11(8):965–971. doi:10.1016/j.cgh.2013.01.021
53. Marinelli C, Savarino EV, Marsilio I, et al. Sleep disturbance in inflammatory bowel disease. Prevalence and risk factors: A cross-sectional study. *Sci Rep*. 2020;10(1):507. doi:10.1038/s41598-020-57460-6
54. Ali T, Madhoun MF, Orr WC, Rubin DT. Assessment of the relationship between quality of sleep and disease activity in inflammatory bowel disease patients. *Inflamm Bowel Dis*. 2013;19(11):2440–2443. doi:10.1097/MIB.0b013e3182a0ea54
55. Ou G, Bressler B, Galorport C, et al. Rate of corticosteroid-induced mood changes in patients with inflammatory bowel disease: A prospective study. *J Can Assoc Gastroenterol*. 2018;1(3):99–106. doi:10.1093/jcag/gwy023
56. Jain A, Marrie RA, Shafer LA, et al. Incidence of adverse psychiatric events during treatment of inflammatory bowel disease with biologic therapies: A systematic review. *Crohn & Colitis 360*. 2020;2(1):53. doi:10.1093/crocol/otz053
57. Torres J, Bonovas S, Doherty G, et al. ECCO Guidelines on therapeutics in Crohn's disease: Medical treatment. *J Crohns Colitis*. 2020;14(1):4–22. doi:10.1093/ecco-jcc/jjz180
58. Magro F, Gionchetti P, Eliakim R, et al; European Crohn's and Colitis Organisation (ECCO); Third European evidence-based consensus on diagnosis and management of ulcerative colitis. Part 1: Definitions, diagnosis, extra-intestinal manifestations, pregnancy, cancer surveillance, surgery, and ileo-anal pouch disorders. *J Crohns Colitis*. 2017;11(6):649–670. doi:10.1093/ecco-jcc/jjx008
59. Kemp K, Dibley L, Chauhan U, et al. Second N-ECCO consensus statements on the European nursing roles in caring for patients with Crohn's disease or ulcerative colitis. *J Crohns Colitis*. 2018;12(7):760–776. doi:10.1093/ecco-jcc/jjy020
60. Lamb CA, Kennedy NA, Raine T, et al. British Society of Gastroenterology consensus guidelines on the management of inflammatory bowel disease in adults. *Gut*. 2019;68(Suppl 3):s1–s106. doi:10.1136/gutjnl-2019-318484
61. Mikocka-Walus A, Clarke D, Gibson P. Can antidepressants influence the course of inflammatory bowel disease? The current state of research. *European Journal of Gastroenterology and Hepatology*. 2009;5:48–53.

Advances
in Clinical and Experimental
Medicine

